Solar Powered Paraglider to cross the Atlantic

A feasibility study

T. Buchenau	4060660	R.C. Kuipers	4015819
F. Fortman	4127919	T.L. Mulders	1320327
M.P. Huijts	4118197	L.M.C. Sijbers	4092643
H. Hussain	4048075	D.L. da Silva Rosa	4047990
L. Koomen	4169727	A.J. Vrasdonk	4157400

Final Review Report

Design Synthesis Exercise

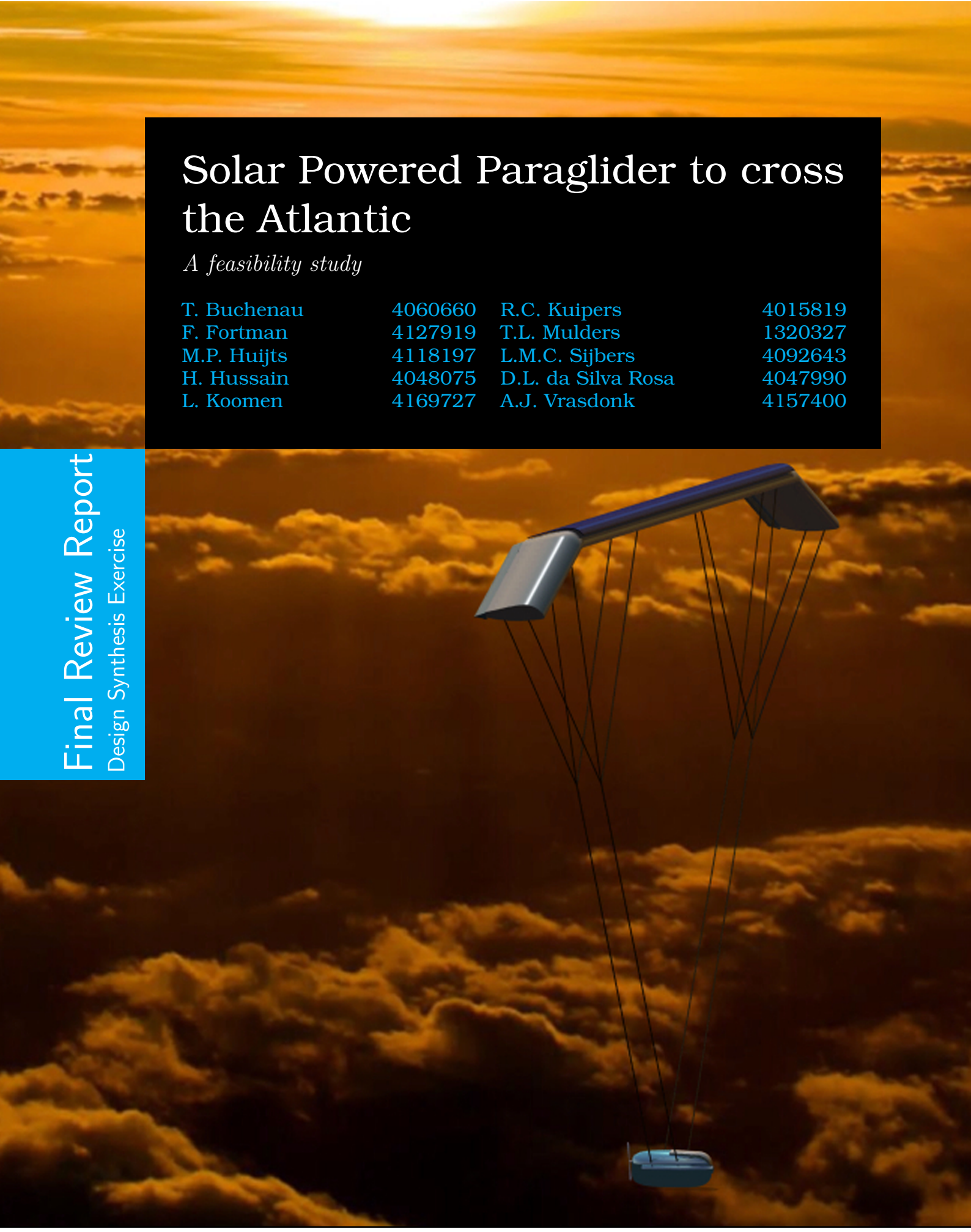

TU Delft Delft University of Technology

Aerospace Engineering

January 27, 2015

Preface

In 1986 the pioneer Henk Brink was the first European to complete a balloon flight over the Atlantic Ocean. In 2014 Mr. Brink proposed the idea for a similar mission to the TU Delft. This time a solar powered paraglider was the vehicle of choice for its sustainability and accessibility to general public. The first step in such a mission is investigate the feasibility before an attempt can be made to gather funds and a design team. This investigation was the subject of a Design Synthesis Exercise at the Faculty of Aerospace Engineering of TU Delft. A group of ten aerospace students were inspired to work on this final bachelor project. The result of nine long weeks is this Final Review Report.

This subject was the first choice out of nine subjects for everyone in this project group, signalling that the whole group was equally motivated. During the project this showed as well in our cohesion prior to deadlines, our communal lunches and coffee breaks at the appropriately named "Fellowship" building.

First and foremost we'd like to thank Mr. Brink for his interesting vision which he trusted with us. Having an inspiring subject certainly made the project more interesting to us.
We'd like to thank the industry experts: Meteorologist Tijmen de Boer, Ozone paraglider test pilot Russel Ogden and Royal Dutch Airforce Medical doctor Erik Frijters for their availability throughout the project. They made us aware off all the facets of such a mission which could prove to be problems. Our gratitude goes towards our tutor ir. Joris Melkert as well as our coaches Dhruv Metha MSc and PhD Jibran Khaliq for their guidance and insightful comments. It was great working under your mentorship. Further thanks to people that were available for questions or facts: Dr. Christos Kassapoglou MSc, Jos Sinke MSc, Nando Timmer MSc, Joep Breuer MSc from Airborne, Nuon Solar team's Bas van Wee. Special thanks to Iliass Azijli for his help on the programming codes. Manfred Kistler from Skywalk, who gave us information about jet flaps, motors and general paraglider characteristics that were of great help to us. Lastly, Geiger Engineering for information about propellers and electromotors.

We've enjoyed working on such a unique project with motivated people all around us. Hopefully the reader reads this report with just as much interest.

Contents

Nomenclature

Abbreviations

2D	Two dimensional
3D	Three dimensional
APU	Auxiliary Power Unit
AR	Aspect Ratio
ASTM	American Society for Testing and Materials
ASM	Aerostructural Static Model
BRR	Baseline Review Report
CAS	Calibrated Airspeed
CFD	Computational Fluid Dynamics
COTS	Commercial Off The Shelf
DC	Direct Current
DOT	Design Option Tree
DSE	Design Synthesis Exercise
EAS	Equivalent Airspeed
EBD	Electrical Block Diagram
FEM	Finite Element Method
FR	Final Review
GR	Glide Ratio
IAS	Indicated Airspeed
LTA	Lighter-Than-Air
MPPT	Maximum Power Point Tracker
MRR	Midterm Review Report
PCHIP	Piecewise Cubic Hermite Interpolating Polynomial
PMS	Power Management System
PPG	Powered Paraglider
PV	Photovoltaic
REE	Rare Earth Elements
RF	Radio Frequency
RoC	Rate Of Climb
RPM	Revolutions Per Minute
TAS	True Airspeed
TSO	Technical Standard Orders
UV	Ultra Violet

Definitions

Atlantic	Atlantic Ocean
Client	Henk Brink
Canopy	Parachute-like part of the vehicle
Fuselage	Subsystem suspended under the canopy
Mission	The operations required to fulfil the mission need statement
Paraglider	Parachute-like glider craft with no rigid parts
Team	The project team set to fulfil the project objective statement

Greek Symbols

α	Angle of attack	$-$
$\alpha_{rotation}$	Angular acceleration	$rad \cdot s^{-2}$
Γ	Dihedral angle	$^{\circ}$
γ	Tensairity ratio	$-$
η_{bat}	Battery coulombic efficiency	$-$
η_{motor}	Motor efficiency	$-$
η_{prop}	Propeller efficiency	$-$
η_{sys}	System conversion efficiency	$-$
$\theta_{rotation}$	Rotation angle	rad
μ_c	Dimensionless weight	$-$
ρ	Density	$kg \cdot m^{-3}$
ρ	Resistivity	$\Omega \cdot m$
σ	Normal stress	MPa
σ	Yield strength	Mpa
τ	Shear stress	MPa
τ_o	Torque	Nm
θ_i	Angle Tensairity®	rad

Roman Symbols

A	Area	m^2
A_{disc}	Actuator disc area	m^2
A_{mr}	Area of jet flap rib	m^2
a	Acceleration	$m \cdot s^{-2}$
acc	Drawing accuracy	$-$
a_r	Height jet flap rib	m
b	Wing span	m
$b_{anhedral}$	Section of the wing span designated for anhedral	m
b_{pv}	Section of the wing span designated for PV cell storage	m
$bubDist$	Bubble distribution	$-$
b_r	Width jet flap rib	m
c	Chord length	m
$c.g.$	Centre of gravity	m
C_D	3D Drag coefficient	$-$
C_d	2D Drag coefficient	$-$
$C_{D_{0w}}$	Wing profile drag coefficient	$-$
C_{f_w}	Skin fiction coefficient of wing	$-$

$C_{d_{minw}}$	Minimum drag coefficient of airfoil	–
C_L	3D lift coefficient	–
C_{L_α}	3D lift curve slope	–
$C_{L_{max}}$	3D max lift coefficient	–
C_l	2D lift coefficient	/∘
C_{l_α}	2D lift curve slope	/∘
C_{l_β}	Increase in roll moment due to sideslip	–
$C_{l_{max}}$	2d maximum lift coefficient	–
C_{l_r}	Increase in roll moment due to yaw rate	–
C_m	Airfoil moment coefficient	–
C_{m_α}	Increase in pitching moment due to angle of attack increase	–
$C_{m_{\dot{\alpha}}}$	Increase in pitching moment due to angle of attack acceleration	–
C_{m_q}	Increase in pitching moment due to pitch rate increase	–
C_{m_u}	Increase in pitching moment due to horizontal speed increase	–
C_{n_β}	Increase in yaw moment due to side-slip	–
C_{n_r}	Increase in yaw moment due to yaw rate	–
C_{X_α}	Increase in forward force due to angle of attack increase	–
C_{X_u}	Increase in forward force due to horizontal speed increase	–
C_{Z_0}	Inverse of C_L	–
C_{Z_α}	Increase in downward force due to angle of attack increase	–
C_{Z_u}	Increase in downward force due to horizontal speed increase	–
c_T	Thrust coefficient	–
d	Distance	m
ds	Surface length	m
d_s	Distance from hinge point a to spring force	m
d_z	Distance from hinge point a to centre of gravity	m
e	Oswald's number	–
E	Young's modulus	GPa
E_2	Energy required during phase 2	J
E_{pv}	Energy delivered by the solar cells per squared meter during sun hours	$J \cdot m^{-2}$
$E_{req_{pv}}$	Required energy to be delivered by the solar cells during sun hours	J
E_{spec}	Energy density	$Wh \cdot kg^{-1}$
E_{vol}	Energy volume density	$Wh \cdot l^{-1}$
f_M	Function of Mach number	–
F_{impact}	Impact force	N
F	Force	N
F_s	Spring force	N
F_{xb}	Horizontal force in back suspension line	N
F_{xf}	Horizontal force in front suspension line	N
F_y	Tensile force in membrane	N
F_z	Gravitational force	N
g	Gravitational constant	$m \cdot s^{-2}$
GR	Glide Ratio	–
GI_p	Torsional rigidity	Nm
h	depth of immersion	m
I	Moment of inertia	$N \cdot m^2$
k	Shape factor	–
K	Column effective length factor	–
K	Tensile force ratio	–
K_Y	Dimensionless moment of inertia of y-axis	–
L	Lift	N
L	Beam length	m
$L_{anhedral}$	Lift over anhedral section	N
L_{helium}	Lift provided by helium	N
L_{total}	Total lift	N

l	Length	m
M_0	Bending moment	$N \cdot m$
M_a	Moment around hinge point a	$N \cdot m$
$M(x)$	Bending moment	$N \cdot m$
m	Mass	kg
m_{bat}	Battery mass	kg
n	Amount of revolutions per second	s^{-1}
n	Amount of bubbles	$-$
$nMembranes$	Amount of cell membranes desired	$-$
O_i	Circle center	m
P	Compressive force	N
P	Pressure	Pa
P_a	Power available	W
$P_{bladder}$	Internal pressure of bubbles	Pa
$P_{buckling}$	Buckling load	N
P_{cr}	Critical buckling force	N
P_i	Point	$-$
P_r	Power required	W
P_{ribs}	Pressure in ribs	Pa
P_{spars}	Pressure in spars	Pa
P_{sub}	Power demand of subsystems	W
p	Overpressure	Pa
$p_{ambient}$	Ambient pressure	Pa
$p_{internal}$	Internal pressure	Pa
$pvDistr$	PV cell distribution	$-$
Q	First area moment	m^3
q	Distributed load	$N \cdot m^{-1}$
$q_{BubbleMax}$	Maximum distributed load over bubbles	N/m
q_{max}	Maximum dynamic pressure	Pa
q_s	Shear flow	N/m
$q_{SparBack}$	Load distribution back spar	N/m
$q_{SparFront}$	Load distribution front spar	N/m
r_a	Ellipsoid semi axis a	m
r_b	Ellipsoid semi axis b	m
r_c	Ellipsoid semi axis c	m
R_gas	Specific gas constant	$J \cdot kg^{-1} \cdot K^{-1}$
R	Resistance	Ω
R	Radius of bubble	m
Re	Reynold's number	$-$
RoC	Rate of climb	$m \cdot s^{-1}$
S_w	Total effective wing surface area	m
$S_{anhedral}$	Anhedral part of the wing surface area	m
S_{wetw}	Wetted wing surface area	m^2
$S_{horizontal}$	Horizontal part of the wing surface area	m
$\frac{s_l}{b}$	Line length per wingspan	$-$
T	Tension in suspension line	N
T	Temperature	K
T	Thrust	N
T_{max}	Maximum available thrust	N
T_b	Tension line force at the back spar	N
T_f	Tension line force at the front spar	N
T_v	Vertical tensile force in outer suspension line	N
t	Thickness	m
t_1	Duration of the first part of darkness of the mission	s
t_2	Duration of the second part of darkness of the mission	s

$t_{bladder}$	Thickness of bladder skin	m
t_{cl}	Duration of the climb phase	s
t_{dark}	Continuous time of darkness	s
t_{des}	Duration of descend	s
t_{sun}	Amount of sun hours per day	s
V	Shear force	N
V	Volume	m^3
v_0	Velocity in front of an object	$m \cdot s^{-1}$
v_g	Ground speed	$m \cdot s^{-1}$
v_{stall}	Stall speed	$m \cdot s^{-1}$
v_t	True airspeed	$m \cdot s^{-1}$
$v_{w_{to}}$	Velocity at which the wing takes off	$\cdot s^{-1}$
W	Weight	N
W_{Canopy}	Weight of canopy	N
$W_{SolarPanel}$	Weight of solar panels	N
W_{tot}	Total weight of the aircraft	N
x_1	X- location of attachment point of front suspension line	m
x_2	X- location of attachment point of front suspension line	m
x_{cg}	X- location of canopy c.g.	m

Abstract

The urge for adventure combined with the global need for increasingly sustainable methods of air transportation resulted in a pioneering idea. What better way to show the possibilities of solar power by altering the accessible and entertaining nature of a paraglider? Personal experience and vision inspired the client to be the first to fly such an aircraft over the Atlantic Ocean to spread awareness for a more sustainable future. The mission was born: "Fly manned, continuously across the Atlantic using a solar powered paraglider."

Crossing the Atlantic requires the typical range of a paraglider to drastically increase. This combined with the current technology in terms of energy storage and solar power generation makes designing a struggle. Duration is a problem due to the slow, inefficient cruise phase. The purpose of this report is to investigate the feasibility of flying a solar powered paraglider over the Atlantic.

The flight route and time of execution were based on the least amount of energy required to make the crossing. This means flying the shortest distance, with the most amount of sun hours per day, the highest solar intensity and the most advantageous tail winds. Impossible to maximise every parameter an optimal mission was determined to fly a rough 3040 km from St. John's, Newfoundland Quebec to Portmagee, Ireland during the late June summer days.

The design mainly evolved around flying with the least amount of energy required whilst still allowing a duration short enough for the pilot to cross without falling asleep. Flying efficiently typically means flying slow, but the aforementioned duration set a lower bound to this. The maximum mission duration was extended as much as possible by techniques such as blue light, stimulating substances, pilot health and pilot entertainment. By designing every part of the paraglider to be as lightweight as possible results in a cycle of less energy required, which in turn allows smaller subsystems, which in turn has lower weight.

The subsystems were designed in a concurrent way. Progress in one part means changed inputs for another part. Integrated MATLAB® tools based on analytic models were created to converge to an optimal design point for the subsystems in relation to each other. The subsystems and final product were analysed for sensitivity of their input values which helped identify the best solution for improvements. The final product was also analysed for its performance in order to check requirement compliance and the actual mission feasibility.

The missions two most important limiting factors are the mission duration and the power required. In order to minimise mission duration the flight speed should increase whilst the opposite is true for the power required. This study revealed that power required was the limiting factor so a lower flight speed was chosen. For the chosen cruise speed of 10 $m \cdot s^{-1}$ the resulting mission duration was 38 hours and the power required ended up to be 3.79 kW. The total mass of the vehicle is 277 kg of which 23% is battery mass and 16% solar cell mass. The high energy density lithium-sulphur batteries are still in development, but are expected to be available within 5 years. Currently available batteries would make the design too heavy.

This study was initiated as a concept study. With a custom designed wing and fuselage the mission is shown to be technically feasible in 5 years time. The limited scope and duration of this project allows for more improvements for which this report can be used as a guideline.

1 Introduction

In modern day aviation there is an ever-increasing drive to develop more sustainable aircraft. In recent years, this drive has resulted in the design of inspiring aircraft that pioneer the use of solar power as a main power source. However, up to this point, no venture has been made in realm of solar powered paragliders. The aim of this Design Synthesis Exercise (DSE) project is to investigate the feasibility of such a concept by attempting to fly a solar powered paraglider continuously across the Atlantic.

Initially the aim was to do this and satisfy the mission need statement: "fly a manned solar powered paraglider continuously across the Atlantic", by using Commercial Off The Shelf (COTS) components. However in the Baseline Review Report (BRR) this was scratched as the mission will not be feasible with this requirement. This Final Review (FR) report is a continuation of the research and findings stated in the Midterm Review Report (MRR). At the end of the DSE the Team aims to deliver a design that shows that it is feasible to cross the Atlantic with a solar powered paraglider. Keeping in mind that additional research has to be done after this feasibility study in fields that are currently outside the scope of the DSE. These have been summarised for future reference at the end of the report.

During this DSE for the investigation of several aspects of the design numerical tools have been developed or existing tools have been adapted to suit the specific purpose of the project. These tools were used to check whether the design meets all the requirements. Validation and verification of the tools used can be found in Chapter 7. When a numerical analysis is not possible a qualitative analysis has been done, e.g. the analysis of the stability in Section 2.1. These qualitative analyses give a general idea of the behaviour of the design in certain situations. Nevertheless further research, experimental or numerical, will have to confirm the results from these analyses.

To achieve all the aforementioned goals the Team, a group of 10 students, has to come up with a design over a period of 10 weeks. The final design has been based on an iterative process, the validation for the number of iteration can be found in Chapter 7. It is important to note that the purpose of DSE is to check the feasibility of the mission, and not necessarily to build a highly accurate tool. The tools will give a feeling of the values that are to be used for the design.

The sections in this chapter form an introduction to the project, its requirements (Section 1.1), the technical risks involved (Section 1.2), project management (Section 1.3), the mission profile (Section 1.4) and project development logice and time planning (Section 8.5). These form a starting point for the subsequent chapters that form the design synthesis. In Chapter 2 the stability and controls of the design have been investigated. Chapter 3 explains the aerodynamic aspects of designing a wing. The structural design of the wing and fuselage have been investigated in Chapter 4 and 5. All the designs for the subsystems as well as the layout of these subsystems in the fuselage has been summarised in Chapter 6. This chapter also contains the approach to sustainability for the project. Chapter 8 contains a performance analysis of the final design. It also explains the sensitivity of the design to changes in the variables, and finally evalutates the feasibility of the design. In Chapter 7 the tools used to calculate the final design are verified and validated. Finally Chapter 9 contains the final conclusions and recommendations based on the results from Chapter 8.

Equation (9.1) shows the formula that characterises the driver behind the design process. During this process the following is always pursued. The power required P_r should be minimised, because every $Watt$ that is required has to be generated or taken aboard, which both will increase the weight. In order to minimise the P_r, the weight W and the velocity v should always be minimised and the measure of efficiency of the design, called the Glide Ratio GR, should be maximised.

$$P_r = \frac{W}{GR} \cdot v \tag{1.1}$$

1.1 Requirements

In the previous phases of this project there have been changes in the requirements list. In this section the current list is presented. These requirements are used to validate the paraglider at the end of the report in Section 8.4.1.

The abbreviations used for this section are TECH: Technical, MIS: Mission, SAF: Safety, COM: Communication, SUS: Sustainability and MSC: miscellaneous.

The top level requirements as stated in the project plan are the following:

- **REQ-MIS-A1** The optimal time frame to cross the Atlantic must be determined, i.e. maximise the availability of solar radiation and favourable wind conditions.
- **REQ-MIS-B1** The transatlantic flight must be continuous or, if proven infeasible, intermediate stops are an option.
- **REQ-MIS-B2** The crossing must at least cover the Atlantic. However, the client has indicated that in addition to the Atlantic, crossing the North Sea is considered highly favourable.
- **REQ-MIS-C1** The paraglider must be manned, this means taking into account human factors such as fatigue, immobility and diet of the pilot.
- **REQ-MIS-C11** The pilot must have food and drinks for the mission.
- **REQ-MIS-D1** The maximum flight altitude must be such that the fuselage does not have to be pressurised.
- **REQ-SAF-A2** In case of landing on water the fuselage must offer survivability long enough to be rescued.
- **REQ-SAF-B1** The safety of the pilot must be guaranteed all throughout the flight.
- **REQ-SAF-B12** The PPG must be able to perform a safe emergency landing.
- **REQ-TECH-A1** The paraglider design must be within the stretched definition of a paraglider, i.e. the canopy is allowed to have semi-rigid parts.
- **REQ-TECH-B1:** The paraglider must be completely solar powered; batteries charged with solar energy are okay.

In order to meet the top level requirements there were certain self-imposed requirements. These give more in depth limitations. These are stated below:

- **REQ-TECH-A11** The canopy must have enough area to store Photovoltaic (PV) cells on.
- **REQ-TECH-A12** The canopy must provide roll and yaw control.
- **REQ-TECH-A13** Canopy material must be UV-resistant.
- **REQ-TECH-A14** The wing must be tear resistant.
- **REQ-TECH-A15** The wing's airfoil must keep its shape
- **REQ-TECH-C1:** The paraglider must be designed to be stable and controllable by a human, i.e. no automated system to counter instability or do control.
- **REQ-TECH-C11** The PPG must have static stability.
- **REQ-TECH-C12** The PPG must have dynamic stability.
- **REQ-TECH-C13** The control forces must not exceed human capabilities.
- **REQ-TECH-C14** The PPG must have trim system.
- **REQ-MIS-B3** The mission duration must be lower than 42 hours or a solution for pilot fatigue has to be found.
- **REQ-MIS-C12** The fuselage must enable to store or get rid of (human) waste.

- **REQ-SAF-A1** The fuselage must be safe in case of an emergency landing both on land as well as on water.
- **REQ-SAF-A21** The floating device must provide visibility for rescue operations.
- **REQ-SAF-A22** There must be an emergency supply of water and food.
- **REQ-SAF-A23** Hazardous equipment must not present harm to the pilot in emergencies.
- **REQ-SAF-A24** An emergency location transmitter must be present.
- **REQ-SAF-B11** The PPG must be designed to avoid collisions.
- **REQ-COM-A1** The pilot must be able to communicate with a control centre throughout the mission.
- **REQ-COM-A11** Ground centre must be able to monitor pilot health.
- **REQ-COM-A12** Vehicle must be capable of sending flight data.
- **REQ-COM-A13** A voice link must be established between pilot and ground centre.
- **REQ-COM-A14** Pilot must be able to receive weather and flight information.
- **REQ-SUS-A1** The project as a whole must be executed in a sustainable way. In operation as well as production and design.
- **REQ-SUS-A2** A valid solution for the after mission life for subsystems must be found.
- **REQ-MSC-A1** A power and weight budget of the design must be made.
- **REQ-MSC-A2** There must be a cost analysis of the project.
- **REQ-MSC-A3** Components with technology in the development phase must be available within five years.
- **REQ-MSC-A4** There must be inboard visibility.

Special attention is given to **REQ-MSC-A3**. The previous top level requirement was considered: "The PPG must be made with commercially off the shelf parts only". However, in the BRR it was determined to be not possible to meet this requirement.[1] Therefore, this requirement was downgraded to self-imposed requirements.

1.2 Technical Risk Assessment

A final technical risk assessment has been made to assess the risks involved with the technology chosen for the final design. In the MRR a choice was made for which type of batteries, PV and electric motor to use. In addition to these technologies Chapter 6 contains an overview of what other technologies have been selected for the remaining subsystems.

Table 1.1 contains a risk map of the technologies involved in the design. As can be seen technologies that have been placed in the categories "critical" or "catastrophic" and are feasible in theory or have a working laboratory model only have been avoided as much as possible. Unfortunately for the canopy design there are no real reference concepts for the design. This is why it has been categorised as "Feasible in theory" and "Critical". Other options for PV cells and batteries have been disregarded as an option in the MRR because their alternative has significantly less technical risks involved. And these technologies will not produce a working version within the time-frame determined for the project.

Table 1.1: Technical Risk Map

	Negligible	Marginal	Critical	Catastrophic
Feasible in theory		l	m	
Working laboratory model				
Based on existing non-flight engineering		b, j	f,p	
Extrapolated from existing flight design	g	a, n, o	e,k	
Proven flight design	d, h, i			

a Battery lithium sulphur
b PV cells triple junction InGAP/InGaAs/Ge
c Brushless direct current motor
d Navigation GPS
e Inflatable wing
f Streamlined fuselage
g Health and safety system
h Life support system
i Communication system
j Emergency rescue system
k Tensairity®
l Conducting lines
m Semi rigid canopy design
n Take-off system
o Steering/control system
p Battery and motor ejection system

Items such as the GPS, life support system and communication system have been based on COTS components that have a proven flight design. Technologies that are in the "critical" column have been assigned additional resources as they are very important to the success of the mission. They are:

- Semi rigid canopy design
- Inflatable wing
- Streamlined fuselage
- Tensairity®
- Battery and motor ejection system

1.3 Project Managment

Planning is essential for a mission to meet its goal. Structure is needed to keep an overview of all the necessary activities, which also are to be chronologically ordered. In this section the necessary planning diagrams are presented. At first the functional flow diagram is presented, followed by the functional breakdown structure.

1.3.1 Functional Flow Diagram

The sequence in which the mission shall be executed is presented schematically in Figure 1.1 and Figure 1.2 on page 6.

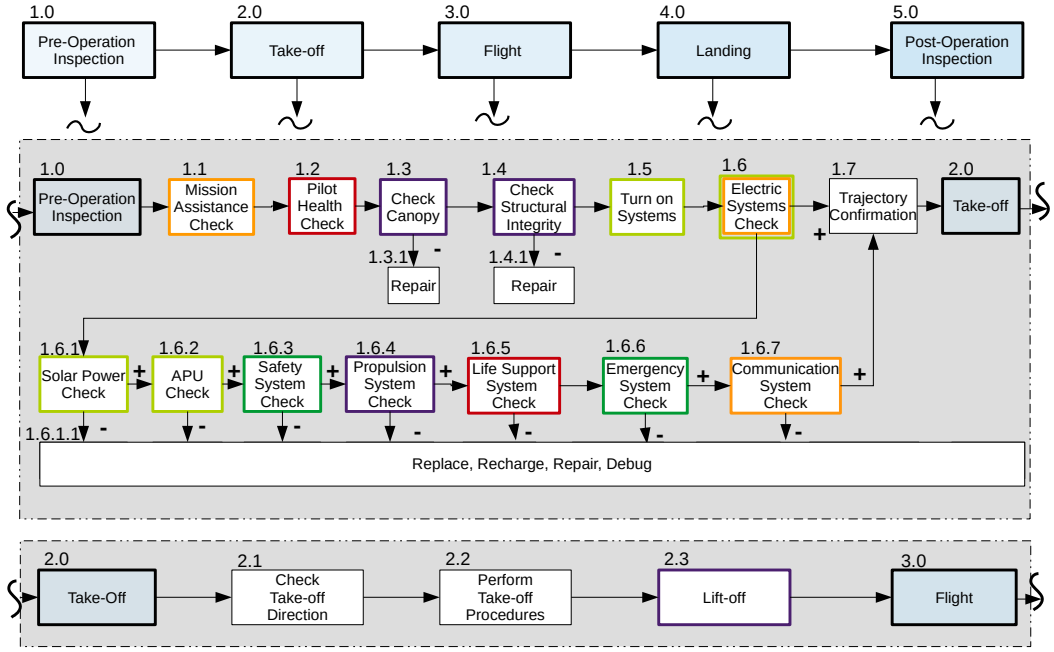

Figure 1.1: Functional flow diagram for the mission

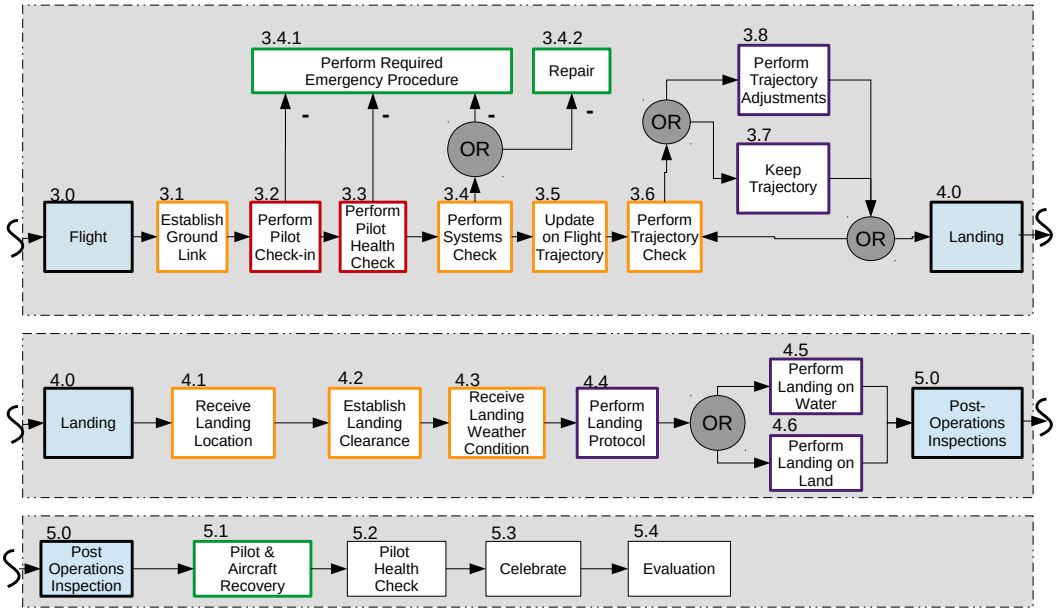

Figure 1.2: Functional flow diagram for the mission continued

1.3.2 Functional Breakdown Structure continued

The functions the PPG and its subsystems have to perform, along with certain low level requirements, are presented in Figure 1.3 on page 7. These entries were divided per technical group so each group could check their compliance later on.

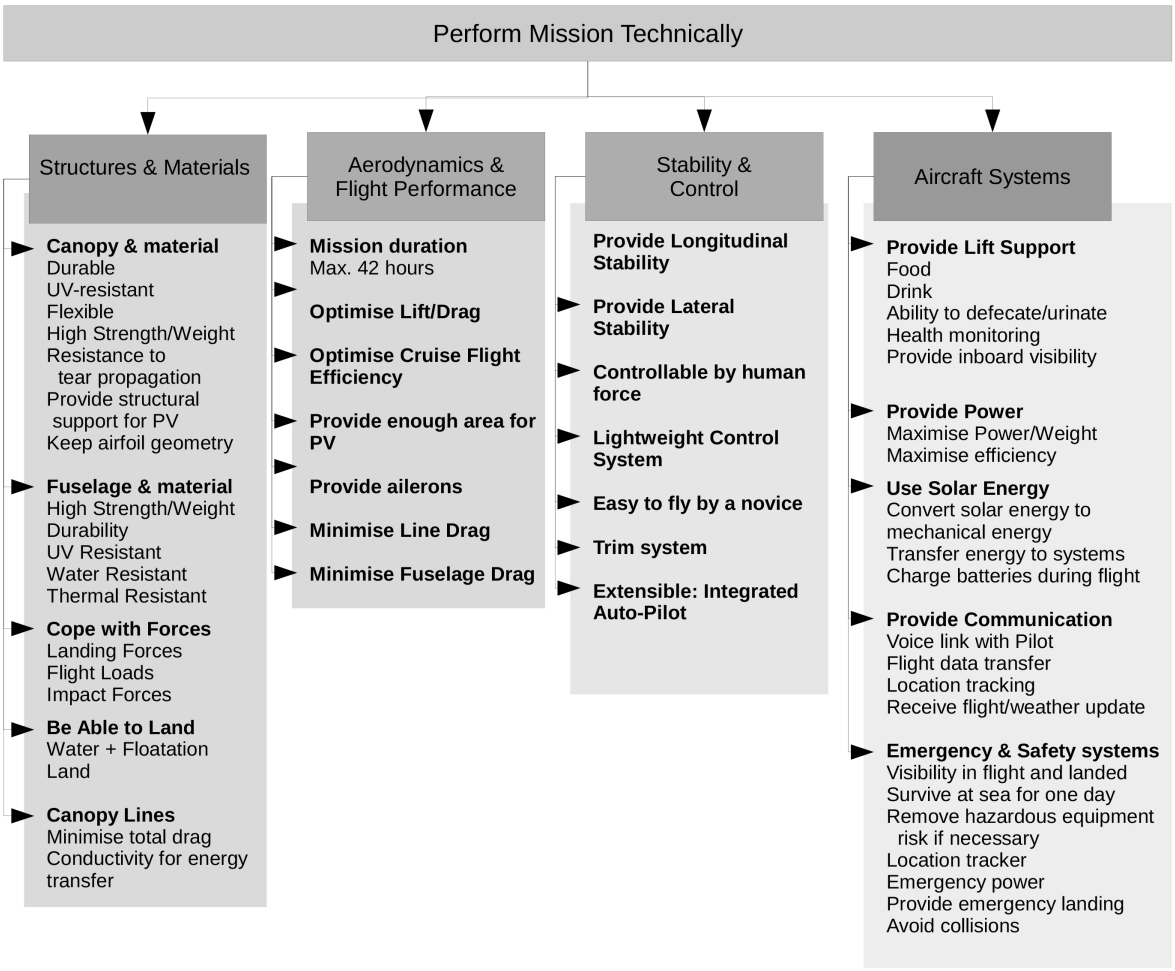

Figure 1.3: Functional Breakdown Structure for the PPG and its subsystems

1.4 Mission Profile

In this section, the way the mission shall be executed and certain mission parameters are specified. The route is shown in Figure 1.5. After the MRR a few mission parameters changed. These are explained in more detail in Section 6.1 and 8.1. The new mission duration is 37.9 h, compared to 26 h in the MRR, being an alternating sequence of night and day hour, starting with 8 h at night. After 16 h in daylight, another 8 h of night time follow before the final hours of the mission pass during day time. This is caused by the changes in cruise speed and wind speed. The cruise speed has been lowered from 12.5 $m \cdot s^{-1}$ to 10.0 $m \cdot s^{-1}$, because with the initial speed the required PV cell area to provide sufficient power would have exceeded the available area on the wing. After consulting meteorologist Tijmen de Boer, our initial assumption of 22.0 $m \cdot s^{-1}$ turned out to be possible albeit very optimistic. Therefore, based on the expert´s advice, the conservative value of approximately 12.0 $m \cdot s^{-1}$ has been used in the subsequent

calculations. A different mission profile, in which take-off is performed in daylight, has been proposed as a recommendation to check if the most optimal mission profile has been chosen for the increased mission duration. The increased mission duration can become critical when looking at the mean relative performance per hour of wakefulness of the pilot. According to research of the Royal Dutch Airforce, the longest sleep deprivation, with the pilot still having the minimum of 65% relative performance, was found to be approximately 42 h, also shown in Figure 1.4.

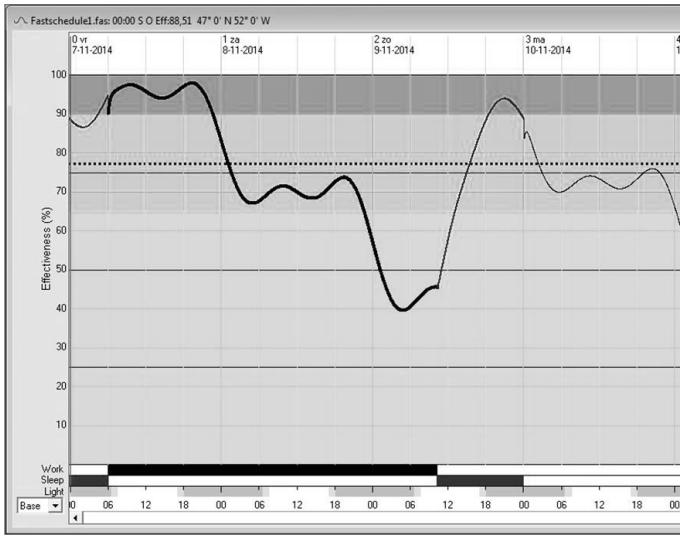

Figure 1.4: Mean relative performance per hour of wakefulness

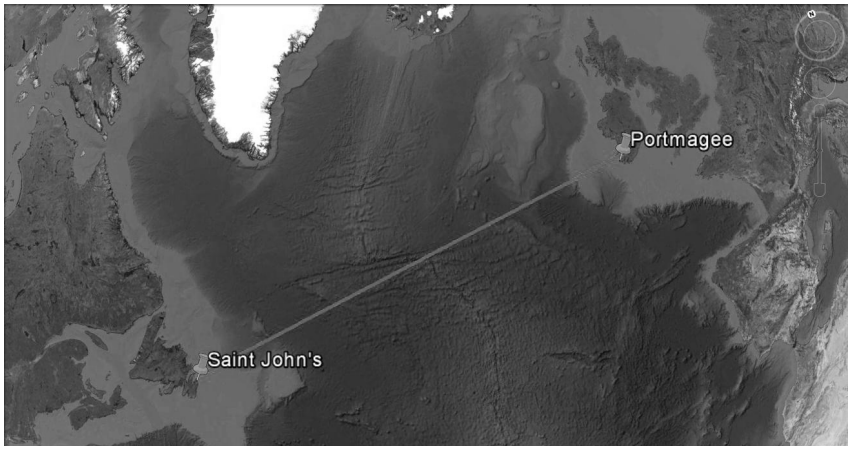

Figure 1.5: Topview of the mission St. John's (start) to Portmagee (finish)

The current mission parameters are presented in Table 1.2.

Variable	Unit	Value
Duration	h	37.9
Distance	km	3040
Sunlight	$h \cdot day^{-1}$	16
Night	$h \cdot day^{-1}$	8
Cruise altitude	ft	10000
Wind speed	$m \cdot s^{-1}$	12
Cruise speed	$m \cdot s^{-1}$	10

Table 1.2: Mission parameters

1.5 Development Logic & Project Design

After the feasibility study is completed start of the preparations can begin. The conclusion of the study can be used to convince industry experts, designers and sponsors to partake in the project.
In this section the activities of post feasibility study are presented. The different activities and their duration were estimated and plotted in a Gantt chart (Figure 8.8). It is understood that the duration may be grossly under- or overestimated as the actual time it takes depends on unknown factors. For example, the time to find a sponsor is likely to depend on economy situations. Also, some extra activities, which are unknown at this point in time, may be necessary or present activities may prove redundant.

Figure 1.6: Time planning of all activities relevant to the mission

1.6 N^2-Chart Of The Design Iteration

Typical for an aerospace design process are iterations. Very often, if not always, inputs for certain calculations are outputs of calculations done later on. This requires these values to be fed back to the earlier calculation, such that the design is iterated. It is important that the iteration converges, otherwise a definitive solution will never be found. To have a good idea of the feedback and the outputs that become inputs for other calculations an N^2-chart is made that shows this in a clear manner. This chart has been shown in Figure 1.7. From this it can be seen that a total of 4 values are output from one of the boxes and fed back into earlier calculation boxes. The parameters that are put in from the top of the chart are external parameters (such as air densities and temperatures), not being output of any of the other calculations.

Underneath, the integrating MATLAB® script and all the different boxes and what their purpose is, are explained.

Main integration file
This script has all the different subscripts integrated. It starts with stating all the different standard parameters such as temperatures at sea and cruise level, the gravitational acceleration and the wind speed at sea and cruise level. In the beginning of this script, also the different kinds of airspeeds are given (Indicated Airspeed (IAS), True Airspeed (TAS) and ground speed). Lastly, the preliminary values of the GR, wing weight and pressurised volume of the wing are stated. These are input for the first 2 boxes, but will only be outputs of later boxes. At the end of this script, the secondary drag contribution (from "Secondary and Total Drag") is used together with the Glide Ratio (GR) that takes into account the drag of the wing (from "Airfoil Sizing") to come up with the final GR that displays the efficiency of the whole design.

Weight and Power Budget of Subsystems
This script calculates all the different masses of all the subsystems, their centres of gravity with respect to the middle of the two suspension lines and if necessary their respective power outputs or inputs. To do so, at first the constants needed for the calculations in this box are provided such as the battery charge efficiency, propeller efficiency and battery energy density. The different amounts of energy needed per stage of flight and their durations are calculated using the GR, which is input from the final stage after the first run.

Lift from Wing and helium
The wing is pressurised using helium and the extra lifting force creating by this, at sea level as well as cruise altitude, is calculated. The available pressurised volume in the wing is an important input for this and is an input after the first loop from the "Structural Wing Weight"-box, also a constant value for the total pressure inside the wing is used in this script.

Airfoil Sizing
In this script, all the airfoil data from Javafoil is read and converted to useable values in 3D instead of just 2D airfoil data. Input for this script are atmospheric conditions at sea and cruise level, the Aspect Ratio (AR), the cruise speed and a preliminary chord length, for which the actual value is calculated in the next box "Wing Sizing". Using the atmospheric conditions, the corresponding air viscosity and Reynolds numbers are calculated, needed for the 2D to 3D calculation and the detailed zero-lift drag approximation of the wing. Using the converted values, the angle of attack, lift coefficient, drag coefficient and moment coefficient related to the maximum lift-to-drag ratio are picked, providing a new GR that takes into account the real drag of the wing. Next to this, also the ratio of the airfoil profile length with respect to the chord is calculated and the influence of a different AR and zero lift drag coefficient of the wing are visualised.

Wing Sizing
Using the needed solar cell area, the lift that has to be generated by the wing only (already taking the subtraction of the lift from the helium into account) and the 3D airfoil parameters, the wing can be sized. The wing span of the horizontal middle part of the wing and the anhedral parts are calculated; the projected and flat total wing area are calculated; using these two values the actual chord of the wing is also an output.

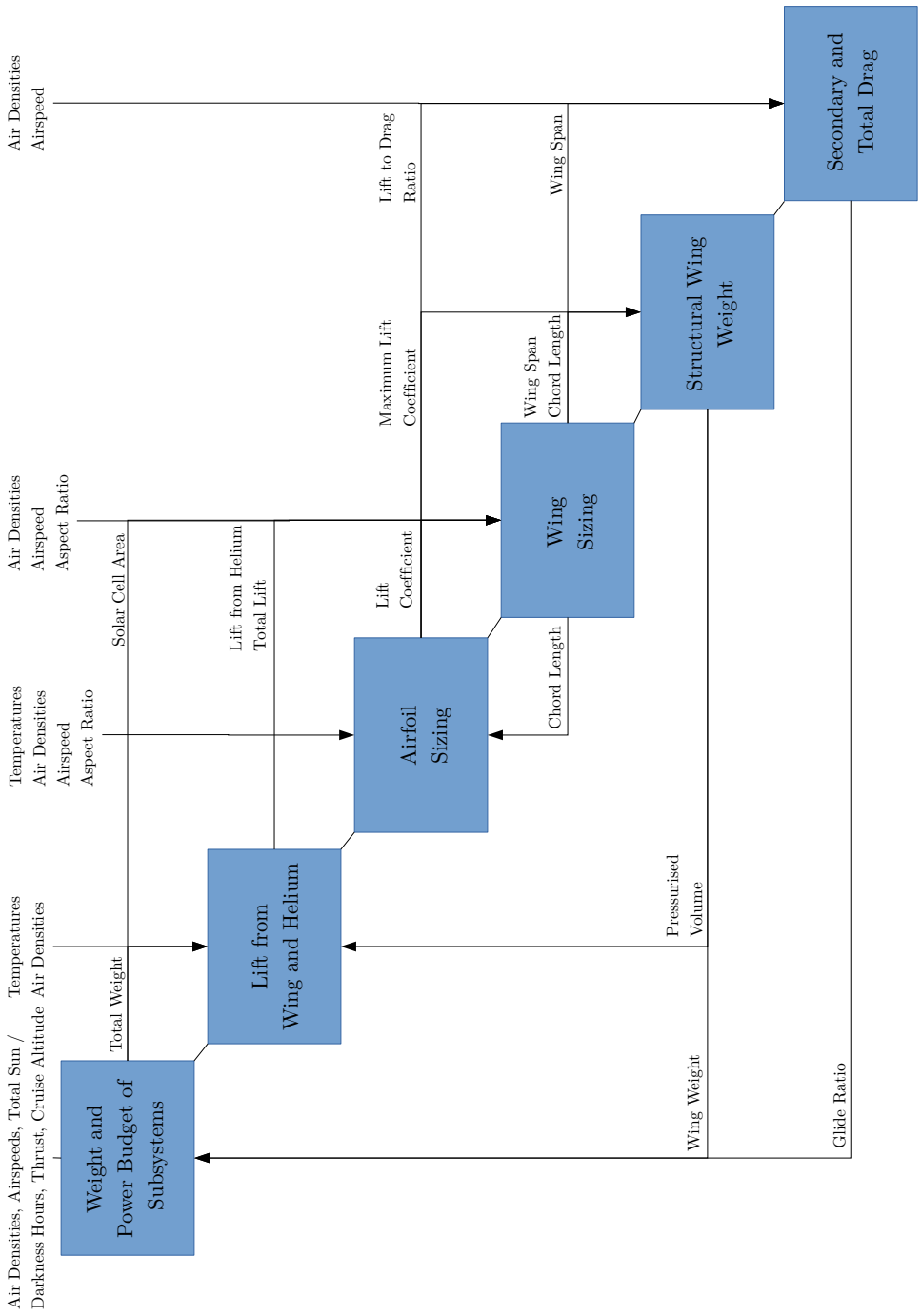

Figure 1.7: N^2 chart of the design iteration

Structural Wing Weight

This script is very stand-alone, and takes into account the maximum lift coefficient, in order to calculate the loads the wing must be able to bear. Input is also the dimensions of the wing to calculate the internal structure and its weight and volume to be pressurised. These two last

parameters are also the main output of this file, and are being used in "Lift from Wing and Helium" and "Weight and Power Budget of Subsystems", respectively.

Secondary and Total Drag

This script is the last one used in the main file. Now that all the parameters are known, the length of the control and suspension lines can be calculated, that are a function of the wing span. From this the respective drag contributions and also that of the fuselage are calculated.

1.7 Market Analysis

In order to actually build the design, all costs need to be covered. A budget estimation for production, logistics, operation pre- and post operation has been made and can be found in section 6.7. The client cannot finance the whole project, therefore partners and sponsors are essential. In this market analysis, the strengths and weaknesses of the concept discovered in the Baseline Review Report (BRR) have been used. The unique selling points have also been quantified in the BRR, these can aid the Team in finding sponsors to finance the project.

During the DSE the Team has had contact with industry experts provided by the TU Delft as well as experts from other industry leading companies. Their enthusiasm has given the Team the confidence to state that there is a large support base within the industry for projects such as this one. However, even though the interest is there, it is important for a potential sponsor to see a certain Return On Investment (ROI). This has been discussed in Section 1.7.1.

1.7.1 Return On Investment

In project such as these which are special one of a kind mission the biggest ROI can be found in the brand exposure. To achieve a maximum brand exposure and thus maximise the ROI there are several steps the Team can undertake in combination with the sponsors. The standard for doing this in the 21^{st} century with social media has been set by the Red Bull Stratos[(i)] mission. By looking at the following fields the maximum ROI is achieved.

- Pre-promotion
- High quality content
- Platform specific content
- Investment
- Community involvement
- Story telling

Companies that sell products or services related to customer groups involved in the paraglider scene approached for a partnership or sponsorship. A company producing paragliders, for example Ozone, can be approached. A company that is related to extreme sports, for instance Red Bull, can be approached for the second customer group. An energy company wanting to raise their public profile in the renewable energy branch, such as Eneco, can also be approached.
The aim is to collect the amount of money from sponsorship that is needed to cover the entire budget. This can also be in the form of partnerships in which companies assist the team in their specialised areas or in a product from their product line that can be used in the mission. In this respect any of the suppliers can be seen as an option for a partnership.

[(i)] `http://www.redbullstratos.com/`

1.8 Operations & Logistics

When the mission is actually performed and the aircraft is built the operations and logistics are an important implementation. To fulfil the mission smoothly the operations and logistics have been planned in advance. For all equipment that has to be rented, a company has been chosen at which this equipment is rented so that the cost analysis is more accurate.

1.8.1 Transport

All the required equipment, including the aircraft itself, has to be transported to the launch site and from the landing site. To take into account sustainability and safety, it has been recommended that the equipment is rented as close as possible, first of all to decrease transport times and second to make sure that spares or a replacement can be delivered fast if needed. Maritime Ontario Freight Lines Ltd[(ii)] has been chosen to provide transportation to and from the launch site as it is based close to the launch site and has the required transportation vehicles in its arsenal. Vanrentals[(iii)] has been chosen to provide transportation at the landing site for the same reason.

1.8.2 Facilities

Facilities to house the equipment and the staff has to be present at both the launch and the landing site. At both the ground station and at the launch site the following people are present:

- Doctors
- Meteorologists
- Emergency services
- Maintenance engineers
- Mission team
- Mission manager

The control centre has been based at the landing site as the landing is more critical than the launch. The decision to aim for a landing site has been made because it is easier to direct the mission from a central point and it creates a place for the media to gather. Doctors are present at the launch site to perform a last check-up for the pilot and the doctors at the ground centre are tasked with monitoring the live data of the pilot.

The meteorologists at the launch site check the take-off conditions and give a GO or a NO-GO for take-off. At the control centre the meteorologists provide up to data weather data to the pilot so that the pilot can direct to a different course when the weather is not optimal.

Emergency services, ambulances and firetrucks, are located at the launch and landing site in case of a failure. Next to that, maintenance engineers are present at the launch site to perform any last-minute preparation.

Last the mission manager is present in the control centre at all times. The mission manager carries the ultimate responsibility concerning the mission. He or she has the power to abort the mission when the pilot is in danger.and has contact to the coastal rescue services at all time. The mission manager is supported by a mission team that takes care of the side issues. The mission team works 12 hours on, 12 hours off during the mission.

These people are housed in portable containers as these are more sustainable and cost efficient than building permanent housing. These are provided by Calnan[(iv)]. A catering service has been appointed to provide food and drinks for the present people.

[(ii)] URL `http://www.m-o.com/index.php`[cited 20 January 2015]
[(iii)] URL `http://www.vanrentals.ie/`[cited 20 January 2015]
[(iv)] URL`http://www.calnan.ie/`[cited 20 January]

1.8.3 Maintenance

Maintenance is performed by the maintenance engineers, as described in previous section. At the launch site, maintenance engineers are present to make sure that there are no malfunctions present in the aircraft prior to launch. If these malfunctions are present, they are fixed to the launch is postponed. The maintenance engineers are responsible for the pre-operation inspection, phase 1.0 according to Figure 1.1. As the mission is only performed once it is not necessary to perform maintenance at the end of the mission. Only if it is decided that the aircraft is used for another mission, maintenance is necessary but this has to be implemented in the new mission design.

1.8.4 Rescue operations

During the mission, real time data is provided by the communication system. The communication system provides both information on attitude of the aircraft as the health of the pilot. During operations the mission team has real-time contact with the pilot. This is to make sure that whenever there is an emergency the control centre can react immediately. The pilot is forced to contact the ground centre every 10 minutes to make sure that the pilot is conscious and awake. The electric shocks are given in an interval of 20 minutes. If the pilot misses two check-ins the mission manager has the ability to abort the mission and start the emergency landing. This time span is small enough as it is smaller than t_{des}. The rescue services will be notified and be instructed with the last known location of the aircraft to start their search.

2 Stability & Control

Perhaps stability and control of a vehicle are its most important parameters. The pilot must be able to safely and effectively fly the craft through different flight phases. In this chapter the longitudinal, lateral and thrust dependant stability are investigated first. Thereafter, the method of controlling the PPG is explained. The required control forces resulted from a 2D panel method that has been transformed to a 3D wing. Lastly, a system has been proposed to translate the control forces to the pilot as well as provide trim control.

Since at present there is not enough data available for a numerical analysis of the current design, the stability and control analysis will function as a guide for the final design. Therefore the technical output for stability presented at the end of this chapter is given in form of a range instead of a fixed number to give the other design groups design range to work with.

2.1 Stability

Stability can normally be investigated analytically or numerically. The fact that a custom designed canopy has been used makes a numerical analysis of the stability difficult; actual stability derivatives are unknown. In contrast, a qualitative analysis provides valuable information and is easier to execute and validate. As the only requirement implicitly involving stability is the safety of the mission, a qualitative analysis is be sufficient. In the end, the paraglider must be easily controllable and have a trimmed and stable cruise phase. If any instabilities come to light, these should be mitigated if necessary.

2.1.1 Directional Stability

A paraglider is inherently stable on the longitudinal (back and forth) axis by the fact that it essentially is a pendulum. The friction caused by small forces in the control lines and aerodynamics cause the oscillation to eventually dampen. The pendulum effect is also valid for lateral(side to side) stability, although more factors come into play there. With use of the Flight Dynamics lecture notes the longitudinal stability was investigated.[2] It has been established that there is a short period and a long period (the phugoid), both of which are stable. The derivation is presented in Appendix A. The time to half amplitude, the parameter how fast it converges to an original position, is important for pilot comfort. A long period might induce airsickness, although this depends on the individual. A study done with a system about half the size of the PPG in this report stated a longitudinal oscillation period of 8 s. [3] The time to damp from a stall to a steady glide was 30 s. This shows that the order of magnitude for this PPG is even larger and might prove an issue if the pilot is prone to motion sickness.

Lateral stability of paragliders was studied back in 1990 by Peter Crimi.[4] According to Crimi a ram-air gliding parachute can exhibit either spiral divergence mode or a lateral oscillatory divergence mode. This depends heavily on the dihedral angle (wingtips upward) Γ, suspension line length per wingspan S_l/b and glide ratio L/D. The question which follows is, what is favourable? A control input is required in order to break from a divergent mode; A long time frame in which there needs to be a correction is easiest for the pilot. Therefore time to double amplitude should be as large as possible. The answer is obvious as the spiral mode's time to double amplitude is nearly 10 times larger than a lateral oscillatory mode.[4] In addition, as demonstrated for NASA's X-38 program[5], the order of magnitude is in the range of 2-3 minutes for a spiral divergence. This is more than enough time for a control input to stop the spiral from diverging too much. Therefore, no actions were taken to achieve spiral stability. As derived in Appendix A the spiral mode is divergent and, according to Crimi, with a minimum s_l/b of 0.81 the oscillatory response is stable.[4]

To give exact numbers for the anhedral angle (wingtips downward) and suspension line length, as mentioned before, is impossible without actual values for stability derivatives. However, a range for the values can be given. Given that there is a static yaw stability $C_{n_\beta} > 0$ and a glide ratio $L/D > 10$ the

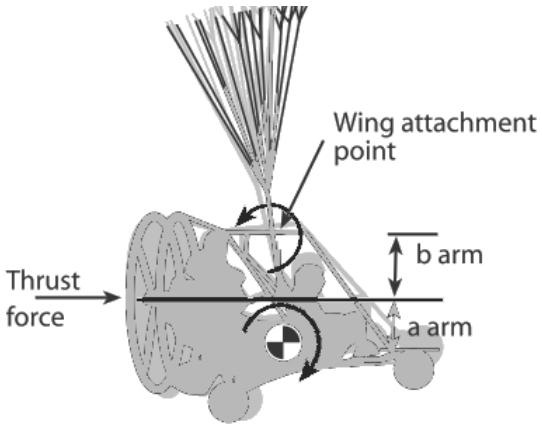

Figure 2.1: Thrust induced oscillations

ranges are presented in Table 2.1.

Table 2.1: Parameter ranges for the canopy design

Parameters	Unit	Lower limit	Upper limit
Line length per wingspan s_l/b	–	0.81	1.8
Minimum dihedral Γ	°	-30	-12

All conclusions in the preceding paragraphs rely on the fact that the parafoil-payload system has static yaw stability. To given a short sensitivity analysis: When the line length per wing span gets shorter than 0.81 it starts to result in oscillatory instability. Having longer lines initially improves spiral and longitudinal stability at the expense of added drag and weight. To stay in the realms of realism the upper bound was given an arbitrary plausible value of 1.8. The required dihedral as specified in Table 2.1 could be appended with an angle of 0° to 30°. These values were discarded for the added complexity in the design of the canopy and the reduced ability of the lines to carry loads.

2.1.2 Thrust dependent stability

A thrust vector that is not aligned with the canopy-fuselage hinge creates a pitching moment around the hinge. This is schematically depicted in Figure 2.1 An excitement of the fuselage's centre of mass then creates a inverse pendulum moment. A back and forth motion occurs when thrust is suddenly increased. This is called porpoising.[6] A similar situation can occur when shutting of the thrust at a high rate of climb. At first the angle of attack increases after which it settles in a steady glide. Both situations are normally not dangerous. Nonetheless, porpoising during a landing can result in a hard landing or even a crash. In order to minimise this problem the vector of thrust should be located somewhere midway between the centre of mass of the fuselage and the hinge point of the canopy lines. On top of that an optional thrust acceleration limiter can be installed for ease of flying.

2.2 Control

The paraglider that has been designed by the Team does not have a control surface for pure yaw control. Therefore the focus of this section will be on the lateral-directional and longitudinal aerodynamics based on X38 Research by NASA.[5][7] The final design has two basic forms of control.

- Throttle: Used to adjust speed magnitude to climb or descend.
- Steering control: Downward aileron deflection at both the left and right side of the wing.

In combination these basic flight controls allow the pilot to control the powered paraglider and can help reduce the pilot's effort required to control the paraglider. The control forces necessary to steer the paraglider have been investigated. These are presented in Section 2.2.1 and the results have been used to design a control system for the wing. In Section 2.2.2 the design for the steering system is explained.

The lateral and longitudinal steering controls of a powered paraglider are governed by three main effects. These effects are: [8]

- **Asymmetric lift** If one of the control lines is pulled, the lift will either increase due to a local change in camber or decrease due to local stall of the wing. This will result in a rolling motion.
- **Drag** A deflection of the aileron will increase the drag. For the calculation of the drag force the profile C_{D_0} is assumed to be constant, hence the change in drag has been assumed to be caused by the induced drag component C_{D_i} only. This will result in a yaw motion.
- **Parafoil warping** This happens when shortening a control line on one side of the paraglider results in a torque that causes wing warp. The warp causes the lift vector on one side of the paraglider to rotate and have a rearward component. This will result in a yaw motion.

The aforementioned effects can not be isolated, they are interrelated, which means that when one occurs due to a deflection of the outward control surface, an aileron for example, another effect will also be at play. However the forces involved in the asymmetric lift and parafoil warping depend on the change in lift via C_L whereas the drag depends on lift via C_L^2. This is why the drag, and the induced drag in particular, has been taken to calculate the control force and the contribution of the other two effects have been neglected.

2.2.1 Control Forces

To calculate the control forces of the paraglider a numerical analysis has been done on the change in C_L due to an aileron deflection. Normally, thin airfoil theory is used, but this is only a good approximation for a thickness to chord ratio (t/c) of less than 12%. This is because in classical thin airfoil theory, the airfoil is simulated by a vortex sheet placed along the camber line, the airfoil is modelled as a flat plate. Hence, this theory does not take the airfoil's thickness into account, therefore it cannot be used to predict the surface pressure distribution of an airfoil section with finite thickness;[9] and this distribution has been used in combination with boundary layer theory to calculate the viscous forces, that in turn have been used for a simple boundary layer analysis to find the airfoil's lift coefficient C_l.
Hence another method based on potential flow, that does predict inviscid pressure distribution, has been used as the current design has a t/c of 26.5%. For the analysis of the chosen airfoil a 2D panel method has been used as described by Anderson[10, Page 361-365]. This method has been applied in JavaFoil[(i)] to find the change in lift coefficient C_l.

To arrive at an actual control force, the 2D lift coefficient C_l had to be transformed to the 3D counter part C_L. The only viable method, albeit inaccurate, was to use lifting line theory which provides a factor to multiply C_l by. The geometry of the airfoil with and without aileron deflections and the air flow around it has been presented in Figure 2.2, 2.3, 2.4 and 2.5.

As described by Anderson[10], the drag of a wing depends on the air density ρ, the flow speed v, the reference area S and the drag coefficient C_D. The only influence that an aileron deflection could have, has been assumed to be on the C_D. The deflection of an aileron causes a change in C_L, this change has been related to the change in C_D as described in Equation (2.1).

$$\Delta C_D = \frac{C_{L_2}^2 - C_{L_1}^2}{\pi \cdot AR \cdot e} \tag{2.1}$$

[(i)] `http://www.mh-aerotools.de/airfoils/javafoil.htm`

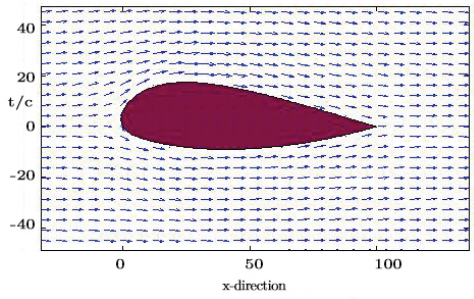

Figure 2.2: NACA54126 airflow with no aileron deflection and the simulated air flow around it.

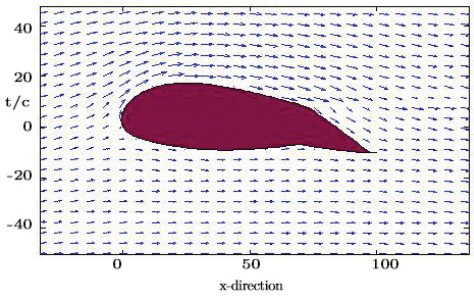

Figure 2.3: NACA54126 airflow with a 20° aileron deflection and the simulated air flow around it.

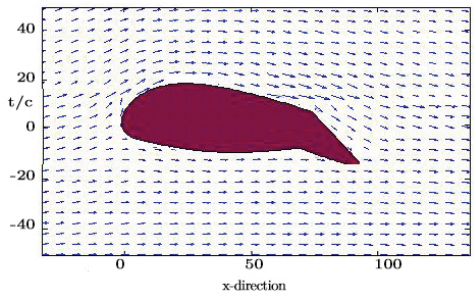

Figure 2.4: NACA54126 airflow with a 30° aileron deflection and the simulated air flow around it.

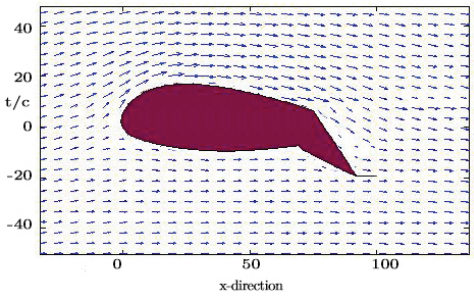

Figure 2.5: NACA54126 airflow with a 40° aileron deflection and the simulated air flow around it.

$$F_{control_{max}} = \frac{1}{2} \cdot \rho \cdot TAS^2 \cdot S_{anhedral} \cdot \Delta C_D \tag{2.2}$$

The impact of different aileron deflections at a range of angles of attack has been investigated and the biggest ΔC_D has been used to determine the control force. The control forces for different angles of attack and aileron deflection are plotted in Figure 2.6. As can be seen the control force has a narrow bandwidth for different angles of attack. The control system has been sized using the maximum control force $F_{control_{max}}$ of 245 N.

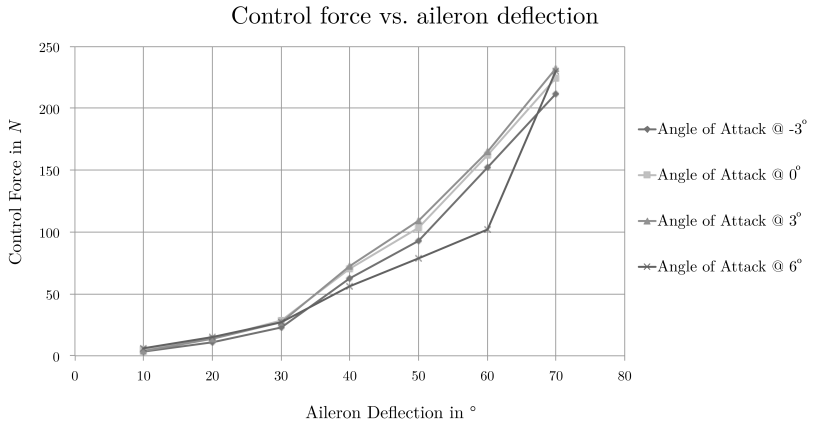

Figure 2.6: Control forces per aileron deflection for different angles of attack

2.2.2 Steering Control System

As mentioned in the introduction of this section the steering system will be foot operated. The design of the 3 pedal system has been illustrated in Figure 2.7. This figure shows the pedals and slider configuration, the control lines originating from each slider will be combined in the "trim box" which contains the trim mechanism. The trim system has been added to prevent the pilot from having to exert a continuous force on the pedals during the cruise phase. It is based on a turn buckles principle that allows the control lines to be shortened or extended by using a turning a dial.

The left and right control lines have been designed to withstand the control force per foot calculated in Section 2.2.1. The middle line is the break of the configuration and therefore has been designed to withstand twice the aforementioned force.

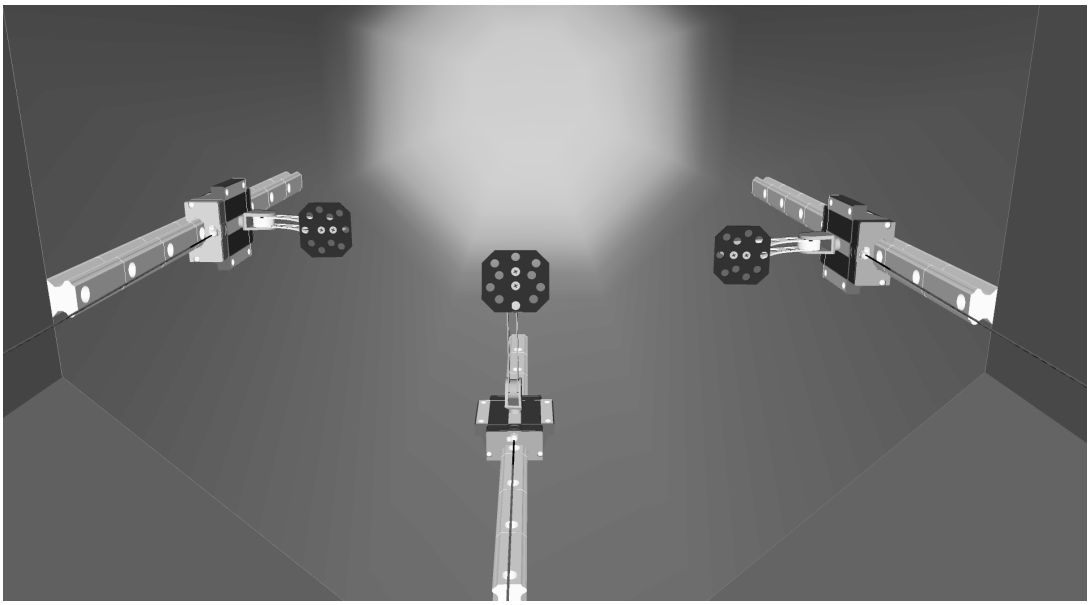

Figure 2.7: Artist impression of the steering system

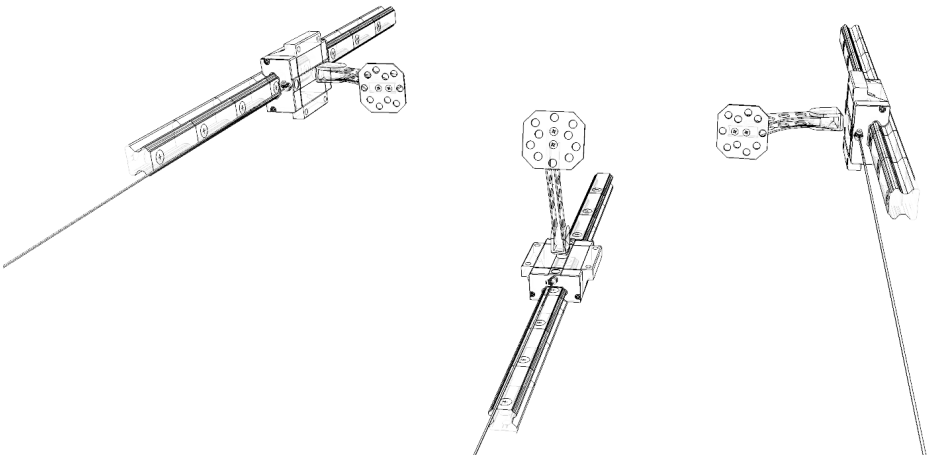

Figure 2.8: Isometric view of the steering configuration

Two additional views of the steering system have been made and is shown in Figure 2.8. It shows

that some motions have been constrained increasing control and creating more comfort for the pilot. To prevent the foot control from moving in more than one direction, a guidance rail has been designed to prevent the pedals from moving in other directions. The total weight of the steering system is assumed to be approximately 2.5 kg, which has been based on numbers by aviation industry expert ROLLON®.[ii]

Control lines

The control force applied to the steering system is transferred to the ailerons via the control lines. A single line with a 0.6 mm diameter, capable of carrying a load of 70 kg, is attached to either steering pedal. This line splits up twice near the aileron to evenly spread the load over the span of the aileron. The lines after both splits are only of 0.4 mm diameter and capable of handling 50 kg each.[iii] The trim box must handle double the load an individual control line has to handle. Therefore the trim box uses 0.8 mm lines capable of handling 100 kg.

For the design a line length per wingspan s_l/b has been chosen of 0.9, this lies within the range determined in Section 2.1. Using this and the wing span calculated in Chapter 3, a line length l_{line} of 23.4 m has been calculated for the control lines. Due to the limited availability of resources a detailed line plan has been determined to be beyond the scope of this DSE. However, to give a good approximation for the total control line length a line plan of an existing paraglider has been used.[iv] Hence a ratio between the junctions has been chosen to be $0.625 \cdot l_{line}$ for the lower part, $0.25 \cdot l_{line}$ for the middle part and $0.125 \cdot l_{line}$ for the upper part of the control lines.

The final technical output from the stability & control group to the other technical groups is shown in Table 2.2.

Table 2.2: Technical output for the stability & control group

	Unit	Value
Dihedral range	°	$[-30, -12]$
Line length per wingspan	–	$[0.81, 1.8]$
$F_{control_{max}}$	N	245
Total control line length	m	81.90

[ii] http://www.rollonnews.com/Rollon_Aircraft_Interiors_Final.pdf

[iii] URL http://www.chainsropesandanchors.co.nz/index.php?route=product/search&search=[Cited 21-1-2015]

[iv] https://www.nova-wings.com/fileadmin/user_upload/glider/Mentor4/files/MENTOR4_manual.pdf

3 Aerodynamics

In this chapter, the design of the canopy, its subsequent aerodynamic properties and its sizing are discussed. To begin with, a preferred lift-to-drag ratio, or L/D for the wing has been decided upon from references. Together with this an aspect ratio (AR) and zero lift drag coefficient have been chosen from references as well. Then, the airfoil selection process is described in Section 3.2. The chosen airfoil and its corresponding aerodynamic properties are displayed. From these details the 3D properties of the wing are calculated. Once this has been done, the C_L corresponding to the optimum L/D is used to calculate the required wing surface area S and the other wing dimensions in Section 3.4.

Then, the additional drag from secondary non lift generating elements; the fuselage, the suspension lines, the control lines and the electrical cables have been calculated in Section 3.5. Once the secondary drag was known, it has been added to the preliminary wing drag, and a new and revised L/D ratio for the whole system is known, which is equal to the final GR. At the end of this chapter a technical output overview of the aerodynamic properties is given in Table 3.4.

It is important to take note of the fact that, during the complete aerodynamic and wing sizing process, frequent and thorough exchange of data and information between the different technical groups has taken place.

3.1 Preliminary Aerodynamic Characteristics

In Section 1.4 the mission parameters have been set, giving the total distance to be covered, the average wind speed on cruise altitude and the average cruise speed. After these parameters have been set, a lift-to-drag ratio, aspect ratio and parasitic drag coefficient have been chosen. From these set parameters, an airfoil has been chosen with its corresponding aerodynamic properties. To complete the planform sizing, the required surface area is then decided upon.

Before continuing though, the different measures of airspeed have been looked at. Since paragliders generally fly at low altitudes, the IAS and v_t are almost the same, however at a height of 10'000 ft they differ by 16%, since the density of the air is less at this altitude. In order to get from IAS to v_t, the IAS has to be transferred to the Calibrated Airspeed (CAS), then to the Equivalent Airspeed (EAS) and lastly to the v_t (IAS $\rightarrow$ CAS $\rightarrow$ EAS $\rightarrow$ v_t). The instrument and position errors are assumed to be zero and the compressibility error too, because of the low cruise speed and relatively low altitude so this has been simplified to just one formula. This formula is presented in Equation (3.1):

$$v_t = IAS \cdot \sqrt{\frac{\rho_0}{\rho}} \tag{3.1}$$

Firstly, In the aforementioned equation $v_t and IAS have to be the same unit, which can be for instance m \cdot s^{-1}$. ρ is the air density given in $kg \cdot m^{-3}$. Using the $v_t and the ground speed, both listed in Table 3.1 together with the differ$

Table 3.1: Overview of Preliminary Aerodynamic Characteristics

Parameter	Unit	Value
Air density at sea level	$kg \cdot m^{-3}$	1.225
Air density at cruise level	$kg \cdot m^{-3}$	0.904
IAS	$m \cdot s^{-1}$	10.0
v_t	$m \cdot s^{-1}$	11.6
Ground speed	$m \cdot s^{-1}$	23.6

Secondly, from references a lift-to-drag ratio of 20 has been taken as a starting value. Since the design of the wing has been made to look like a conventional wing, the whole wing design will have

aerodynamic properties more similar to hanggliders than paragliders. Therefore this lift-to-drag-ratio is taken from hanggliders and is increased, since the wing design will be more aerodynamically optimal than that of a hangglider.[(i)] This also corresponds to another inflatable wing that has been presented at an AIAA conference.[11]

Thirdly, the Aspect Ratio (AR) has been chosen. Other parachutes of powered paragliders have an AR of around 5[(ii)] and the Phoenix inflatable wing has an AR of 6. However, in a paper of the AIAA, it has been found that in history, inflatable wings have never been designed with an AR larger than 9.[11] Since higher aspect ratios for wings reduce the induced drag of the aircraft and the design has a pendulum type of stability which is beneficial, an AR of 9 has been chosen.

Lastly, a value for the profile drag has been chosen. From a private e-mail conversation with a company called Skywalk, that designs paragliders themselves, a profile drag coefficient of $C_{D_0} = 0.012$ has been received. [12]

3.2 Airfoil Selection

Now that the preliminary aerodynamic characteristics have been decided upon, the airfoil selection process is described. Certain airfoil characteristics have been kept in mind when choosing and designing the airfoil. The nature of these airfoil characteristics and the subsequent reasons for deciding upon them are delved into.

Thickness The thickness of the airfoil is critical, since thicker airfoils show more gradual stall characteristics. They are beneficial for providing a higher wing volume, which is important for the function of storing helium. However, thick airfoils create more drag and flow separates over them more easily. The location of the maximum thickness is also of importance. The closer it is to the leading edge, the higher the C_{lmax} is.

Camber It is important for the wing to be able to generate lift at $\alpha = 0°$. As a consequence, the airfoil must not be symmetric and have some amount of camber.

Reflex profile A reflex profile ensures that for a certain range of α the pitching moment C_m is positive. For the longitudinal stability of the paraglider, C_m must be positive and as close to 0 as possible. Since the paraglider is designed to be a tailless aircraft, a nose-up pitching moment is beneficial. Hence, the decision of looking into reflex cambered airfoils has been taken.

Keeping the described characteristics in mind, the Team has chosen a set of airfoils that can be seen in Table 3.2.

From Table 3.2 a selection of eight airfoils can be seen. These airfoils have been chosen for various reasons. To start with, the airfoils labelled MH78, MH80, MH81 and MH92 have been taken from the UIUC Airfoil Database.[(iii)] These airfoils are existing and in use for either hang-gliders or parafoils. The contour coordinates of these airfoils have been brought into the XFLR5 airfoil design software. Along with the existing ones, three completely new airfoils have been designed. These newly designed airfoils are labelled in Table 3.2 as HG-RFLX-1, HG-RFLX-2 and HG-RFLX-3. These airfoils have been designed to have a higher thickness than their existing counterparts. Similar to the ones previously described, they too are reflex profiles. The final airfoil, NACA54126, is a standard NACA 5 digit reflex airfoil. This airfoil has been designed, since thorough data on it can be generated in another software, JavaFoil. Using

[(i)] URL `http://www.a-i-r.de/ger/air_07.php?kat=154&gp=7&stl=Download` [cited November 19 2014]
[(ii)] URL `http://www.a-i-r.de/ger/air_07.php?kat=154&gp=7&stl=Download` [cited January 17 2015]
[(iii)] URL `http://m-selig.ae.illinois.edu/ads/coord_database.html` [cited December 11 2014]

Table 3.2: Characteristics of the different airfoils

Airfoil	Thickness $\%(t/c)$	C_m positive α range $\circ$	L/D	α_{stall} $\circ$
HG-RFLX-1	26.70	-5 to 14	21.70	16
HG-RFLX-2	25.50	-5 to 12	21.62	14
HG-RFLX-3	26.25	-5 to 11	21.68	20
MH78	14.45	-5 to 21	21.69	18
MH80	12.70	-5 to 18	21.33	15
MH81	12.98	4 to 5	21.70	15
MH92	15.47	-5 to 22	16.91	16
NACA54126	26.30	-5 to 6	21.39	26

JavaFoil to simulate the behaviour of this airfoil helps with the work flow between the technical groups Structures and Stability and Control. The NACA54126 airfoil has been designed, keeping in mind the thickness and camber requirements mentioned previously. For these reasons, a decision has been made to choose the NACA54126 airfoil as the basis for designing the wing.

The shape of the NACA54126 airfoil can be seen in Figure 3.1. Its drag coefficient curve is shown in Figure 3.2, the lift coefficient curve is in Figure 3.3 and its moment coefficient curve is shown in Figure 3.4.

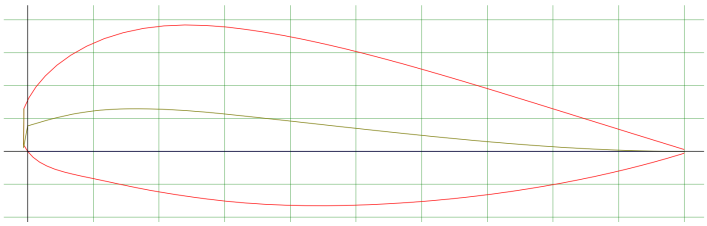

Figure 3.1: NACA54126 airfoil contour

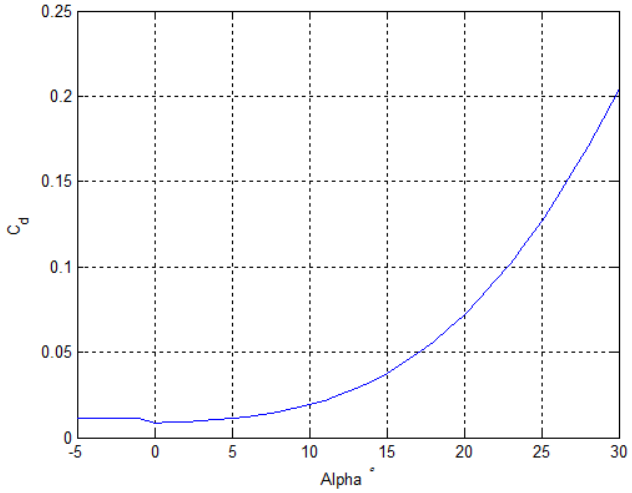

Figure 3.2: $C_d - \alpha$ curve for NACA54126 airfoil

3.3 Airfoil To Wing Conversion

Now that the airfoil has been selected, the wing's aerodynamic performance with the selected airfoil is determined. Using JavaFoil, certain data for the aerodynamic behaviour of the airfoil has been made available. For instance, the behaviour of the airfoil lift coefficient C_l, the airfoil drag coefficient C_d and the coefficient of moment C_m with respect to the angle of attack α is known. These parameters have been taken with a Reynolds number that was calculated using Equation (3.2), with a preliminary wing chord of 2.9 m. In the end this has proven to be 2.89 m, because of this difference being really small, it has been decided that the difference is not significant enough to recalculate the airfoil parameters, within the scope of this project.

$$\mu = \left(\frac{T}{T_0}\right)^{\frac{3}{2}} \cdot \left(\frac{T_0 + 110}{T + 110}\right) \cdot \mu_0 \tag{3.2a}$$

$$Re = \rho \cdot v_t \cdot c_{wing} \cdot \mu \tag{3.2b}$$

In Equation (3.2), μ is the air viscosity, given in $kg{\cdot}(m{\cdot}s)^{-1}$ and μ_0 is the reference value for this taken at sea level, together with T_0, which are $1.79{\cdot}10^{-5} kg^{-m{\cdot}s}$ and 288 K respectively and T is the temperature in K. ρ is the density of the gas given in $kg \cdot m^{-3}$; $v_t is the true airspeed of the aircraft and c_{wing}$ is the chord length of the wing. The Reynolds number at take-off is 2.5 million and during cruise 1.9 million.

In order to more accurately simulate the aerodynamic behaviour of the 3D wing with respect to a 2D airfoil, certain perturbations must be made to the airfoil C_l to convert it to a 3D wing C_L. A 2D airfoil only represents the cross sectional area of the wing. The 3D wing on the other hand, is the complete wing, taking into account the surface area, wingspan and aspect ratio. The addition of a span changes certain parameters in the aerodynamics of the wing, which can be seen in this section. Accurately modelling the 3D aerodynamic behaviour of wings is either done using experimental set ups in wind tunnels, or with the help of computational fluid dynamics (CFD). However, due to time and resource constraints and the fact that CFD is currently beyond the scope of the Team, a different approach has been undertaken. The use of Prandtl's 3D lift curve slope formula has been made as shown in Equation (3.3).

$$C_{L_\alpha} = \frac{C_{l_\alpha}}{1 + \frac{C_{l_\alpha}}{\pi \cdot AR \cdot e}} \text{ (iv)} \tag{3.3}$$

Assuming the airfoil $C_{l_\alpha} = 2\pi$, using the $AR = 9$ as decided in Section 3.1 and using an Oswald factor $e = 0.78$ for a rectangular wing, the ratio between the 3D and 2D lift curve slopes $\frac{C_{L_\alpha}}{C_{l_\alpha}} = 0.78$. Using this ratio, the subsequent C_L values for the wing have been calculated. It should, however, be noted that Prandtl's 3D lift curve slope formula Equation (3.3) is not entirely accurate for the Team's case since the NACA55126 airfoil has a $t/c = 26.3\%$ which is very high. The formula is usually associated with airfoils having a lower t/c. However, after consultation with experts at the Aerodynamics department of the TU Delft, the Team came to the conclusion that using the Equation (3.3) would be a reasonable approximation given the time and resource limitations.

$$C_D = C_{D_0} + \frac{{C_L}^2}{\pi \cdot AR \cdot e} \tag{3.4}$$

The calculation for the 3D coefficient of drag C_D Equation (3.4) follows from the C_L values that have been calculated and the assumption of using a $C_{D_0} = 0.012$ Section 3.1. Following that, the wing's aerodynamic behaviour with respect to the angle of attack has been calculated and is shown in Figure 3.3, 3.4 and 3.5.

Looking at these figures, the aerodynamic behaviour of the wing is analysed. It can be seen that at $\alpha = 6°$, highest $L/D = 21.39$ for the wing is achieved. A 3D lift coefficient of almost 2 is high with respect to what is know from conventional aicraft, however the chosen airfoil is very thick which creates large pressure differences and thus high lift coefficients. The values have been checked with Javafoil and are correct.

Before sizing the wing, it is important to investigate the sensitivity of the wing's aerodynamic behaviour when certain parameters are changed. Since the AR is one of the characteristics that determine

(iv) `http://www.dept.aoe.vt.edu/~lutze/AOE3104/airfoilwings.pdf` [cited 9 January 2015]

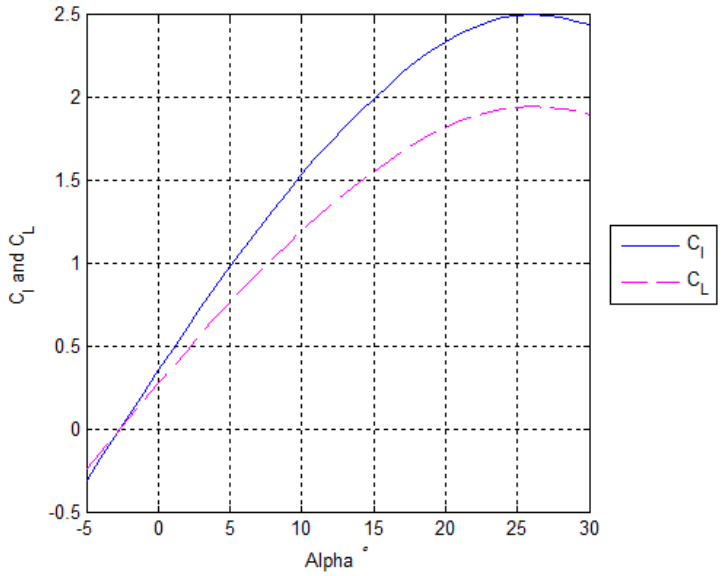

Figure 3.3: $C_L - \alpha$ and $C_l - \alpha$ curve for NACA54126 wing

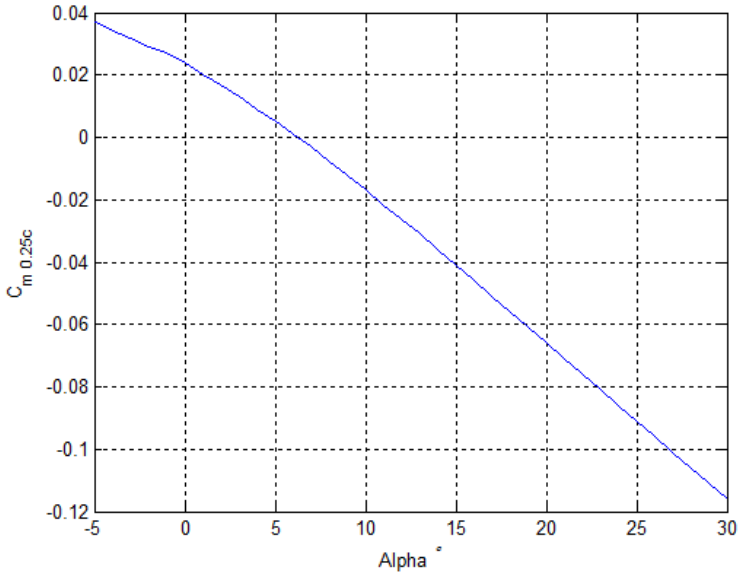

Figure 3.4: $C_m - \alpha$ curve for NACA54126 wing

the 3D aerodynamic behaviour of the wing, its effect on the L/D must be investigated. Moreover, the $C_{D_0} = 0.012$ that was provided as a reference value, must also be manipulated to investigate its effect on the L/D of the wing. Changing these two parameters and investigating the changes, gives an overview of the sensitivity of the wing's L/D with respect to the parameters

It can be seen from Figure 3.6, that the L/D is, as expected, sensitive to AR. The higher the AR the higher the L/D for that α. It has been concluded that the higher the AR the higher the C_L and L/D for a given α. When it comes to the sizing of the wing, it has been kept in mind that a higher AR is preferable for its aerodynamic performance. Hence, it has been decided to keep the $AR = 9$. A higher AR is harder to manufacture, but since our reference stated that pressurised wings have already been

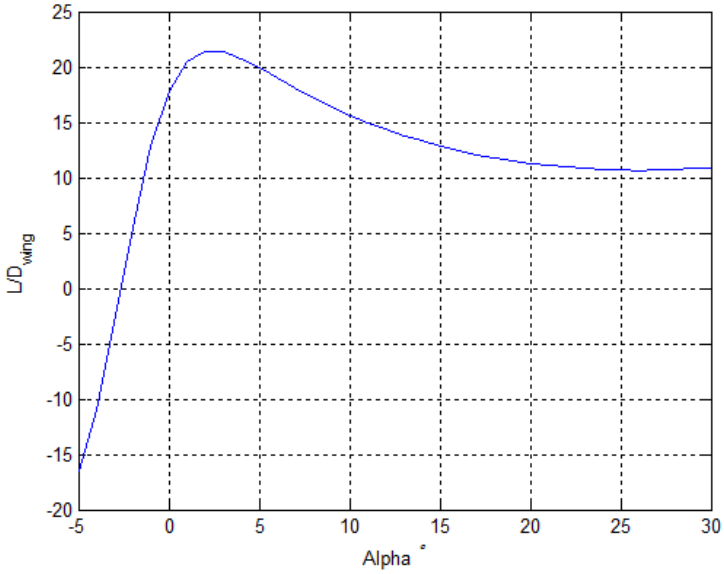

Figure 3.5: $C_L/C_D - \alpha$ curve for NACA54126 wing

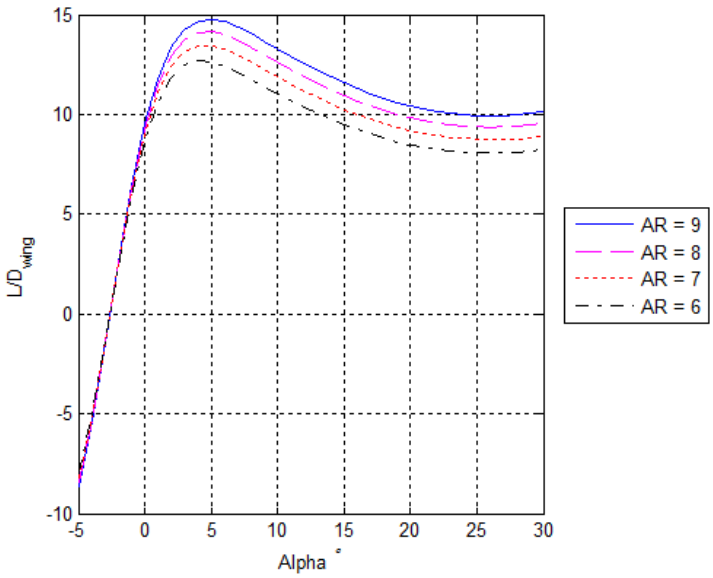

Figure 3.6: $C_L/C_D - \alpha$ curves for NACA54126 wing with changing AR

built with an AR of 9, this value is picked.[11]

From Figure 3.7 it can be seen that the aerodynamic performance of the wing is very sensitive to any perturbations in C_{D_0}. For instance if the C_{D_0} is changed from 0.012 to 0.024, there is a significant drop in the maximum L/D from 21 to 15. This heightened sensitivity of the L/D to C_{D_0} has given the team the incentive to further investigate into reliability of the current $C_{D_0} = 0.012$.

Further investigation into the nature of profile drag, or C_{D_0}, led to an equation that helps to give a more accurate representation of C_{D_0}.[13]

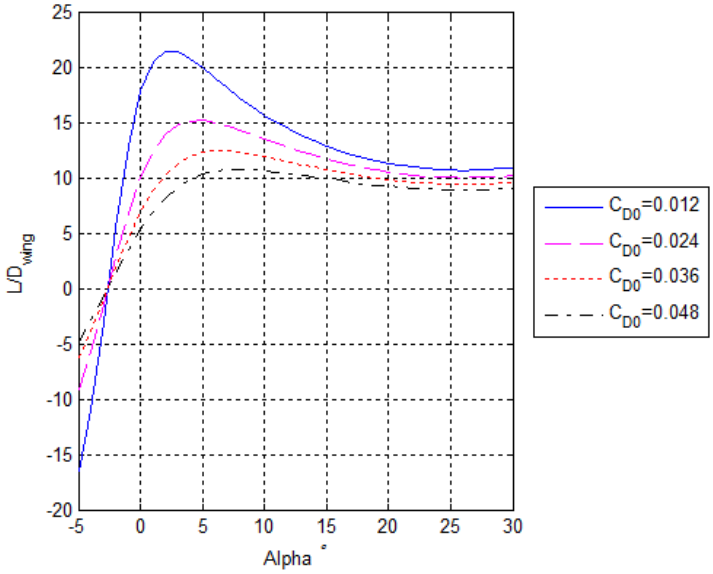

Figure 3.7: $C_L/C_D - \alpha$ curves for NACA54126 wing with changing C_{D_0}

$$C_{D_{0_w}} = C_{f_w} \cdot f_{tc_w} \cdot f_M \left(\frac{S_{wet_w}}{S}\right) \left(\frac{C_{d_{min_w}}}{0.004}\right)^{0.4} \tag{3.5a}$$

$$C_{f_w} = 0.455/(\log_{10} Re)^{2.58} \tag{3.5b}$$

$$f_{tc_w} = 1 + 2.7 \cdot \left(\frac{t}{c}\right)_{max} + 100 \cdot \left(\frac{t}{c}\right)^4_{max} \tag{3.5c}$$

$$f_M = 1 + 0.08 \cdot M^{1.45} \tag{3.5d}$$

In Equation (3.5a) for the wing's profile drag coefficient $C_{D_{0_w}}$, certain terms have not yet been described. They are described as follows. The parameter C_{f_w} is the skin friction coefficient of the wing and is a function of the Reynold's number, taken at cruise, Re which has been calculated using Equation (3.2). This formula can be used for airfoils that are predominantly in a turbulent flow which is the case if the Reynolds number is around 2 million or higher, which is the case for this mission. The $f_{tc_{max}}$, which is known as well. The third parameter, f_M is a function of the Mach number M, which is known. The fourth entry in the equation, S_{wet_w}/S is a ratio between the wetted surface area of the wing S_{wet_w} and the wing surface area S, and has been calculated to be 2.14. The final characteristic, $C_{d_{min_w}}$ is the minimum drag coefficient for the airfoil, which is known as well to be 0.0085. Plugging in estimated and known values for the described parameters in Equation (3.5a) gives a value for $C_{D_{0_w}} = 0.025$. Compared to the previously used reference value of 0.012, the revised value is higher. Hence, design accuracy wise, it has been a useful decision to actually calculate the $C_{D_{0_w}}$ rather than using a reference value. Looking back at the assumption of $C_{D_{0_w}} = 0.012$, this was rather low when different references are looked at that give a value that is around 0.020[(v)] and when an paragliding instructor was asked about it.

As can be seen in Figure 3.8 and Figure 3.9, by implementing $C_{D_{0_w}} = 0.025$, the C_D with respect to α has increased as expected. Moreover, the L/D of the wing with respect to α has reduced, also as expected.
The new optimal wing $L/D = 15$ at $\alpha = 5°$.
However, it must be noted that this is just the wing's L/D and not the total system's L/D or Glide Ratio GR. In order to optimise and calculate that, the drag from the secondary system elements is calculated

[(v)] URL `http://sci-fix.blogspot.nl/2010/08/paragliding-aerodynamics.html` [cited January 26 201]

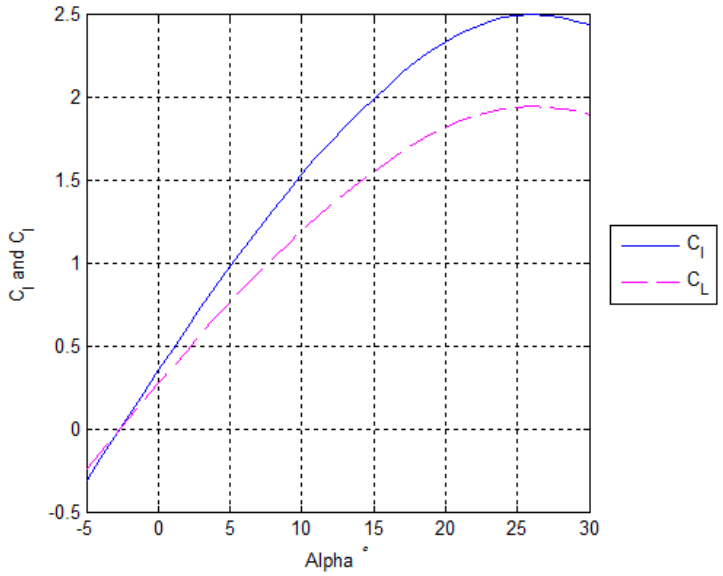

Figure 3.8: New $C_L - \alpha$ and $C_l - \alpha$ curve for NACA54126 wing

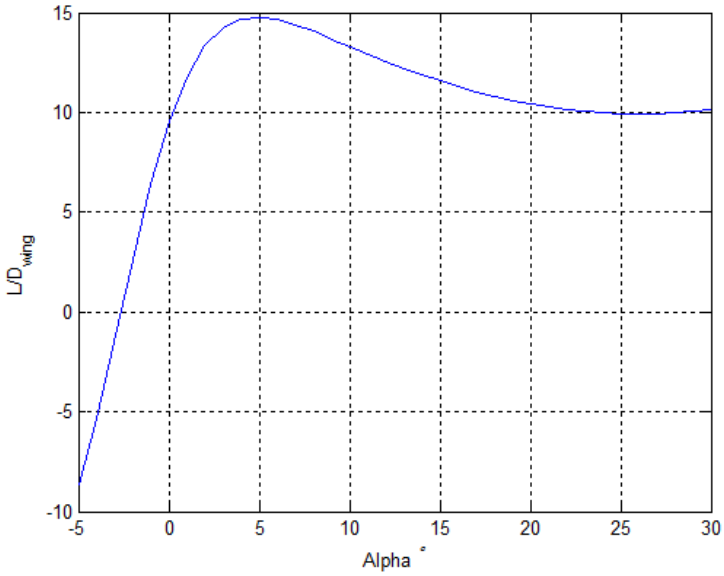

Figure 3.9: New $C_L/C_D - \alpha$ curve for NACA54126 wing

in Section 3.5. The stall speed with the 3D properties is calculated for the maximum lift coefficient of 1.94 and is 6.15 $m \cdot s^{-1}$.

The use of high lift devices to improve the aerodynamic performance of the paraglider wing, has not been decided upon. However, a decision has been made by the Team to use jet flaps. Jet flaps, a technology developed by the paraglider manufacturer Skywalk, are a part of the trailing edge section of the wing. Traditionally, jet flaps are used as high lift devices to manipulate the aerodynamic behaviour of the paraglider wing. However, the Team's decision to use jet flaps is not for aerodynamic reasons but for reasons of structural integrity and stability and control. In the context of the structural make-up of

the wing and the stability and control of the wing, jet flaps are delved into further detail in Chapter 4. It is important, however, to understand the changes in the aerodynamic behaviour of the wing due to the use of jet flaps. In consultation with experts at Skywalk, certain points have been brought to the Team's attention. The increase in the drag coefficient C_D, due to the use of jet flaps, is negligible [12]. Hence, the Team has decided to not include any changes in drag due to the addition of jet flaps. Another point that has been brought to the Team's notice by Skywalk, is that at low speeds the C_L increases by 8% [12]. No speed range or further information on the C_L increase was made available. So this increase was not taken into account for the lift coefficient, but it is used for increasing the stall speed which because of this becomes 5.66 $m \cdot s^{-1}$.

3.4 Wing Sizing

In Section 3.2 the aerodynamic properties of the airfoil have been calculated. Furthermore the aerodynamic values for the wing and the aspect ratio have been determined in Section 3.3. This information has been used to size the wing together with the input from Chapter 2 to achieve the most stable and controllable wing design.

To start with, the total wing surface area needed to lift the total weight is calculated. Its mass has at first been assumed to be 300 kg and has in the end been calculated to be 277 kg. Calculating the surface area needed has been calculated using the standard lift equation given in Equation (3.7a).

$$L = \frac{1}{2} \cdot \rho \cdot TAS^2 \cdot S_w \cdot C_L \tag{3.6}$$

Where L is given in N, ρ in $kg \cdot m^{-3}$, the TAS in $m \cdot s^{-1}$, the wing surface area S_w in m^2 and C_L is the 3D lift coefficient of the wing. The total effective wing area is given in Table 3.4. As can be read in Section 2.1.1, for directional stability, some form of anhedral is required to achieve lateral stability. The qualitative analysis has produced a range for the anhedral angle Γ, for the wing sizing the maximum value has been selected as this results in the fastest damping when a disturbance occurs. Considering the reasons discussed in Section 2.1 to refrain from performing a numerical analysis, the size of the deflected part, in span direction, has to be calculated using a different approach.

For structural reasons discussed in Chapter 4 as well as for efficiency reasons mentioned in the MRR [14, Section 4.2] the PV cells have to be placed on the horizontal part of the wing. An optimisation loop has been used to obtain the geometry of the wing and the resulting characteristics.

The loop that is described in this section has multiple iterations, the reasoning for this can be found in Section 7.1.4. The middle span section designated for the PV cells has been denoted b_{pv} in Figure 3.10 and is calculated by using the PV cell area A_{pv} in m^2 and the section of the chord that is available for support of the PV cells c_{pv} calculated in Chapter 4. The remaining span has been divided by two to find the span of the anhedral section $b_{anhedral}$. This is shown in Equation (3.7).

$$b_{pv} = \frac{A_{pv}}{c_p v} \tag{3.7a}$$

$$b_{anhedral} = \frac{b - b_{pv}}{2} \tag{3.7b}$$

From the geometry of the wing a new corrected lift can be calculated using a simple calculation of the individual lift vectors per section as shown in Equation (3.8).

$$\eta_{cor} = \frac{c \cdot (2 \cdot b_{anhedral} \cdot cos(\Gamma_{anhedral}) + b_{pv})}{S_{wing}} \tag{3.8}$$

The final geometry of the wing is shown in Figure 3.10 and 3.11. This geometry has been used to size and calculate the internal structure of the wing.

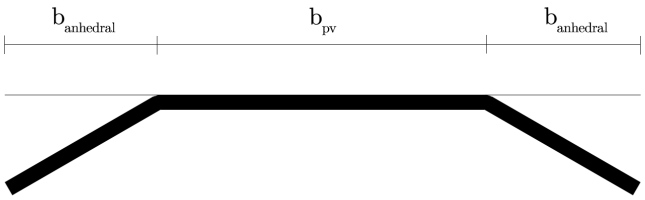

Figure 3.10: Front view of the wing

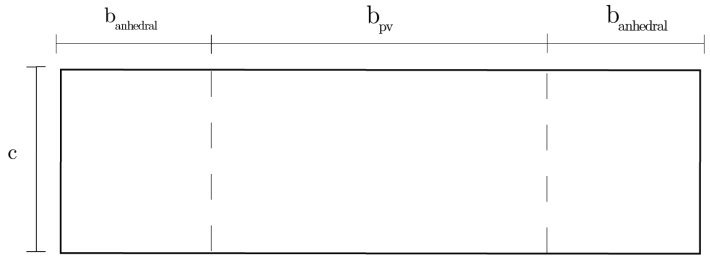

Figure 3.11: Top view of the wing

3.5 Secondary Drag

Next to the drag that is coming from the wing, as described in Section 3.3, other drag sources can be distinguished as well: suspension lines, electrical cables, control lines and the fuselage. In the end, the total drag that arises from flying the design has been calculated and an ultimate lift to drag ratio and GR have been established. All three different drags have been calculated using Equation (3.9), for which a frontal surface area S_{front} has to be calculated and a drag coefficient is to be established as well.

$$D = \frac{1}{2} \cdot \rho \cdot TAS^2 \cdot S_{front} \cdot C_D \tag{3.9}$$

3.5.1 Suspension lines and electrical cables

The suspension lines are the lines that run the fuselage to the wing and transfer the lifting loads. Four of these lines are connected at the fuselage and after about two-thirds of the total line length, each line splits into three separate lines, giving a total of twelve lines connecting to the wing. The drag coefficient of these lines is approximated using a circular steel rod that has a drag coefficient of 1.2.[10]

A total of two electrical cables run next to the suspension lines to transfer the electrical power from the PV cells to the fuselage. In Section 6.2 it can be read that the thickness of these cables is around 2 mm. Since this thickness is greater than that of the suspension lines an aerodynamically beneficial solution is thought of for the integration of these two lines. For a total of two suspension lines the electrical cables are integrated with them. Making the insulation of the cables also run around the suspension lines in a symmetrical airfoil shape, will reduce the drag coefficient of these lines to 0.12. This design can be seen in Figure 3.12. The black line is the suspension line and the orange one is the electrical cable. They are incorporated this way such that the shape will always want to face towards the airspeed vector because the centre of rotation is in the suspension line, not the electrical cable. The number of suspension lines, with their respective frontal areas and drag coefficients have now been determined, which all sums up to a drag of 11.5 N.

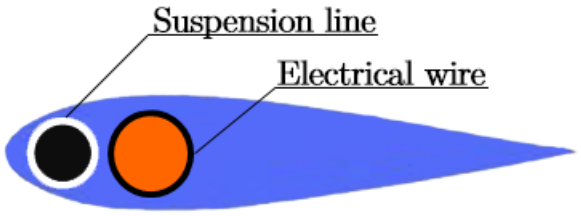

Figure 3.12: Integration of suspension line (black) in the insulation of electrical wires (orange)

3.5.2 Control lines

Also the control lines, that run behind the suspension lines from the fuselage to the trailing edge of the wing create drag. Their configuration is a little more complicated than that of the suspension lines. From the fuselage, one line on either side of the fuselage starts, splitting into two lines after 62.5% of the total length. At 87.5% of the total length, these two lines split into a total of five lines. This means a total of ten control lines is attached to the wing. The forces on these lines are much smaller than those on the suspension lines and therefore their radii are smaller as well as can be read in Section 2.2.2. Using the drag coefficient of 1.2 gives a total drag of 2.8 N.

3.5.3 Fuselage

The drag of the fuselage has already been investigated in the MRR yielding a drag coefficient of 0.12 and a frontal surface area of 1 m^2. This gives a total drag of 7.3 N.

All these different drags add up to a total secondary drag of 21.7 N. Together with the total drag of the wing being 169 N makes the total lift to drag ratio or GR 13.1.

The technical output from all the sections of this chapter has been summarised in Table 3.4. These values have been communicated to the other groups. This has been done to create the optimum synergy within the Team and enable the optimum result. A resulting glide ratio of 13.1 has been found, which is a lot lower than the ratio of 20 that was assumed in the MRR. Together with a cruise speed of 10.0 $m \cdot s^{-1}$ instead of 12.5 $m \cdot s^{-1}$ as had also been assumed in the MRR, there is a large increase in mission duration between these two reports.

Table 3.4: Technical output of the aerodynamic characteristics

	Unit	Value
IAS	$m \cdot s^{-1}$	10.0
v_t	$m \cdot s^{-1}$	11.6
Ground speed	$m \cdot s^{-1}$	23.6
Stall speed	$m \cdot s^{-1}$	5.66
Airfoil	–	NACA54126
$\left(\frac{t}{c}\right)_{max}$	–	0.263
$\frac{C_L}{C_l} conversion$	–	0.779
$C_{L_{opt}}$	–	0.762
$C_{L_{max}}$	–	1.94
$C_{D_{opt}}$	–	0.0516
$C_{m_{opt}}$	–	0.0500
α_{opt}	$^\circ$	5.00
Oswald factor	–	0.78
$C_{D0_{wing}}$	–	0.0254
AR	–	9.00
S_{wing}	m^2	75.1
b_{wing}	m	26.0
c	m	2.89
b_{pv}	m	19.2
$b_{anhedral}$	m	3.41
η_{cor}	–	0.965
D_{wing}	N	169
$D_{fuselage}$	N	7.35
D_{lines}	N	14.3
GR	–	13.1

4 Canopy Structures & Materials

This chapter discusses the canopy structural design and the materials used. Section 4.1 explains the canopy design method and in Section 4.2 the structural concept of the canopy is explained. The Tensairity® concept is explained in Section 4.3. Section 4.4 presents the structural layout and in Section 4.5 the multibubble structural concept is explained. In Section 4.6 the pressurisation with helium is discussed. Section 4.7 shows the structural solution for the trailing edge of the canopy, the jet flap. In Section 4.8 the numerical approach and code are discussed at length. Furthermore, Section 4.9 contains the specification of the materials used for the canopy. Finally Section 4.10 suggests accuracy improvements by reviewing the used assumptions and gives the technical output.

4.1 Canopy Design Method

The canopy system has to fulfil the functional requirements outlined in the requirement discovery tree in Section 1.1. The requirements relevant to the structural design of the PPG are in the top level requirements "be structurally sound" and "be able to fly with a canopy". For the canopy structure and materials the following requirements have to be met.

- Materials
  - High strength
  - Lightweight
  - UV resistant
  - Water resistant
  - Withstand temperatures encountered during the mission
  - Resistant to tearing
  - Flexible structure
  - Possibility to reuse
- Cope with forces encountered
  - Landing forces
  - Flight loads
  - PV panel weight
  - Internal cylinder pressure
  - Suspension lines
  - Vibrations
- Aerodynamic design
  - High lift, low drag
  - No induced vibration in the structure

In addition to these primary requirements, secondary requirements are given by the interfaces with the other technical groups. These include but are not restricted to the following list.

- Aerodynamics: Airfoil shape, canopy planform design (chord, span, surface area), anhedral span, minimum amount of suspension lines to decrease line drag
- Flight performance: maximum usable volume of helium
- Subsystems: solar panel surface area, conductivity of suspension lines

- Stability & control: integration of control lines, anhedral angle for yaw stability
- Fuselage structures & materials: suspension line attachment points on fuselage, center of gravity range

As usual for aerospace applications, the requirements should be met while ultimately minimising the weight of the structure. This is particularly important for this mission since the power required is to be minimised by means of weight reduction.

The objective of the canopy design method is to meet all the aforementioned requirements. The design process is as follows. First the applied loads are determined by drawing free body diagrams of conceptual sketches. Then a choice is made between the two structural concepts that were presented in the MRR [14, Section 4.4.2]. The most critical load cases have been defined and the numerical inputs needed to model them have been collected.

A plan is made to build a numerical simulation of the critical load cases on the selected design concept. This plan includes the input design parameters, the main functional blocks and the failure checks of the structure as outputs. Once the numerical model is constructed, an initial design is made which sustains the load cases. The influence of the various input parameters on the performance of the structure is then analysed. This knowledge is iteratively used to further optimise the design, e.g. find the configuration with the lowest weight. The design has been changing continuously during the iterations. Only the final design has been detailed in this report.

Due to limitations in resources the structural analysis is reduced to the least amount of elements necessary in order to reduce complexity of the system.

Throughout this chapter the body reference frame is used where the x-axis is in flight direction, and thus along the chord length; the y-direction is along the wingspan; and the z-direction points upwards completing the reference system. This reference system is shown in Figure 4.1.

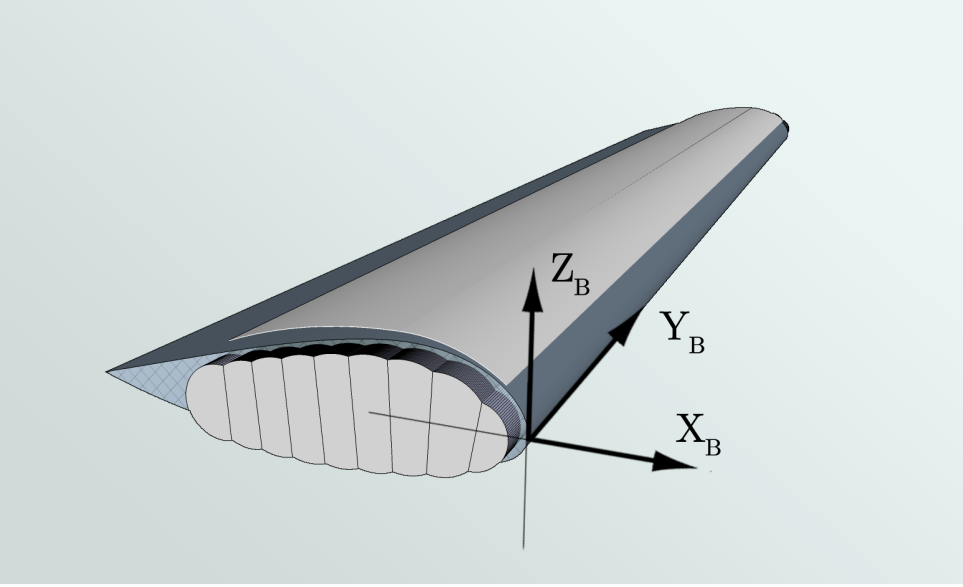

Figure 4.1: Body reference frame for a paraglider canopy

4.2 Canopy Structural Concept

The top level requirements dictate that a powered paraglider is to be designed. The problem dealt with is an energy problem. A stiffer structure generally enables higher wing aspect ratios, yielding higher lift over drag than flexible wing designs such as a conventional paraglider canopy. However, even though the paraglider definition may be stretched, in essence the structure of the canopy still needs to be flexible and collapsible. This train of thought has led the Team towards inflatable wing concepts. These combine both the required collapsibility while offering relatively high stiffness compared to traditional ram-air paraglider canopies. The high stiffness is obtained when the structure is pressurised.

Two canopy concepts were presented in the MRR. The "Phoenix" concept, shown in the left of Figure 4.3, has pressurised tubes aligned in y-direction and the conventional "Paraglider concept", shown in the right of Figure 4.3, has pressurised tubes aligned in x-direction. These two concepts were to be analysed, numerically compared, and a decision for the best concept based on a trade-off has been made. When starting the final design phase however this approach method was altered. Instead of choosing one concept or the other it was decided to integrate both concepts into the "Phoenix glider" concept. The main idea of this concept will shortly be explained below. The rest of the chapter will go into a more detailed investigation and analysis of this concept. The goal is to optimise this concept design with a numerical and analytical approach.

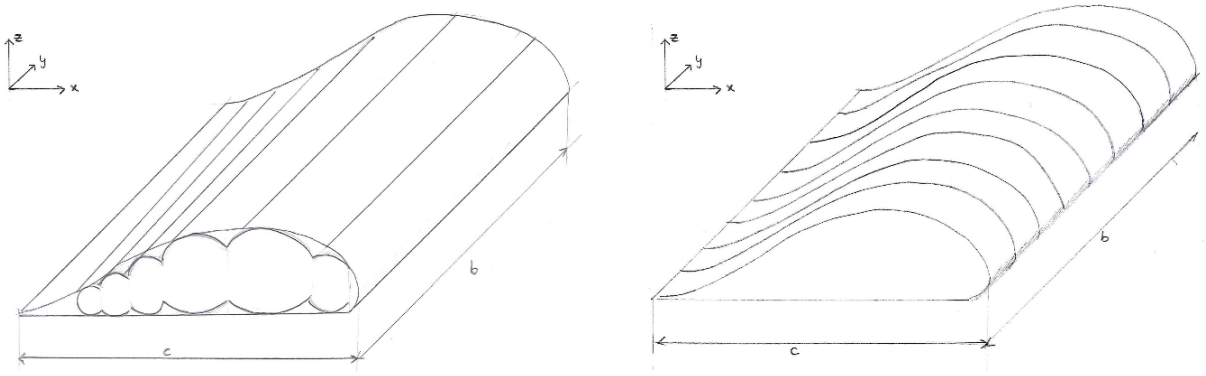

Figure 4.2: Multibubble design "Phoenix" (left) and conventional canopy design "Paraglider" (right)

The "Phoenix glider" concept has a multibubble design in the xz-plane, which approximates the chosen airfoil geometry as accurately as possible, and is divided in several sections along the wingspan. At each dividing line between the sections a suspension line is attached and a rib is placed. The suspension lines are thus located at the two ends of one section. Also, at these intersections, a rib has been implemented to carry the bending moments in xz-direction. Several spars will be implemented in each section to carry the bending moment in yz-direction. Both the ribs and spars are based upon the concept of Tensairity®[15] which has been explained in Section 4.3.

4.3 Tensairity®

The name Tensairity® is a combination of tension, air and integrity. In past years several studies have been conducted to investigate the potential of the concept in inflatable wing structures. Notable contributions have been made by the Swiss company "Prospective Concepts"[(i)], by Swiss Federal Laboratories for Materials Science and Technology (EMPA) and by the faculty of Aerospace Engineering of the Delft

[(i)] URL `www.prospective-concepts.ch` [cited on 20 December 2014]

University of Technology [16][17].

The principle of Tensairity® is a means of structurally reinforcing inflatable structures to enhance their load bearing capability. In essence any air-inflated cylinder may be reinforced by integrating both a compression element tightly connected to the airbeam and two tension elements which run in a helical form around the airbeam as shown in **??**. [15]

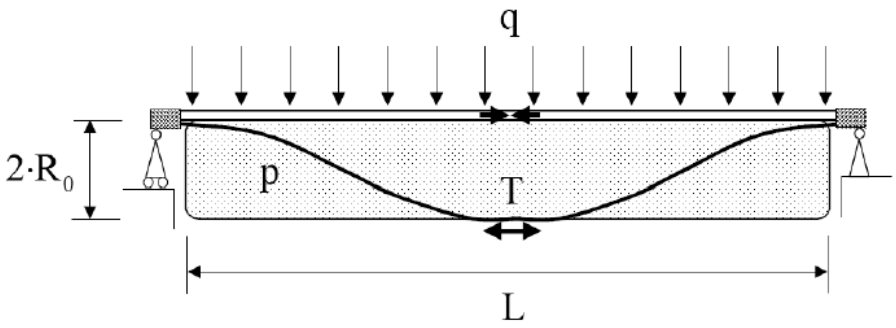

Figure 4.3: Forces in a Tensairity® beam. [18]

Under a distributed load the tension in the cable can be approximated with Equation (4.1):

$$T = \frac{1}{8} qL\gamma \tag{4.1}$$

$$\gamma = \frac{L}{2R_0} \tag{4.2}$$

The buckling load is independent of the length of the beam and is given by Equation (4.3) [15]:

$$P_{buckling} = 2\sqrt{\pi pEI} \tag{4.3}$$

Where p is the overpressure in Pa, E the modulus of elasticity in Pa and I the moment of inertia of the compression element in m^{-4}. By defining a proper moment of inertia for a given material and overpressure results in a buckling load which can be higher than the yield load. The yield load then becomes the limiting factor and the compressive force can be defined by equation Equation (4.4).

$$P = \sigma A \tag{4.4}$$

With σ in Pa as the yield stress and A the cross-sectional area of the compressive element in m^4. Equation (4.1) and Equation (4.3) can be set equal to each other and combined into one single equation Equation (4.5); which then yields both for the compression and tensile element.

$$q = \frac{8\sigma A}{\gamma L} \tag{4.5}$$

Where σ and A are the yield stress and area of either the tension or compressive element.
Another important quantity in Tensairity® is the overpressure since the cables press into the membrane. A relationship between the optimal pressure and applied distributed loading is given by Equation (4.6).

$$p = \frac{\pi^2 q}{2} \tag{4.6}$$

Furthermore, according to Breuer, Ockels and Luchsinger, Tensairity® beams can be improved by implementing a web membrane between the compression and tension element of two adjacent inflated tubes [16]. Load testing has revealed that the web tensairity beam is both lighter and about 2.5 times stiffer than a spindle Tensairity® beam; Figure 4.4 shows both the spindle and web configurations.

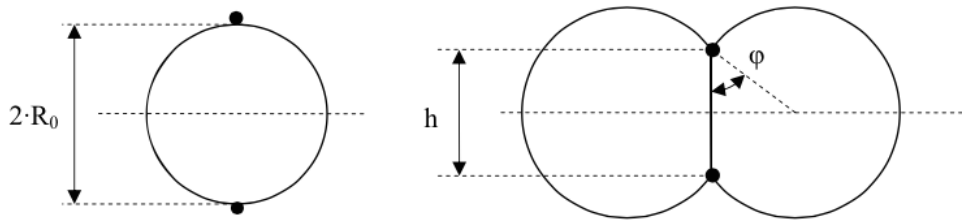

Figure 4.4: Cross-section of a Tensairity® spindle (left) and a Tensairity® web spindle (right). The black dots indicate tension and compression elements. [16]

The web Tensairity® element seems suited to strengthen cylinders in spanwise direction at spar locations in the airfoil section and ribs in chordwise direction. Prototype testing with inflatable kites has shown the potential of this concept. [18]

4.4 Canopy Structural Layout

The overall layout of the canopy structure is shown in Figure 4.5, this figure does not represent the final design. The components that make up the canopy are indicated by the numbers in the figure.

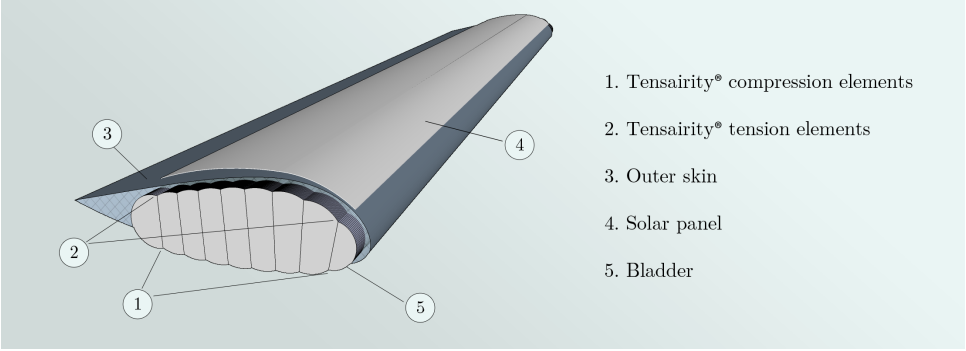

Figure 4.5: Structural layout of a straight canopy section with main components

The layout of the inner pressure cylinders, also called 'bubbles' or as a single element 'bladder', is designed such that the desired airfoil is approximated. An outer skin is wrapped around the internal pressure cylinders for the part that is not covered by the PV cells in order to increase the smoothness of the exterior to improve the accuracy of the airfoil shape. The Tensairity® compression and tension elements increase the strength of the canopy structure. They are integrated into specific cylinders to reinforce them. This has enabled those reinforced cylinders to act as spars and ribs. The webs are formed by the sides of two adjacent cylinders. The wall thickness has thus twice the thickness of the bladder material. This has reduced the membrane stress due to the overpressure.

A top view of the final structural layout of the canopy is shown in Figure 4.6. The figure is a rough sketch and is not scaled with respect to the final dimensions of the canopy design. The figure shows a sketch for the amount and location of ribs and spars, which are all supported with Tensairity® elements. There are 6 ribs and 10 spars in total. The spars in the middle have all the same length.

The bladder is pressurised with helium since this will add to the lift provided by the wing. The working principle is explained in Section 4.6. Helium is more volatile than air; this means that it consists of smaller molecules which can easier escape through the material. Therefore the bladder is made of Mylar®, a material which can contain this gas relatively well compared to other materials. Details are

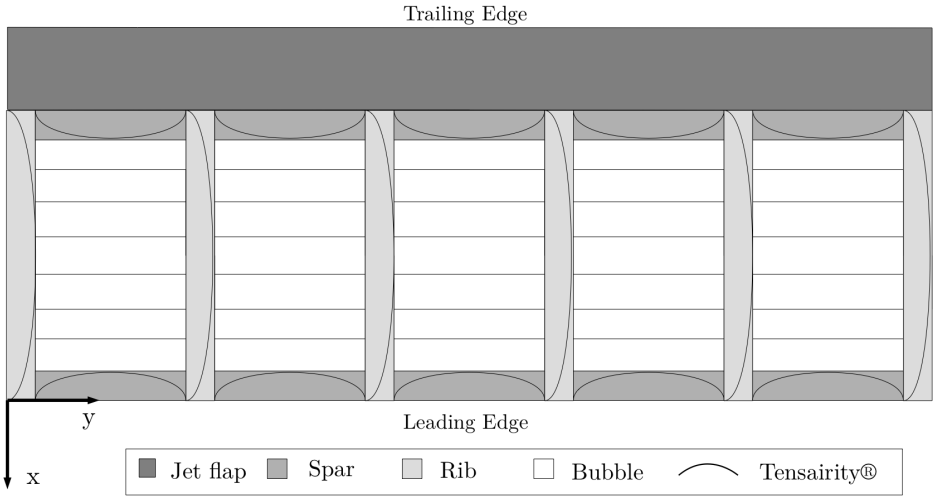

Figure 4.6: Structural layout of canopy with Tensairity® elements

specified in Section 4.9.

The 'bridle' consists of the suspension lines which connect the fuselage to the canopy structure. They are the structural interface between the two structural parts. The solar panels are part of the power system and are strictly speaking payload to be carried on the canopy structure. However they are incorporated into the structure of the canopy for an integrated design. The design of the suspension lines is depicted in Figure 6.15.

4.5 Pressurised Multibubble Design

The multibubble is a concept introduced in 2011 at the Delft University of Technology by Geuskens, Bergsma, Koussios and Beukers [19]. The multibubble is a structurally efficient pressure vessel which optimally combines inner pressure with geometric variables. Cylindrical or spherical members are pressurised and their structural integrity is enhanced by adding inner walls and reinforcement members. The loads and forces in a multibubble are solely dependent on the geometry of the configuration, given the cylinders are identically pressurised. The most elemental configuration described by Geuskens is the single-row multicylinder depicted in Figure 4.7. The analysis of this concept is used to determine the stress in the membrane between the cylinders in the airfoil section.

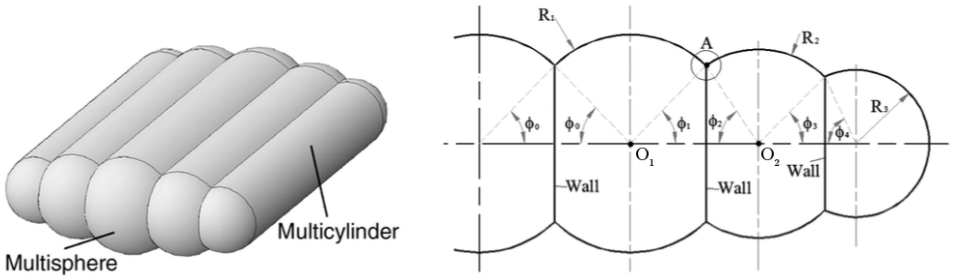

Figure 4.7: Left: Multicylinder geometry. Right: Multicylinder cross-section. [20]

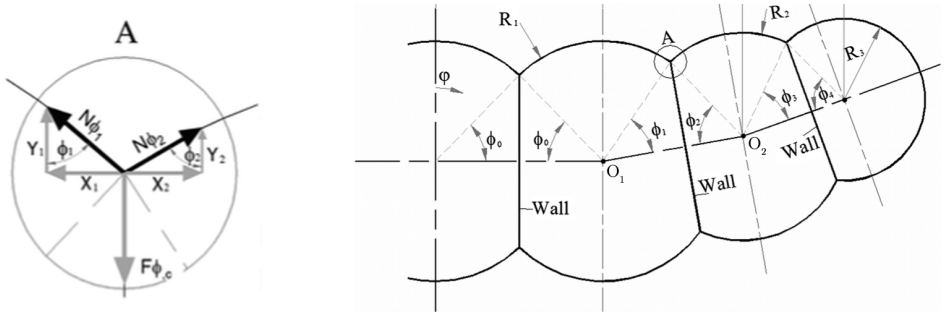

Figure 4.8: Left: Force equilibrium at point A. Right: variation of the single-row multicylinder [20]

Regarding the cross-section depicted at the right in Figure 4.7, the basic single-row multicylinder consists of circles with their respective centres O_i aligned. R_i is the radius of each circle shape used to construct each bubble. Walls between the circles are constructed at the intersections of the circles. In case of force equilibrium at the upper point of a wall as depicted on the left in Figure 4.8. Equation (4.7) can be used to determine the force acting on the wall. In order to create layouts where the circles are not aligned as shown on the right in Figure 4.8. Equation (4.8) should be used to find a geometry which ensures force equilibrium in the walls. The angle θ_i is the angle between the circle centre O_i and the intersection point A.

$$F_y = p \cdot |O_1 O_2| \tag{4.7}$$

$$R_2 sin(\theta_2) = R_1 sin(\theta_1) \tag{4.8}$$

The force F_y can be used with the thickness of the wall to determine the wall stress. If the material properties are known the wall can be checked for failure.

To incorporate the pressurised multibubble design in the canopy structure the wing geometry is first designed in the xz-plane. The aerodynamics group has chosen an airfoil which has been the starting point for the chordwise airfoil structure design. One of the first objectives of the structural design has been the realisation of the numerical 2D multicylinder design. An approach has been developed to trace the layout of the canopy structure within any desired airfoil.

Taking the airfoil as a starting point of the design, the mean camber line is traced first. Circles are drawn inside the airfoil with their respective center on the mean chord line while at the same time selecting a radius which fits the circle perimeter exactly on the upper and lower airfoil skin. The circles span the airfoil shape from leading edge up to 70% of the chord length towards the trailing edge. The upper and lower intersection points of adjacent circles are then determined. Wall membranes are drawn between the pairs of intersection points such that the walls are perpendicular to the mean chord line. Only the top and bottom sections of the circles in between the adjacent intersection points are conserved. The circles are thus reduced to an upper and lower arc section. Figure 4.9 shows the selected airfoil with a bubble geometry drawn inside. The left side of Figure 4.9 contains 5 membranes and the right side has 8 membranes.

The two geometries illustrate the trade-off between airfoil shape approximation and weight. If more circles are drawn the desired airfoil shape is more accurately obtained. A shape that accurately copies the ideal design airfoil is beneficial for the aerodynamic performance. However if more circles are drawn there are more intersection points. This means the number of walls increases and consequently the weight of the structure will increase. Additionally if more circles are drawn the pressurised structure becomes less efficient for dealing with wall stresses. Wall stresses increase when the angles at wall intersections become smaller. This effect is shown in Figure 4.10.

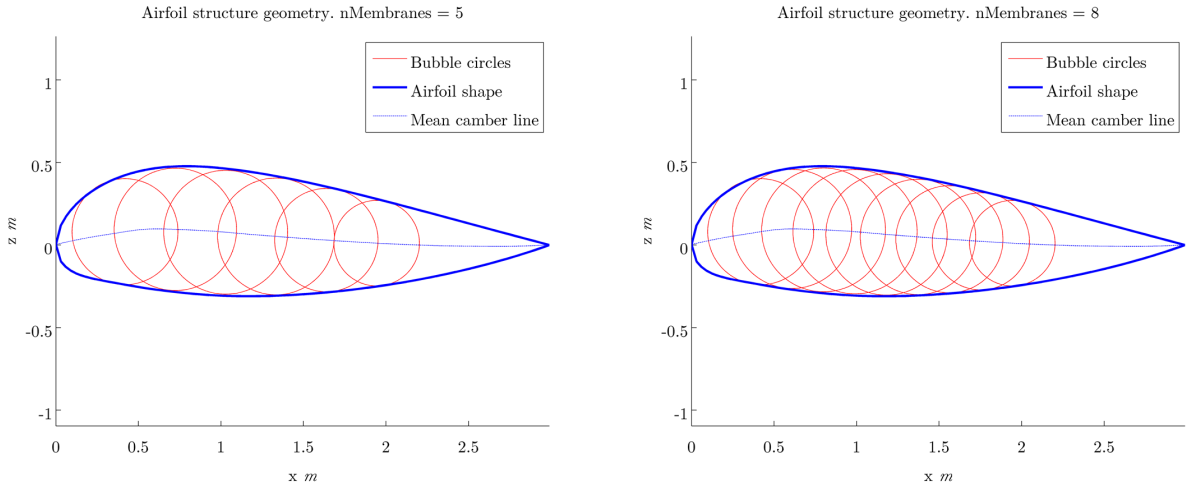

Figure 4.9: Airfoil geometry for 5 membranes (left) and 8 membranes (right)

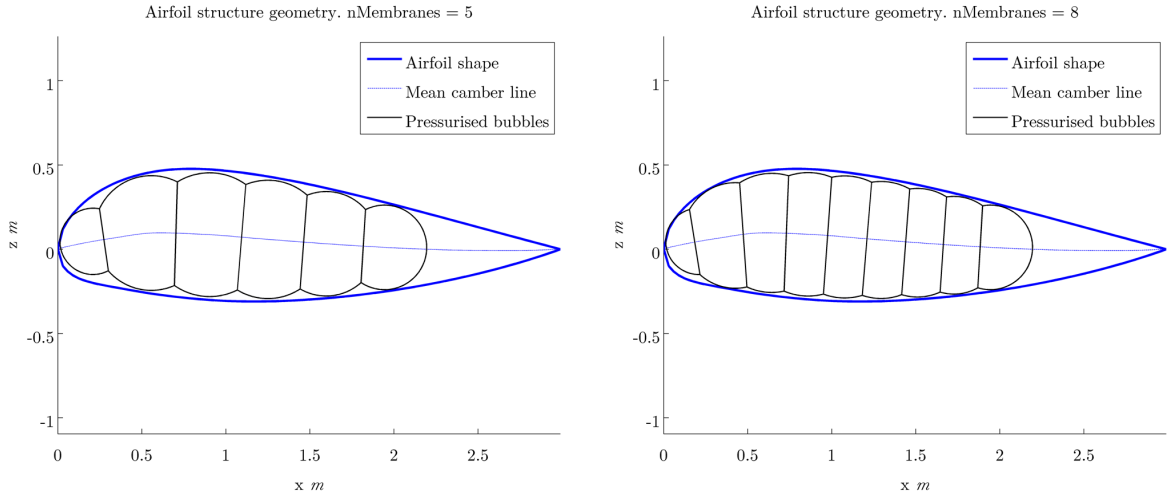

Figure 4.10: NACA 54126 airfoils with wall structure. Left: $nMembranes = 5$, right: $nMembranes = 8$

The numerical implementation of the aforementioned design approach has made this design step relatively fast and flexible once the program had been written. Another advantage is a relatively easy optimisation of the amount of bubbles used in the final design. Purely based on geometry an estimate of the aerodynamic performance and the structural weight can be found. The entire numerical program for the structural canopy design is explained in Section 4.8. The exact functionality of the multibubble design functions is explained in Section 4.8.1.

4.6 Helium Pressurisation

Already since 1783, humans have explored the world of lighter-than-air balloons using hydrogen as the gas being lighter than air to provide lift.[21] The two most common gases used for this purpose are helium and hydrogen, because of these gases being the two lightest ones known to man. Hydrogen is the lightest of the two with a density of only 0.0899 $kg \cdot m^{-3}$ and with helium having a density of 0.1786 $kg \cdot m^{-3}$, in comparison to air that has a density of 1.225 $kg \cdot m^{-3}$. The major reason for helium being used more often instead of the lighter hydrogen is that hydrogen is very flammable, whereas helium is an inert gas meaning it cannot catch fire.

As can be read in Section 4.4 the wing of the design is pressurised, which creates the option to fill the wing with a gas lighter than air. Placing electronics on top of the wing, can create unsafe conditions when put next to a large volume of hydrogen. Therefore the choice has been made to fill the wing with helium in order to provide a lifting force next to the aerodynamic lifting force. Since helium is much more volatile than air, measures have been taken to contain the helium inside the wing, using Mylar® as the material for the inside of the wing instead of ripstop nylon, since it has a lower permeability. This is further explained in Section 4.9.1, where it has been said that the permeability is low enough to sustain the mission.

In Equation (4.9) the formulae for lift provided by the helium are shown.

$$\rho_{gas} = \frac{p_{gas}}{R_{gas} \cdot T_{gas}} \tag{4.9a}$$

$$W_{gas} = V_{wing} \cdot \rho_{gas} \cdot g \tag{4.9b}$$

$$L_{helium} = W_{air} - W_{helium} \tag{4.9c}$$

In the aforementioned equations the density of the gas, ρ, is given in $kg \cdot m^{-3}$; the pressure of the gas, p, is given in Pa; the specific gas constant, R, is given in $J \cdot (kg \cdot K)^{-1}$; the temperature of the gas, T, is given in K; the weight of the gas, W_{gas}, is given in N; the pressurised volume of the wing, V_{wing}, is given in m^3; the gravitational constant, g, is given in $m \cdot s^{-2}$; the lift provided by the helium, L_{helium}, is given in N.

4.7 Structural Integrity Through Jet Flaps

It has been established in Section 4.5 that the inflated cells only fill up to about 70% of the wing's cross sectional chord length starting from the leading edge. The guaranteeing of the structural integrity of the trailing edge with the use of jet flaps is discussed in this section.

Jet flaps, a technology incorporated by paraglider company Skywalk, are traditionally inflated by neighbouring cells. They are divided in sections and independent from the main wing section. In the Team's design of the paraglider, the trailing edge incorporates the use of jet flaps in the way that is depicted in Figure 4.11.

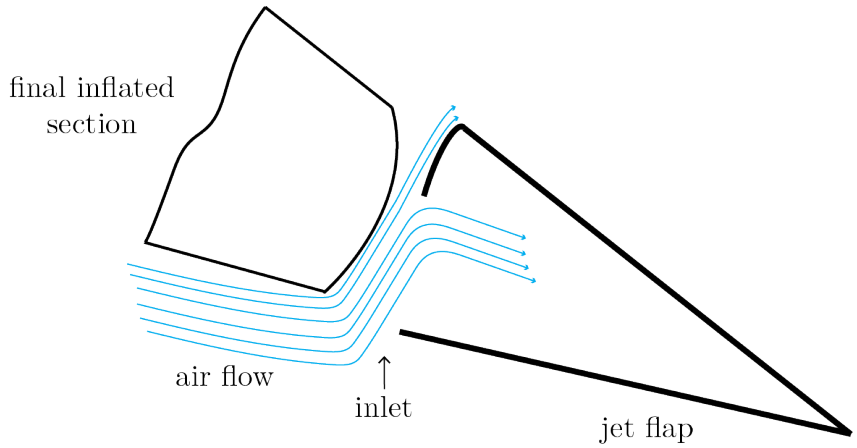

Figure 4.11: Modified jet flap in the trailing edge

In Figure 4.11, the airflow around jet flaps, which are located after the last inflated air bubble, is depicted. The inlet in the bottom part of the jet flap lets some of the air enter it, pressurising it and giving it the shape that is required to approximate that of the selected airfoil. This helps in structurally shaping the trailing edge. The air entering the section through an inlet is based on the same principle of pressurising a ram air inflated wing paraglider [22]. Some of the air enters the section, while some of

the air goes out, flowing over the upper side of the trailing edge. The effect on drag of the jet flaps is to be investigated. The manufacturer, Skywalk, claims the effect is negligble but this remains to be verified.

Using jet flaps not only helps the structure of the trailing edge, but also helps in the control of the paraglider as the full rear segment of the wing on the sides can be deflected, as described in Section 2.2.

Minor ribs are placed throughout the wing to obtain the desired shape through the jet flaps. These are lightweight structural reinforcements. The spacing of the minor ribs is such that the trailing edge section can not collapse in case the inlet flow of the jet flap is obstructed or perturbed.
The construction of the jet flaps is further discussed in Section 4.9.4.

4.8 Numerical Code For Structural Canopy Design

The canopy has to be structurally supported with spars and ribs that make use of the principle of Tensairity®, in combination with pressurised cylinders. The design of the stiffening elements supporting the structure is a function of the external loads and how these loads are introduced in the system. External loads may translate into shear, torsion, bending and buckling. A numerical code is written to optimise this structural canopy design based upon the requirements mentioned in Section 4.1.

The numerical model will give a rough estimation of the weights and pressures needed to carry the external loads, related to a specific number of ribs, spars and pressurised bubbles. By playing with these three design parameters the optimum weight can be found. The amount of ribs, spars and bubbles, alters the local wing loading and the pressures needed to support this loading. The principle loads that are to be considered are bending and torsion. First the model is built to design a wing that can carry the bending loads. This means that the internal pressures of the bubbles, and stiffness of the Tensairity® elements will have to provide enough rigidity to carry these loads. The internal pressures and bending moments will also introduce stresses into the material skin and must stay within an acceptable range for the material to not rip or buckle.

For torsion, research on calculation methods has been done. The methods found to calculate these loads will be briefly explained in Section 4.8.7. However it has not been implemented in the code due to the complexity of determining the torque for a multibubble inflatable wing and the results found so far show very low deformations on a multi bubble design. Also the exactness of these torsion models is to be questioned since most numerical reference values are found by performing experiments on the prototype itself. Since this canopy design deviates from any wing design built so far these numerical models are not considered applicable to give a good estimate of the torsional loads introduced in the canopy system.

With these criteria in mind the optimum design is thus obtained for the bending moments and skin stresses through an iterative process of the numerical model. The accuracy of the model is restricted by the assumptions and simplifications made. It is important to recall that the purpose of the project is to check the feasibility of the mission, and not necessarily to build a highly accurate model. This model will give a feeling of the values that are dealt with and the following assumptions made are considered acceptable for this specific purpose:

- The solar panel is placed in between bladder walls. Its weight is proportionally distributed over the bubbles it is placed on.
- The lift distribution is simplified to the lift at stall condition proportionally divided over the bubbles.
- The bubble centers are placed on a single line. The requirement for multibubble geometry in Equation (4.8) is not respected.
- The chordwise spacing in between bubbles is equal for all pairs of adjacent bubbles.
- The thickness of used materials is so low that all calculated geometry can be represented by points and lines. The thickness of various elements is not taken into account in the calculations.

- Each bubble is formed by its own enclosed area. Webs consist of two bonded sheets of material, they are twice as thick as the circular sections of the bubbles.
- The suspension lines act vertically on the canopy.
- The bubbles in airfoil design are assumed to behave as pressurised cylindrical beams.
- Constant distributed load over span due to rectangular wing shape.
- Zero angle of attack.
- The effect of disturbances such as wind gust or control forces are neglected.
- $C_m = 0$ for the airfoil.
- The system is in equilibrium thus steady symmetric flight.
- The wing and fuselage are symmetric about the z-axis.

In order to increase the accuracy of the model and achieve an even lighter design these assumptions could be altered, or left out. This will be further discussed in Section 4.10

The numerical model is composed of several functions or blocks that have to be integrated with each other. A flow chart gives an overview of the directional flow of data and functions. This is presented in Figure 4.12.

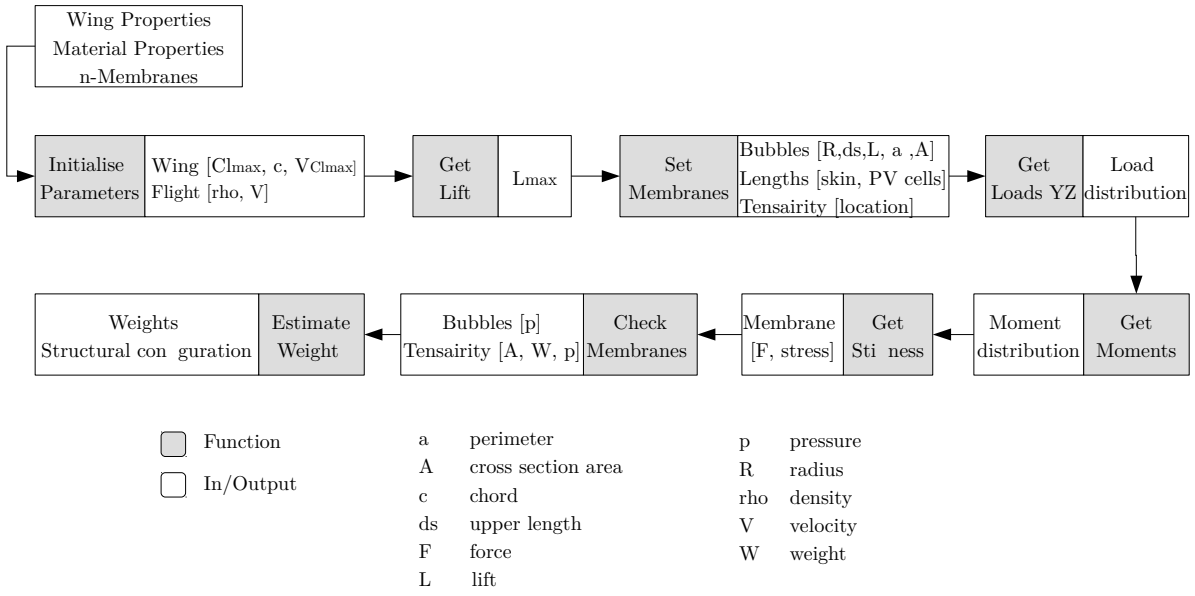

Figure 4.12: Flow chart for the canopy numerical design tool

In the following subsections the theory used to built the numerical model is explained.

4.8.1 Numerical Multibubble Design

The numerical multibubble design is a software implementation of the approach explained in Section 4.5. The program is made in MATLAB®, which has sufficient built-in functions to speed up this first geometrical design block. The multibubble block is the first one to be called by the main structures function. It is called "setMembranes" since its primary goal is to find the internal geometry of the pressure membranes.

The code takes the following inputs:

- Airfoil coordinates, loaded as a *.dat* file
- Chord length c
- Bubble distribution $bubDist$: chordwise start and end locations of pressurised cylinders
- $nMembranes$: number of wall membranes desired
- Solar cell distribution $pvDistr$
- Drawing accuracy acc, set within the function itself

The airfoil shape is provided as a file containing coordinates by the aerodynamics group. The maximum number of coordinates is set in JavaFoil to obtain an accurate description of the airfoil shape. The file is imported in the function and run through a preprocessor. In some cases the JavaFoil program does not correctly align the chord line of the designed airfoil with the x axis. In this case also the chord may be other than unit length. The preprocessor determines the two points at the leading edge and trailing edge. It then scales and rotates the airfoil to correct for the incorrect Javafoil output. The airfoil coordinates are sorted into separate vectors for the lower and upper skin section. All coordinates are scaled to the input chord dimension.

The upper and lower airfoil shapes are approximated by a piecewise cubic hermite interpolating polynomial (PCHIP) to be able to evaluate the airfoil shape at any desired x coordinate. 150 points are available for each section. Therefore the interpolation is made of a maximum of 150 coefficients which is sufficiently accurate for this study. The MATLAB® command PCHIP conserves the original shape. The interpolating functions are then used to evaluate the airfoil at a number of points in both the upper and lower sections, set by the accuracy setting that the user can manipulate.

The multibubble design should be such that the bubbles support both the upper and lower skin of the canopy. To automatically place the bubbles at the correct locations, the mean camber line is needed. It is probably easiest to implement the equations used to analytically trace NACA airfoils. These include the definition of the mean camber line. However at the start of the aerodynamic design and airfoil selection it was unclear whether a NACA airfoil would be used. Therefore a numerical solver was built to find the mean camber line of any possible airfoil. Support has been provided by aerodynamics PhD student Iliass Azijli.

The mean camber line solver starts with an initial guess by vertically averaging the upper and lower skin of the airfoil. For each point on the previous guess the line is found which minimises the distance between the intersection points of this line with the upper and lower skin. The point halfway that line is added to the next guess of the camber line. This process is iterated until an approximate mean camber line is found. The convergence of this method is however not guaranteed. It has been found that the solution found is off by a maximum of 3% at the front of the selected airfoil. Efforts to fix this inaccuracy have been undertaken but the potential improvement was too low for the amount of resources needed. Therefore a quick fix has been implemented which manually corrects the cylinders drawn near the leading edge.

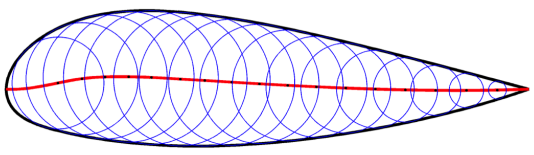

Figure 4.13: Illustration of the mean camber line solver

Once the mean camber line is found, the bubble distribution inputs are used to find the coordinates of the bubble centers on the mean camber line. The bubbles are equally spaced. The spacing between them is based on the minimum and maximum chordwise location and the number of bubbles. By using a subfunction of the mean camber line solver the intersections points of the bubbles on the upper and

lower skin are found and used to set the radius of each bubble. If the mean camber line were perfectly accurate, the upper and lower intersection points would have been at the same radius from the bubble center. By inspection this has not been the case within $x < 0.1 \cdot c$.

The bubble coordinates and radiuses are known. The MATLAB® function "circcirc" is used to find the intersections between adjacent bubbles. The membranes or walls are defined as the lines between the pair of intersection points of two adjacent circles. These are drawn, this step can be seen in the left side of Figure 4.14. The intersections points are further used to find the remaining arcs of the bubbles in between the walls. A function "getArc" has been written which returns coordinates of an arc running from point $P1$ to $P2$ with a circle center O. The arcs defined by the first and last bubbles are drawn as well by a variant of this function "getEndArc". The right side of Figure 4.14 shows the geometry obtained.

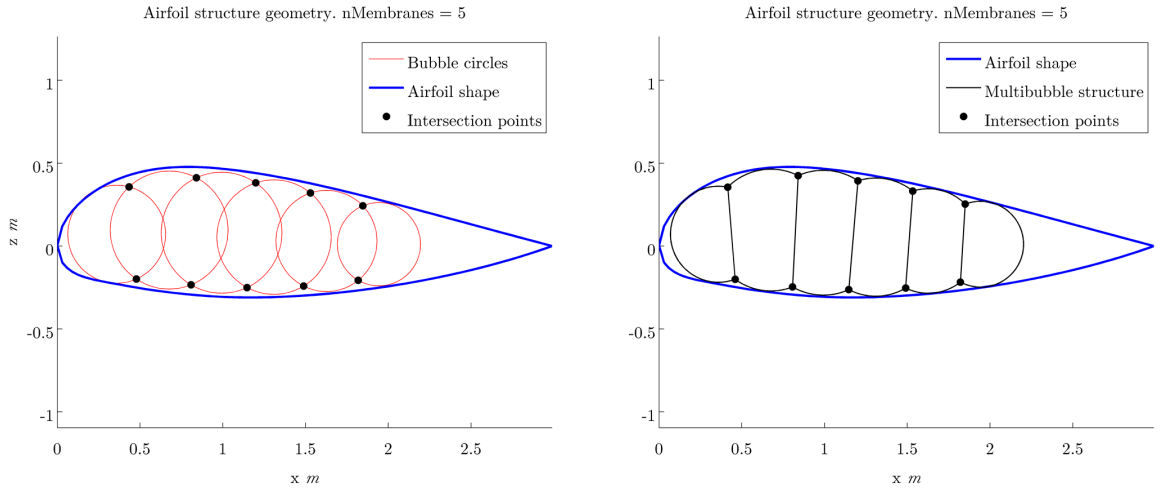

Figure 4.14: Example airfoil geometry with bubble intersection points (left) and membrane walls and connecting arcs (right)

Two geometrical elements are added. Firstly the locations of the Tensairity® webs is determined. Manual manipulation has shown that the optimal positions are at the most forward and aft webs. Secondly the chordwise placement of the solar cell is determined by covering the region delimited by the reinforced webs. At the leading edge the solar panel is limited by the rounding of the airfoil. The inclination with respect to the sun becomes too significant. At the rear the solar cell placement is limited by the reinforced web. Figure 4.15 shows the placement of the PV cells by the program.

The last chordwise 30% of the wing structure is pressurised through the ram-air principle. This section is not designed for the load due to the solar cell and therefore the solar cell is not placed behind the last rear web. The control forces calculated in Section 2.2.1 have taken into account that the chordwise rear 30% of the wing can be used to make control deflections. If the last bubble is moved aft, then the control forces would have been higher.

The next block of code has determined various outputs from the defined geometry which are used for the stress calculations and for determining various other wing parameters. A simple function has been written to determine for any geometrical element its length. This is used to calculate solar cell length, outside skin length and total bladder length. The total length of upper skin supported by bubbles is calculated and used to approximate the respective lift contribution per bubble. For this the maximum total lift is calculated by assuming the maximum 2D lift coefficient, the air density at sea level and a maximum airspeed of 65 $km \cdot h^{-1}$. Most commercial canopies have lift polars specified up to 55-60 $km \cdot h^{-1}$ [(ii)]. This basic calculation of the lift distribution is deemed sufficiently conservative since the maximum

[(ii)] URL `http://para2000.org/wings/index.html` [cited 20 January 2015]

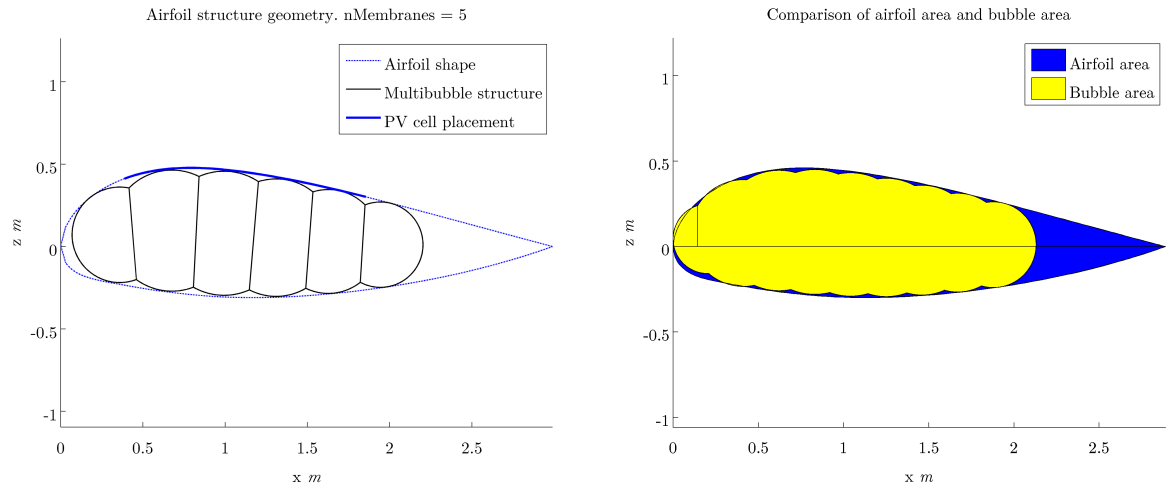

Figure 4.15: Left: PV cell placement for $nMembranes = 5$. Right: airfoil area vs. bladder area for $nMembranes = 8$

total lift is distributed over the bubbles only, excluding the rear section. The 2D maximum lift coefficient of 2.493 has been obtained from JavaFoil and is a theoretical upper limit for the actual 3D lift coefficient.

The calculated lengths are output for a 2D weight estimation and for the calculation of the total available solar panel area. An array is built containing all bladder segments which together form a contour inside the ideal airfoil shape. An integrating function is used to calculate the area inside the contour and the area of the airfoil shape itself. The ratio between the bladder contour area and the airfoil area is used to indicate how well the airfoil shape is approximated by the cylinders. The bladder contour area is also an output to estimate the total available pressurised volume per span. The right side of Figure 4.15 contains a geometrical illustration of the airfoil and bladder areas. The left side of Figure 4.16 shows the progression of the area ratio when $nMembranes$ increases from 3 to 30.

The total 2D length of the bladder has been calculated and plotted as a function of $nMembranes$ at the right of Figure 4.16. This length is a measure of the structural weight of this element.

A trade-off has been made for the number of bubbles in the chordwise cross-section. As can be seen in the right side of Figure 4.16 the weight of the cross-section seems to linearly increase with the amount of bubbles. This seems intuitive since approximately the same amount of material is added for each additional bubble. The left side of Figure 4.16 shows the bubble area ratio when the number of membranes increases from 3 to 30. The y-axis scale indicates that the improvement is relatively low, as the minimum value for 5 membranes is about 0.79 and the maximum plotted value is about 0.874 for 30 membranes. The plot has confirmed that the airfoil is better approximated for an increasing amount of membranes. However the rate of change is low and decreases rapidly after $nMembranes = 6$. Thus the increase of membranes becomes increasingly less beneficial for the airfoil shape approximation. The curve shows an asymptote at an area ratio of about 0.875. This value can be approached but never attained using the numerical tool built.

The stress in the walls increases as the bladder shapes become more rectangular. As more bubbles are added the wall stress becomes critical. The check for the wall stress is explained in Section 4.8.6. After consultation of the aerodynamics group and while considering that the weight increases linearly with $nMembranes$ it has been decided to set the number of $nMembranes$ at 8. The efficiency increase after this number is low while the same weight is added for each membrane. This results in a number of 9 bubbles spanning the mean chord line. The outside of the wing will be covered by the solar panels and by additional skin to protect the bladder and to decrease the bumps in the airfoil shape. The final 2D multibubble design is shown in Figure 4.17.

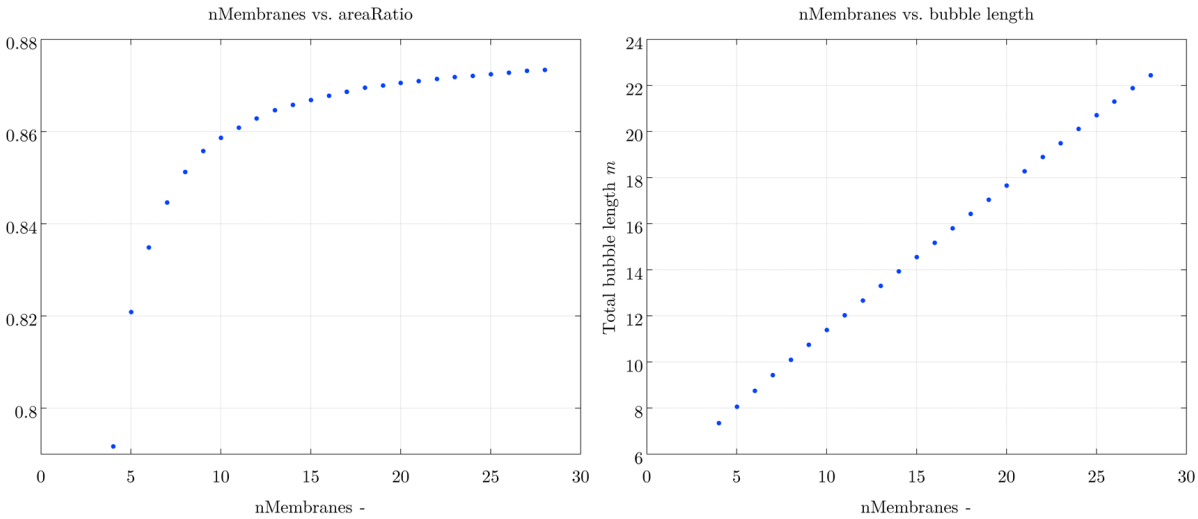

Figure 4.16: Left: Area ratio as a function of $nMembranes$. Right: Total 2D bladder length as a function of $nMembranes$

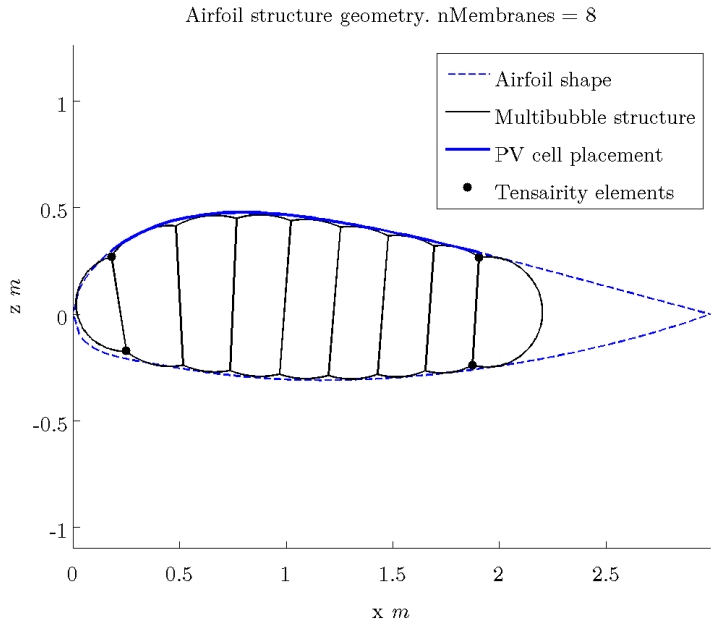

Figure 4.17: Final design for airfoil structural multibubble design

4.8.2 Bridle

The canopy is subjected to several external forces. These will create a moment C_m about the centre of gravity if not set to equilibrium by some counteracting forces. It is desired for stability that the moment about the canopy's centre of gravity (c.g.) is in equilibrium. The bridle is defined by the number and location of the suspension lines. The bridle of the lines will be designed such that the tension in the suspension lines provide this state of equilibrium. For a 3D object, front view and side view must be considered. It is assumed that disturbances such as wind gust, or control forces can be neglected. Also

the airfoil is designed to approach an as low as possible moment coefficient as explained in Section 3.2, therefore it is assumed that C_m can be set equal to zero to simplify the analysis.

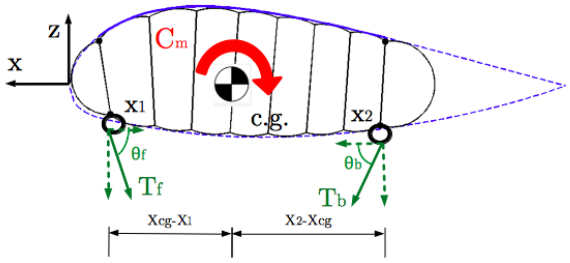

Figure 4.18: Line bridle forces - Side view

The moment about the c.g for side view is a function of C_m and the tension in the suspension lines as shown in Figure 4.18. Since C_m is assumed to be zero, moment equilibrium only becomes a function of the forces in the suspension lines. Taking force equilibrium in x-direction:

$$\Sigma F = 0 : F_{xf} - F_{xb} \tag{4.10}$$

where F_{xf} and F_{xb} are the horizontal components of the tensile force in N, in the front and back suspension line. The two horizontal forces are thus equal to each other. Another simplification is made by saying that the two attachment points have the same y-location (the difference is considered negligibly small). This simplifies the moment equilibrium equation to only two contributing forces: the vertical components of the front and back suspension line force. By taking moment equilibrium about the c.g. a ratio K can be found between the two suspension line forces T_f and T_b. The moment arm is the horizontal distance between the c.g. and the attachment points.

$$K = \frac{x_2 - x_{cg}}{x_{cg} - x_1} \tag{4.11}$$

where x_1 is the location where the front suspension line is attached to the canopy in x-direction, x_2 where the back suspension line is attached and x_{cg} the c.g. location in m. This means that T_f is K times larger than T_b and the front spar is to carry K times more load than the back spar. This ratio is implemented in the numerical code when designing for the front and back spars.

For front view, the main concern is the outer suspension line has to be strong enough to keep the wing anhedral section in place. As shown in Figure 4.19 a resultant lift force $\sigma L_{anhedral}$ acts on the anhedral section. When taking force equilibrium it is found that the bridle of the front view lines must thus be designed such that the tension in the outer line T_v counteracts the resultant lift force $L_{anhedral}$ of the anhedral section.

$$\Sigma F = 0 : \Sigma L_{anhedral} - T_v \tag{4.12}$$

The final design consists of four suspension lines which split into three smaller lines after two thirds of the total length. In total this makes 12 connections to the canopy and four to the fuselage. The layout is illustrated in Figure 6.15.

4.8.3 Bending Moments

The design of the stiffening elements is a function of the external loads and how these loads are introduced into the canopy. As explained in Section 4.3, the area of the Tensairity® elements is a function of the distributed load over the beam and determined with Equation (4.5). The distributed load is thus to

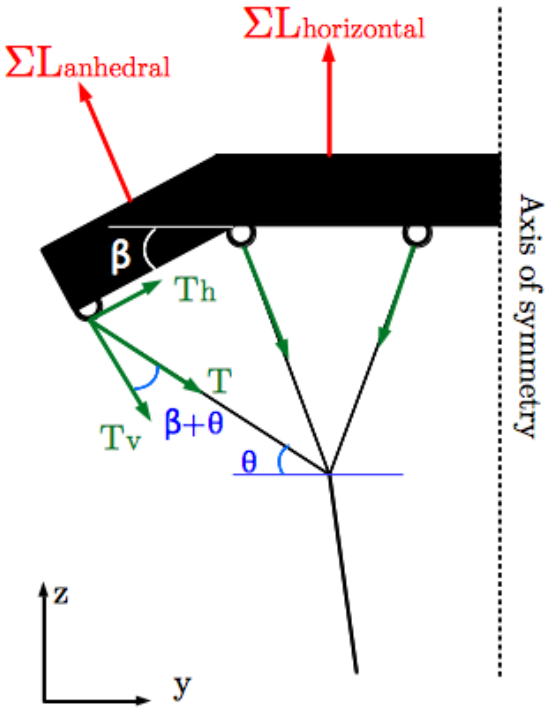

Figure 4.19: Line bridle forces - Front view

be found for the spars and ribs. A safety factor of 1.5 is applied for the distributed loads to compensate for the assumptions made and to provide a conservative wing design. As for the bridle of the suspension lines the forces must be considered for front view and side view.

First the value for the distributed load q over the spars is determined for side-view (xz-plane). In the xz-plane, the spars have to carry the lift over the wing, the weight of the wing and the weight of the solar cells (1.234 $kg \cdot m^{-2}$. This 2D distributed load q is then assumed to be constant over the length of a spar in the yz-plane since the wing is rectangular shaped; q is then distributed such that the front spar carries K times more load than the back spar as explained in Section 4.8.2. There are thus two distributed loads, $q_{SparFront}$ and $q_{SparBack}$. The values are multiplied with a safety factor of 1.5.

$$q = L_{Total} + W_{Solarpanel} + W_{Canopy} \tag{4.13}$$

$$q_{SparFront} = q \cdot \frac{K}{K+1} 1.5 \tag{4.14}$$

$$q_{SparBack} = q \cdot \frac{1}{K+1} 1.5 \tag{4.15}$$

For the first iteration the weight of the canopy elements is added to the lift over the wing as shown in Equation (4.13). Once a weight of the wing is determined, the weight is added to the lift calculation as explained in Chapter 3. A new value is found for the lift and so the code can be run again with a new lift distribution without having to add the weight of the canopy. This is an on going design process. A more detailed flow diagram of the inputs and outputs is given in Figure 4.12.

For the ribs the highest load value q over a bubble, located in the region between the two spars, is chosen as design value. The highest value is taken instead of the average to provide a conservative design. The average distributed load over each bubble is calculated by dividing the total distributed load

q by the surface length ds above each bubble. The highest value is taken as q_{rib} and is then considered constant over the wingspan and constant over the rib length:

$$q_{rib} = q_{BubbleMax} \cdot l_{spar} 1.5 \tag{4.16}$$

Having determined the distributed load, both the spars and ribs are looked at as simple supported beams under a constant distributed loading q. The bending moment is then given by the parabolic function Equation (4.17) for $0 \leq x \leq L$:

$$M(x) = q \cdot \frac{Lx - x^2}{2} \tag{4.17}$$

Where L is the length in m of the spar or rib segment.

The maximum moment for the anhedral and horizontal section are presented in Table 4.1. The overpressure needed in the Tensairity® elements to support this load is also given. Even though the load is lower for the ribs, a higher overpressure is needed. This is because the ribs are spindles which have lower load bearing capacity than the spars which are webs, as explained in Section 4.3.

Table 4.1: Maximum bending moment and overpressure

Parameter	Unit	Front spar	Back spar	Rib
Max moment (anhedral)	Nm	222.94	148.17	52.71
Max moment (horizontal)	Nm	3055.80	2030.90	296.65
Overpressure	Pa	559.72	316.37	691.40

Plots of the bending moments can be found in Figure 4.20, 4.21, 4.22 and 4.23
The moment diagrams for the horizontal section of the spars and rib are shown in Figure 4.20 and 4.21. The figures show a parabolic function, where the moment increases up to the middle of a spar or rib where it reaches its maximum and decreases again as it approaches the next attachment point. The same can be observed in figure Figure 4.22 and 4.23 but with lower values since the span is much lower than for the horizontal section. Also, for both sections it can be observed that the front spar carries higher loads than the back spar. This is due to the bridle as explained in Section 4.8.2.

4.8.4 Tensairity® Elements

The Tensairity® beams are composed of a compression and tension element. Now that the distributed load over the ribs and spars has been determined, an estimation of the cross-sectional area of the Tensairity® elements can be found with Equation (4.18)

$$A = \frac{q_{\gamma} L}{8\sigma} \tag{4.18}$$

As explained in Section 4.3, the same equation can be applied for the tension and compression elements. The tensile element has a circular cross-section and the compressive element a rectangular cross-section.
The areas needed for the Tensairity® are given in Table 4.2 for the front spar, back spar and ribs. The resulting values show that the front spar of the horizontal section has Tensairity® elements with highest needed area. This makes sense since this is the part of the wing that must support the highest loads. Tensairity® elements make out usually 16% of the total weight of a Tensairity ® spindle [18]. The calculated percentage is 18% which seems reasonable with respect to the 16%.

The compression and tensile elements are made out off different materials as presented in Section 4.9. With the needed area and the density of the material the total weight of the Tensairity® is estimated and presented in Table 4.3.

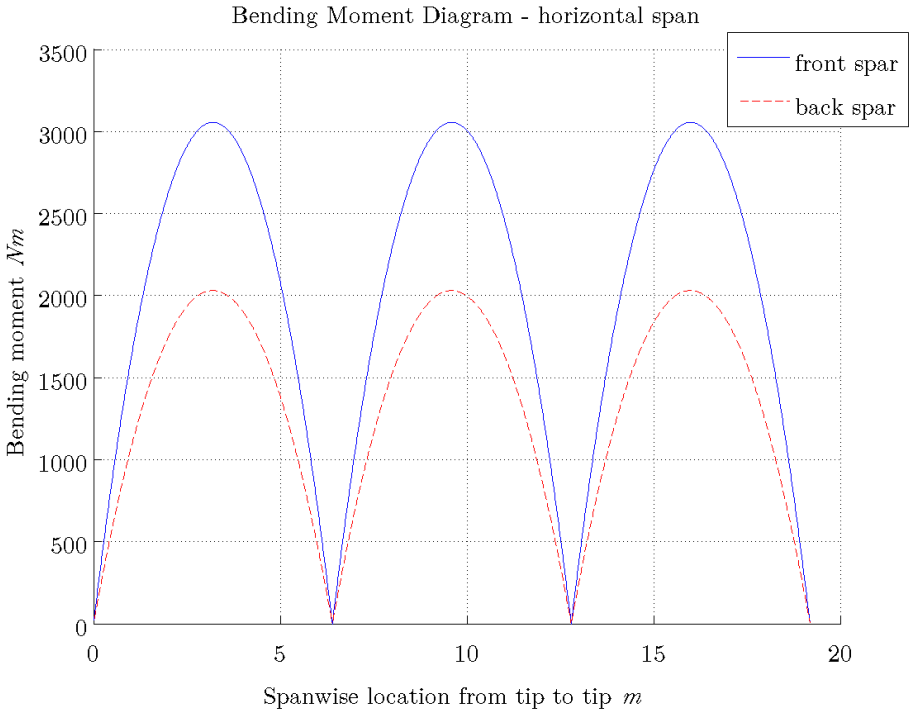

Figure 4.20: Moment diagram spars horizontal section

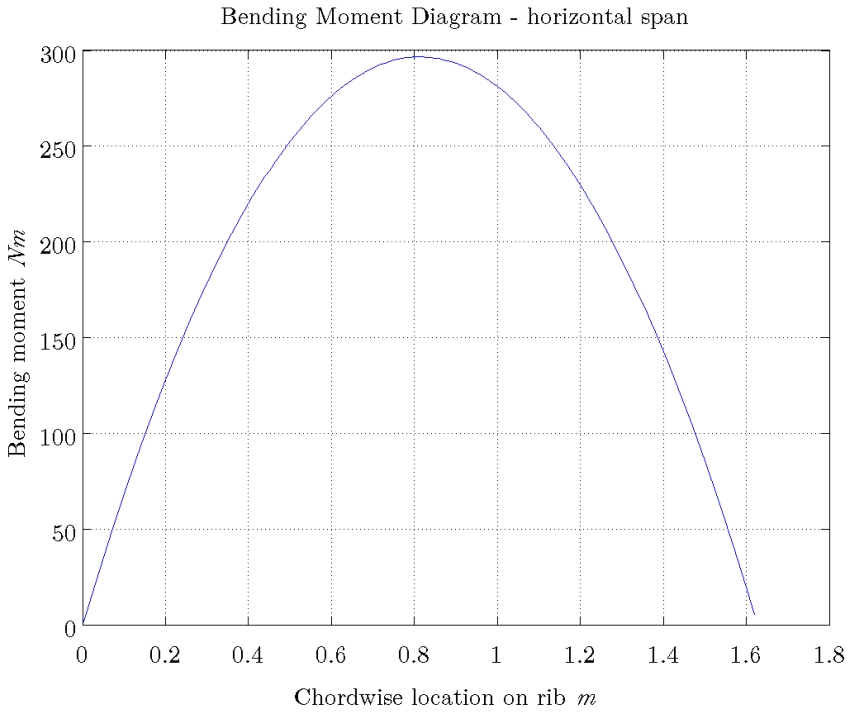

Figure 4.21: Moment diagram ribs horizontal section

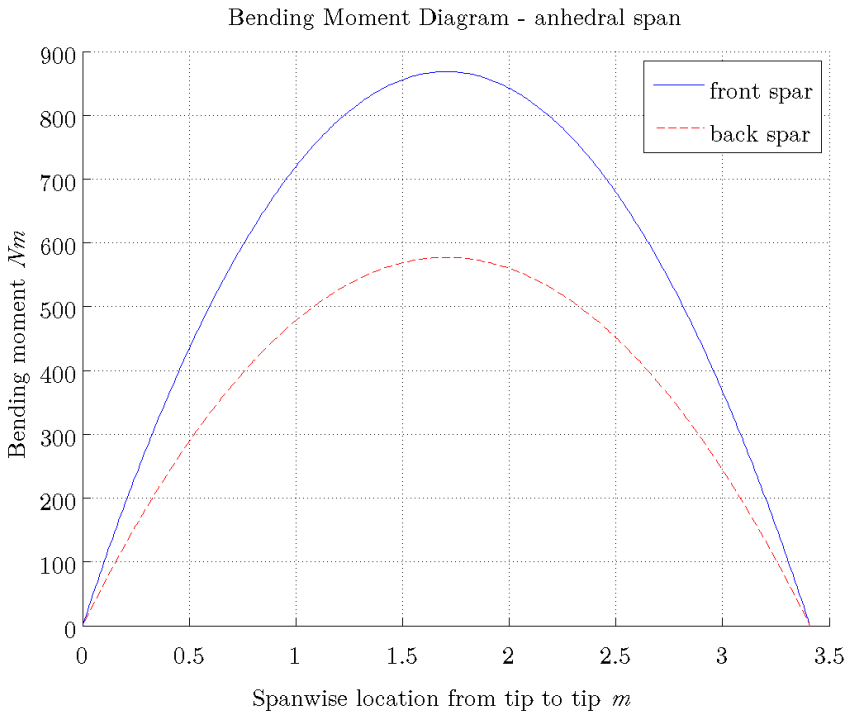

Figure 4.22: Moment diagram spars anhedral section

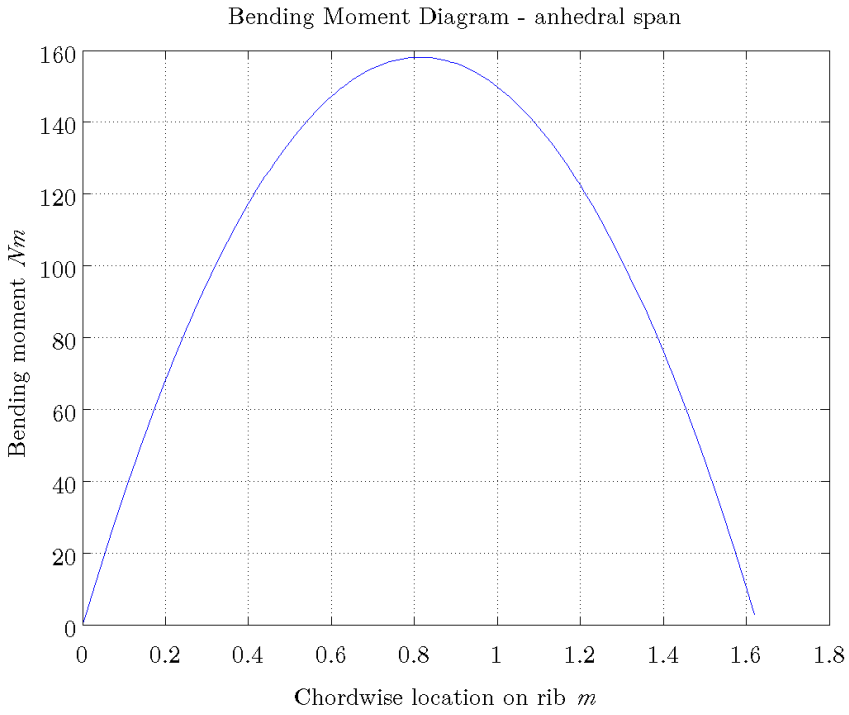

Figure 4.23: Moment diagram spars anhedral section

4.8.5 Overpressure

For the spars the Tensairityy® elements consist of two adjacent pressurised bubbles as shown in Figure 4.7. The internal pressure needed is a function of the angles θ_1 and θ_2 and the radius R of the

Table 4.2: Area Tensairity® Elements

	Unit	Front spar		Back spar		Rib	
		Tension	Compression	Tension	Compression	Tension	Compression
Anhedral	mm^2	0.55	1.10	0.27	0.55	0.23	0.46
Horizontal	mm^2	1.92	3.86	0.97	1.94	0.80	1.61

Table 4.3: Weights of Tensairity® elements

	Unit	Front spar	Back spar	Rib
Anhedral	kg	0.1123	0.0626	0.1749
Horizontal	kg	0.3625	0.0683	0.4308

pressurised bubble as discussed in Section 4.5:

$$p_{spars} = \frac{q}{sin(\theta_1)R_1 + sin(\theta_2)R_2} \tag{4.19}$$

The ribs have to carry much lower loads, and are therefore single cylinders (spindle), as the increase in stiffness provided by the web Tensairityy® element is not needed. The overpressure can then be calculated with equation Equation (4.20).

$$p_{ribs} = \frac{\pi^2}{2} q \tag{4.20}$$

Two different equations can be used to determine the required overpressure in the bubbles that are not strengthened with Tensairity® elements. Both equations are valid and are used as a verification by checking whether they give comparable results. The first is based on a cylindrical approximation for the inflated bubbles, and is determined by Equation (4.6); it is a function of the distributed load [23]:

The second equation is also appplicable for a cylindrical inflated beam, only now the overpressure is a function of the moment M_0 over the beam and the radius R as shown in Equation (4.21) [24].

$$p_{bladder} = \frac{2M_0}{\pi R^3} \tag{4.21}$$

In Table 4.4 the internal pressures needed for the bubbles to support the bending loads that act on the canopy are presented. As discussed, two different calculation methods are utilised for verification purposes. Bubble one, two, eight and nine (marked in grey) are to be strengthened with Tensairity® elements. These pressures are thus not of interest. Since the anhedral and horizontal section are of different size and have a different amount of ribs the internal pressures differ. The bubbles in the horizontal section must have a higher internal pressure according to the results. Since the canopy is to be designed for the same pressure in every bubble, the highest pressure is taken for a conservative design. A higher pressure is also favourable in terms of stiffness and torsional rigidity. The internal pressure for the bubbles has a value of 11'540 Pa to which the ambient pressure still has to be added; this gives a design pressure of 113 kPa.

4.8.6 Membrane Stresses

A function is integrated to check the stresses in the walls. The function uses the coordinates of the bubble centers, the calculated values for the overpressure in the bladder, the thickness of the bladder material $t_{bladder}$ and the tensile strength of the bladder material $\sigma_{bladder}$. First the distance between the bubble centers is calculated for each pair. Then using Equation (4.22) the maximum internal overpressure $p_{internal}$ is added to the ambient pressure $P_{ambient}$ to obtain a total internal pressure p_{total}. This is used for all bubbles since all bubbles are to be pressurised at the same design pressure p_{total} for convenience when the canopy is pressurised before the mission.

Table 4.4: Internal pressures bladder

Wing Section	Anhedral		Horizontal	
Bubble	Method 1	Method 2	Method 1	Method 2
	Pa	Pa	Pa	Pa
1	4696	10433	16524	36712
2	2394	3336	8424	11739
3	1735	2421	6167	8518
4	1266	2199	4465	7737
5	1316	2297	4633	8083
6	1449	2620	5099	9218
7	1452	**3279**	5110	**11540**
8	1799	4490	6331	15799
9	3584	6833	12610	24043

$$p_{total} = max(p_{internal}) + p_{ambient} \tag{4.22}$$

Equation (4.7) is transformed into Equation (4.23) to determine the tensile force in the wall membrane. Each web consists of twice the material thickness since the sides of two cylinders are bonded.

$$\sigma_{wall} = p_{total} \cdot \frac{|O_1O_2|}{2t_{bladder}} \tag{4.23}$$

The resulting σ_{wall} is compared to $\sigma_{bladder}$. An output is given indicating whether the wall fails or not. A safety factor has already been included in the load calculation as specified in Section 4.8.3. A load factor for the failure check is therefore not needed. The numerical function outputs both the wall stress as well as the failure check result. The resulting wall stresses are presented in Table 4.5 and are discussed in Chapter 7.

Table 4.5: Wall stresses

	Unit	Anhedral	Horizontal
Pressure	Pa	327.9	1154
Membrane Force	N	707.21	2488.6
Membrane stress	$N \cdot m^{-2}$	$2.30 \cdot 10^7$	$4.32 \cdot 10^7$

4.8.7 Torsion

The wing stiffness is a function of the inflation pressure, and thus areo-elastic behaviour is a concern. The main concern for the canopy when considering torsion, is the resultant angle of twist at the tips. To examine wing tip deformation due to torsion, several static load tests were performed on inflated wings by Webber [25], Veldman [26] and Harvey [27]. However these analysis were restricted to circular cylindrical beams, while this wing structure is composed of a multibubble section.

A more recent study presents a simplified aerostructural static model (ASM) for inflated wings which takes into account a multicell design [28]. The airfoil used for the static model is a symmetric, NACA four-digit airfoil with 14 cells and a chord length of $0.384m$ and a torsion rigidity of 140 $N \cdot m^2$ was estimated. The tip deflection was studied for aspect ratios between 3 and 10. The results showed tip torsion angles of less than $0.6°$ at maximum dynamic pressure q_{max} for all aspect ratios. Torsional rigidity increases with the radius of a cylinder or the volume of a structure. Consequently, since this wing is at least 10 times larger than the prototype wing used for the ASM discussed, the deflection angle would

be even lower than 0.6°. However the magnitude of deflection appears to monotonically decrease with increasing inflation pressure.

The maximum pressure used for the ASM was 2.43 kPa which is much smaller than the 113 kPa used for this wing design. Since the volume ratio is much larger and so is the design pressure (which means higher rigidity), torsion is considered as a non-critical design criteria for the structural design. However, more detailed analysis of torsional rigidity is recommended for further analysis.

Following a method to estimate the torsional rigidity of this wing will be presented. The method consists of treating the wing as a linearly elastic cantilever beam with a torque load at the tip. The flexural rigidity can then be calculated with Equation (4.24) [29]:

$$GI_p = \frac{TL}{\phi} \tag{4.24}$$

Where GI_p is the torsional rigidity in $N \cdot m$, T the applied torque load, L the beam length and ϕ the angle of twist.

The total torque for a multibubble structure is the sum of the torques in each bubble:

$$T = T_1 + ... + T_n \tag{4.25}$$

Where n is the number of bubbles in the design. The torque for each bubble is a function of the shear flow q_s in N/m and the cross-sectional area A in m^2:

$$T = 2Aq_s \tag{4.26}$$

By determining the shear flow in each bubble the total torque can be determined. The rate of twist decreases with a higher internal pressure [29], thus a maximum allowable angle of twist can be set, and the internal pressure can be estimated with respect to this. Implementation of this method is left out of the numerical code due to its complexity while lacking precision, and more importantly that torsion is not considered to be critical for this design according to the literature discussed above.

4.8.8 Helium Lift Calculation

Using Equation (4.9a), the density of the helium in the wing has been calculated. The overpressure in the wing is 11.5 kPa at take-off, as has been calculated in Section 4.8, making the total pressure inside 1061 hPa. An assumption that has been made here is that the pressurised volume of the wing is assumed to be constant, so the wing structure is not expanding when located in lower air pressures at higher altitudes. This also means that the total pressure within the wing remains constant. The specific gas constant R for helium is 2077 and for air 287. The temperature T at take-off is 288.15 K and during cruise 268.15 K.

The pressurised volume of the wing will be 32.3 m^3. From this volume the weight of the air and the helium that can fit within the pressurised part of the wing has been calculated for take-off and cruise conditions using Equation (4.9b). Using Equation (4.9c), the lift provided by the helium has been calculated for take-off and cruise conditions, which is 329 N and 227 N, respectively, making the fraction of lift delivered by helium during cruise 8.3%.

4.8.9 Weight Optimisation

The final step in the code is to calculate the weight of the whole structure which includes the weight of the Tensairity® elements, bubbles and extra skin material to provide a smooth surface. Once the number of bubbles is fixed, the weight is calculated as a function of the number of ribs and thus attachment points for suspension lines.

The decision on amount of ribs for the canopy design was based on a trade-off between complexity and decrease in weight. The total weight of the canopy with a certain amount of ribs is presented in

Table 4.6. As can be observed for the anhedral section, the decrease in weight is small when increasing the rib from two to a higher number. Therefore a selection of two ribs has been chosen for the anhedral part. For the horizontal section the weight decreases considerably up to an amount of four ribs; after that the decrease is small, while adding to more lines would increase the drag considerably. Having 2 ribs at the anhedral sections and 4 ribs at the horizontal section leads to total structural wing weight of $6.7kg$. The two most outer ribs of the horizontal section overlap with the two most inner rib location of the anhedral section. Therefore a total amount of 6 ribs instead of 8 is counted. A graphical interpretation of the rib and spars location is sketched in Figure 4.6.

Table 4.6: Resulting weights for different number of ribs

Number of ribs	Unit	Anhedral	Horizontal
2	kg	**0.88**	8.12
3	kg	0.86	5.48
4	kg	0.86	**4.98**
5	kg	0.856	4.80
6	kg	0.85	4.72
Total weight	kg		6.75

4.9 Canopy Materials

The structure of the canopy consists of various components. The material of each component has to meet the requirements specific to the functions the component has to fulfil within the structure. In addition, a set of requirements common to all components flows down from the mission definition. The material design process starts with a functional description of each component in the canopy. The common requirements are added to this set. The set of requirements of each component is used as a validation to verify the materials meet the requirements in the final design.

The requirements common to all are the following:

- Environmental resistance (UV, temperature and moisture)
- Lightweight
- Available within 5 years
- Manufacturing process compatible with interfacing components
- Material and processing costs
- Low flammability
- Acceptable resistance to cyclic loading

The canopy structure is designed to withstand the amount of load cycles imposed during test flights and the mission flight itself. It is assumed that the amount of cycles is low compared to a standard commercial canopy. Therefore the fatigue resistance of the materials has not been a critical criterion during the selection process.

4.9.1 Bladder Material

The following criteria are used to judge whether a material is suitable for the multibubble bladder:

- Helium permeability
- Tensile strength and modulus
- Layer bondability, handling and joint strength

The selected bladder material is Mylar®. This high performance plastic film is widely applied to contain helium in lighter-than-air (LTA) applications such as ballooning and as heat insulation in space applications [30]. For example, in 2012 the record-breaking spacejump "Red Bull Stratos" by Felix Baumgartner utilised an helium inflated Mylar® balloon. The balloon is depicted in Figure 4.24. Mylar®'s tensile strength is high enough to withstand the wall stresses in the multibubble design. Its elasticity is low since it is a polyethylene, this ensures the canopy does not deform much as the cruise altitude is reached.

Figure 4.24: The Mylar® balloon used for the the Red Bull Stratos mission

Polyester films such as Mylar® are used for their high tensile strength, toughness, chemical and dimensional stability, gas barrier properties, high temperature resistance and low coefficient of friction. Additionally the material is creep resistant compared. Table 4.7 presents the relevant material properties for Mylar®.

Table 4.7: Material properties for Mylar® [(iii)]. TD means polymer orientation transverse of machine direction.

Property	Typical Value	Unit
Tensile strength TD	193.05	MPa
Modulus TD	4.9	GPa
Gas permeability helium at 0 $°C$	$1.47 \cdot 10^5$ [(iv)]	$m^3 \cdot m^{-2} \cdot h^{-1}$
Density	1390	$kg \cdot m^{-3}$
UL94 Flame Class	94VTM-2: Slow self extinguish	–
Approximate Cost	2 [(v)]	$€ \cdot m^{-2}$

The helium permeability is reported by the manufacturer to be 70 $cc^{-1} \cdot 100in^{-2} \cdot 24h^{-1} \cdot atm^{-1} \cdot mil^{-1}$ at a temperature of 0 $°C$. Assuming a material thickness of 0.35 mil (9 µm) and an 0.11 bar overpressure this is converted to $1.47 \cdot 10^5 m^3 \cdot m^{-2} \cdot h^{-1}$. According to Table 4.7 the flammability of Mylar® has to be dealt with to incorporate it in the canopy. A solution could be to extend the outside skin of ripstop nylon

[(iii)] URL `https://www.tapplastics.com/uploads/pdf/ProdData-PolyesterFilm.pdf`[cited on 20 January 2015]

[(iv)] URL `http://usa.dupontteijinfilms.com/informationcenter/downloads/Chemical_Properties.pdf`[cited on 20 January 2015]

[(v)] URL `http://www.professionalplastics.com/MYLARFILM`[cited on 20 January 2015]

such that it forms a fire protection layer between the solar cells and the bladder. Possibly aluminised Mylar® may also be used to effectively reduce the helium permeability and increase the heat resistance of the material [31][32].

Gluing techniques for laminates may be used to join the Mylar® layers [17]. These include hot-melt gluing (Ultra Bond™) and radio frequency (RF) activated gluing (Q-Bond™). The resulting joints can be stronger than the material itself. The joint strength may be limited by stress concentrations and possible delaminating. Acrylic tapes are also an alternative bonding method. In any case sowing is to be avoided as this creates leaks in the bladder material.

4.9.2 Skin Material

The PV cells are placed on top of the canopy. The remaining exposed bladder is then spanned with an outer skin made of ripstop nylon. This woven material is widely used in paraglider canopies and kite applications. Table 4.8 shows the relevant material properties for the ripstop nylon Skytex 27 and Figure 4.25 illustrates the texture of the material.

Table 4.8: Material properties for Skytex 27 ripstop nylon [(vi)]

Property	Value	Unit
Fibres	Polyamide (Nylon)	-
Thickness	6.6	μm
Surface Break Tension	13.12	kN
Weight Density	27	$g \cdot m^{-2}$
Approximate Cost	5 [(vii)]	$€ \cdot m^{-2}$

Figure 4.25: Skytex 27 ripstop nylon [(viii)]

The ripstop is tensioned when the bladder is pressurised. It then acts as an external skin which ensures the flow of air around the canopy collides with a surface which is smoothed of the bumps due to the multibubble structure. Ripstop has the advantages of being creep resistant, waterproof, water resistant and fire resistant.

[(vi)] URL https://www.tapplastics.com/uploads/pdf/ProdData-PolyesterFilm.pdf [cited on 20 January 2015]

[(vii)] URL http://www.opale-paramodels.com/index.php/en/shop-opaleparamodels/fabrics-nylon/fabrics/

4.9.3 Tensairity® Member Materials

The Tensairity® members serve two different purposes, namely tension and compression reinforcement. Therefore also two types of materials are selected for these members. Their characteristics are detailed in this section.

For the compressive reinforcement members carbon fibre composite rods are selected. Carbon fibre composite rods have a 60% higher strength to weight ratio compared to aluminium alloys. They are exceptionally stiff as well. Their outstanding weather resistance properties make them very suitable for stiffening the canopy. They are available in a wide range of standard dimensions, but can be made in custom dimensions as well.

The properties of this material are shown in Table 4.9.

Property	Value	Units
Compressive Strength	1.90	GPa
Compressive Modulus	131	GPa
Glass Transition Temperature	100	^oC
Density	1480	$kg \cdot m^{-3}$
Fiber Density	67	%
Approximate Cost	15 [ix]	$€ \cdot kg^{-1}$

Table 4.9: Typical material properties of carbon rods [x]

The tensile reinforcement members are made of Zylon®, a material consisting of PBO[xi] fibres. Zylon® is one of the strongest commercially available fibers. It is used by NASA in LTA weather balloons for long-duration data collection. Braided Zylon® strands reinforce the Mylar® superpressure structures. Zylon® has low weight, high tensile strength, and excellent thermal properties. Figure 4.26 illustrates flat Zylon® braids. Table 4.10 presents the relevant material properties.

Figure 4.26: Flat Zylon® braids used for sailboats

The cost of Zylon® is publicly unavailable. The reported value is a rough estimate. Furthermore, it is reported that the strength of Zylon® is significantly decreased by exposure to high humidity or high

[ix] URL `https://goodwinds.com/carbon/solid-flat.html`[cited on 20 January 2015]
[x] URL `http://gwcomposites.com/carbon-rods/`[cited on 20 January 2015]
[xi] poly(p-phenylene-2,6-benzobisoxazole))
[xii] URL `http://kiss.caltech.edu/study/airship/smoot.pdf`[cited on 20 January 2015]
[xiii] URL `http://www.toyobo-global.com/seihin/kc/pbo/Technical_Information_2005.pdf`[cited on 20 January 2015]

Property	Typical Value	Unit
Tensile Strength	5.8	GPa
Tensile Modulus	270	GPa
Glass Transition Temperature	650	^oC
Density	1560	$kg \cdot m^{-3}$
Approximate Cost	1'170 [xii]	$€ \cdot kg^{-1}$

Table 4.10: Typical material properties of Zylon® HM (high modulus) fibres [xiii]

temperature, and UV and visible light. Since the Zylon® fibres are to be laminated in between the walls of the reinforced members, this should not be a problem in this implementation. The manufacture of a prototype should confirm whether this is indeed the case. Otherwise Dyneema® fibres are a suitable alternative with slightly lower strength properties [33].

The Zylon® fibres are to be bonded to the bladder material. Most standard forms of bonding are suitable for fabrication including adhesive bonding, heat welding, ultrasonic welding, and laser enhanced bonding zylon.

4.9.4 Jet Flaps

Though the jet flaps get inflated with the principle of the ram air inflated paraglider wing, it is important to add extra reinforcements to make sure that the inflation results in the desired airfoil shape. To tackle this issue, the use of multiple minor ribs throughout the span of the trailing edge has been decided. Minor ribs are a common feature in reinforcing the trailing edge shape in paragliders. Since the outer trailing edge material is essentially just ripstop nylon, the minor ribs will play an important role in maintaining the shape.

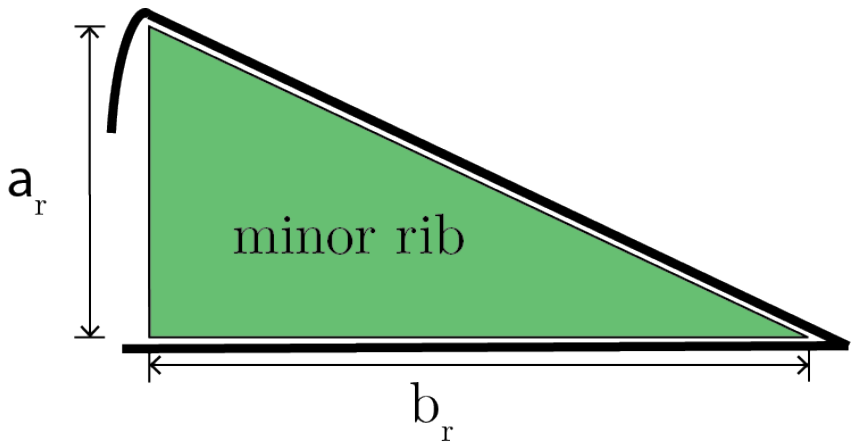

Figure 4.27: Trailing edge jet flap with minor rib

In Figure 4.27, a simple depiction of a minor rib is presented. The green shaded area represents the placement of the minor rib. The triangular shape of the minor rib is represented with the dimensions a_r and b_r. Since it is known that the jet flap, and subsequently the rib as well, accounts for 30% of the chord length, an estimation can be made for b_r and a_r. It has been calculated that for a chord length $c = 2.99\ m$, the dimensions of the rib are $a_r = 0.45m$ and $b_r = 0.90m$. Subsequently, the area for each minor rib has been calculated, with $A_{mr} = 0.20\ m^2$.

The Team has decided to use minor ribs made of a durable fibre Skytex 9017 and an E38A coating.

This decision has been made since these materials are used for minor ribs of other reference paragliders such as the Marvel[(xiv)] and the Envy[(xv)]. The materials for the minor ribs have an area density of 0.04 kgm^{-2}. Though minor ribs are used extensively in many paragliders, relevant data on the appropriate number required per length of wingspan is not available. Hence, the Team an educated estimation of the number of minor ribs required per length of wingspan is made. This has resulted in 4 minor ribs per meter throughout the entire span. For a wingspan b = 26.89 m the number of minor ribs required is 108. The total added mass due to the minor ribs is calculated at 0.87 kg.

4.10 Effect of Assumptions

One way of improving the accuracy of the numerical code is to adjust the assumptions made. The following list contains recommendations to improve the numerical design tool.

- *The solar panel weight is proportionally distributed over the bubbles it is placed on.* A more accurate description of this load can be made to increase the accuracy of the bending moment calculations.
- *The lift distribution is simplified to the lift at stall condition proportionally divided over the bubbles.* The pressure distribution calculated by the 2D airfoil software can be integrated over each section to increase the accuracy.
- *The bubble centres are placed on a single line.* The requirement for multibubble geometry in Equation (4.8) is not respected.
- *The chord wise spacing in between bubbles is equal for all pairs of adjacent bubbles* The bubble spacing may possibly be optimised to increase the accuracy of the airfoil approximation.
- *The thickness of used materials is so low that all calculated geometry can be represented by points and lines.* For manufacturing the thickness of the materials needs to be taken into account to obtain more accurate material calculations.
- *The suspension lines act vertically on the canopy.* The angle of the bridle w.r.t. the surface of the canopy is left out of the calculation for simplicity. The effect of neglecting the angles can lead to a slightly over-designed structure since the forces act now vertically, while an angle may also translate some of the load horizontally.
- *The bubbles in airfoil design are assumed to behave as pressurised cylindrical beams.* The more a pressurised object deviates from a circular contour, the higher the introduced bending stresses in the wall and the lower the structural efficiency become. Modelling this more precisely could lead to a heavier structure.
- *Constant distributed load over span due to rectangular wing shape.* A more optimal design could be reached by making the wing elliptical. This would alter the lift distribution, especially at the tips, where it tends to be lower. Since the outer suspension line is designed to keep the anhedral section in place, this suspension line could be designed for lower load cases. Furthermore an elliptical wing distribution has other advantages such as a higher Oswald factor. Further analysis on this could be done to optimise the wing design even more.
- *Zero angle of attack.* The wing will have an angle of attack during flight, especially during landing and take-off. For now the structural design was mainly focused on the cruise phase. The loads introduced in the system are a function of the lift provided by the wing. Since the lift is dependent on the angle of attack, so is the structural design if you incorporate it as a variable. The accuracy of the model can this way be improved and lead to a more efficient design.

[(xiv)] URL `http://www.macpara.com/en/marvel.html`[cited January 10 2015]
[(xv)] URL `http://www.macpara.com/en/paraglider-envy.html`[cited January 10 2015]

- *The effect of disturbances such as wind gust or control forces are negligible for the structural calculations.*These might introduce higher loads than expected. Therefore a safety factor must be applied. By incorporating a description of these forces intro the model will give a better idea of how big the safety factor should be, and whether these are critical for the design.
- $C_m = 0$ *for the airfoil.* This includes lift and drag forces. This is assumed for lateral stability. A positive or negative moment coefficient would alter the force distribution in the two suspension lines as described in Section 4.8.2.
- *The system is in equilibrium thus steady symmetric flight.* In order to analyse the applied forces of a structure, force and moment equilibrium are the first step. To simplify this cruise condition is assumed. To approximate landing and take-off conditions better the model must be adjusted for parameters such as angle of attack, flight velocity and thrust.

Table 4.11 contains the output to the other technical groups. These parameters are used as input in the design integration script and in all other calculations. The total canopy cost is a broad approximation. It is based on the raw material cost and the labour cost for a month of 5 constructors (assuming 5 workers required would be a cost of €15'000 a month).

Table 4.11: Output data from the canopy structures group

Parameter	Unit	Value
Canopy Structural Weight	kg	6.75
Canopy Internal Volume	m^3	32.3
Helium Lift Take-off and Landing	N	329
Helium Lift Cruise	N	227
Bladder Design Pressure	kPa	113
Total Canopy Cost	€	16'800
Total Bridle Line Length	m	140.4

5 Fuselage Structures & Materials

The fuselage of the PPG is the housing of the majority of subsystems as well as the protection for the pilot. The pilot has to be protected during flight and emergency situations. This chapter talks about the fuselage, its structure and all the materials involved in it. In Section 5.1 the different load cases for the fuselage are explained. The different failure modes and the fuselage model are described in Section 5.2. Section 5.3 shows the results of the investigation of sensivity of the results. Section 5.4 the materials for the fuselage are discussed. In Section 5.5 the load carrying frame structure is explained. The canopy connectors and the motor frame are presented in Section 5.6 and Section 5.7, respectively.

5.1 Load Cases

The fuselage has to carry all the loads during operation and during extreme circumstances. For the design of the fuselage the following load cases have been taken into account.

- In-flight loads
  - Cruise flight with fully loaded aircraft at full thrust
  - A turn of $2G$ with a fully loaded aircraft at full thrust
- Controlled belly landing
- Emergency water landing

With the load cases a safety factor of 1.5 will be implemented in the fuselage design, as required by American Society for Testing and Materials (ASTM) regulations.[34]

5.1.1 Flight loads

The flight loads at cruise have a load factor of 1 with a fully loaded aircraft at full thrust and a 2 G load factor for a turn. In Figure 5.1 the flight load case is shown. The weight of the fuselage frame is distributed over the different components of the airframe structure.

5.1.2 Belly landing loads

Figure 5.2 shows the forces acting on the fuselage during a belly landing. The thrust will be set to zero. After completing the full mission, the PPG will perform a controlled belly landing. Limits have been set for the maximum approach speed, which shall not be greater than 5 $m \cdot s^{-1}$, and the maximum approach angle has been set to a value of 5°. Further assumptions that have been made are:

- The weight is a point load acting on the c.g. of the fuselage.
- The skin carries no loads.
- The thrust force is set to zero (during approach phase).

Using these assumptions an analytical solution for the belly landing has been calculated. In Figure 5.4 the simplified free body diagram and kinetic diagram are shown. Via Newton's second law the horizontal and vertical component of the impact force have been found, as shown in Equation (5.1a) and 5.1b.

$$F_{impact,x} = m \cdot a_x \tag{5.1a}$$

$$F_{impact,y} - W_{fuselage} = m \cdot a_y \tag{5.1b}$$

The time frame of impact is in the order of 0.2 s [35]. Combining the time frame with the velocity, the relation for the declarations a_x and a_y can be found. The impact forces are found to be 4.5 kN in vertical direction and 2.4 kN in horizontal direction. Dividing the impact force over the length results in a (uniformly) distributed impact load for the belly landing.

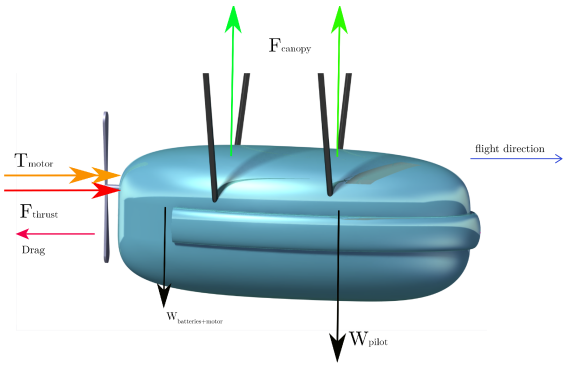

Figure 5.1: Flight load

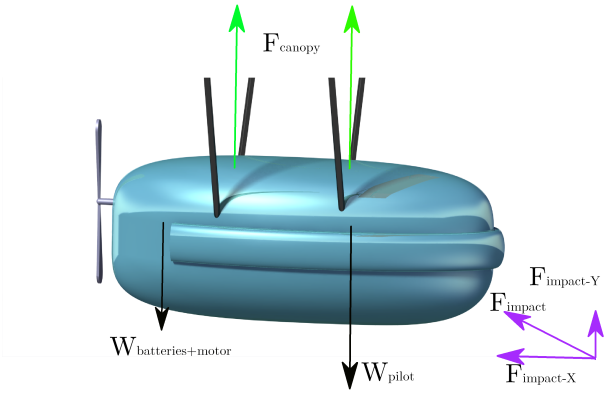

Figure 5.2: Belly landing load

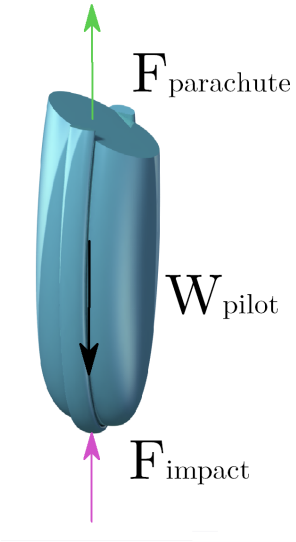

Figure 5.3: Water landing load

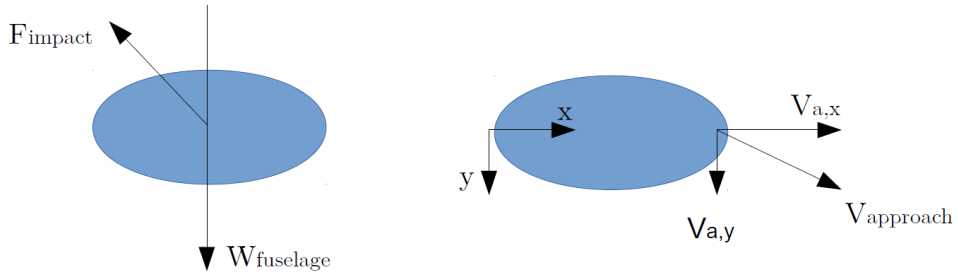

Figure 5.4: Free body diagram and kinetic diagram for the belly landing

5.1.3 Emergency water landing loads

The emergency water landing will be the most critical load case for the fuselage design. Figure 5.3 shows the loads acting on the fuselage during the water landing. During emergencies the motor and batteries are ejected and therefore not shown in the free body diagram. The peak impact force will be the determining factor for the fuselage sizing, after a material choice for the frame structure is made in Section 5.4.

The most critical load case for the fuselage structure is the load when performing an emergency landing on water. The emergency parachute will decelerate the fuselage when falling, such that the vertical impact velocity on the water is (equal to the parachute sink rate) $v_0 = 5.5\ m \cdot s^{-1}$. For the following calculations a number of assumptions have been made.

- Drag, weight and buoyancy forces are disregarded.
- The geometry of the fuselage is approximated by a cone.
- The instant of impact is neglected, since the impact force will be infinitely large at that moment.
- The water surface is assumed to be undisturbed during impact (e.g., no waves).

A first order estimation can be made using the 2D method of Von Karman [36]. This method assumes the conservation of momentum at impact, as shown in Equation (5.2). The starting point has been used to derive a 3D equation. It is implied that the impacting body moves a certain volume of water, which is used to find the mass after impact [37], together with the ocean´s density $\rho_{water} = 1027\ kg \cdot m^{-3}$ [(i)]. m_0 is the mass of the fuselage without batteries and propeller (since they are dropped before the emergency landing), v_0 is the impact velocity, m_v the (virtual) mass of water moved by the impact and v is the velocity after impact.

$$m_0 \cdot v_0 = (m_0 + m_v) \cdot v \tag{5.2}$$

The shape of the fuselage is approximated by a cone with circular base of radius $R_{eq} = 0.81\ m$ and a total height of $h = 3\ m$, based on the fuselage dimensions, shown in Figure 5.5, while its actual shape is close to an ellipsoid with $r_a = 0.5\ m$, $r_b = 0.65\ m$ and $r_c = 1.5\ m$, visualised in Figure 5.6, explained in more detail in **??**. The equivalent base radius, R_{eq}, was found using an equivalent volume of an ellipsoid with the mentioned dimensions. The centre of gravity is assumed to be located at the line of symmetry of the fuselage.

Virtual mass of the (partial) sphere of water is now calculated using Equation (5.3) [37], with a shape factor of k=0.75, as used in [38], and h the depth of immersion.

$$m_v = \frac{4}{3}\pi h^3 \left(\frac{R_{eq}}{h_{max}}\right)^3 \rho_{water} k \tag{5.3}$$

As can be seen in Equation (5.3), the virtual mass is dependent on the depth of immersion, which determines the local radius of the fuselage at the water surface, x.

$$x = h\left(\frac{R_{eq}}{h_{max}}\right) \tag{5.4}$$

[(i)] URL `http://www.windows2universe.org/earth/Water/density.html`[cited 12 January 2015]

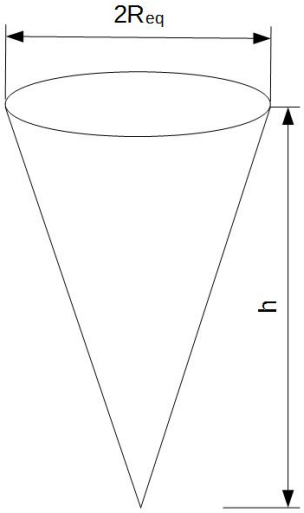

Figure 5.5: Approximated cone shape

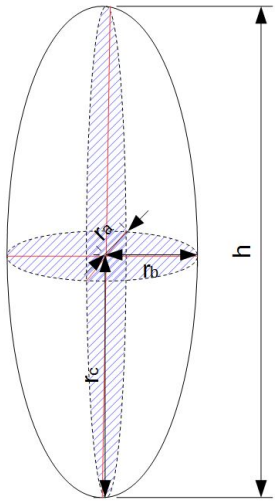

Figure 5.6: Ellipsoid geometry of the fuselage

The expression in Equation (5.3) can now be substituted in Equation (5.2) to find an expression for the velocity V as a function of x.

$$V = \frac{m_0 v_0}{m_0 + \frac{2}{3}\rho_{water}\left(\frac{h_{max}}{R_{eq}}\right)^6 x^3 \pi k} \tag{5.5}$$

$$\begin{aligned} a &= \frac{dV}{dt} \\ &= \frac{d^2h}{dt^2} \\ &= \frac{d^2x}{dt^2}\left(\frac{h_{max}}{R_{eq}}\right) \end{aligned} \tag{5.6}$$

with

$$\frac{d^2x}{dt^2} = \frac{d}{dx}\left[\frac{1}{2}\left(\frac{dx}{dt}\right)^2\right]$$

The G-load can be derived by using the derivative definition of acceleration and velocity, as shown in Equation (5.6). In Equation (5.7) the acceleration is given in terms of x. Figure 5.7 shows the loading ratio a/g vs. x, with a peak load of 15 G, as well as the velocity change during impact. Comparing the peak load with reference values for reentry vehicles, the value seems to be in a reasonable order of magnitude [38][39].

$$a = \frac{{m_0}^2 {v_0}^2 \frac{R_{eq}}{h_{max}}}{\left[m_0 + \frac{2}{3}\rho_{water}\left(\frac{h_{max}}{R_{eq}}\right)^6 x^3 \pi k\right]^3}\left[-2\rho_{water} x^2 \left(\frac{h_{max}}{R_{eq}}\right)^6 \pi k\right] \tag{5.7}$$

5.2 Fuselage Model

Before describing the fuselage model in Section 5.2.2, the frame´s failure modes are briefly explained in Section 5.2.1.

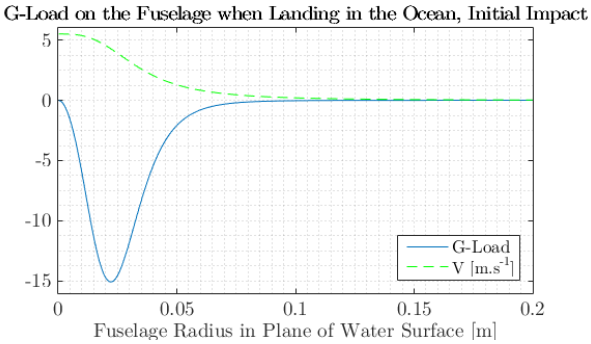

Figure 5.7: G-load for initial impact

5.2.1 Failure Modes

For the fuselage frame two failure mode checks have been done, the first one being the Von Mises stress criterion and the second failure mode being buckling. With the Von Mises stress criterion, shown in Equation (5.8), a beam fails when the Von Mises stress times the safety factor of 1.5 is larger than the yield stress of the material. A beam fails under buckling when the applied normal forces exceeds the buckling load of the beam. For buckling the safety factor of 1.5 is applied as well. The buckling equation is given in Equation (5.9). Factor K in Equation (5.9) depends on how the beam is supported. For simply supported beams K equals 1 and for clamped beams K is equals to 0.5.

$$\sigma_{vm} = \sqrt{\sigma_x^2 + 3\tau^2} \tag{5.8}$$

$$P_{cr} = \frac{\pi^2 EI}{(KL)^2} \tag{5.9}$$

5.2.2 Model description

To model the impact, the fuselage has been represented as a simply supported beam with a distributed load (see Figure 5.9). To model the fuselage frame as a beam, the equivalent moment of inertia of the fuselage frame has been calculated. The equivalent moment of inertia of the fuselage is taken with respect to the cross-section of the fuselage. A representation of the cross-section can be found in Figure 5.8. To find the equivalent moment of inertia, Steiner´s theorem has been used, as shown in Equation (5.10). In the beam model the curvature of the beam has been neglected, while in reality the frame structure follows the fuselage´s ellipsoidal shape.

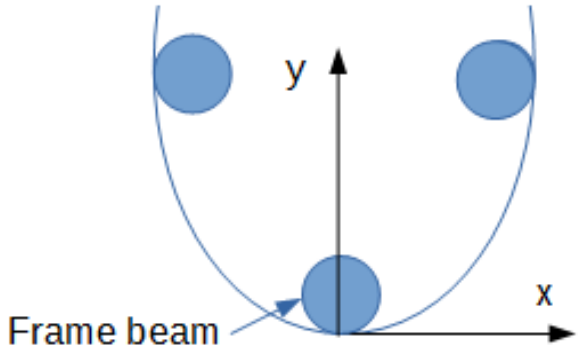

Figure 5.8: Cross-section of the fuselage frame

$$I_{equiv} = I + A \cdot dy^2 \tag{5.10}$$

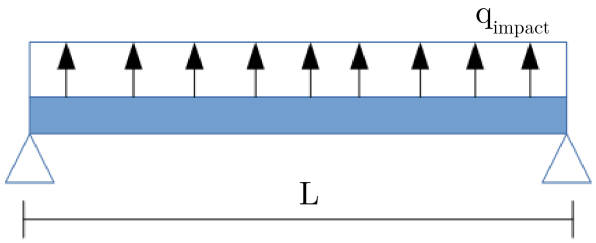

Figure 5.9: Simply supported beam with distributed load

The normal stress has been found using Equation (5.11), The shear stress distribution is given by Equation (5.12). The maximum shear stress occurs at the neutral axis of the beam. For this case the first moment of area, Q, is found using Equation (5.13).

$$\sigma_x = \frac{My}{I} \tag{5.11}$$

$$\tau = \frac{VQ}{It} \tag{5.12}$$

$$Q = \frac{1}{2} \cdot (R_o + R_i)(\pi R_o^2 - \pi R_i^2) \tag{5.13}$$

Normal and shear stresses from Equation (5.11) and 5.12 have been substituted in Equation (5.8) to check for failure. Using this method the inner and outer radii for the beams can be sized accordingly. As already mentioned, the critical load case is the emergency water landing. The load is, with a value of 15 G far bigger than the belly landing loads. The initial impact will be on the nose of the fuselage (see load cases Figure 5.3 as reference), which will be modelled as a beam with a length equal to the width of the airframe. Checking the beam model for the emergency impact load for Von Mises stress and buckling failure will result in a minimum inner and outer radius of the beam model to support the load. The beam radii found for the emergency water landing load case will be implemented in the entire fuselage frame. Further calculations and a more accurate (numerical) model will show that not all members of the frame structure have to support equal loads which will most probably result in them having different thicknesses (e.g., different inner and outer radii) .

5.3 Sensitivity

The design load case for the fuselage is the emergency landing on water. The calculations of this load case depend on the mass of the fuselage and the downward velocity. To check the sensitivity, one parameter has been changed while keeping the other one constant. In Figure 5.10 and 5.11 spider plots of changing the mass or the velocity have been made. The standard case is for mass of 40 kg with an impact speed of 15 $m \cdot s^{-1}$ and an impact load of 15 G.

When the mass was increased by 50%, the G-load decreased by 15%. The inner and outer radii for the fuselage frame will remain the same, resulting in an equal fuselage weight.

Increasing the velocity by 50% will give a load increase by a factor of two. This will result in a weight increase of 50%. Decreasing the velocity by 50% will decrease the G-load by 80%. This G-load will be in the same range as the load of the belly landing. Reducing the speed of impact during a water landing has a great effect on the total G-load. Additional research on how to decrease the impact velocity is desirable.

5.4 Fuselage Materials

The fuselage has to guarantee the safety of the pilot at all times during operation. In order to do so, suitable materials have to be chosen. Certain requirements have been set for the frame material:

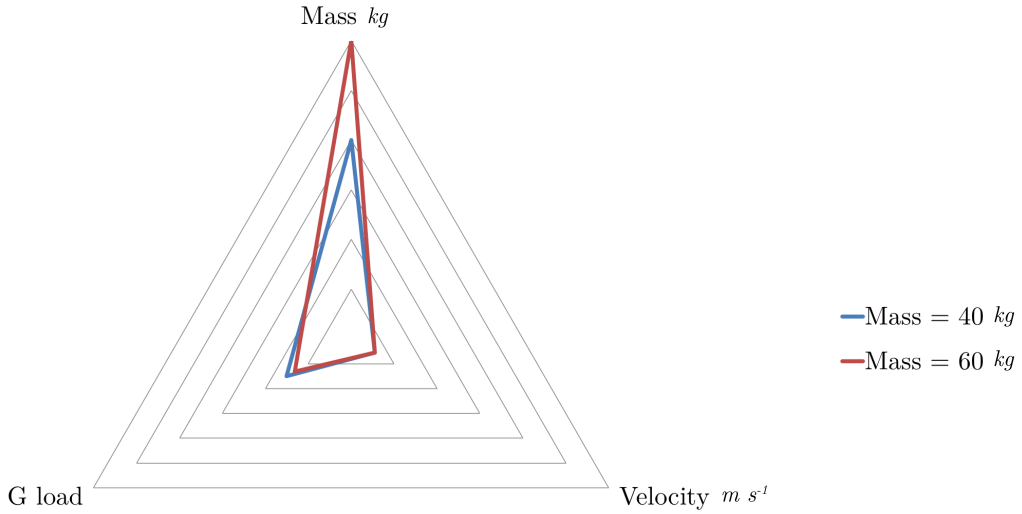

Figure 5.10: Spider plot showing sensitivity to change in mass

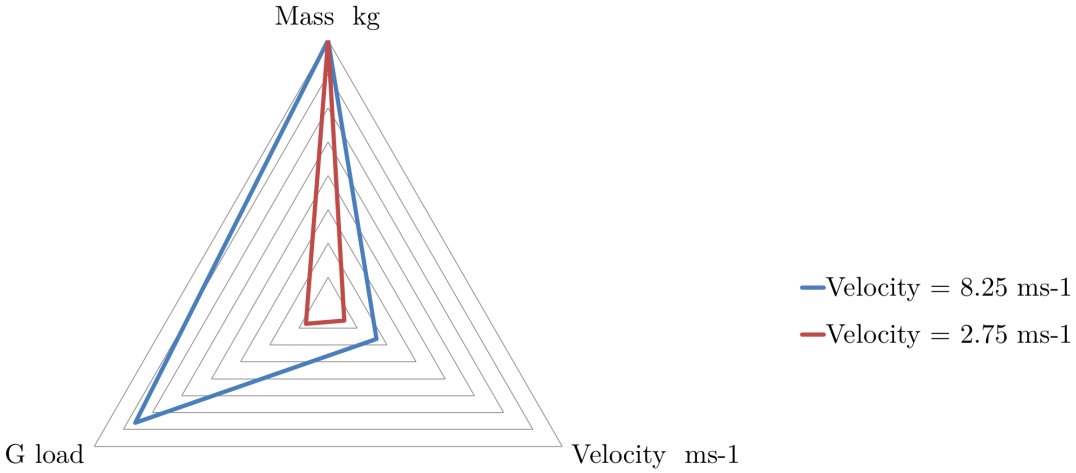

Figure 5.11: Spider plot showing sensitivity to change in velocity

- Perform under different types of loading: Bending, torsion, shear, tension and compression
- High strength combined with low density
- Manufacturability in curved shapes
- Water resistance
- Water tightness

During the trade-off, materials like steel and titanium were taken into account. Yield strength and Young's modulus of steel and titanium are promising, but because of their high densities they where discarded. Aluminium has a high strength in combination with a relatively low weight and seems to be the suitable for the load carrying structure. Aluminium is also widely used in aerospace applications. For the frame structure aluminium 6061 T651 has been chosen. Al-6061 T651 is able to carry the loads for all load cases and is cheaper than stronger aluminium alloys. After a more detailed analysis of cost and loads it might be chosen for a different material if weight can be saved ore safety increased.

For the skin of the fuselage the choice to use a carbon composite has been made. It has been chosen to use TORAYCA® T300, which is also used in aerospace applications. The composite structure uses a Toray 250°F epoxy resin and the values of the composite are normalised to 60% fibre volume.

The pilot needs a way to look outside and to check the canopy. Therefore in the front of the fuselage a window will be placed. Certain requirements have been set for the window.

- Impact resistant
- Watertight
- Airtight

For the window of the fuselage a reference window has been chosen. This has been done since the current fuselage model does not give a load distribution across the skin of the fuselage. As a reference window a window made of PLEXIGLAS® has been chosen. PLEXIGLAS® windows are used in the general aviation and comply with aviation regulations. The values for the materials chosen for the design are shown in Table 5.1.

Table 5.1: Material properties chosen in the fuselage design

Material	Young's modulus GPa	Yield strength MPa	Density kgm^{-3}	Cost €$\cdot kg^{-1}$
Aluminium 6061 T651 [(ii)][(iii)]	68.9	310	2700	4.0
TORAYCA® T300 [40][41]	130	1570	1760	14.0
PLEXIGLAS® [42]	3.3	80	1190	

5.5 Fuselage Frame

The beams of the fuselage frame will have a circular cross-section with a constant inner and outer radius. The fuselage frame can be seen in Figure 5.12. The fuselage frame consist of a central ring, a bow structure and three vertical rings. The two rings at the back will be used for the connection of the canopy and the fuselage structure. On the front ring, the window frame will be attached. The window frame is represented by two beams from the bow of the fuselage to the central ring. The total mass of the fuselage frame will be 40 kg which will cost about € 335 in materials. See Table 5.1 for the material details of the fuselage. The fuselage will have a length of 3.0 m, width of 1.0 m and a height of 1.3 m. The production of the fuselage should take place as close as possible to the take-off site. The average (gross) monthly salary in the USA is $ 2928[(iv)]. Assuming 5 workers required would be a cost of € 13'000 a month.

5.5.1 Window

An important design criteria for the window is that the window will remain watertight. During as emergency water landing, the fuselage will be submerged for a short period of time. Thus a good watertight sealing of the window is critical. The window also acts as a door for the pilot to enter the fuselage. For future research in window design, see the recommendations in Section 9.2.

During landing procedures the pilot has to be able to see the runway. Therefore the window has to be placed such that the pilot can look over the nose of the fuselage. The overnose angle, the angle defined by the pilots view to look over the nose of the aircraft, has to be between 5 to 10°[43] for general aviation. The overnose angle is defined by Equation (5.14)[43]. Using the approach speed and angle defined in Section 5.1.2, an overnose angle of 6.5° has been found.

$$\theta_{nose} = \alpha_{approach} + 0.04 \cdot v_{approach} \tag{5.14}$$

[(iv)] URL `http://www.worldsalaries.org/manufacturing.shtml` [cited 20-01-2015]

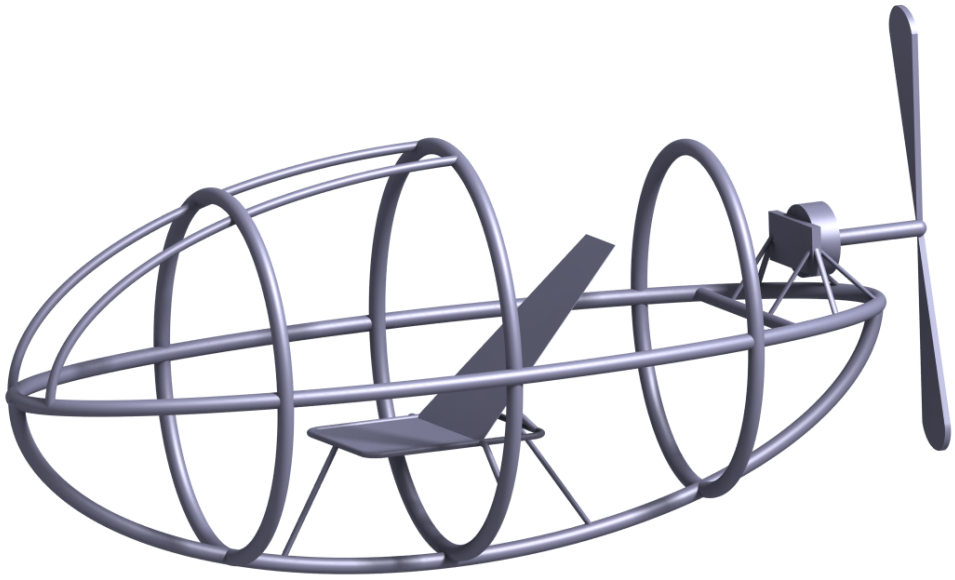

Figure 5.12: Fuselage frame structure

5.6 Canopy Connectors

The fuselage of the PPG is suspended below the canopy. Therefore the lifting force of the canopy needs to be transferred to the fuselage a the connecting system. The connection systems has to be able to hold a $2G$ turn with a safety factor of 1.5. Assuming that one side will hold up to 70% of the total lifting force, results in a 3.1 kN force per line on the loaded side. The lines between the canopy and the fuselage will be SL Dyneema® fiber braided paraglider rope [(v)]. The lines from the fuselage will be the 12 by 1 strand with a diameter of 2 mm. The 12 by 1 strand has a breaking load of 4.3 kN. Near the canopy, the lines split up into three different lines. From the split up point, the lines will be the Dyneema® 4 by 1 strand with a diameter of 1 mm and a breaking load of around 1.1 kN.

The attachment points for the canopy are located at the top side of the fuselage. In total there are four points, two on either side. As a way to connect the lines to the fuselage the choose has been made to use U-bolts (see Figure 5.13). For the attachment point the PSB-UBOLT[(vi)] has been chosen. The break load of the PSB-UBOLT is 110 kN. The PSB-UBOLT is over designed for the load case, this is due to the emergency system. In case of an emergencies the canopy has to be able to detach from the fuselage. For this a 3-ring release system will be implemented. In Figure 5.14 a representation of a 3-ring system is shown. When the pilot pulls the release lever, all the pins in the 3-ring system will be pulled, which releases the canopy from the fuselage. Therefore the biggest diameter of the three-ring system has to fit through the PSB-UBOLT. The four U-bolts will have a total mass of 0.6 kg and an assumed cost of € 40. The four three-ring system will have an assumed mass of 2 kg and a cost of € 140[(vii)].

5.7 Motor Frame

The motor frame has to hold three types of load: weight, thrust and torque. The motor will be attached to an aluminium plate via four bolts. This plate is supported by a frame. Two bars on the side of the

[(v)] URL `http://www.jeelysports.com/e_productshow/?179-Dyneema-Spectra-Braided-Paraglider-Rope-179.html` [cited 14-01-2015]
[(vi)] URL `http://www.pegasusdesigns.com.au/` [cited 15-01-2015]
[(vii)] URL `http://www.aerofoam.com/3_ring_release.htm` [cited 16-01-2015]

Figure 5.13: U-bolt[a]

[a] URL http://www.hardwin.in/product.html[cited 25-01-2015]

Figure 5.14: Three-ring system[a]

[a] URL http://houston.skydivespaceland.com/3-ring-maintenance/[cited 25-01-2015]

plate to support the motor and four bars diagonally attached to the main fuselage frame. All the beams of the motor frame will have the same radius and thicknesses. Certain beams will therefore be over designed. For ease of manufacturing and assembly of the frame this has been decided. A representation of the motor frame structure can be seen in Figure 5.15.

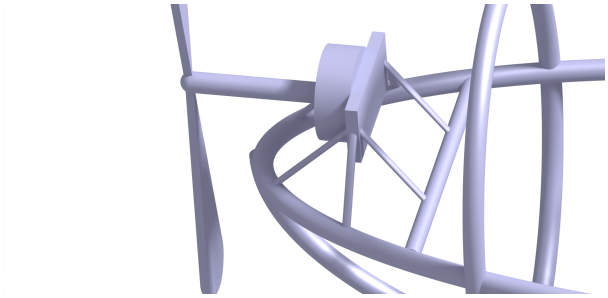

Figure 5.15: Motor frame structure

Table 5.3 summarises the most important output data for the calculations of the fuselage group. The only output used as an input by other groups was the fuselage mass with a value of 40 kg.

Table 5.3: Output data from the fuselage structures group

	Unit	Value
Skin thickness	m	0.001
Frame element R_o	m	0.025
Frame element thickness	m	0.003
Impact load	G	15
Structural fuselage mass	kg	40

6 Aircraft Subsystems

Several subsystems are required in order to fly safely across the Atlantic. The PV cells on the canopy are the main source of power for this flight, but this power should be transferred to the motor and the electric subsystems, therefore a power system is designed. In addition to the power system, the power management system is designed. The power system, accompanied with the power management system, make sure that the right amount of power is provided at the right time during the mission. Furthermore, the pilot should have access to information regarding the heading, velocity and altitude of the paraglider throughout the flight. The health and safety of the pilot should be ensured. The paraglider uses a take-off cart system to take off in a safe manner. The configuration of the aforementioned subsystems is treated as well. An overview of the total system is presented to show the interactions between all the systems used in the paraglider. The decision has been made to use COTS components when available, since these systems are more reliable and easier to validate.
The most important subsystems that are discussed in this chapter are the following; The power system is discussed first, followed by the power management system in Section 6.2. Then the navigation and communication is discussed, followed by health and safety, the take-off and landing system and the configuration of the subsystems in the fuselage. Finally an overview of the subsystems is given in Section 6.7.

6.1 Power System

In order to power the paraglider a power system is needed. This system contains both a method to generate power and a mechanism to store the generated power when it is abundant. The power system consists of:

- PV Cells
- Battery
- Motor
- Propeller

For each of these components either the configuration has been determined in [14, Chapter 4] or at least the required specifications have been determined with help of Design Option Trees (DOTs). The Power Management System (PMS) is treated separately in Section 6.2. To be able to size the power system the mission profile has been determined first. The power system has been sized to be able to sustain steady, climbing flight conditions during climb phase.

6.1.1 Power profile

To be able to size the power system the mission profile and duration has been determined. In Figure 6.1 the mission profile is found. As treated in Section 1.4 the cycle of the mission is 32 h after which the cycle starts at t_{sun} again. The power system has been designed to sustain one cycle. When the cycle is completed the mission will continue in the phases during t_{sun} and t_2. In the phase during t_{sun} the battery is charged for the phase during t_2 so no extra batteries or PV cells are needed to complete the mission.

The mission profile consists of five parts, it starts off with t_{cl} which is the required time to reach cruise altitude. After this phase, the phase of t_1 is initiated. During t_1 the aircraft is in cruise phase during darkness and is operated by the batteries which are charged beforehand. When t_{sun} starts the aircraft receives daylight and the aircraft is powered by the power generated by the PV cells. The fourth phase is the second cruise phase in darkness and has a duration t_2. The required energy for this phase is generated in the cruise phase during daylight and stored in the batteries. When t_2 ends the cycle starts over again from t_{sun} to t_2. The power system has been designed to have no limitation to the amount

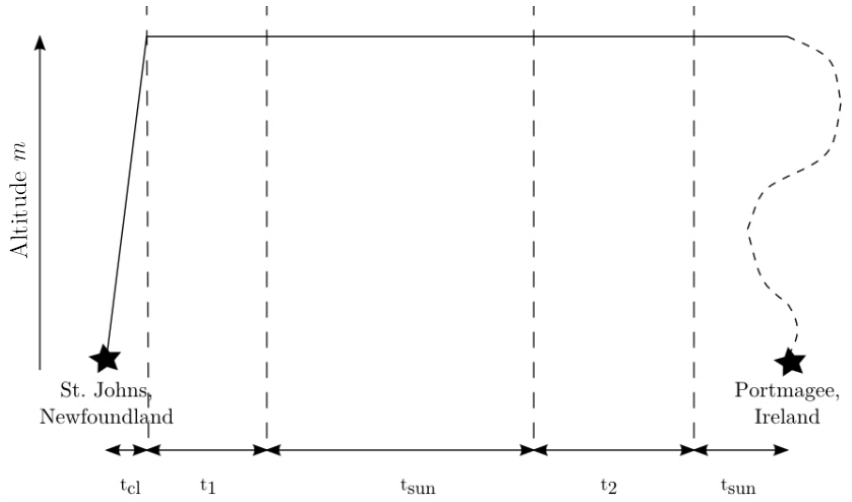

Figure 6.1: Mission profile

of cycles performed during the mission, to ensure this a safety factor for the required energy has been implemented so that the aircraft can reach the destination at cruise altitude after exactly one cycle. When the destination has been reached the aircraft will loiter until it has landed. The duration of this period is specified by t_{des}.

6.1.2 Power budget tool

Using the mission profile the power system has been sized. This sizing is done with help of a power budget tool, which has been built in MATLAB®. With this tool the required power at every moment during the mission has been calculated. For the climb phase the available power has been calculated using Equation (6.1) and the power system for this phase has been sized accordingly. It is desirable to exit the climb phase as soon as possible, so the aircraft operates with the maximum power that is accessible.

$$P_a = T_{max} \cdot v_t \cdot \eta_{prop} \tag{6.1}$$

in this equation P_a is the power available in W, T_{max} is the maximum thrust that can be delivered by the propeller in N, v_t is the true airspeed in $m \cdot s^{-1}$, η_{motor} is the motor efficiency and η_{prop} is the propeller efficiency. The available power is limited by the thrust that can be produced by the propeller. The power system has been sized such that it can deliver the maximum available power to the propeller. Therefore the available power is limited by the maximum thrust of the propeller, compensated by the efficiency of the propeller. This power available is set equal to the power required during climb phase.

During cruise phase the power system has been designed to deliver the power required. This required power is calculated with Equation (6.2).

$$P_r = \frac{W_{total}}{GR \cdot \eta_{sys} \cdot \eta_{prop}} \cdot v_t + P_{sub} \tag{6.2}$$

in this equation P_r is the power required in W, W_{total} is the total weight of the aircraft in N, GR is the glide ratio of the aircraft, η_{motor} is the motor efficiency, η_{prop} is the propeller efficiency and P_{sub} is the power demand of the subsystems in W. The required power depends on the power that is needed to perform sustained flight, then the required power is multiplied with the efficiencies of the system and the propeller and the added power that is required to power the subsystems to find the total required power as described in Equation (6.2).

The duration of the mission has been calculated by calculating the duration of each phase. The maximum continuous time that the aircraft operates in darkness is calculated utilising Equation (6.3).

$$t_{dark} = 24 - t_{sun} \tag{6.3}$$

where t_{dark} is the continuous time of darkness in h and t_{sun} is the amount of sun hours per day in h. As the duration of the period of darkness is calculated, the size of the PV cells and the battery can be calculated. The method for calculating the specifications of the PV cells and the battery mass are discussed in more detail in subsections 6.1.3 and 6.1.4. The duration of the cruise speed has been determined by dividing the remainder of the to be covered distance of 3'040 km, by the ground speed of 26.5 $m \cdot s^{-1}$. This has resulted in a mission duration of 38 h. The mission set-up and duration of each phase can be found in Table 6.1.

Table 6.1: Mission set-up

	Unit	Value
t_{cl}	h	1.5
t_1	h	5.7
t_{sun}	h	16
t_2	h	8
t_{des}	h	1
t_{dur}	h	38

6.1.3 PV Cells

PV cells are required to generate enough power for the aircraft during cruise phase in daylight and to generate enough power to store in the batteries for the second phase in darkness. As stated in the MRR the PV cell of choice is the ZTJ. The ZTJ is a triple junction InGAP/InGaAs/Ge cell; it's specifications are found in Table 6.5[(i)]. To transform the efficiency to PV panel efficiency, the PV cell efficiency has been multiplied with the smallest conversion factor of the remaining examined PV cells of 0.85. This results in a PV panel efficiency of 25%.

Table 6.3: PV cell characteristics

	Units	ZTJ
Type of cell	-	Triple junction InGAP/InGaAs/Ge
Efficiency	-	0.295
V_{oc}	V	2.726
J_{sc}	$A \cdot m^{-2}$	174
V_{mp}	V	2.41
J_{mp}	$A \cdot m^{-2}$	165
Area	m^2	$2.66 \cdot 10^{-3}$
Area density	$kg \cdot m^{-2}$	0.84

The PV cells have to generate enough power for both the duration of t_{sun} and t_2 during the period of sunlight. To determine the amount of area of required PV cells the irradiation has been calculated and the conversion efficiencies of the system have been determined. Using Equation (6.4) the required area of PV cells has been calculated.

[(i)] URL `http://www.emcore.com/wp-content/uploads/ZTJ-Cell.pdf`[cited 9 January 2015]

$$A_{pv} = \frac{E_{req_{pv}}}{E_{pv} \cdot \eta_{pv} \cdot \eta_{sys}} \tag{6.4}$$

in which A_{pv} is the PV cell area in m^2, $E_{req_{pv}}$ is the required energy to be delivered by the PV cells during sun hours in J, E_{pv} is the energy delivered by the PV cells per squared meter during sun hours, all safety factors included, in $J \cdot m^{-2}$, η_{pv} is the PV cell efficiency and η_{sys} is the conversion efficiency. The curvature of the canopy is, for simplicity, not included in the calculation.

This required PV area has been multiplied with a safety factor of 1.05 to take into account the fact that the given area in Table 6.5 is for a PV cell only and not for a PV module, which will have a reduction in energy delivered per squared meter as elements are added that do not contribute to the generation of PV power.

To calculate the mass of the PV cells the energy density is required. Again, only the specifications are given per PV cell. Based on tests of the respective solar cells[44] the energy density has been determined to equal 1.234 $kg \cdot m^{-2}$. The specifications of the PV panel have been presented in Table 6.5. A safety factor of 1.05 has been included in the design of the PV cells to take into account any shading, collecting dust on the PV panel or any other defunct that can result in a lower power output. This safety factor is included in E_{pv} as well. The safety factor is low as a safety factor already has been incorporated in the mission profile, since the mission profile incorporates a safety factor.

Table 6.5: PV panel specifications

	Units	
$E_{req_{pv}}$	J	$3.38 \cdot 10^8$
E_{pv}	$J \cdot m^{-2}$	$1.28 \cdot 10^7$
A_{pv}	m^2	33.2
Energy density	$kg \cdot m^{-2}$	1.234
m_{pv}	kg	41.0

The PV cells are located on top of the canopy. This is such that the PV cells have maximal sun coverage and it is easier to implement in the design. When the PV cells are located on the structure the angle of inclination is smaller and the cells can be covered in the shadow of the canopy. Next to that it would add complications during an emergency landing. As has been found that the required area of PV cells fit on the canopy the option to place PV cells on the structure has not been thoroughly investigated.

A sun tracking system has also been deemed undesirable as the required amount of solar power can be generated with the available canopy surface. Adding a sun tracking system would only increase the weight and complexity of the design.

The lay-out of the PV panel should be such that it delivers the right amount of power, voltage and current for the system. To provide the maximum amount of power a Maximum Power Point Tracker (MPPT) is implemented. A MPPT searches for the optimal point in the I-V curve of the PV cell or panel and makes sure it operates at that point to maximise its power output[45]. Two MPPTs per module have been implemented. This is due to the fact that too many MPPTs will severely increase the weight and complexity of the panels, but too few will limit the efficiency at which the PV cells operate. The MPPTs are located at the canopy, their detailed working is explained in Section 6.2.

Voltage and current of a PV panel can be controlled by setting a number of cells in parallel or series. The two main recipients of power from the PV cells are the battery and the motor. The voltage and the current are however controlled by the power cables in this case. The power cables have to transfer the power from the canopy to the fuselage. Therefore as many cables as possible are desirable to split the load. However, due to increased drag the cables should be kept to a minimum. Therefore the power is transferred through one cable, rated at 600 V. As the current that is required is to be kept to a minimum

for safety and dividing the cells into modules reduces the risk. When one of the modules experiences a fatal failure the other modules can still deliver power.

Another constraint for designing the PV lay-out is the number of cells. To deliver the required power for cruise phase a total number of 7'021 PV cells are required. Modules should however consist of equal numbers of PV cells. The modules have been designed such that the excessive amount of PV cells is kept to a minimum to limit the weight of the PV system. This has resulted in the PV cells being split up in 10 panels of 3 cells in parallel by 249 cells in series. A total number of 7'470 cells have thus been implemented in the PV array. Bypass diodes are implemented for every string of 24 cells.

6.1.4 Battery

The task of storing the power generated by the PV cells is performed by the battery. As has been concluded previously the battery of choice is a Li-S battery[14]. For the final design a type of Li-S battery has been chosen that fits the need of the aircraft, however this product is not COTS and is still in development. It has been proven in the MRR that the mission is not feasible using a COTS battery. The specifications of the battery are found in Table 6.7.

Table 6.7: Battery characteristics[46]

	Units	Li-S
Specific capacity	$Ah \cdot kg^{-1}$	1.675
Discharge rate	C	<6
Charge rate	C	<3
Cycle life	–	>1500
V_{cell}	V	1.5-2.8
E_{spec}	$Wh \cdot kg^{-1}$	500
E_{vol}	$Wh \cdot l^{-1}$	625
η_{bat}	–	>96.3

At the start of the mission the battery is fully charged using solar power from generated by the PV panels to maintain a fully solar powered paraglider. The battery is sized to provide enough power during t_2. The determining factor in this calculation is the specific energy. The mass of the battery is calculated with Equation (6.5).

$$m_{bat} = \frac{E_2}{E_{spec} \cdot \eta_{sys2}} \tag{6.5}$$

where m_{bat} is the battery mass in kg, E_2 is the required energy during phase 2 in J, E_{spec} is the energy density of the battery in $Wh \cdot kg^{-1}$ and η_{sys2} is the conversion efficiency of the system from the battery to the motor. Note that the efficiency of the battery is included in η_{sys2}. The battery mass is 59.6 kg. A safety factor of 1.05 has been applied to the mass of the battery to account for the casing of the battery. This mass has been included in the fuselage mass. The volume of the battery is calculated using the energy volume density. The battery may be split up in several blocks if this is necessary for the division of the weight in the monocoque for stability and control reasons.

The battery is considered to be fail-safe. Designing a back-up battery in case of failure is unrealistic as the added weight of the second battery would not allow the paraglider to take off. The auxiliary power unit (APU) has been designed to deliver enough power for the emergency systems but not to continue the mission. In case of fire or an other malfunction to the batteries, the batteries are dropped before they can harm the pilot in any way.

6.1.5 Motor

A motor is required to transform electric power to mechanical power. Using a rotor and a stator the electrical power is transformed using armature winding. The available power is the upper boundary con-

dition for choosing a motor's rated power. As given by Equation (6.1) the available power is determined by the motor only as v_t is fixed. As the available power is greater than the required power the rate of climb (RoC) is the determining factor. It is desirable to climb as fast as possible as at cruise altitude where the wind speed is more favourable. Therefore a large RoC is beneficial. The RoC is calculated using Equation (6.6).

$$RoC = \frac{P_a - P_r}{W_{tot} - L_{helium}} \tag{6.6}$$

in this equation RoC is the rate of climb in $m \cdot s^{-1}$, P_a is the power available in W, P_r is the power required in W, W_{tot} is the total weight of the aircraft in N and L_{helium} is the lift provided by helium in N. Having a higher available power enables the paraglider to reach cruise altitude more rapid. The lift provided by helium is assumed to be constant throughout the climb phase. There is no limit to the amount of power available, a larger motor delivers more power. During cruise flight this abundance of power is a waste as it remains unused. Therefore a motor has been chosen that delivers a reasonable rate of climb but does not have too much excess power during cruise flight. For this reason the Geiger Engineering HPD 13.5 has been favoured. The specifications of this motor have been given in Table 6.9. This motor delivers a maximum of 13.5 kW, before efficiencies are applied, which results in a RoC of 0.57 $m \cdot s^{-1}$. Using a smaller motor results in a small mass reduction, but increases the required time to reach cruise altitude. In a further study it can be examined which situation is optimal.

Table 6.9: Motor specifications[(ii)]

	Units	HPD 13.5
Maximum voltage	V	58
Rotational speed limit	rpm	2500
Rated current	A	260
Rated input power	W	13'500
η_{bat}	$-$	>93
E_{vol}	$Wh \cdot l^{-1}$	400
η_{bat}	$-$	>96.3
k_T	$Nm \cdot A^{-1}$	0.22
m_{motor}	kg	4.7

6.1.6 Propeller

Propellers are designed to fit a certain motor. As the motor has been chosen the respective propeller has to match the motor. Luckily the company that produces the motor also has produced a propeller that fits the motor. The propeller that fits the motor is the Geiger Engineering HK25 K 1.40, the specifications of which have been given in Table 6.11. This propeller is a fixed-pitch propeller and is pitched for cruise speed.

The propeller has been located on a shaft attached to the the back of the monocoque. This is to prevent that the air flow that reaches the propeller becomes too turbulent and so that the centre of gravity on the z-axis is favourable. The motor is located at the same position to provide an easy connection to the shaft.

The efficiency provided by Geiger Engineering is very low. Propellers reach efficiencies up to 90 % nowadays. The reason that the efficiency is low is due to the fact that this efficiency is based on full load. The details of the motor and propeller in part load are however unknown. The derivation of the

[(ii)] URL `http://www.geigerengineering.de/fileadmin/templates/PDF/Bedienungsanleitung_HPD_xx_V1.1.pdf`[cited 12 January 2015]

[(iii)] URL `http://www.geigerengineering.de/fileadmin/templates/PDF/Handlingsanleitung_Propeller_V1_0_englisch.pdf`[cited 12 January 2015]

Table 6.11: Propeller specifications[iii]

	Units	HK25 K 1.40
m_{prop}	kg	1.0
d	m	1.40
T	N	678
τ_o	Nm	61.5
Maximum received motor power	VA	13'500
η_{prop} at $40km \cdot h^{-1}$	–	0.45
Rotational speed limit	rpm	2200
Noise emission at $70m$	dB	<49

relation between thrust and efficiency is given in the MRR[14, Chapter 5] and the relation is once more given in Equation (6.7).

$$\eta_{prop} = \frac{2}{1 + [\frac{T}{A_{disc} \cdot {v_0}^2 \cdot \rho \cdot 0.5} + 1]^{\frac{1}{2}}} \tag{6.7}$$

in this equation η_{prop} is the efficiency of the propeller, T is the thrust in N, A_{disc} is the area of the actuator disc area in m^2, v_0 is the airspeed in front of the propeller in $m \cdot s^{-1}$ and ρ is the density of air in $kg \cdot m^{-3}$. This is the theoretic propeller efficiency, when comparing the value with experimental data it is noticed that there is a deviation and thus the real propeller efficiency is up to 10% lower.

As can be seen in Equation (6.7) the efficiency of the propeller is solely dependant on the thrust as the other variables in the equation are constant. Thus to increase the efficiency for cruise speed the thrust has to be decreased. The combination of the motor and the propeller has been examined to find a way to decrease the thrust and thus the efficiency of the propeller. As seen in Equation (6.8) the thrust is linearly related to the power available. So, in order to increase the efficiency the power that the motor delivers to the propeller should be decreased. This can be achieved by either decreasing the voltage, thereby altering the revolutions per minute (RPM), or the current, thereby altering the torque (τ_o).

$$T = \frac{P_a}{v} \tag{6.8}$$

Hereby T is the thrust in N, P_a is the power available in W and v is the flight velocity. The thrust varies with RPM as seen in Equation (6.9).

$$T = c_T \cdot \rho \cdot n^2 \cdot d^4 \tag{6.9}$$

for which T is the thrust in N, c_T is the thrust coefficient, ρ is the density of air in $kg \cdot m^{-3}$, n is the amount of revolutions in s^{-1} and d is the diameter in m. Decreasing the RPM results in a quadratic decrease in thrust. This can be done by changing the voltage or using a gear box. A gear box however has a low efficiency ranging between 0.7-0.9 so that is not desirable. Changing voltage has been chosen as the method to vary the RPM. As c_T is unknown for the propeller that has been used it can not be stated with what value the voltage has to decrease in order to get a favourable RPM. It is designed to have an efficiency of 0.76, equal to the propeller efficiency at maximum thrust. During cruise phase the aircraft will not fly on T_{max}.

It has been decided that thrust vectoring will not be implemented in the design. This is due to the fact that the vertical thrust added by vectoring the thrust does not equal the same amount of lift. Effectively the lift thus increases less than the weight increases due to the system that produces the thrust vectoring.

6.2 Power Management System

To enable the power to be distributed to the correct system a PMS has been designed. A PMS has to perform the following tasks

- Transport electric power
- Distribute electric power
- Convert electric power to mechanical power
- Regulate the power so that maximal efficiency is obtained

Utilising the electric system to its fullest potential requires the system to perform these tasks with the least amount of components.

6.2.1 MPPT

As has been stated in Section 6.1, MPPTs have been included in the PV modules. Two MPPTs are added per module, resulting in a total of 18 MPPTs. The MPPT that has been implemented is based on a fixed-step incremental conductance system. This system is more complex than the traditional perturb and observe system. However, as the power budget is crucial for this mission, optimal performance of the MPPTs is demanded and the fixed-step incremental conductance method shows the best power tracking characteristics.[47]

6.2.2 Wiring

To transfer the power between components electric wiring is required. The most important component of the wiring are the cables that transfers the power from the canopy to the monocoque. As the cables are released whenever one of the cables break it is not useful to implement redundancy as all the cables will be released when one fails. For this task a EPR Hypalon cable has been chosen, which conducts up to 3'500 V. A cross-section of 3.3 mm^2 is required to deliver the power to the fuselage with an insulation of 0.762 mm is required for these cables[(iv)]. The resistance of the cables has been calculated using Equation (6.10)

$$R = \frac{\rho \cdot l}{A} \tag{6.10}$$

in which R is the resistance in Ω, ρ is the resistivity in Ωm, l is the length of the cable in m and A is the area of the cross section in m^2. The total length of the two cables is 45.15 m, resulting in a wire resistance of 0.30 Ω a power loss of 51 W and a mass of 1.3 kg.

Inside the fuselage the power is fed through the same kind of cable. After the converter a lower voltage is obtained, while the current is higher. Therefore a thicker cable with the same characteristics is required for this part.

6.2.3 Auxiliary Power Unit

An APU is added to the system to provide power in case of failure in the power system. When the power system fails it is removed from the fuselage, thus resulting in no available power. The APU has been placed in the part of the monocoque that is not dropped when the emergency procedure is initiated. To be able to ensure the rescue and the safety of the pilot, the APU has been designed to provide power for the health, safety and emergency systems for 24 h. The APU has to deliver 15 W over a period of 24 h or 360 Wh. The APU has to be reliable thus a conventional battery is preferred. A lead-acid battery can range up to 42 $Wh \cdot kg^{-1}$, resulting in a mass of 8.57 kg which is too heavy. A conventional Alkaline AA-battery delivers 3.9 Wh, which is too small as 93 of these batteries would be needed thus a larger alternative had to be investigated as the internal resistance would be too large[(v)]. Using a Lithium-Ion

[(iv)] URL `http://www.omnicable.com/spec-sheets/600v-durasheath-eprhypalon-use-2-power-cable-600-volt-aluminum-wi` `html`[Cited 16 January 2015]

[(v)] URL `http://data.energizer.com/PDFs/BatteryIR.pdf`[Cited 15 January 2015]

battery with an energy density of 180 $Wh \cdot kg^{-1}$ results in an acceptable mass of 2 kg for the APU. This APU has been constructed in a different mesh so that it can deliver power to the emergency system even when the cycle is interrupted when the batteries and PV cells have been dropped.

6.2.4 Electrical Block Diagram

As all the electric subsystems are now treated it is possible to create an electrical block diagram (EBD). An EBD is a schematic representation of the electrical system and is found in Figure 6.2. Note that the PV system is not represented accordingly in the schematic. In reality there are nine modules but to keep the EBD organised only two have been drawn for clarity. The PV modules and their MPPTS, of which there are two per PV module, are the only components located on the canopy. Wires transfer the power to the fuselage where it is fed to the controller. The controller calculates whether the power is transferred to the converter or the battery. The controller also determines whether the motor is powered by the PV cells or the battery. If the power is fed to the battery the battery manager determines the state of charge. If the battery is fully charged, the extra power is dumped to make sure that the battery is not overcharged. The battery manager also contains a DC-DC converter to regulate the current and voltage to the battery. Before the power is transferred to the motor it is fed through a converter to acquire the correct voltage and current for the motor and subsystems. Then the power is split between the subsystems and the motor. The motor, guided by the motor controller, then rotates the shaft to which the propeller is attached.

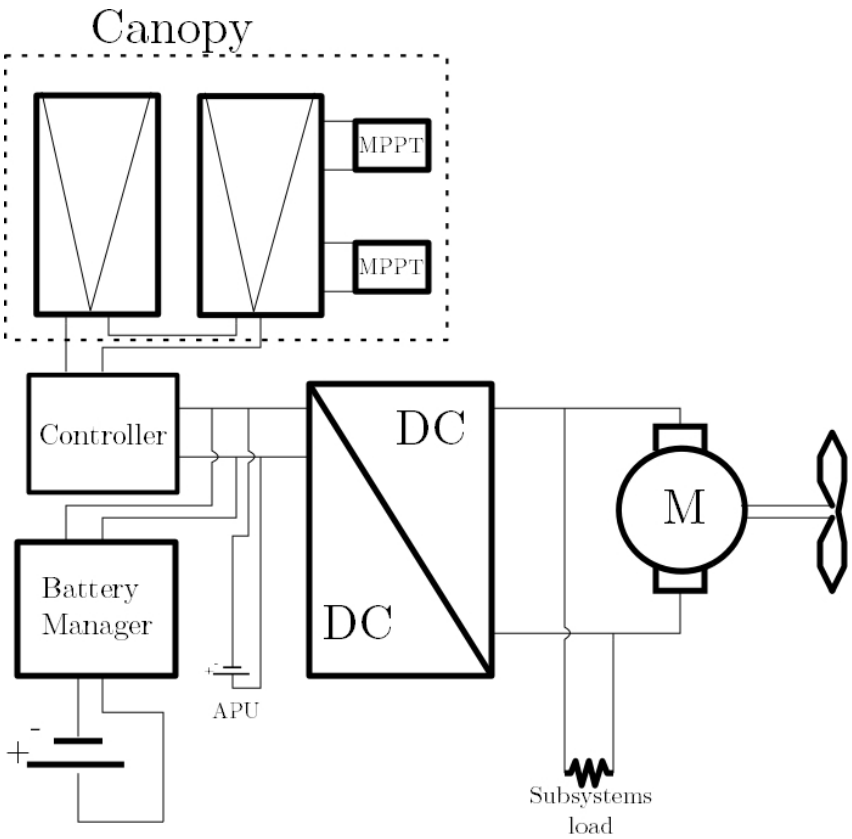

Figure 6.2: Simplified electrical block diagram

6.3 Navigation

The pilot of the paraglider needs to know the attitude of the aircraft at any time in order to know his location. The following parameters are considered relevant for the pilot at any moment in flight.

- Data transmission
- Heading
- Altitude
- Speed monitoring

These features of the system are evaluated and based on the requirements a decision is made what components are used. The decision is made to stick to the Federal Aviation Administration technical standard orders (TSO). The TSO are used for small aircraft and are a minimum technical standard for civil aircraft. The paraglider is not a standard civil aircraft, but for safety matters the TSO are used in the paraglider.

6.3.1 Data transmission

The pilot of the paraglider needs to be able to communicate with the ground system at all times. There are various reasons why this is important. Firstly, when something goes wrong, the pilot should be able to call for help. Secondly, the ground station provides the pilot with weather data at certain intervals. Finally, the pilot is flying alone. Usually this is not a problem, but since the pilot is alone for more than a day, it is quite essential that he is at least able to speak to people at the ground station to prevent loneliness. The data transmission system is of vital importance and therefore a backup system is required as well.
The decision was made to use an Ipad Mini 3[(vi)] with an Iridium Go[(vii)] for communication. The Ipad Mini is not a communication device itself, since it does not receive a cellular signal or mobile data, but the screen can be used to view live data or type messages for the ground station. The Iridium Go is used for the required signal. The Iridum Go receives satellites signals and provides a Wi-Fi hotspot for the Ipad and basically turns the Ipad into a satellite phone. In order to make sure that the Ipad Mini 3 does not malfunction it is covered in a shock resistant, waterproof case.[(viii)]
The Ipad Mini 3 is required since various subsystems will use bluetooth to send data to the Ipad Mini as well. The most lightweight option would be a smartphone, but since a slightly bigger screen is more comfortable, the decision was made to use an Ipad Mini 3.
The Iridium Go is an Ipad extension. Since the Ipad is used anyways, it is beneficial to pick an extension compared to a separate satellite phone. The most important parameters of a satellite phone, in this case the Iridium Go, were considered to be the mobile coverage, talk time, standby time and whether a wi-fi signal could be set up. As a backup for the Iridum Go, the Iridum 9575 is used. This is a separate satellite phone, which is used in case the Ipad Mini 3 or the Iridium Go fails. The Iridium 9575 also supports wi-fi, which makes it a better option than its competitors. Other satellite phone companies have worse coverage or do not provide an Internet signal. Therefore for data transmission the Iridium Go in combination with an Ipad Mini 3 and an Iridium 9575 has been chosen.

6.3.2 Heading

The pilot spends the most of his mission above the open sea, with no reference point for his flight direction. The view will be exactly the same around the vehicle, water as far as the eye can see. Therefore the heading needs to be monitored at all time. The Garmin GPS 165 TSO[(ix)] is used since it has a really accurate GPS functionality, it is lightweight, small and it meets the TSO.
In addition a Polar V800 Watch[(x)] is used, but not primarily because of the GPS functionality. The V800 watch is multi-functional. The GPS watch is light, has a heart-rate monitor, altitude meter and

[(vi)] URL `https://www.apple.com/nl/ipad-Mini-3/` [cited 8 January 2015]
[(vii)] URL `https://iridium.com/products/Iridium-GO.aspx?productCategoryID=29` [cited 8 January 2015]
[(viii)] URL `http://www.lifeproof.com/shop/us_en/ipad-mini-cases/ipad-mini-3-case-fre/?color=Black+2F+Black`
[(ix)] URL `https://buy.garmin.com/en-US/US/in-the-air/discontinued/gps-155-tso/in-the-air/discontinued/gps-165-tso/prod27.html` [cited 18 January 2015]
[(x)] URL `http://www.polar.com/us-en/products/maximize_performance/running_multisport/V800` [cited 9 January 2015]

thermometer as well. The data of the V800 watch can be easily send to the Ipad Mini 3 using blue-tooth. The battery life is 50 h in GPS low power mode. So the watch may need to be charged during flight, since a lot of features of the watch will be actively used. It is therefore necessary to bring the charger for measurements at certain intervals. Due to the low price and independence of electric energy a simple compass is brought as well for back-up.

6.3.3 Altitude

The altitude is one of the most important variables to measure during flight. Firstly, the amount of oxygen in the atmosphere is limited. If the pilot exceeds the 10'000 ft altitude, he will not be able to breathe properly. Secondly, for optimal flight efficiency, the flight should be steady and horizontal. Deviations from cruising altitude cost a lot energy as the optimal wind speed occurs at cruise altitude. Finally, in case of emergency, the pilot has to know the altitude with respect to the water surface accurately. If there is an emergency situation, it is really important that the pilot is able to measure the altitude accurately. The impact of the emergency landing is highly dependent on the altitude and pilot should be able to prepare himself for impact. Estimating the altitude at sea with your eyes may seem easy, but it is very difficult and inaccurate, as the water level is constantly varying because of the waves. The altitude can be measured with the v800 watch for instance, but the accuracy is simply insufficient for emergencies. The Polar v800 watch will therefore only be used as a backup. The Garmin GRA5500[(xi)] is used as the primary altitude meter. The Garmin GRA5500 has an accuracy of 1.5 ft and the radar altitude meter is mostly used in helicopters. The mass is 1.6 kg. The Garmin GRA5500 is accompanied by a GI-205[(xii)], a small simple screen which shows the altitude. The backup, the Polar V800 Watch is less accurate and is only used if the Garmin GRA5500 fails. The accuracy is approximated in several tests and is 20 ft at best.

6.3.4 Speed monitoring

The speed of the paraglider consists of two important components. The v_t and the wind speed. The v_t is the speed that the system has with respect to the wind. The wind speed is the speed of the wind. The wind is a vector and the component in flight direction is considered positive tailwind. The ground speed (v_g) is the sum of these two components. The v_g determines how long the flight will take if the distance is known. Therefore the v_g should be measured at all time and the GPS system described earlier is used to do so.
The accuracy of the Garmin GPS 165 is sufficient since it meets the TSO. As a backup, once again the Polar v800 Watch is used. Both the speed monitoring systems are lightweight (90 g and 79 g respectively) and multi-functional. The Polar v800 watch has a speed accuracy of 2 $km \cdot h^{-1}$[(xiii)].
In addition to measurement of the ground speed, the v_t should be measured. The wind data in combination with the GPS data are not sufficient for the the v_t measurements. There are basically two options that could have fatal consequences on the mission. The v_t could be too low; The paraglider should always fly above stall speed v_{stall}. At v_{stall} the lift becomes insufficient and the semi-rigid wing could collapse. In order to measure v_t thoroughly a pitot tube with speed indicator is used. The pitot tube measures the air pressure and with he use of Euler's equation the v_t can be computed. In this way the pilot always knows when he should adjust his thrust in order to fly at a safe range from the v_{stall}.
The other option is that the air speed is too high. This means that the system is flying too fast. It is designed for a certain v_t and the batteries and PV cells are sized for that v_t. The batteries and the PV cells are a limited energy source and flying at the wrong speed reduces the efficiency of the paraglider. A small pitot tube has been chosen that is small and lightweight[(xiv)]. Its mass is 0.190 kg and is connected to a small monitor and is visible in Figure 6.3. The accuracy is 0.3 $m \cdot s^{-1}$, which is assumed to be sufficient, since the difference between the cruise speed and v_{stall}Section 3.3 is $10 - 5.66 = 4.34\ m \cdot s^{-1}$.

[(xi)] URL https://buy.garmin.com/en-US/US/in-the-air/avionics-safety/helicopters/gra-5500/prod135561.html [cited 9 January 2015]
[(xii)] URL https://buy.garmin.com/en-US/US/in-the-air/avionics-safety/radar-altimeters/gi-205/prod503232_013-02121-00.html [cited 9 January 2015]
[(xiii)] URL http://www.runningmetronome.org/polar-v800-review/ [cited 9 January 2015]
[(xiv)] URL http://www.kimouk.com/MP120-portable-anemo-manometer-pressure-air-velocity

Figure 6.3: pitot tube with speed monitor

6.4 Health & Safety

Health and safety are of great importance to this mission. The mission takes place above the Atlantic. There is no land nearby, the sea is rough and is the natural habitat of deadly animals. Due to the fact that the pilot is all by himself at a remote location, his health state is crucial and should therefore be monitored. This section will be split up in health and safety.

6.4.1 Health

The pilot is subjected to different atmospheric conditions at 10'000 ft and he is sitting in a fuselage for the whole mission duration. The health of the pilot is influenced by these conditions and should therefore be monitored. For instance the temperature at 10'000 ft is -5^o C. In addition, there is less oxygen at cruise altitude and the pilot may have problems due to a lack of oxygen, for instance Hypoxia. The topics that are dealt with, regarding the health of the pilot, are summarised by:

- Monitor heart rate
- Photo-plethysmographic health monitoring
- Check consciousness
- Measure body temperature
- Body movement
- Excessive noise cancellation
- Visual
- Human waste
- Drinks
- Food

Heart rate

The heart rate of the pilot needs to be monitored at all time. This is essential, since partial failure of the heart is critical. The heart rate will be measured by the Polar V800 watch and send to the Ipad Mini 3, which is able to send the data periodically to the ground station. In addition, a heart rate monitor ring with bluetooth is used as backup. This ring is also capable of measuring other health statuses and will be discussed later on.

Photo-plethysmographic health monitoring

The health system has to be capable of monitoring sleep deprivation. This can be done using photo-plethysmographic signals. A ring is used that measures blood volume with light[48]. It is expected to weigh less than 200 g, which is just an estimate, since the system is not COTS. Basically, the system measures the heart rate, arterial blood oxygenation, blood pressure and respiratory rate. These measurement are sent to the ground station as well and the medical team inspects the values and acts when necessary. In order to do so, the ring should have bluetooth capability. This way, the information can be send to the Ipad Mini 3 and therefore to the ground station.

Consciousness

During normal operations the pilot should be focused. Therefore some periodic actions need to be performed by the pilot. Informing the ground station with the newest measurements is a periodic action, which keeps the pilot alert. Other tasks, such as checking the functionality of the control lines can be performed periodically in order to prevent boredom. In addition, video games of the pilot's choice are installed on the Ipad Mini 3. Apart from entertainment, these video games increase the focus and give an opportunity for the pilot to move. The pilot is awake for many hours during this mission, however, the

pilot must remain conscious. If any of the systems fail, the pilot should be able to take action. To avoid the risk of having the pilot fall asleep certain precautions should be taken. The inboard lighting should be of a blue colour as this slightly increases the alertness of human beings.[49] Also, substances that can be taken by the pilot to increase alertness include caffeine or modafenil. Like Royal Air Force pilots in World War 2 or B2-bomber pilots anno 2014, amphetamines (known as "speed" or "pep") could be applied if the pilot is tested to be physically capable. As a last resort, the pilot may be awakened using small electric shocks. These shocks can be given to the pilot using the photo-plethysmographic ring with an interval of 20 minutes. If all fails to awaken the pilot the mission must be aborted resulting in an emergency landing.

Body temperature

The pilot is flying at an altitude at which the temperature is -5^o C. The clothes of the pilot are warm enough to comfortably endure this temperature. Still, the body temperature of the pilot is influenced by the outside air temperature. Therefore the body temperature needs to be monitored. Once the temperature is too high or too low, the pilot should be notified of this and cope with this by putting on more or less clothes. Therefore a Braun Thermoscan 7[(xv)] is used for periodical body temperature measurements. The system warns the pilot when necessary. The pilot has to be instructed to keep his body temperature at 37^o C as this is the regular temperature of a human.

Body movement

Ideally, the pilot would be stationary in the fuselage, but this is not the case. A person is not able to sit idle in a chair for multiple hours straight. The blood has to flow and normally gravity makes the blood flow to the feet. When a person is moving, the blood can easily flow upwards as well and the whole body is furnished with blood. Therefore the pilot should be able to move his legs.

The pilot's feet are also used for controlling the control lines. Basically, the volume of the pilot is not the volume that is being sized for, since there is no room for movement then. At the legs of the pilot there is therefore significant space implemented for movement.

Noise

The pilot is subjected to the noise of the propeller during the flight. The pilot is seated only a meter away from the propeller. Therefore, the noise characteristics of this design must be looked at.
The different parts of the design that produce noise are the turbulence of the airflow around the wing, the propeller, the electrical motor, the pilot and the internal subsystems. The pilot and internal subsystems will produce the least amount of noise, and is therefore neglected with respect to sources such as the propeller. Of all these noise sources, the propeller will be the source producing the most amount of noise. As mentioned in Table 6.11, the maximum sound level being produced by the propeller at 70 m distance is 49 dB. Noise produced by the wing and the electrical motor are very hard to estimate, but the electrical motor turns at relatively low rotational speeds of 2500 RPM maximum and will therefore not produce much noise. The wing turbulence will also not be significant due to the low speeds and therefore these contributions are assumed to be negligible as well with respect to the propeller. The wing is also so far from the pilot that the wing turbulence effects are not critical for the pilot.

The known noise produced by the propeller has been extrapolated to larger and smaller distances using equation Equation (6.11)[(xvi)].

$$I_2 - I_1 = \log_{10} \frac{R_2^2}{R_1^2} \tag{6.11}$$

in this equation, I_2 and I_1 are the noise levels in dB at location R_2 and R_1 in m, respectively. The outcome of this has been displayed in Figure 6.4.

[(xv)] URL `http://www.brauntherms.com/our-products/thermoscan-7` [cited 9 January 2015]
[(xvi)] URL `http://www.sengpielaudio.com/calculator-distance.htm` [cited 16 January 2015]

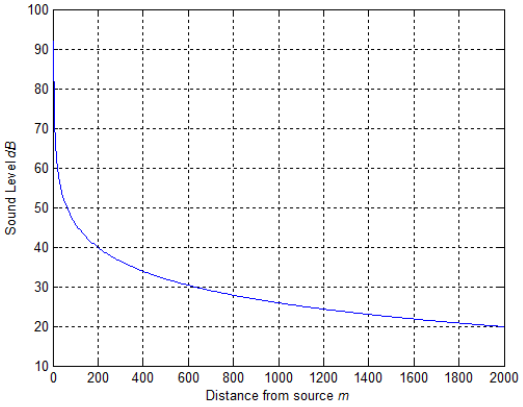

Figure 6.4: Distance from noise source vs. sound level

From Figure 6.4, it can be seen that the noise level at 0.5 m is 91 dB, which can cause hearing damage when exposed to for more than 8 hours. Section 6.4 describes what measures are taken for the pilot to prevent this damage from happening. Also, this will make any audio communication from the fuselage to the ground a problem. This problem is also solved in Section 6.4. The graph also shows that the overall noise production stays well under the 100 dB and at 20 m distance one can already have a conversation and at a distance of 200 m the sound level is equivalent to the sound level in a quiet library.[(xvii)] Next to this, most of the mission will be flown over the ocean, where not many creatures or people are disturbed by the sound, so there is no problem with the noise with respect to the external environment.///

Ear protection is thus required, but the question is: Is it possible to communicate with the ground station in this noise? The Cessna 172 general aviation aircraft, shows a peak noise level between 93 dB and 102 dB. In aircraft like these a noise cancelling headset for the pilot is suitable noise protection. Therefore the assumption is made that it is still possible to communicate with a proper headset like the EM-1® ANR Headset[(xviii)], since this is also possible in the Cessna 172. The headset reduces the noise level peak to a significantly lower 72 dB [(xix)]. Of course this does not mean that the ground station has a better reception of what the pilot says, since only the noise towards the pilot's ears is reduced. Tests in 90+ dB noisy environments with the EM-1® ANR Headset should determine whether the communication is actually possible or that the fuselage should be reinforced with noise cancelling material in the fuselage.

Visual

There are two main difficulties regarding the visual of the pilot. At first, the pilot is subjected to sunlight during daytime. Therefore sunglasses with significant UV protection are required to protect the pilot's eyes. Furthermore, during the flight in darkness, the pilot needs lights in order to see. Inside the fuselage, LED-strips are the source of light, so the pilot is able to see all subsystems. LED-strips are both more efficient and compacter when compared to common lightbulbs with the same luminosity.

[(xvii)] URL `http://www.sengpielaudio.com/TableOfSoundPressureLevels.htm` [cited 16 January 2015]

[(xviii)] URL `http://anr-headsets.com/Html_folder/HI-EM1.html`[cited 16 January 2015]

[(xix)] URL `http://www.lightspeedaviation.com/content/lightspeedaviation/CustomPages/ANR-101-A-Tutorial-on-Active-Noise-Reduction/Section-3-Airplane-Issues.htm`[cited 16 January 2015]

Human waste

The system has to be capable of dealing with the human waste that is inevitably produced during flight. The urine can be turned into water again using the Forward Osmosis Purifier[(xx)]. Approximately 30 l of water can be made with only 1.1 kg purifying gel and the urine itself. The system is small and light (2 l and 1 kg) and is therefore easy to take along. Underneath the seat of the pilot the Hassock Portable Lightweight Self-Contained Toilet[(xxi)] is stored. It is a simple, relatively small toilet of 50 l that weighs 2.5 kg. The Forward Osmosis is validated for its efficiency. If the system is beneficial for the total weight, it is implemented. The following procedure has been done in order to validate the effectiveness of the HTI Forward Osmosis.
As stated in the MRR,[14] the HTI Forward Osmosis can make 30 l of water using 30 l of urine and 1.1 kg purifying gel. The mission duration is 38 h and in combination with the emergency landing and pick up the mission duration is at max approximately 48 h. An average human produces 0.8-2 l of urine per day[(xxii)]. The average of 1.4 l is used. This makes a total 2.8 l of urine for the mission. This requires 0.1 kg of purifying gel. The total mass of 1.1 kg for the HTI Forward Osmosis produces 2.8 l of water, so 2.8 kg, which makes the HTI Forward Osmosis beneficial to taking along the required water.

Drinks

An average human male needs approximately 3 l of water per day. The mission duration is at max two days so 6 l of water would be sufficient. The Forward Osmosis Purifier is capable of converting the urine to water, so the pilot can use more than 2.8 l of water using that system. Therefore 4 l the extra water by the Forward Osmosis Purifier should be sufficient. Studies regarding the efficiency of the Purifier may change the amount of water for this mission.
The water is improved by adding green tea. The green tea adds anti-oxidants, which increases the endurance of the pilot.[50] For muscle recovery cherry juice is used. The cherry juice reduces the muscle sourness after exercise.

Food

Apart from drinks, food is required as well. The following food, with a total of 4 kg is taken for this mission: Walnuts (calories), chia seed (amino acids), energy bars (calories, anti-oxidants), vitamin capsules (vitamins) and soy powder (proteins). The food is carefully chosen with respect to their nutrients and the demands of the human body. A total of 4 kg is used since an average person requires approximately 2 kg of food per 24 h.[1]In the worst case scenario the mission takes 38 h plus the 24 h to be picked up at the middle of the ocean. This makes a total of 62 h, but this value is over estimated since the pickup time is shorter if the mission duration is near the total of 38 h. The pick up time is also a function of the location at which the system lands at sea. If for instance the paraglider lands precisely in the middle of the ocean between Ireland and Canada, the mission duration is approximately 20 h and the pickup time is at its maximum of 24 h here. This makes a total duration of 44 h. The assumption is therefore made that the total mission duration including floating at sea is less than 48 h, which makes 4 kg of food sufficient.

6.4.2 Safety

The mission is required to be safe. The pilot should have a comfortable Atlantic crossing and during emergencies any risk should be mitigated. In order to improve the safety of the mission, the following subsystems are integrated.

- UV lights
- Chair
- Life raft

[(xx)] URL `http://www.htiwater.com/technology/forward_osmosis/` [cited 12 January 2015]
[(xxi)] URL `http://www.amazon.com/dp/B000FIDZLI/?tag=znt0323-20` [cited 11 January 2015]
[(xxii)] URL `http://www.nlm.nih.gov/medlineplus/ency/article/003425.htm`

Figure 6.5: Representation of the chair system

- Life jacket
- Parachutes
- Battery drop system

UV lights

The lines between the fuselage and the wing are critical. If one of the lines snaps, the mission can not be completed and the emergency procedures take place. Therefore it is crucial that there are no objects that hit the lines during flight. Birds are the main reason for concern regarding control line collision. Therefore small, pulsating UV lights have been installed at the lines to prevent bird from coming close.[51]

Chair

The pilot spends the entire mission in a chair and the chair should therefore be comfortable and safe. During an emergency landing, the fuselage drops nose-down in the ocean or at land and therefore the pilot is thrown out of his chair without a proper safety belt system. A five point seat belt is used in order to ensure the pilot's safety during an emergency landing. The actual seat belt is the G force Black Pro Series.[(xxiii)] The chair that is being used is a modification of a paraglider chair is used. Since there needs to be a zipper in the chair in order to dispose human waste and the bag to store the canopy in basically becomes redundant it is removed. A representation of what the chair is going to look like is given in Figure 6.5.

Life raft

There are different outcomes for this mission. The vehicle either lands on land or at sea. Assuming that the fuselage is able to bear the landing collision in both cases, the pilot is still in great danger once he lands at sea. Therefore a life raft is integrated. Since the fuselage can be used as a floatation device, the decision is made to incorporate the fuselage in the life raft. The fuselage is surrounded by a folded life raft that is going to be inflated using CO_2 cylinders. A COTS component was preferred, but to get maximum efficiency out of the fuselage this concept is used. In order to inflate the life raft CO_2 cylinders are used. The pressure of these capsules make the life raft inflate rapidly during emergency

[(xxiii)] URL `http://www.ebay.com/itm/G-Force-Black-Pro-Series-5-Point-Shoulder-Harness-Racing-Seat-Belts-SFI-2-Sets-200960240165`

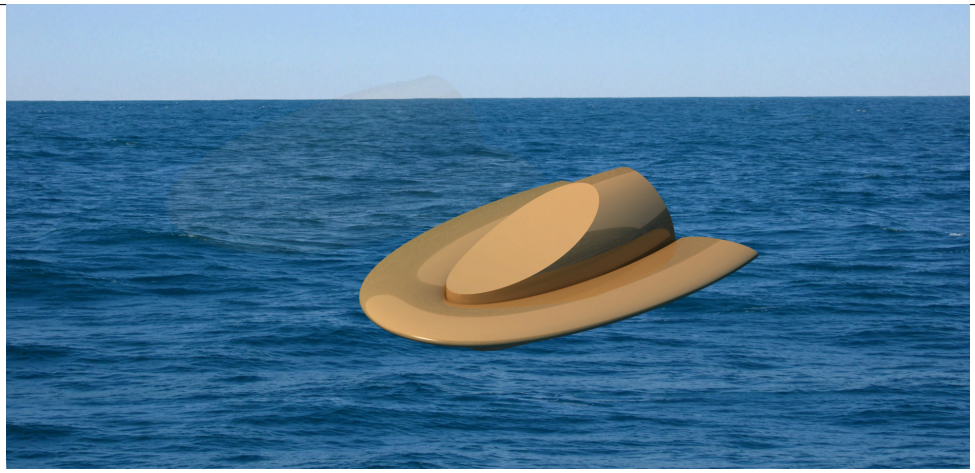

Figure 6.6: Liferaft inflated

cases. The exact moment of inflation is determined by a water sensor, the Seahawk SDZ.[(xxiv)] This is a simple system that uses the conductive capabilities of water to determine whether the system is in water or not by having an open circuit that is closed once it hits the water. Once the Seahawk SDZ is in contact with water, the electric circuit is completed and the sensor gives a signal to the life raft and the CO_2-capsules inflate the life raft and safety on the water is realised. A visualisation of this system can be found in Figure 6.6.

Life jacket

The WAB-H18 life jacket is used since it is TSO-C85 approved. This means that it has a certain quality standard and it can therefore be safely used when necessary. In case the pilot lands in the water, the WAB-H18 life jacket is used to prevent the pilot from drowning and to remain above the water surface.

Parachutes

In the case the mission is aborted in-flight it is necessary to have emergency parachutes. The parachute should be light, easily and compactly storable, have a reasonable descent rate, and be quickly deployable. There are multiple different parachutes available on the market that fit the description. For a maximum weight of 300 kg the Magnum 300 Speed Softpack[(xxv)] can be used. The descent rate is lower than 5.5 $m \cdot s^{-1}$, which is an acceptable speed. For redundancy another reserve parachute is available, which can be deployed if necessary.

Battery drop system

The batteries will be stored in an eject-able rear section of the fuselage. This section is a elliptical cone with a volume of 0.270 m^3. With specifications mentioned in Table 6.7 it was calculated that the batteries volume would approximately be 0.082 m^3. This is not accounting for any casings or safety material. Still, it is assumed that the 0.270 m^3 is more than enough for all batteries and the motor. The rear section is clamped to the fuselage with a spring in between. The potential energy from the spring will make the rear section eject away from the fuselage to avoid entanglement of the propeller with the parachute or canopy lines as well as get rid of potential hazardous batteries. There is no solid requirement for the ejection speed, so a rotation of 90 degrees in 1 sec was assumed. The required spring force is calculated in Chapter B to be 838 N. The design could easily incorporate springs that deliver

[(xxiv)] URL `http://rletech.com/our-products/spot-leak-detectors/sd-z/`

[(xxv)] URL `http://www.businessaircraftcenter.com/articles/private-aircraft-pilots-hearing-loss-art0312.htm` [cited 11 January 2015]

this amount of force[xxvi]. Clamps, which hold the eject-able section firmly to the fuselage, are connected to the first reserve parachute so the whole move is done in a rapid sequence, saving time. A simplified sequence prior to parachute deployment is presented in Figure 6.7.

6.5 Take-off & Landing

The PPG can not take off without a horizontal velocity. Therefore a take-off cart is designed, since the fuselage is not equipped with wheels. The take-off cart makes sure that the system has a v_t that is higher than the stall speed (v_{stall}). The cart is thrusted by the propeller and it will take off in head wind conditions. The head wind is used to inflate the wing during the take off. At some point, the TAS is sufficient to lift the fuselage from the take-off cart. The take-off cart is given in Figure 6.8. The take-off cart's design is based on comparable systems like a boat trailer. The fuselage is supported at three points and the frame is made structurally sound in order to prevent a collapse of the take-off cart when it carries the weight of the fuselage.

In order to prevent buckling, plates are placed in the structure to prevent column buckling due to the fuselage weight. The take-off cart design is made out of aluminium besides the wheels. The aluminium tubes have an r_o and r_i which are unknown at this stage in design. The weight of the take-off cart is not critical for this mission, but further research should determine the exact dimensions of the aluminium tubes in order to prevent overdesigning the structure.

A structural analysis with the exact loads at take-off should be done in order to check whether a system like this is sufficient to take off in real life conditions.

The length and width of the take-off cart are logically based on the dimensions of the fuselage. The fuselage should fit in the vertical semi-rings and therefore the size of those rings are based on the fuselage design.
The height of the system is not an issue, since the propeller diameter is 1.40 m, which is not critical as the height of the fuselage itself prevents the propeller from hitting the ground. If the size of the propeller would increase, the tip of the blade should be at least 0.20 m from the ground in order to prevent that the blade touches the ground during take-off. The 0.20 m is simply considered a safe margin, but as mentioned earlier this is not relevant in the current case. The wheels are sized based on reference vehicles, like the boat trailers mentioned earlier. There is no release mechanism required in this system. Once a speed of 1.2 times v_{stall} is reached the system lifts itself from the take-off cart. In order to make sure that the system does not take off earlier than at 1.2 times v_{stall}, extra weight is added and released at take-off. The total system with fuselage is presented in Figure 6.9.

The wing is filled with helium and it is capable to lift its own weight at a lower airspeed than v_{stall}, which makes the take-off easier. In Equation (6.12) the velocity at which the wing takes off is given.

$$v_{w_{to}} = \sqrt{\frac{(W_{PVs} + W_w - L_{helium})}{S_w} \cdot \frac{2}{\rho} \cdot \frac{1}{C_{L_{\max}}}} = \sqrt{\frac{(393 + 64 - 329)}{75.1} \cdot \frac{2}{1.225} \cdot \frac{1}{2.49}} = 1.06 \quad m \cdot s^{-1} \tag{6.12}$$

In Equation (6.12), $v_{w_{to}}$ is the velocity at which the wing takes off, W_{PV} is the weight of the PV cells, W_w is the wing weight, S_w is the effective surface area of the wing, ρ is the density, in this case at ground level, and $C_{L_{max}}$ is the lift coefficient with the jet flaps deployed. The $v_{w_{to}}$ is only 1.06 $m \cdot s^{-1}$ and the wing supports its own weight during the take off procedure, while the cart has to accelerate to 1.2 times v_stall before the total system takes off.

The landing subsystem is incorporated in the fuselage, there are basically 2 options: A landing at sea and a landing at land. The landing on land is a simple belly landing and the landing at sea, an emergency landing, is a vertical drop in which the fuselage frame carries the loads. There are no additional subsystems required in order to land.

[xxvi] `http://www.leespring.com/uk_compression_spec.asp?springType=C&forWhat=Search`[cited 17 january 2015]

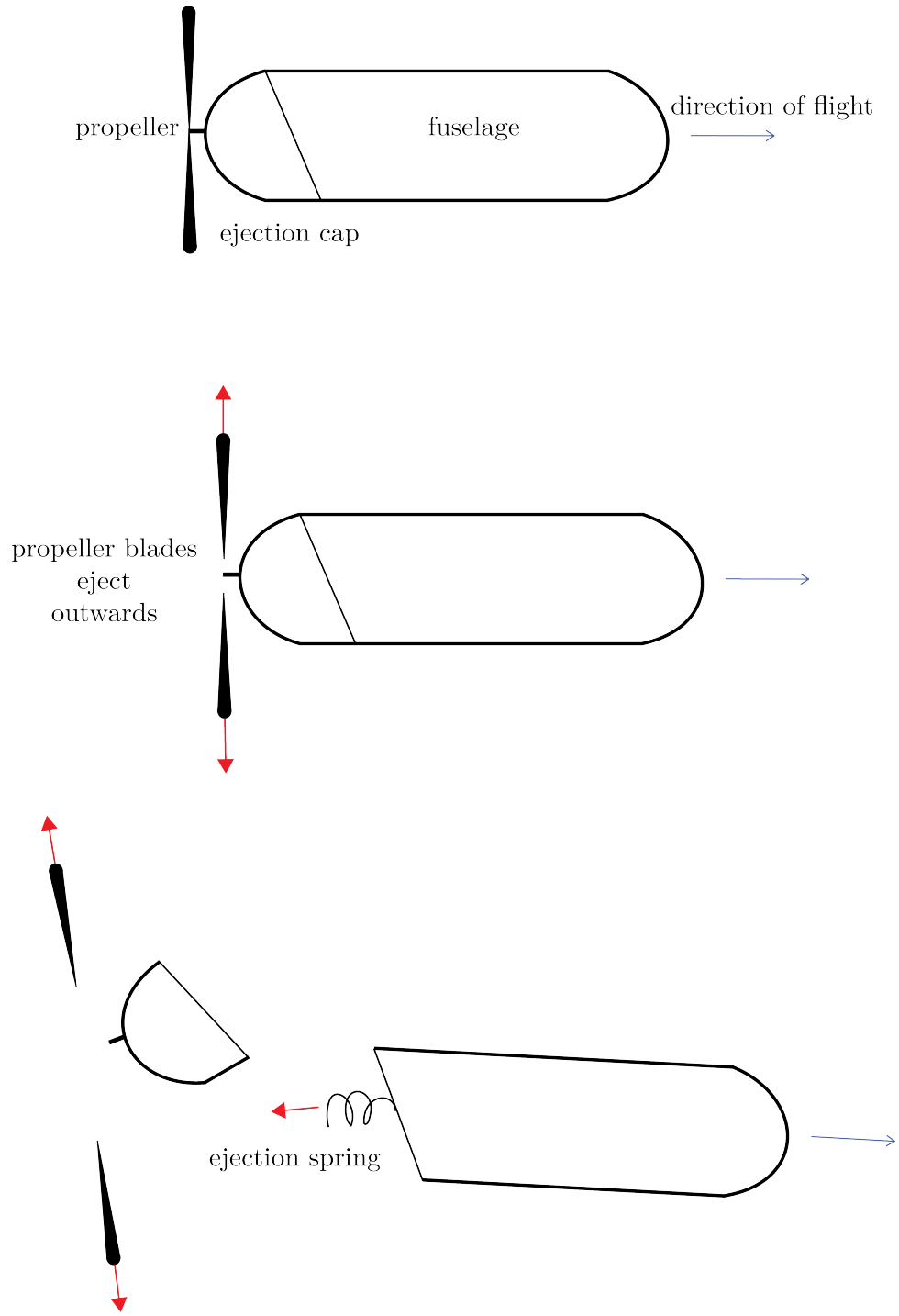

Figure 6.7: Simplified ejection mechanism for droppable batteries and motor

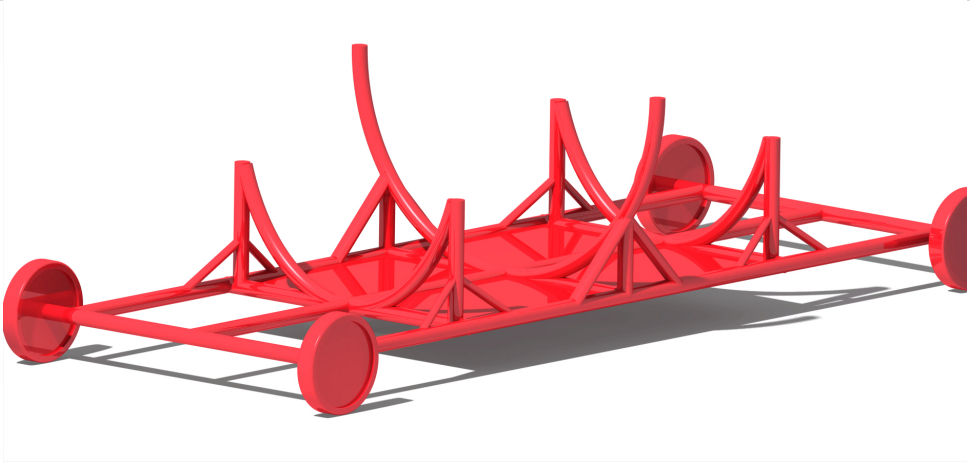

Figure 6.8: Take-off cart

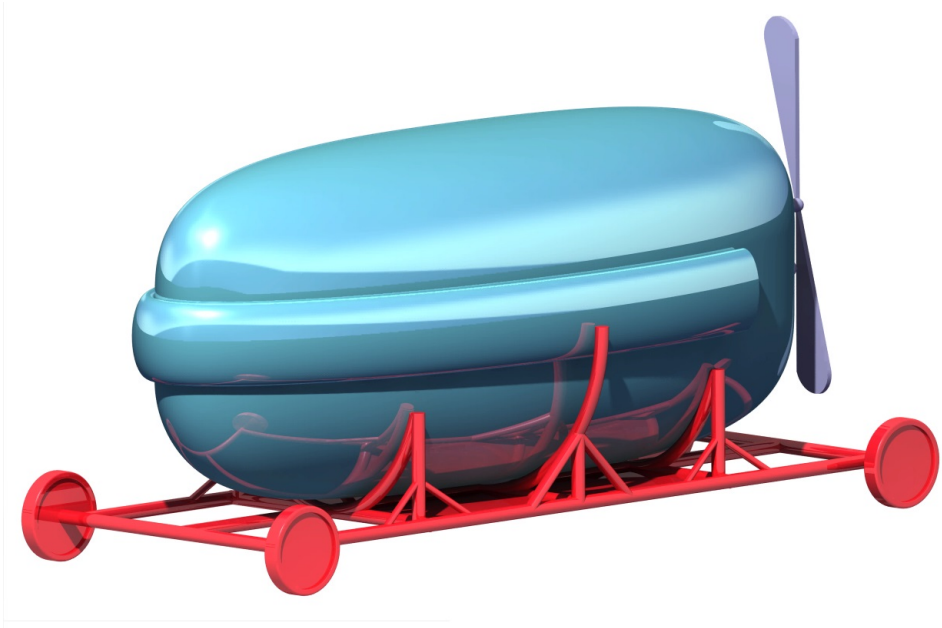

Figure 6.9: Take-off cart with fuselage

6.6 Configuration

The fuselage contains the subsystems mentioned in the previous sections and since all those subsystems have weight, they should be stored in the fuselage such that they provide moment equilibrium. The c.g. has been chosen to be in between the attachment points of the control lines. In that way, the fuselage is most stable. Several subsystems have fixed locations based on their usage. For instance, the batteries, the motor and the propeller are stored at the back of the fuselage and the pilot is positioned in such a way that he is able to look out of the window an move his legs and arms. The fuselage structure itself also has a c.g. and the emergency parachutes are stored in the back of the fuselage for the emergency procedure.
There are several other subsystems that can be stored anywhere in the fuselage. The only question is whether the pilot should be able to reach the subsystems during flight. The subsystems such as food, drinks and the life vest for instance should be close enough to the pilot to grab them. The datum line for the c.g. calculation is the nose of the aircraft. The subsystems that have a fixed location are dealt with first. The following subsystems are constrained at a certain location:

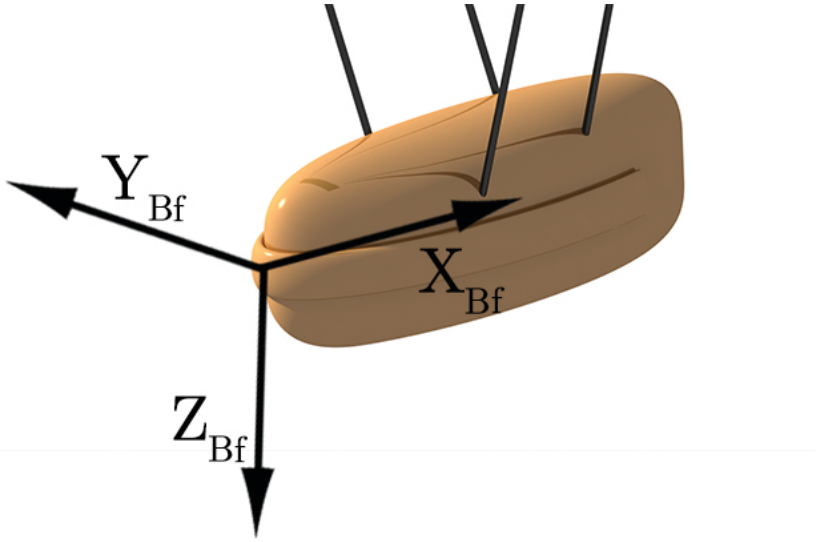

Figure 6.10: Body axis system

- Batteries
- Propeller
- Motor
- Frame
- Pilot
- Parachutes
- Life raft
- Monitors
- Control line system
- Electric wiring
- Other subsystems

6.6.1 Centre Of Gravity Contributors

In this subsection each component with a significant influence on the centre of gravity is briefly discussed. The axis system used is given in Figure 6.10.

In y_{bf} direction moment equilibrium is ensured by equally spacing the subsystems from the x_{bf} axis. The z_{bf} location is not relevant for stability. The z_{bf} location should be as low as possible in order to lower the c.g. when the system is floating in the emergency case when the life raft is inflated at sea. The z_{bf} location of the parachutes is also relevant. This is the case since the upward force of the parachute should have its line of action through the total c.g. of the system. The location in x_{bf} direction is discussed in this subsection.

Batteries The batteries are stored in the back of the fuselage, since they are dropped in during the emergency landing. They are stored as far to the back as possible. Based on the available volume and the battery volume the exact location is picked. The c.g. with respect to the nose is 2.70 m.

Propeller The vehicle has one thruster and it is stored behind the end of the fuselage. The propeller is therefore 0.10 m behind the fuselage, therefore the c.g. is 3.10 m.

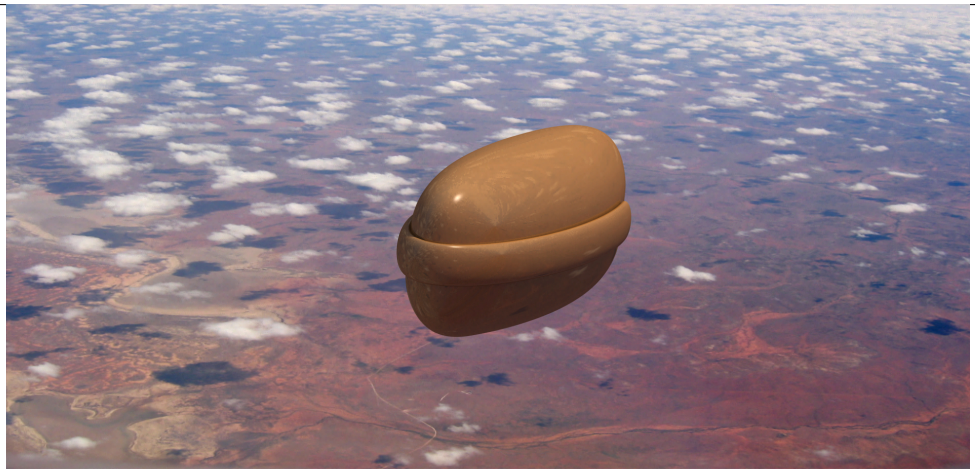

Figure 6.11: Liferaft as situated during flight

Motor The motor is the device that makes the propeller rotate and is therefore stored behind the batteries, as close to the back of the fuselage as possible. It is stored above the batteries, which makes the c.g. 2.70 m. The motor weighs 4.7 kg.

Frame The frame is fixed and the c.g. is at the middle of the fuselage, since the design is almost symmetric. The supportive rings for structural stiffness at impact shift the centre of gravity together with the window frame. The frame is designed such, that with the spacing of the rings and the thicknesses of the bars the c.g. is exactly in the middle of the fuselage. Therefore the c.g. of the fuselage frame is 1.50 m.

Pilot The pilot's location is also fixed. Basically the pilot was moved to the nose as much as possible. There should be however, enough space for his feet to move and due to the elliptic shape of the fuselage, the pilot cannot be moved entirely to the nose of the vehicle as the height of the fuselage decreases towards the nose. Based on the volume of the chair and the small toilet under the pilot, the c.g. is approximated at 1.45 m. The pilot mass and his c.g. are a summation of the pilot, the chair and the toilet. The pilot is sitting right before the middle of the fuselage, since most of his body is located before the middle.

Parachutes The parachutes are located at the back of the fuselage. When the batteries are dropped, the parachutes are deployed at the location where the fuselage is split up. Therefore the nose of the fuselage is pointed downwards during the emergency drop in the water.
Both of the parachutes are at this location at 0.70 m from the rear end of the fuselage, so the c.g. is 2.30 m. One of the parachutes deploys automatically if the batteries and propeller are dropped. The other parachute is deployed manually once the other parachute is not working.

Life raft The life raft is located around the fuselage. Therefore the c.g. is relatively close to the middle of the fuselage. However, the life raft can not surround the fuselage entirely, since the back of the fuselage is dropped during emergencies. Therefore, the packed life raft is U-shaped around the fuselage, as shown in Figure 6.11. The life raft during flight is given in Figure 6.11

Monitors The TSO monitors, mentioned in Section 6.3, are positioned 0.50 m in front of the pilot, since the pilot should be able to read the screens during flight. Therefore the c.g. becomes 1.0 m.

Control line system The pilot uses his feet to control the control lines as explained in Section 2.2.2. This system has a mass of 2.5 kg and is assumed to be located at 0.70 m from nose of the fuselage .

Electric wiring From the PV cells at the canopy, two electric wires are used for the transfer to the fuselage. The c.g. location of the electric wires is assumed to be in between the 2 rings from the fuselage structure, namely at 1.925 m from the datum line. This way the electric wires do not contribute to the c.g. location, since the moment arm is 0 with respect to the c.g. location that is described in Section 6.6.2.The electric wires are mainly used for a connection between the PV cells and the motor, but also to the subsystems that require electric power.

Other subsystems Now what is left are several subsystems that can be stored anywhere in the fuselage. Some subsystem should be in the reach of the pilot though. For instance the food, drinks and the life vest should be within reach of the pilot. This distance is estimated to be 0.5 m.
The subsystems that weigh less than 1 kg are ignored since they do not have a significant contribution.

6.6.2 Centre of gravity overview

The centre of gravity is determined using the forces generated by the tension lines. The rings in the fuselage that provide stiffness are also the location at which the tension lines are attached. By placing the c.g. precisely between these rings, the resultant moment at the fuselage is 0 Nm. Since the drag is equal to the thrust during steady symmetric flight and their arm with respect to the c.g. is assumed to be equal, the only contributors to the moment with respect to the x_{bf} -axis are the tensile forces of the control lines and the fuselage weight. The rings that carry the tension lines are located at, with the nose of the fuselage as a datum line, 1.50 m and 2.35 m. Therefore the c.g. is aimed to be at 1.925 m. In order to achieve this, the moment of each component with respect to this point is given in Table 6.13 In this table the $c.g._{effective}$ represents the c.g. with respect to the aimed c.g. of 1.925 m, so for instance the c.g. of the pilot becomes 1.50-1.925=-0.42 m.

Table 6.13: Center of gravity overview

Subsystem	c.g m	$c.g._{effective}$ m	Mass kg	Moment $N \cdot m$
Batteries	2.70	0.775	63.3	481.3
Motor	2.70	0.775	4.70	35.7
Propeller	3.10	1.175	1	11.5
Frame	1.50	-0.42	40	-167.0
Pilot	1.45	-0.425	80	-294.26
Parachutes	2.35	0.425	14	58.4
Life raft	1.50	-0.425	10	-41.7
Monitors	1	-0.925	6.48	-58.8
Control line system	0.70	-1.225	2.50	-30.0
Total	1.925	0	230.5	**-4.86**
Other subsystems	*1.97*	0.046	10.8	**4.86**

In Table 6.13, "Other subsystems" contains all the subsystems that weigh less than 1 kg plus the food, drinks, HTI Forward Osmosis and the spare battery. These subsystems should be within the range of the pilot, which is the case, since the pilot is located at 1.45 m from the front, the pilot can easily reach the food, drinks and the HTI Forward Osmosis. 0.52 m should be doable for the pilot. The total moment of -4.86 $N \cdot m$ is the moment that should be countered by the "Other subsystems". In order to do so the c.g. of the subsystems should be 1.97 m.
In Figure 6.12 the layout in longitudinal direction can be found.

6.6.3 Volume distribution

The fuselage shape is an ellipsoid, as shown in **??**. The a-axis is associated with the width, the b-axis with the height and the c-axis with the length. The volume of the fuselage is easily computed using Equation (6.13).

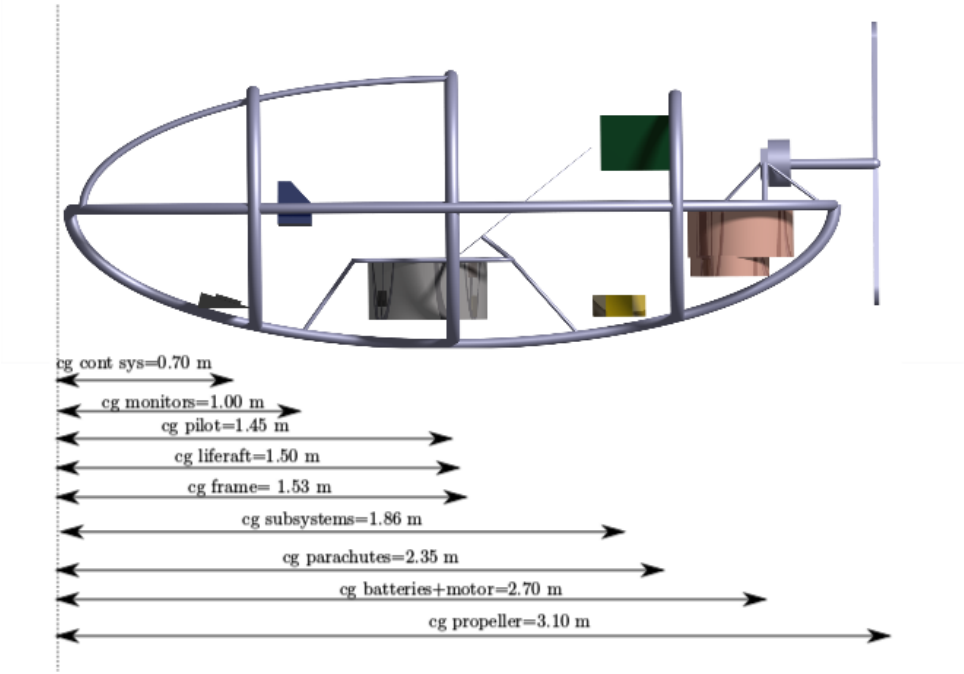

Figure 6.12: Layout fuselage in longitudinal direction

$$V_{ellipsoid} = \frac{4}{3} \cdot \pi \cdot r_a \cdot r_b \cdot r_c \tag{6.13}$$

Where r_a, r_b and r_c are the semi-axes of the ellipsoid. The height of the fuselage has been chosen to be 1.30 m, since this height is required for a person to fit. The pilot sits in a chair with the backrest of the chair under an angle of 45° with respect to the fuselage centre line.

The width is fixed by the dimensions of a person as well. The width of an average person is 0.65 m. This width is the distance between the shoulders of a person. The shoulders of the pilot are located at approximately z_{bf}=-0.80 m. The width at this z_{bf} location is less than the maximum width due to the elliptic shape of the fuselage. The width has therefore been chosen to be 1.00 m. The width at z_{bf}=-0.80 m is then still sufficient to fit a person.

The fuselage length was basically determined by 2 main factors. The pilot and his seat take up approximately the first 1.75 m of the fuselage. This is the case, since the pilot cannot be stored all the way at the front and a person has a certain length (assumed to be 1.80 m).
Apart from the pilot, the main contributor, as a requirement, to the fuselage length is the battery drop system. This system is located at the back of the fuselage (x_{bf}=2.40-3.00 m) For safety reasons, this 0.60 m is stretched to 0.75 m as the battery drop system requires some extra space in order to actually drop the rear end. With 0.75 m reserved for the battery drop system and 1.75 m for the pilot, the fuselage should be at least 2.50 m long.
The decision is made to make the total fuselage length 3 m. The extra 0.50 m is reserved for future changes. The fuselage length of 3.0 m makes it easier to store the subsystems and the extra 0.50 m is not a main contributor to the mass of the fuselage; only 3 kg extra. The profile drag is not significantly influenced by the length of the fuselage. The c.g. is easily placed in between the rings that carry the control line forces. In addition, the impact at an emergency landing should most likely be countered by a damper system. Therefore it is nice to have some longitudinal space reserved for such a system.
So in conclusion, the height is fixed, which makes r_b=0.65 m. The width is fixed, which made r_a=0.50 m. The length was variable within certain constraints and the decision was made to stretch the minimum of 2.50 m to 3.00 m, making the r_c 1.50 m. The total volume of the fuselage therefore is 2.04 m^3 or 2040 l.

6.7 Overview

In this section an overview is given of the subsystems. The mass, volume, c.g. location and the price are given in Table 6.14. Most of these systems are stored in the fuselage, however, the wing, PV cells and control lines are not.

Table 6.14: Overview of subsystems

Subsystem	Mass kg	Volume l	C.g. m	Cost €
Stimulants	0.001	0.001	1.97	7
Sunglasses	0.007	0.05	1.97	149
Ipad 3 Mini with case	0.38	0.24	1.97	399
Iridium Go	0.295	0.298	1.97	700
WAB-H18 Life Jacket	0.053	0.043	1.97	40
Compass	0.05	0.04	1.97	7
GPS 165 TSO	1.5	2	1	2'466
Garmin GRA5500	1.69	0.98	1	12'112
Garmin G600	2.90	3.6	1	25'911
v800 watch	0.079	0.004	1.5	470
Electric wiring	1.8	0.002	1.952	100
Ring sensor	0.070	0.002	1.5	200
Braun Thermoscan 7	0.15	0.04	1.97	35
HTI Forward Osmosis	1.1	2	1.97	80
Seahawk SDZ	0.093	0.05	1.97	100
Isatphone 2 Inmarsat	0.318	0.456	1.97	849
LED cabin light	0.10	0.22	1.97	12
Geiger Engineering HPD13.5	4.7	3.03	2.7	8'132
Green tea	4	4	1.97	3
Food	4	4	1.97	20
Propeller	1	N/A	4.00	6'000
Parachutes Magnum 300	14	23.52	2.60	4'758
Pitot tube	0.19	-	1.50	326
Life raft[(xxvii)]	10	30	1.50	1'298
Batteries	59.6	75	2.7	12'600
Spare battery	2	2	1.97	300
Hassock portable toilet	2.2	52	1.50	37
Control system	2.5	3.0	0.70	150
Pilot	80	150	1.50	-
Chair	3	100	1.50	100
Fuselage frame	40	2040	1.53	38'500
Total$_{fuselage}$	227.8	457	1.952	116'312
Wing[(xxviii)]	6.5	32'380	-	16'800
PV cells[(xxviii)]	41.0	-	-	1'307'250
Control lines[(xxviii)]	1.3	0.38	-	800
Trike	12	N/A	N/A	600
Total	**277.6**	-	-	**1'441'162**

[(xxvii)] Around fuselage

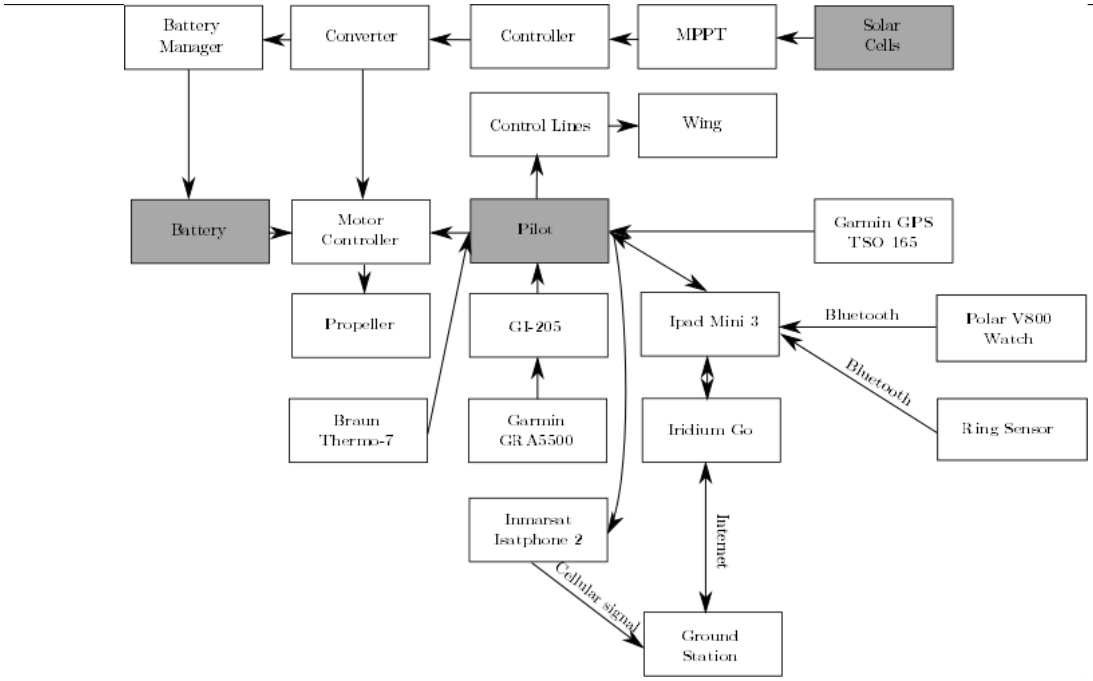

Figure 6.13: Subsystem interaction chart

Each subsystem has a certain role for the total system. The subsystems and their interactions with the pilot, battery and the PV cells. These systems are considered to be the most important. An overview of the subsystems and their interactions is given in Figure 6.13.

A visual representation of the subsystems can be found in Figure 6.14. As seen in the overview all the subsystems fit in the fuselage and there is plenty of moving space for the pilot.

(xxviii) Not in fuselage

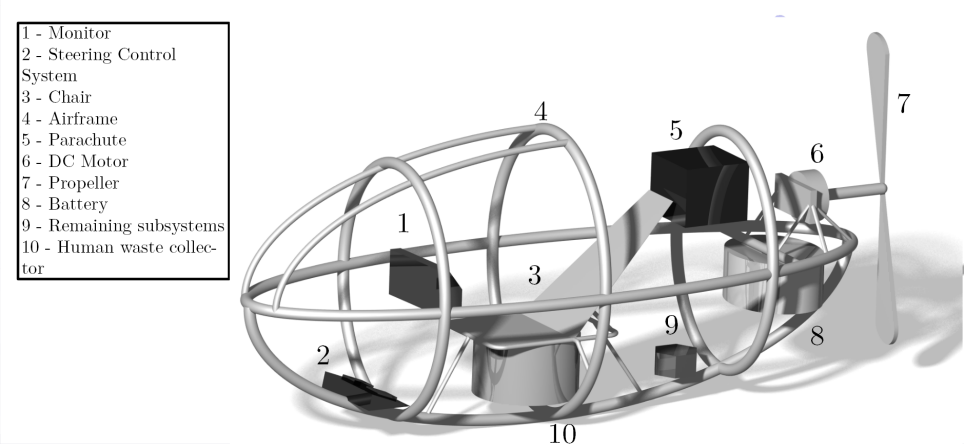

Figure 6.14: Caption Luuk

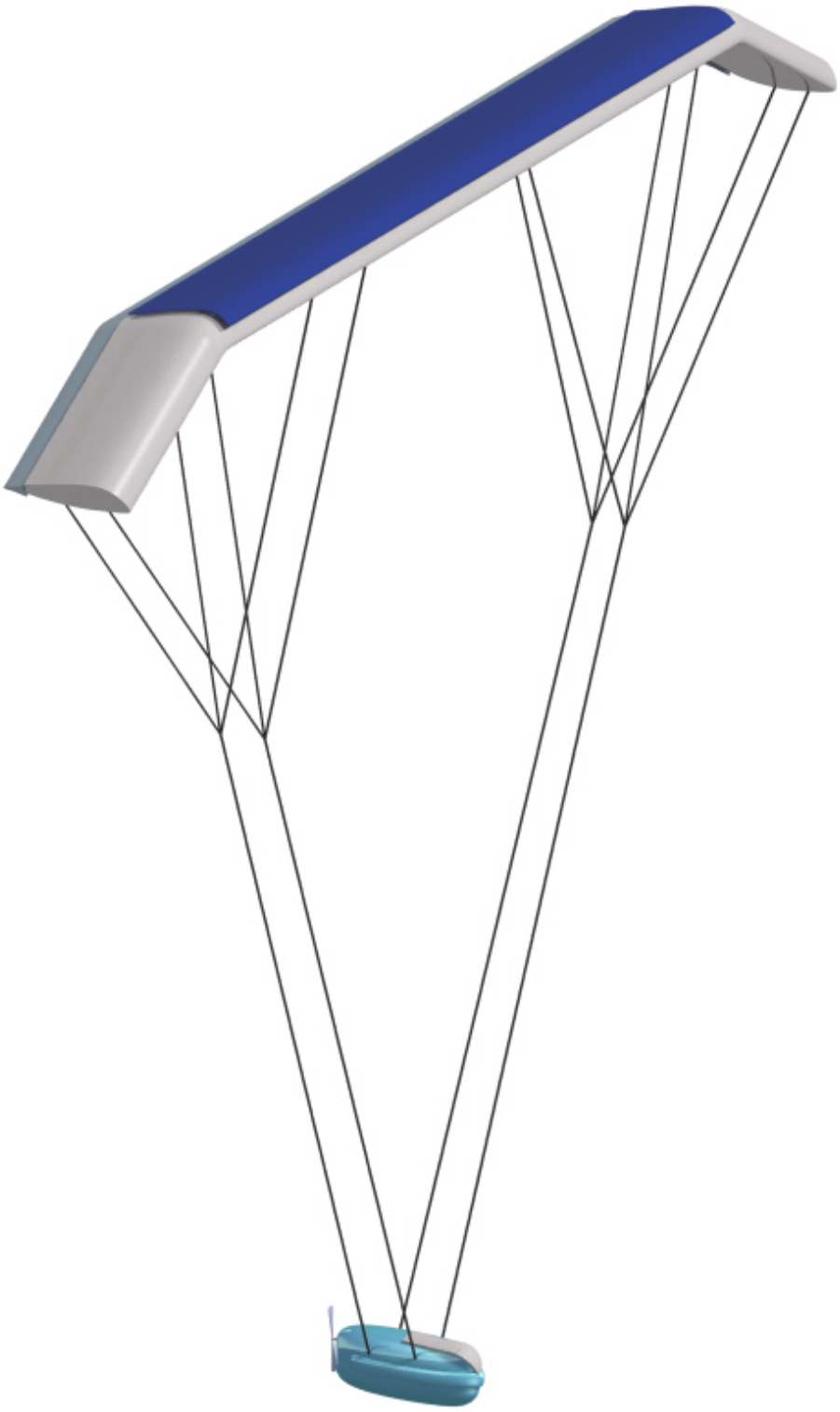

Figure 6.15: The paraglider during flight

7 Verification & Validation

For all the tools used in calculations and design iterations a verification and validation has been done to investigate the validity of the obtained results. To ensure that the results obtained are accurate.

7.1 Verification

Verification is used to confirm whether a tool or calculation and its specification are actually doing what the Team intends it to do. In essence this section should, for all the tools and calculations involved, answer one simple question:"Are we building the tool right?"

7.1.1 Qualitative Stability Analysis

In order to determine the stability the Flight Dynamics lectures notes have been used.[2] This gave a qualitative description of the PPG. After due research it has been verified with papers from NASA[5][7], Rochester Institute of Technology[52] and Textron Defense Systems[4] that the qualitative stability was indeed correctly calculated. However, it did not clearly determine the specific influences such as the anhedral angle and pendulum motion due to suspended loads. For proper accurate values, calculations with more complexity such as aerodynamic modelling should be done.

7.1.2 Airfoil Selection

In this part, the choice of the airfoil selection is verified. To begin with, the characteristics of the chosen NACA54126 airfoil are discussed. The NACA54126 airfoil has been chosen based on three characteristics. These are: thickness, camber, and reflex profile. The choice of using a relatively high thickness $t/c = 26.3\%$ is mainly due to the reason that, at low speeds, the stall angle of the airfoil is very high. This can be seen in Section 3.2 where $\alpha_{stall} = 23°$. Moreover, having a high thickness for the airfoil, provides a larger cross sectional surface area for the wing, in turn providing a larger internal wing volume. This is beneficial for the technical group dealing with the canopy structure. A larger internal volume for the wing also leads to more storage space for Helium, and this is verified in Chapter 4 since the storage volume for helium is known as 32.3 m^3. The reason for having chosen an airfoil with a certain amount of camber was so that it can provide lift at even $\alpha = 0°$. As can be seen in Figure 3.3, the NACA54126 airfoil has a $C_{l_{\alpha=0}} > 0$. The reason, to use an airfoil with a reflex camber, was such that the airfoil (and subsequently the wing) could provide a positive pitching moment (nose-up) for a certain range of α. The justification for using reflex airfoils has been verified by the already mentioned examples in Table 3.2, which exist in use for parafoils and hang-gliders. Apart from these, reflex airfoils are also extensively used by reputed paraglider manufacturers like Dudek, Skywalk and Ozone. For the NACA54126, it can be seen in Table 3.2 that for a range of $-5 \leq \alpha \leq 6$, the coefficient of moment C_m is positive.

7.1.3 Airfoil To Wing

In Section 3.3, a conversion from 2D airfoil data to 3D wing data has been made. This conversion is mainly based on Equation (3.3). Using this, Prandtl's 3D lift curve slope formula, and assuming the 2D Airfoil $C_{l_\alpha} = 2\pi$, a ratio between the 3D and 2D lift curve is found, $\frac{C_{L_\alpha}}{C_{l_\alpha}} = 0.78$. In order to see the wing's aerodynamic behaviour more accurately, either the use of CFD or experimental tests in wind tunnels must be undertaken. This is currently beyond the scope of the project due to resource limitations. However, to verify the use of Equation (3.3), as an appropriate estimation for 3D behaviour of the wing for a given airfoil, experts at the Aerodynamics department of the TU Delft have been consulted. They have suggested the team use the same approach as an appropriate approximation of 3D wing C_{L_α} as Equation (3.3).

7.1.4 MATLAB Iterations

In the programming files, multiple iterations have been performed. In order to make sure that all the optimums have been reached, the change in the values for the parameters have been investigated to see if they converge. In Figure 7.1, 7.2 and 7.3 some of these final parameters are shown and how they converge. From this it can be seen that the iterations converge. The code could be made more efficient, because from these figures it can be seen that the iteration could be stopped earlier in all cases, however, this does nicely illustrate that the codes fully converge.

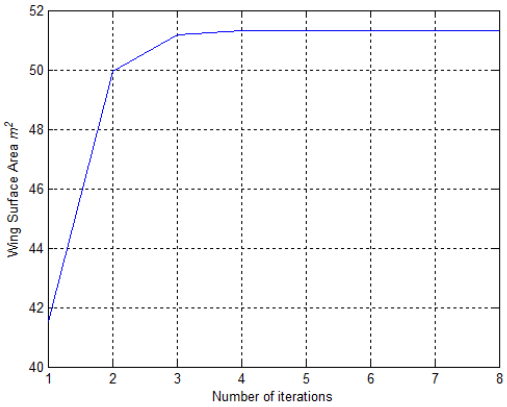

Figure 7.1: Iteration Convergence of the Wing Surface Area

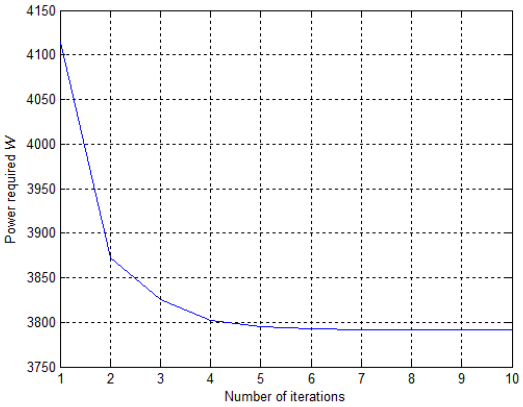

Figure 7.2: Iteration Convergence of the Power Required

7.1.5 Canopy Structural Tool

Verification is performed in order to check whether the numerical model works correctly and is coherent with the theory used to build the tool. The verification is divided in two main test: the unit test and the system test. The unit test is a qualitative check of each sub-function or block in the code. The system test is performed to verify the model as a whole; it checks whether all the functions (blocks) put together result in a reasonable output.
The unit tests or qualitative analysis for the numerical tool of the canopy design are explained below:

- *Multibubble design*: Verification of the mean camber line finder has consisted of testing a variety of different airfoils to visually inspect the results. The solution found has been judged very accurate

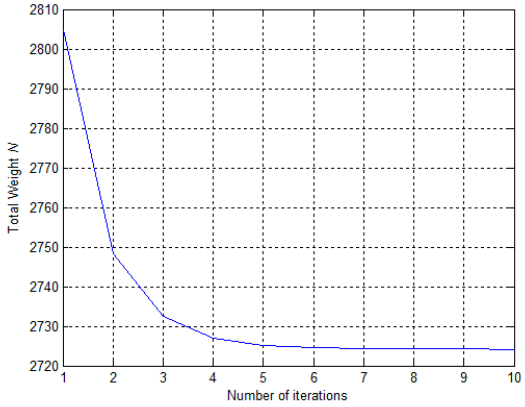

Figure 7.3: Iteration Convergence of the Total Weight

in between 0.5 and 0.95 $\frac{x}{c}$. Near the leading and trailing edge the mean camber line is up to 6% off. The functioning of the tool has been sufficient for the scope of this study. Therefore, even though a mathematically better performing solution had been found, it was decided not to numerically implement it. A quick fix with a manual scaling factor has proved convenient in this case.
Verification of the bubble geometry finder has consisted of visual inspection of plots obtained with different input parameters. Increasing the number of membranes has decreased the bubble spacing. Changing the inputs for the determination of the first and last bubble positions has yielded the desired geometry. As the mean camber line estimation was correct on a large portion of the chord length, the calculation of the bubble radius by means of the intersection points with the PCHIPs of the airfoil shape has been very accurate.
The calculation of output parameters of the bubble geometry finder has been verified by manual calculation and by critically assessing the validity of the output values one by one. The total material lengths have been approximated through calculation in a separate spreadsheet program. The bubble area output has first been verified by manually estimating the area of the airfoil to compare with the results of the code. The various input parameters for the amount and positions of the bubbles have also been used to conclude the correct functioning of the multibubble geometry finder.

- *Lift*: The function for the calculation of the maximum lift is verified by manually performing comparison calculations. By varying the airspeed, the lift coefficient, the density and the chord length the expected results have been obtained through this function.
- *Bending moment*: The plots found for the bending moments showed the expected parabolic function for both the spars and ribs. The highest loads were found for the front spar which is coherent with the fact that the front suspension line has to carry higher loads for moment equilibrium. Furthermore, by playing with variables such as the span length, chord length, and number of bubbles it could be checked whether the loads increased or decreased as expected.
- *Tensairity® elements*: Since the tensile elements have a higher yield strength than the compression elements, a lower needed area was expected and also found. They differ by a factor of 2 in yield strength, and so in the area needed which is coherent with Equation (4.18).
- *Overpressure*: The internal pressures depend on the radius of the bubble and the load applied according to equations explained in Section 4.8.5. This functional block was verified by finding highest needed pressures for the bubbles of smallest radius and highest applied load.
- *Wall stress*: The function for the calculation of the wall force and wall stress has been verified by manually performing calculations to compare with those of the tool. A plot has been made to verify the correct behaviour with varying distance between bubbles and internal pressure. By varying the thickness and the strength of the material the failure check has been verified. In case the calculated wall stress exceeded the failure stress the function indeed displayed the conclusion of material failure.

The total weight of the canopy structure is the final outcome of the integrated model. If the value found is within an expected range and varies accordingly when changing input parameters, the model works correctly as a whole. A total weight of $6.7kg$ was found for a the final design which consists of 9 bubbles, 10 spars and 6 ribs. When increasing the number of ribs the total weight of the structure decreased. The spar length would decrease with more ribs, and so the total needed area for the Tensairity® elements. The Tensairity® elements are quite heavy compared with the skin material, this would explain the drop in weight. When increasing the amount of bubbles however the weight increased due to an increase in material needed.

7.1.6 Fuselage Structural Tool

The fuselage has been modelled as a simply supported beam using MATLAB®. In order to verify the analytical solutions of the program, a calculation has been made by hand to compare the results. For the beam representation the moment of inertia of the frame beams has been taken as an equivalent moment of inertia as described in Equation (5.10). Filling in the values for the equivalent moment of inertia in

x-direction grants that $I_{equiv,x} = 2.00 \cdot 10^{-4} m^4$. Comparing the value with of the model results in the same value. From the beam model the normal stress has been calculated using Equation (5.11). The maximum normal stress will occur at the middle of the beam (highest moment). Calculating the normal stress for the maximum moment equals to $\sigma = 0.38 MPa$. Comparing the calculation with MATLAB® results in the same value. The other equation to verify is Equation (5.12). Checking the value for the maximum shear stress has been found to be $\tau = 0.21 MPa$. The model in MATLAB® supplies the same value for the maximum shear stress. The models checks out with the analytical calculations.

7.1.7 Impact Load Calculation Tool

The expressions used and method used in the tool for calculating the impact load for an emergency landing on water are shown in Section 5.1.3. It can be seen that the only variable changing during the impact is x, which is the momentary radius of the fuselage at the water surface. As specified in Equation (5.4), this radius is dependent on the depth of immersion h. h is defined as a vector between zero and h_{max} in steps of 0.001, the tool hence calculates the load for a new radius every time it moves 0.001 m further into the water. In order to verify the tool, the values for the intermediate steps have been checked by hand and rounded to four significant digits. The results are presented in Table 7.1. It can be seen that the values differ by a maximum of 0.0058 (m_v) and it therefore can be concluded that the tool is functional.

Parameter	Unit	Value code	Check
h	m	0.5000	0.5000
x	m	0.1344	0.1344
m_v	kg	7.8270	7.8328
V	ms^{-1}	0.0852	0.0852
a	G	0.0044	0.0044

Table 7.1: Impact load verification

7.1.8 Power Budget Tool

The power budget tool has been verified. To check whether the mission that has been designed is indeed the optimal mission, several variations were adapted. First, a mission was designed that took of during daylight. Next, a mission has been investigated that required two times more energy during one of the darkness phases. Keeping the other inputs the same, it has been analysed in what case the mass of the power system is minimal. The results are presented in Table 7.2. The mission profile that has been selected for the preliminary design was considered as reference point. Note that these tests have not been performed using the final values, this has, however, no influence on the ratio between the weights.

Table 7.2: Power system masses for verification of power budget tool

	Mass kg
Original mission profile	258.3
Mission start in daylight	Unable to take-off
Unequal energy division during darkness	350.1

From Table 7.2 it is clear that the original mission profile is the optimal mission. When the energy division between the darkness phases was set to be twice as large between the dark mission parts, the mass increased with almost 100 kg. When the mission starts in daylight the aircraft is unable to take-off as the PV system has not been designed to deliver the required power for climbing. A recommendation has been included to investigate the changes in the design when the power budget is sized for take-off in daylight.

To indicate that the best mission profile is calculated correctly, it has been needed to verify the calculations performed in the tool. The influence of the wind speed and the airspeed were investigated. It was expected that the duration of the mission increases when either of these values is decreased. When halving both of the speeds the duration increased twofold. Increasing either of the speeds resulted in a decrease of the duration.

Second, the impact of glide ratio is analysed. When the glide ratio is doubled, the required power halves based on Equation (7.1). When this adjustment was made in the tool the required power indeed changed as expected.

$$P_r = \frac{W}{GR} \cdot v \tag{7.1}$$

To size the PV panels, the true solar influx is needed. The value obtained in the tool was compared to the value obtained in the MRR, which is 831 $W \cdot m^{-2}$. The value obtained is 842 $W \cdot m^{-2}$, which defers by 1.3%. To make sure that the consumed energy during both parts of the mission are equal the required energy per part have been fixed in the final tool, so that the required energy stored in the battery for both parts are identical.

The efficiency of the propeller is determinant for the mission. A decrease in propeller efficiency results in a larger mass of the the aircraft. As the mission is performed at a low airspeed the efficiency is not high. The efficiency has been assumed to be 0.76, based on reference values and theoretic data. The propeller has to be tested to find out if the motor and propeller can indeed deliver the given efficiencies. If the test data notify that the propeller does not meet this requirements with any RPM the propeller diameter has to be increased to a maximum diameter of 2.1 m, at which the wing tips reach 0.88 M. A study for noise reduction has to be done in this case as well.

The wind speed during climb phase has been assumed to be a constant which has the value of the average wind speed between the ground wind speed and the wind speed at cruise altitude. In reality the wind speed increases exponentially up until the cruise altitude. The assumption that has been made thus overestimates the wind speed during climb phase. A linear relation between the covered distance would have resulted in the same average wind speed, but an exponential relation has less area under the graph and thus the real average wind speed is lower as is proven by Jensen's inequality theorem.[53]

A safety factor of 1.05 has been included in the design of the PV cells as the cells have been formatted in a module to provide a realistic value for the efficiency of a PV module due to the packing density. As the PV cells have a square shape the packing density is maximised.

During last stages of the design it has been concluded that the tool is not completely correct. This has come to notice during the sensitivity analysis presented in Section 8.3.3. The power required is computed using the total weight of the design, without the helium contribution, even though it should have done this. The helium contribution can be incorporated by basically treating it as a weight reduction of the whole design. This has been done for all the other tools, but was wrongly communicated and therefore wrongly used in this tool. The influence of this is that the power required is calculated to be higher than it should actually be, making the whole energy budget of the design overdesigned. Too many PV cells and batteries are incorporated, which also increases the mass in two ways. The influence of this on the feasibility of the design is the following: if it is to be concluded that the design is feasible, it is overdesigned and if it is concluded to not be feasible by a small margin, it could still be feasible and this needs to be investigated. This will be reflected upon in Section 8.4.

7.2 Validation

It is important to note that even though validation has been done separate from verification in some cases, the activities are complementary. The validation of numerical and calculation tools is very important to establish the compliance between the tools and the real situation.In essence this section should, for all the tools and calculations involved, answer one simple question: "Are we building the right tool?" However when comparing experimental and theoretical results for the validations of calculation tool the

assumption has been made that the experimental results do not perfectly resemble the real situation. This is why there can be small differences even though the tool is completely accurate.

7.2.1 Qualitative Stability Analysis

The best method to find out if the PPG's stability is positive is through experiments. This is currently impossible as it is not a physical vehicle yet. The next step would be to simulate and receive some numerical values for the different stability derivatives. This was also impossible as the canopy, the biggest influence, was not designed yet as well. The same problem arises when the turn rate, pitch rate, thrust dependant oscillation etc. need to be modelled. This made the sizing of ailerons quite difficult and thus no exact values can be computed. As the PPG needs to be designed for a steady sustained cruise the most important ability is to have positive stability and that it must be able to alter its direction, even if this means it turns slowly compared to normal paragliders.

For stability, the biggest hurdle is to prove the parafoil-payload model accurately models the PPG that is being designed. This could be overcome by using dedicated software such as developed by Dutch Space to model gliding parachute delivery systems.[54] Also, all literature uses a parafoil with either no anhedral or with a continuous poly anhedral. The difference this makes with a canopy with only anhedral tips should be investigated properly. This is left as a recommendation for further improvements.

7.2.2 JavaFoil

The first step in calculating the control forces is finding the lift coefficient C_l for different angles of attack α, this has been done using JavaFoil. The well known tool interface is shown in Figure 7.4. The developer of the tool, Martin Hepperle, has done validation for the tool and Figure 7.5 shows a typical comparison between both theoretical analysis methods and experimental results at low Reynolds numbers. This figure shows the results for a comparison between XFOIL (numerical) and PROFIL (numerical) which are similar calculation tools with data from the Althaus experiment.

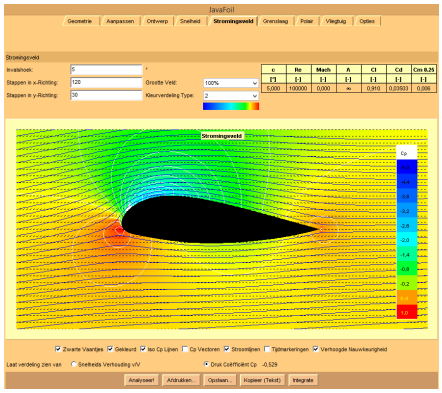

Figure 7.4: JavaFoil interface used to obtain values for C_l at α

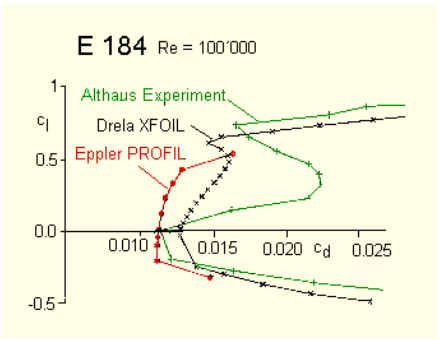

Figure 7.5: Typical comparison between both theoretical analysis methods and experimental results at low Reynolds numbers [(a)]

[(a)] URL `http://www.mh-aerotools.de/airfoils/index.htm`

The biggest discrepancy between the experimental data and the numerical data can be explained by the laminar separation bubble. As can be observed in Figure 7.5 this phenomenon has an impact on the drag coefficient for certain values of C_l. This potential addition to C_d has been taken into account, however because no actual numbers are known for the drag of the wing this problem has been noted and requires experimental research beyond the scope of this DSE. By noting this and the fact that a Reynold's number above 2'000'000 has been used, the validity of the results obtained in Chapter 2 and Chapter 3 is not compromised.

7.2.3 Line drag

In Section 3.5, the drag of the all the lines has been calculated to be 14.3 N. From reference, it has been taken that the line drag is typically around 10% of the total drag.[55] For this case it is a little less, around 7.5%, but since this design has minimised the amount of lines and the number of lines is less than for conventional paragliders, the value found for line drag is deemed acceptable.

7.2.4 Canopy Structural Tool

The structural design of the canopy is unique and thus no tests have been done with a prototype of this design so far. Therefore one cannot completely rely on the numerical values found from tests on similar inflated wings. However, it can give a feeling of whether the resulting values are within an acceptable range. An acceptable range is considered to be within the same order of magnitude. The parameters that can be validated within this perspective are the weight, internal pressure and stresses which can be compared to numerical values of other inflatable wing designs.

According to Gal-rom and Raveh in their "Simplified Aerostructural Static Model for Inflated Wings" the stresses in the membrane lie around 20-100 MPa.[28] The maximum stresses found for the anhedral and horizontal section were 23 MPa and 43.2 MPa respectively which falls within this range.
The internal pressures are quite different from aircraft to aircraft as is shown in Table 7.3.[56] Some aircraft have very high pressures while having a small wingspan, while others lower pressures and a higher wingspan. There is thus no fixed pattern to be found. This is because each wing design is different and so is the pressurisation needed to support the loads. Also the mission differs from vehicle to vehicle, altering parameters such as flight velocity, height and duration. Therefore it is impossible to validate with certainty the pressure found for this wing. However the pressures range from 48-1240 kPa, the design value of 113 kPa falls within this range as well.

Table 7.3: Parameters inflatable wing vehicles

Vehicle	Pressure	Span
Unit	kPa	m
Apteron	185	1.55
ERADS	895	8.8
Inflatoplane	48	6.7
I2000	1240	1.6

For aircraft weights the most comparable designs are the paragliders. A paraglider usually weights around 8 kg, has a wing area of about 30 m^2 and has about 90 cells[(i)]. This wing weights about 6.8 kg which is lighter than the usual paraglider. This can be explained by the fact that the materials used are lighter, stronger and the wing is sealed and pressurised with helium which adds more rigidity and thus less material is needed to support the loads.

As shown, it is difficult to validate the model with already existing numerical values based on references. It is recommended to further research to perform tests with a prototype of the wing itself to validate and test the accuracy of the numerical model.

7.2.5 Fuselage Structural Tool

For the validation of the model, reference calculations of a similar set up where compared. As a reference calculation a simply supported beam with a distributed load has been used [(ii)]. The difference between the model and the validation is that the geometry validation has a rectangular cross-section. Therefore the model has been adjusted to represent similar problem. For the calculations the moment of inertia

[(i)] `http://www.paragliding.org/book/en/11-1.htm`
[(ii)] URL `http://www.merc.zju.edu.cn/htw/files/2013/032713-chap5a.pdf` [cited 21-01-2015]

was changed appropriately. The model implemented with the changes grant the same results as the reference calculation. In Table 7.4 the values can be found.

Table 7.4: Validation of the fuselage structural tool

Symbol	Unit	Validation	Model	error
σ	MPa	6.25	0.375	0
τ	MPa	6.25	0.375	0

7.2.6 Impact Load Calculation

The impact load calculation gives reasonable outputs when comparing to reference values for space craft, but it has to be kept in mind that reentry vehicles and space probes differ quite a bit in shape compared to our fuselage.[38][37] Due to the major assumptions made in Section 5.1.3 the real value for the peak load can differ quite a bit. A better simulation of the load case can be made by building an FEM tool to simulate the point loads and local stresses more accurately.

8 Feasibility

Now that the paraglider is designed and sized, a feasibility of the design integration is done. This chapter deals with certain aspects of the entire feasibility of the design. To start with, the flight profile is briefly described in Section 8.1. Then, a performance analysis of the system on a whole is done in Section 8.2 to check if all the parts of the design comply with its overall performance. Once this is done, the system's sensitivity is analysed in Section 8.3 with respect to changing certain parameters. Then, a feasibility check of the whole system is done in Section 8.4, to make sure any changes added to the design benefit its performance. Along with that a requirement compliance is conducted in Section 8.4.1 to check off all the system's performance attributes with respect to the top and lower level requirements. Following that, a plan for the future of the project is made in Section 8.5 and the way sustainability is involved in this project is discussed in Section 8.6. Then, a RAMS characteristics study is conducted in Section 8.7. And finally, the chapter ends with a cost analysis of the entire project in Section 8.8. This crucial chapter is decisive in showcasing the success of the feasibility of the Team's design.

8.1 Flight Profile

The mission profile and its characteristics have already been described in Section 1.4 and Section 6.1. This section summarises the most important flight parameters.

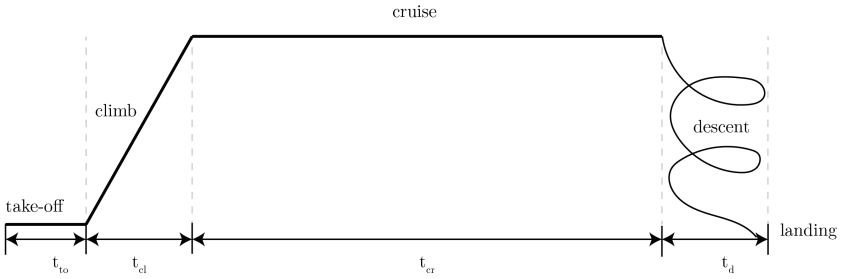

Figure 8.1: Flight profile diagram

In Figure 8.1, the overall mission profile is shown. As can be seen in the figure, the flight is broken down into distinct phases: Take-off and climb, cruise, and descent and landing. These phases and their respective aerodynamic performance requirements are discussed briefly in the upcoming subsections.

8.1.1 Take-off

From the point where the wing is inflated, is suspended in the air and the motor is started, to the point where the pilot is flying in a stable manner and will start climbing, is considered as the take-off phase. It will not last longer than the first few minutes of flight, represented by t_{t0} in Figure 8.1. During this part, the paraglider will start driving on the ground up, pushed by the propeller, until the point where the wing starts generating enough lift to carry all the weight of the whole system. The carriage that is underneath the fuselage will then be dropped such that the paraglider can climb without the extra weight.

8.1.2 Climb

In Section 6.1, the motor has been chosen and this has provided a Rate of Climb (RoC) of 0.57 $m \cdot s^{-1}$. With this RoC it will take about 1 *hour* and 29 *minutes* to reach cruise altitude, within time span t_{cl} in Figure 8.1. During climb, the density of the air will decrease. This would affect a reciprocating engine or

gas turbine, but only hardly or even positively affect the RoC for an electrically driven propeller design. Therefore a constant RoC has been used.

8.1.3 Cruise

When the paraglider reaches the cruise altitude of 10'000 ft the cruise phase start. In this phase, the optimum GR is around 13.2 and the velocity is steady at 10 $m \cdot s^{-1}$. This is the most time intensive part of the flight and the duration for the cruise is 35 h and 17 min, shown as t_{cr} in Figure 8.1.

8.1.4 Descent and landing

After the cruise phase, the final phase of the flight is the descent and landing. In the case of the flight of the paraglider, the descent occurs in a downward spiral, with a GR of -12. The velocity is decreased until the landing velocity is reached. The duration of this phase is the smallest with 57 min, depicted between time t_d in Figure 8.1. Once the paraglider has safely landed, the flight is complete.

8.2 Performance Analysis

In the previous chapters, the whole design has been specified and at this moment all the design parameters are known. The parameters that define the performance most for the design are listed in Table 8.1. In this table, four different cases can be seen. Case 1, 2 and 3 differ on the cruise speed (IAS) and the fuselage mass being: 12.5 $m \cdot s^{-1}$ and 53.0 kg, 10.0 $m \cdot s^{-1}$ and 53.0 kg, 10.0 $m \cdot s^{-1}$ and 40.0 kg, respectively. This sequence of values originates from the fact that when this project was started a cruise speed of 12.5 $m \cdot s^{-1}$ had been assumed. This was the maximum cruise speed found for reference paragliders, that operate within a cruise speed range of 10.0 $m \cdot s^{-1}$ and 12.5 $m \cdot s^{-1}$ as has been mentioned in Section 1.4. With this maximum value the mission duration would be the smallest and at that moment in time it was thought that mission duration was the limiting factor of this mission. However, near the end of the design process it became clear that the design was not feasible, as has been explained in Section 8.4. Mission duration was no longer the limiting factor, but available wing area for PV cells seemed to be limiting the design. For this reason, the power required had to be reduced and a more efficient speed of 10.0 $m \cdot s^{-1}$ had been decided upon and this cruise speed has been used throughout the report, this is Case 2. In an even later stage the fuselage mass has been changed from 53.0 kg to 40.0 kg which again changed all the performance parameters. This led to the design set of parameters called Case 3, the set of parameters used in the report. The design process that has been involved in these changes is elaborated upon in Section 8.4.

Lastly, Case 4 is described in the final column. This is the case for which a correct power budget tool has been used, in contrast to the other cases. In Section 7.1.8 on verification it has been stated that during the sensitivity analysis of the power budget tool, it has come forward that this tool is not completely correct. The design is overdesigned with respect to the power budget and because of this it is also too heavy. In Table 8.1 one can see the consequences of this correction. Whether or not this is a decisive factor for the design is reflected upon in Section 8.4.

8.3 Sensitivity Analysis Of The Full Design

It has been concluded, that with the current parameters, the system is feasible. However, it is important that the Team conducts a sensitivity analysis of the whole system's response to changes in certain parameters. This helps the Team in understanding the behaviour of the paraglider with respect to some main design parameters. This understanding of the systems response to changes in parameters helps the team streamline into a specific re-design if necessary.

The parameters that have been manipulated for this sensitivity analysis are: total system mass, propeller efficiency, pressurisation gas, wing profile drag coefficient and cruise speed. The sensitivity analysis is conducted for Case 1 Table 8.1, which is with a cruise speed of 12.5 $m \cdot s^{-1}$. A sensitivity

Table 8.1: Performance Analysis

Parameter	Unit	Case 1	Case 2	Case 3	*Case 4*
Indicated airspeed	$m \cdot s^{-1}$	**12.5**	**10.0**	**10.0**	*10.0*
Mission duration	h	33.6	38.3	37.9	*37.5*
Climb phase duration	h	1.34	2.18	1.68	*1.07*
Cruise phase duration	h	31.5	35.2	35.3	*35.4*
Descent phase duration	h	0.75	0.96	0.95	*0.95*
Total mass	kg	324	297	277	*266*
Battery mass	kg	80.1	63.4	59.6	*52.6*
Photovoltaics mass	kg	55.0	43.6	41.0	*36.2*
Fuselage structure mass	kg	**53.0**	**53.0**	**40.0**	*40*
Power required at cruise	kW	5.08	4.02	3.79	*3.34*
Rate of climb at cruise	$m \cdot s^{-1}$	0.72	0.44	0.57	*0.79*
Area of PV cells	m^2	44.6	35.3	33.2	*26.3*
Wing span of PV cells	m	30.6	19.7	19.2	*17.2*
Wing surface area	m^2	53.2	80.3	75.1	*72.4*
Wing span	m	21.9	26.9	26.0	*25.5*
Available PV cell surface area	m^2	31.9	48.3	45.1	*43.5*
Helium lift at cruise	N	161	246	227	*219*
Wing lift at cruise	kN	3.02	2.67	2.50	*2.39*
Total drag at cruise	N	238	205	194	*183*
Glide ratio at cruise	–	12.9	13.2	13.1	*13.0*

analysis of this case has been done, since the system is infeasible and a sensitivity analysis helps narrowing down on the specifics of a re-design.

8.3.1 Total System Mass

The changes in the system's total mass are analysed here. Currently the mass of the system, as mentioned in Section 8.2, is $M_{tot} = 303.46kg$. Changing the system mass, leads to the some changes. Table 8.2 shows the changes in the system's behaviour with respect to changes in mass of the system.

Table 8.2: Performance sensitivity to changes in total mass

Total mass kg	Power required kW	Wingspan m	PV span m
303	4.79	21.6	29.9
243	4.67	18.9	27.7

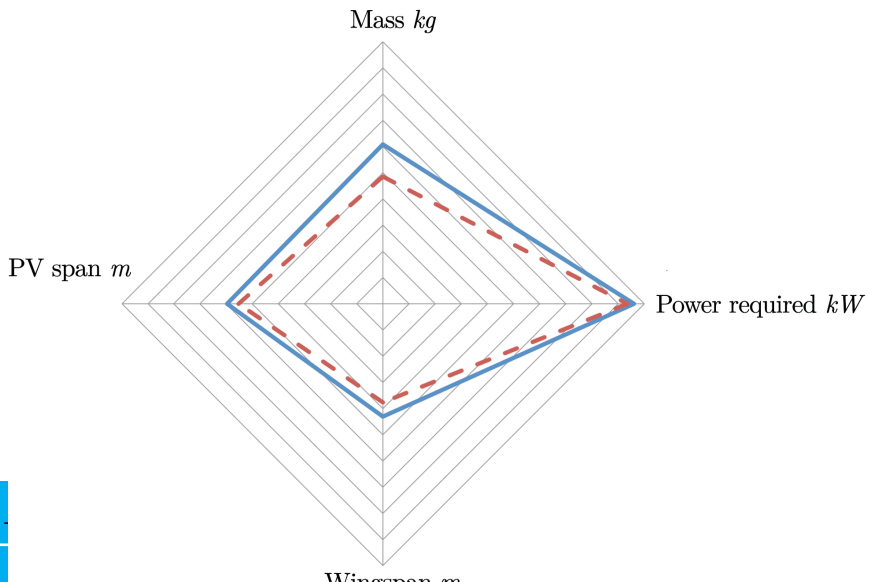

Table 8.4: Performance sensitivity to changes in propeller efficiency

Propeller efficiency	Total mass kg	Power required W	Wingspan m	PV span m
0.76	303	4.79	21.6	29.9
0.92	273	3.66	20.4	23.7

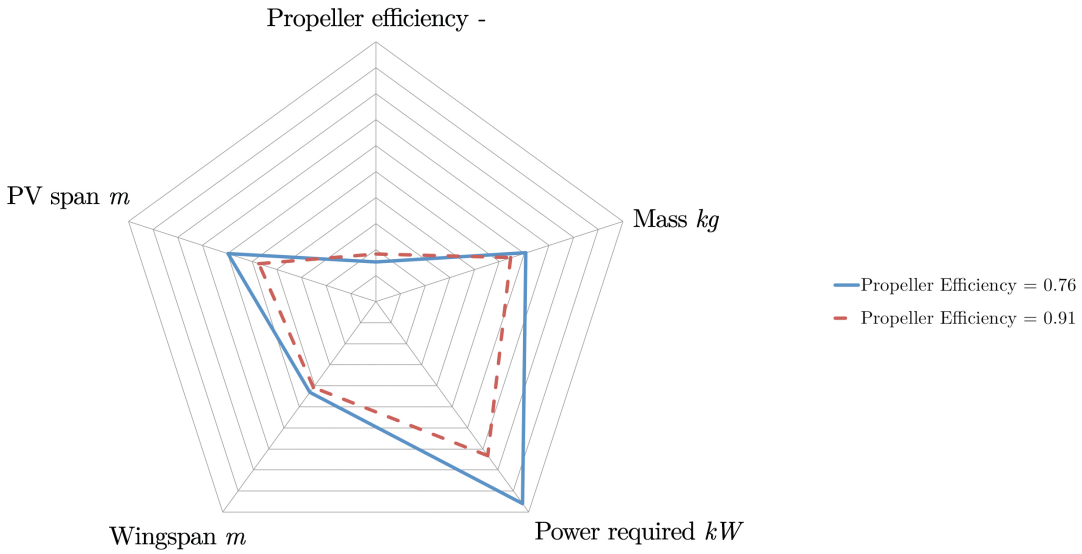

Figure 8.3: Spider plot showing system sensitivity to change in propeller efficiency

8.3.3 Pressurisation Gas

The Team has decided to use helium as the gas for pressurisation of the wing. However, it is important to see the performance of the wing if air is used instead of helium.

Table 8.6: Performance sensitivity to changes in pressurisation gas

Pressurisation gas	Total mass kg	Power required W	Wingspan m	PV span m
Helium	303	4.79	21.6	29.9
Air	302	4.75	21.8	28.7

Table 8.6 and Figure 8.4 represent the changes in the system's behaviour with respect to change in the pressurisation gas from helium to air. As can be seen, the sensitivity of the systems response to changing the gas to air is very minimal.

The changes that do happen seem counter intuitive at first, but can be explained. When removing the helium from the wing, the aerodynamic lift to be generated by the wing increases, but only slightly increases its drag. Because of this the GR will increase, which decreases the power required and thus also the required PV cell area and span. Since more aerodynamic lift needs to be generated, the total wingspan will increase. The reason the calculation works this way, is because for power required the total weight of the design has been used, whereas the total weight minus the contribution of the lift from

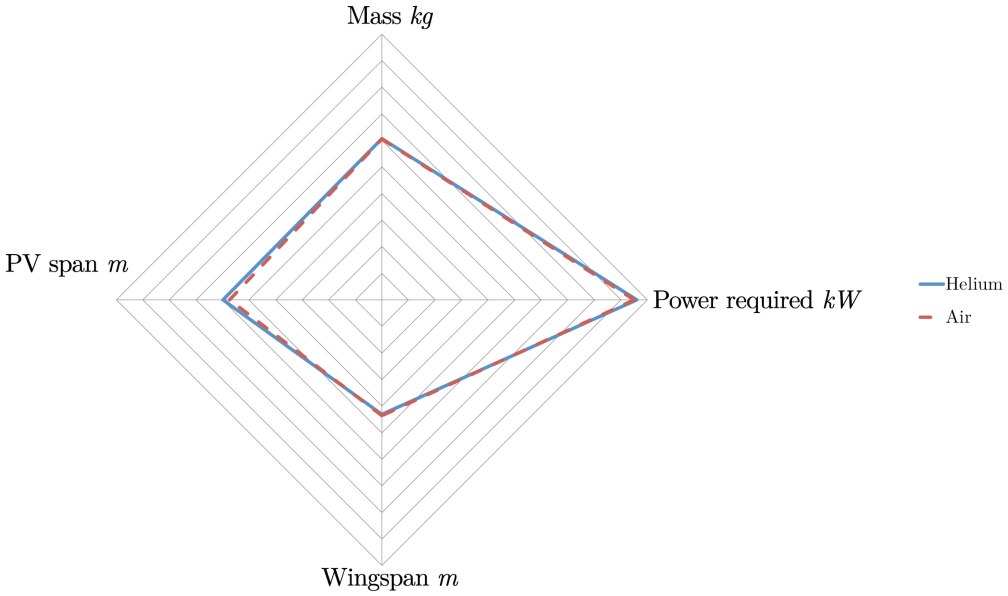

Figure 8.4: Spider plot showing system sensitivity to change in pressurisation gas

the helium should have been used. The tool used is not completely correct, as has already been stated in Section 7.1.8 and the consequences of this have already been shown in Section 8.2. In Section 8.4 it has been stated whether or not this error is decisive for the mission. The altered table and spider plot can be seen in Table 8.8 Figure 8.5.

Table 8.8: Correct performance sensitivity to changes in pressurisation gas

Pressurisation gas	Total mass kg	Power required W	Wingspan m	PV span m
Helium	266	3.34	25.5	17.23
Air	277	3.74	27.2	18.07

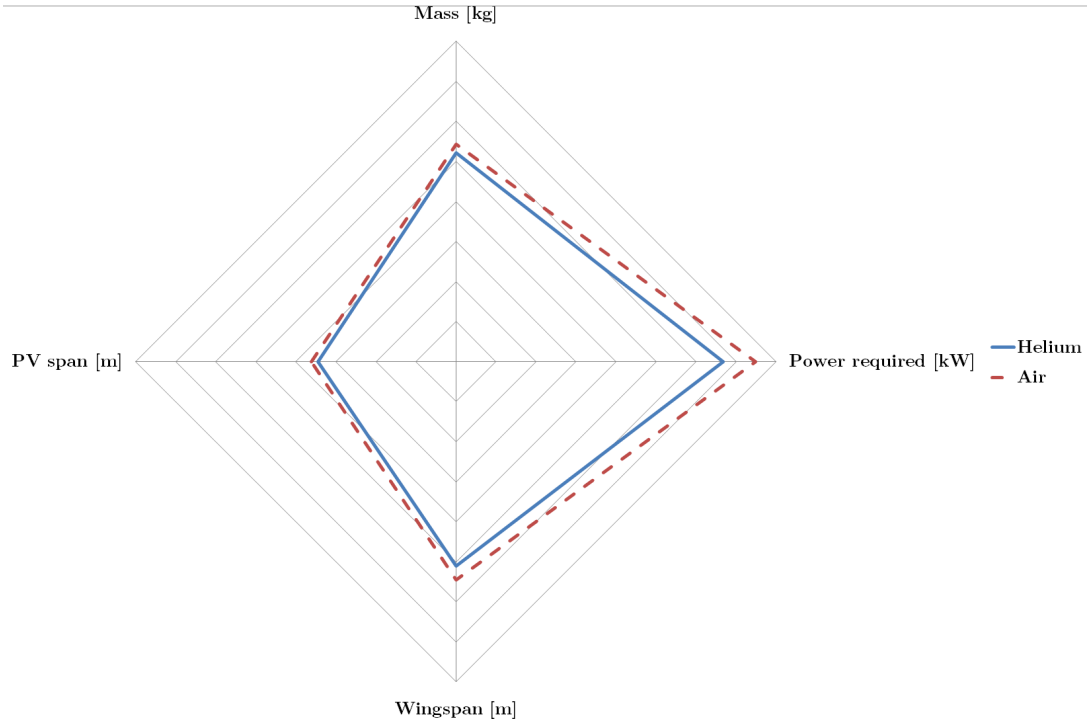

Figure 8.5: Spider plot showing correct system sensitivity to change in pressurisation gas

From this figure (Figure 8.5, it can be seen that changing the pressurisation gas from helium to air

However, doing this doesn't let the MATLAB® script run since the system fails in the second darkness phase of the flight. The team has, hence, decided to check the sensitivity with a drag increase of 10%.

Table 8.10: Performance sensitivity to changes in drag

Drag N	Total mass kg	Power required W	Wingspan m	PV span m
221	303	4.79	21.6	29.9
243	325	5.59	21.7	34.0

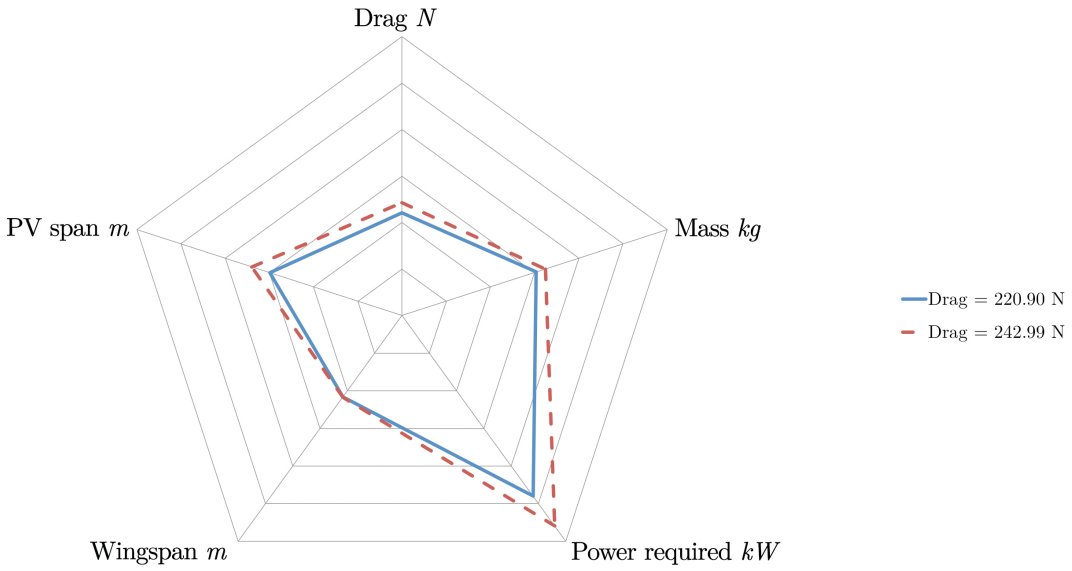

Figure 8.6: Spider plot showing system sensitivity to change in drag

Table 8.10 and Figure 8.6 represent the sensitivity of the system towards a 10% increase in drag from 221 N to 243 N. This increase in drag leads to a significant increase in the PV span, further making the flight unfeasible with the given wing area.

8.3.5 Cruise Speed

The cruise speed has been chosen as 12.5 $m \cdot s^{-1}$. As already mentioned, it is a reasonable number as it corresponds within a suitable range of reference paraglider speeds. However, choosing a different speed within the range and analysing its effect on the system's overall performance is important.

Table 8.12: Performance sensitivity to changes in cruise speed

Cruise speed $m \cdot s^{-1}$	Total mass kg	Power required W	Wingspan m	PV span m
12.5	303	4.79	21.6	29.9
10.0	278	3.79	26.0	19.20

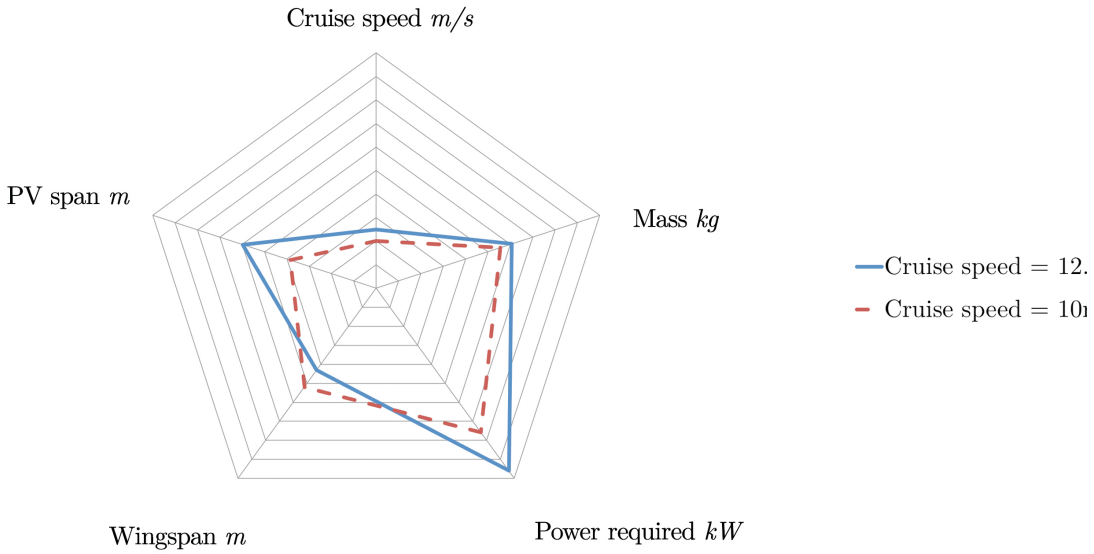

Figure 8.7: Spider plot showing system sensitivity to change in cruise speed

When the cruise speed is reduced by 20% to $10ms^{-1}$, the changes in the system's behaviour are significant. Apart from significant reductions in mass and power required, the PV span reduces significantly while the wingspan increases. The PV span is no longer larger than the wingspan, implying that the PV cells can fit on the wing.

8.4 Feasibility Check

As has been said in the introduction of this chapter, if a close look is taken at Case 1 in Table 8.1, the span of PV cells that is needed to deliver the power required is larger than the total wing span of the complete wing. Of course this is not a feasible design, since for this design, it has been decided that no PV cells are to be placed on the fuselage and for Case 1 this would mean that not enough power can be produced by the PV cells on the wing to sustain flight for a long duration. Another remark to be made, which can be read in Section 4.8.3 is that only the middle section has been designed for taking the weight of the PV cells. Also, only 60% of the chord is to be covered with PV cells because of the leading edge not being able to be used nor the jet flap area. Because of this, the wing surface area and PV cell area are not to be compared with each other, but the required span value for PV cells has to be compared to the total wing span. It can be concluded that the main two problems are; that the power that is required is too large with respect to the amount of lift that has to be created or the area allocated to deliver the required amount of power is too small. Multiple solutions for these problems can be thought of, with their respective drawbacks and advantages:

Use of a correct power budget tool

As has been stated in Section 7.1.8 and proven in Section 8.3.3, the power budget tool was not completely correct. The power required is calculated to be 12% higher than it would actually be if for this calculation not the total weight of the design had been used, but the helium lift contribution would have been added to this. Therefore it has been investigated whether fixing this error can completely fix the problem of the required wingspan for PV cells being larger than the available wing span. It has been found, that even with a correct calculation that requires less PV cells, the available wing span is still not sufficient. A shortage of 7 m wing span is still encountered.

Increase the wingspan

To allocate the required PV cell area, one could simply increase the wingspan and thus the wing area of the design to allocate the PV cells. However, this would provide redundant lift and make the whole design heavier as well, because of a larger wing. Since this is not efficient and far from optimal, this is not a preferred solution.

Decrease Drag

To decrease the power required, one could strive for decreasing the total drag of the design. However, the drag of the fuselage is already very low, and already very few lines are used between the fuselage and the wing, so not much is to be gained on these parts. The drag created by the wing is the main contributor to the total drag, so one could look for drag reductions here. However, this would call for a redesign of the airfoil and/or wing. For instance, a higher aspect ratio of the wing would be decrease the induced drag, but at this stage of the design, making such a large design change is not possible anymore. A thinner airfoil would also help decrease the profile drag, but this is also not feasible since this also imposes a smaller lift coefficient on the design and with the chosen low airspeed, this would require a very large wing area, which would again increase the drag and make the whole design heavier.

Put photovoltaic cells on the fuselage or the anhedral wingtips

Another way of allocating the required PV cells, is by looking for new areas to put them on. The anhedral sides of the wing could be made structurally sound to put the PV cells on. However, this would slightly increase the structural weight of the wing, requiring a little more PV cells. Also, at this moment, the total area on the wing available for PV cells, is not large enough to hold the PV cells required. Another area to use for placing PV cells is the fuselage. This has two major drawbacks though. Firstly, this would only help with about 6 m^2 and secondly, the inclination angle with respect to the sun is so high during midday, that the efficiency of the PV cells would be very low and thus would not help much and mostly add much weight as has also been discussed in the MRR [14, Section 4.2].

Higher percentage of chord suitable for PV cells

The requirement that limits the percentage of the chord to be covered with PV cells could be changed. For structural reasons the aft limit for placing PV cells is determined by the last pressure

bubble in the wing structure. The wing could be designed to have the last bubble move more backwards, but this would leave less area available for control surfaces and this would increase the control forces. Increasing these would require a pulley system to reduce the load, but this would increase the weight and also require the pilot to exert the force over larger areas, requiring a larger fuselage, which would again increase the weight etc. Therefore, this is not a feasible solution.

Lower cruise speed

The way both the area available for PV cells is increased and the total required PV cell area can be decreased is by lowering the cruise speed. With the same lift coefficient, a larger wing area is needed to provide the same amount of lift (see Equation (3.7a)) and the drag decreases because the drag coefficient for the systems almost stays the same, as will the related surface area (see Equation (3.9)). The wing will become a little larger, but the wing weight is very low, so even a 100 % increase would only increase the mass with around 7 kg.

From this list of solutions, the last solution is clearly the easiest and most effective way of solving the problem. Also, since the resources were not available anymore to investigate all the other solutions into much depth and perhaps decide upon a combination of the above, the solution of changing the cruise speed is chosen. Since this parameter was chosen to be 12.5 $m \cdot s^{-1}$, based on a range of flying speeds from paragliders and its sensitivity is very high, as can be seen in Section 8.3, changing this parameter to solve the problem is very sensible. Lowering the speed to 10.0 $m \cdot s^{-1}$ will completely solve the problem and is still within the range of paraglider speeds as was mentioned in Section 1.4. As has been stated in the introduction of this chapter.

The new performance parameters that correspond to the new cruise speed are displayed in Table 8.1 as Case 2, in which it can be seen that the available PV cell area is much larger than the needed area. The fact that the required PV cell area is less than the available PV cell area, means that in Case 2 there is room again for anhedral tips, which are required for stability. The only parameter that does not change is the fuselage mass, because this is only dependent on the fuselage subsystem mass, excluding the battery and propeller, the pilot's mass and it's own mass, which are all not influenced by the cruise speed. As expected, a major change occurs to the power required which is reduced by 26%. The lower speed increases the total duration of the mission by 14%. However, the limit for mission duration has been set at 42 h in Section 1.4, so the new mission duration of 38.3 h is still within the limits. Also the total mass of the whole design changed significantly, reducing it by 9%. The main reason for this is that the paraglider will fly slower during the dark, so less energy is needed and hence the number of batteries can be reduced and because it is also flying slower during the day less PV cells are needed to generate the reduced power required.

As has been stated in the introduction of this chapter, the fuselage weight has been changed near the end of the design process, because of a revision of the load case which lead to a lighter fuselage. The mass changed from 53 kg to 40 kg, and the influence of this change is displayed as Case 3. This decrease in weight also changed almost all parameters given in the Table 8.1, but the major ones are the following. Firstly the rate of climb is increased by 28%, which results in a decrease of climb duration of 30%. A famous aerospace design phenomenon can be witnessed here as well, which is the mass snowball effect. This effect describes the weight reduction of the other subsystems when one subsystem becomes lighter. So with a 7% decrease in the total weight, because of the reduction in fuselage weight, the battery weight and PV cell weight both decrease with 6.3%. The lower weight requires a smaller wing area, which has proven to be a potential problem, however, the available and needed PV cell area still differ 35% which leaves enough room for the anhedral wing parts.

The last alteration that is made from Case 3 to Case 4, using the corrected power budget tool, has had a large influence. The main differences in the parameters are the following. Firstly, because of the power required is now calculated using the weight of the design minus the helium lift contribution, this parameter decreased by 12%. This decreased the PV cell area by 12%, also decreasing the required horizontal span of the wing by 10%. The mass of the PV cells and the batteries both decreased by 12% as a result as well, note that even though it might look this way, the relation between these parameters is not directly proportional. The thrust that can be delivered by the motor stays the same and power

required decreased, so therefore the RoC increased by 39% decreasing the climb time by 36%.

Case 4 is not the case that has been investigated in the report, and therefore this analysis is only made for future use and to show the impact of the change. The final feasibility is checked using Case 3.

Table 8.14: Values used to confirm mission feasibility

Parameter	**Unit**	**Required value**	**Calculated value**	**Feasibility check**
$P_{r_{cruise}} => P_a$	kW	3.79	5.15	✓
L => W	kN	2.72	2.73	✓
Distance	km	3040	3040 + loiter	✓
$S_{anhedral} > 0$	m	0	3.41	✓
$t_{duration} < 42$	h	42	37.9	✓

8.4.1 Requirement Compliance

The requirements as stated in Section 1.1 were evaluated to see if the overall design meets the top-level and lower-level requirements. In Table 8.16 and Table 8.18 a check mark (✓) for compliance or a cross (✗) for non-compliance was given for each of the requirements. All top level requirements are met. As can be seen one low level requirement that has not been met is the dynamic stability due to the possibility of having just stable mode. This was discussed in Section 2.1. The other low level requirement that was failed to be met is the emergency landing safety. This is due to the fact that calculations for impact loading were beyond the scope of the bachelor courses and the Team's current knowledge. Therefore, in order to compensate, extra volume and weight was added so a future design team has a technical budget to work with. Theoretically speaking the PPG is a valid solution for the mission. Table 8.16 and 8.18 can be used for future design as a validation tool as well.

Table 8.15: Compliance of Top Level Requirements

Requirement handle	Explanation	Achieved
REQ-MIS-A1	The optimal time frame to cross the Atlantic must be determined, i.e. maximise the availability of solar radiation and favourable wind conditions.	✓
REQ-MIS-B1	The transatlantic flight must be continuous or, if proven infeasible, intermediate stops are an option.	✓
REQ-MIS-B2	The crossing must at least cover the Atlantic. However, the client has indicated that in addition to the Atlantic, crossing the North Sea is considered highly favourable.	✓
REQ-MIS-C1	The paraglider must be manned, this means taking into account human factors such as fatigue, immobility and diet of the pilot.	✓
REQ-MIS-C11	The pilot must have enough food and drinks for the mission.	✓
REQ-MIS-D1	The maximum flight altitude must be such that the fuselage does not have to be pressurised.	✓
REQ-SAF-A2	In case of a landing on water the fuselage must offer survivability long enough to be rescued.	✓
REQ-SAF-B1	The safety of the pilot must be guaranteed all throughout the flight.	✓
REQ-SAF-B12	The PPG must be able to perform a safe emergency landing.	✓
REQ-TECH-A1	The paraglider design must be within the stretched definition of a paraglider, i.e. the canopy is allowed to have semi-rigid parts.	✓

Requirement handle	Explanation	Achieved
REQ-TECH-B1	The paraglider must be completely solar powered; batteries charged with solar energy are okay.	✓

Table 8.17: Compliance of Low Level Requirements

Requirement handle	Explanation	Achieved
REQ-TECH-A11	The canopy must have enough area to store Photovoltaic (PV) cells on.	✓
REQ-TECH-A12	The canopy must provide roll and yaw control.	✓
REQ-TECH-A13	Canopy material must be UV-resistant.	✓
REQ-TECH-A14	The wing must be tear resistant.	✓
REQ-TECH-A15	The wing's airfoil must keep its shape.	✓
REQ-TECH-C1:	The paraglider must be designed to be stable and controllable by a human, i.e. no automated system to counter instability or do control.	✓
REQ-TECH-C11	The PPG must have static stability.	✓
REQ-TECH-C12	The PPG must have dynamic stability.	✗
REQ-TECH-C13	The control forces must not exceed human capabilities.	✓
REQ-TECH-C14	The PPG must have trim system.	✓
REQ-MIS-B3	The mission duration must be lower than 42 hours or a solution for pilot fatigue has to be found.	✓
REQ-MIS-C12	The fuselage must enable to store or get rid of (human) waste.	✓
REQ-SAF-A1	The fuselage must be safe in case of an emergency landing both on land as well as on water.	✗
REQ-SAF-A21	The floating device must provide visibility for rescue operations.	✓
REQ-SAF-A22	There must be an emergency supply of water and food.	✓
REQ-SAF-A23	Hazardous equipment must not present harm to the pilot in emergencies.	✓
REQ-SAF-A24	An emergency location transmitter must be present.	✓
REQ-SAF-B11	The PPG must be designed to avoid collisions.	✓
REQ-COM-A1	The pilot must be able to communicate with a control centre throughout the mission.	✓
REQ-COM-A11	The ground centre must be able to monitor pilot health.	✓
REQ-COM-A12	The vehicle must be capable of sending flight data.	✓
REQ-COM-A13	A voice link must be established between pilot and ground centre.	✓
REQ-COM-A14	Pilot must be able to receive weather and flight information.	✓
REQ-SUS-A1	The project as a whole must be executed in a sustainable way. In operation as well as production and design.	✓
REQ-SUS-A2	A valid solution for the after mission life for subsystems must be found.	✓
REQ-MSC-A1	A power and weight budget of the design must be made.	✓
REQ-MSC-A2	There must be a cost analysis of the project.	✓
REQ-MSC-A3	Components with technology in the development phase must be available within five years.	✓
REQ-MSC-A4	There must be inboard visibility.	✓
REQ-TECH-B1	The paraglider must be completely solar powered; batteries charged with solar energy are okay.	✓

8.5 Future Project Planning

After the feasibility study is completed start of the preparations can begin. The conclusion of the study can be used to convince industry experts, designers and sponsors to partake in the project.
In this section the activities of post feasibility study are presented. The different activities and their duration were estimated and plotted in a Gantt chart (Figure 8.8). It is understood that the duration may be grossly under- or overestimated as the actual time it takes depends on unknown factors. For example, the time to find a sponsor is likely to depend on economy situations. Also, some extra activities, which are unknown at this point in time, may be necessary or present activities may prove redundant.

8.6 Sustainable Development

Sustainability has been set as one of the key requirements in the project plan. As nowadays sustainability is a big issue it is a mandatory aspect of every aerospace design project. Sustainability can be obtained in two ways, the first by designing a sustainable aircraft and the second by designing an aircraft sustainable. In this DSE project it has been aimed for to obtain sustainability as much as possible.

Obtaining a sustainable aircraft has been pursued by creating an aircraft that uses only solar power. Combining PV cells to generate solar power and batteries to store this solar power the aircraft can run continuously without creating any waste. During operation no fossil fuels are used and no additional CO_2 and greenhouse gasses are released.

To design the aircraft with a sustainable method is has been aimed for to perform several tasks with one component. This has especially been beneficial in the design of the subsystems. The core of the subsystems design revolves around the iPad Mini 3, which provides communication, wi-fi, attitude and health visualisation and leisure activities. Combining it with the Iridium GO it transforms into a satellite phone as well.

Another way in which this idea is incorporated is the control lines. The control lines provide control, attachment of the canopy to the monocoque and they also conduct electricity from the wing to the fuselage. Next to that the fuselage also serves as a liferaft in case of emergency.

After designing an aircraft with as few components as possible, the next option is to design components with as few materials as possible. The battery and PV cells are made using complex methods, which require a lot of energy. Therefore using as few as possible of these materials is beneficial for the environment and also for the design. A lighter design requires less required power for sustained flight which then again indicates a decrease in mass. The design has been optimised to require as few mass as possible. Especially the mission profile for the power budget has been chosen to minimise the mass of the power system. Also carbon fibres have been implemented in the design of the fuselage and the canopy to keep the weight of the aircraft to a minimum.

Lastly parts of the aircraft can be recycled at the end of life of the aircraft. As the mission is unlikely to be repeated in the near future it has been decided that the aircraft will be split up into components that are useful for other projects and reuse or repair of the entire aircraft has not been considered.

The battery is high tech and can be used in for instance a PV solar plant or used as an experimental car battery. The PV cells are of space grade quality and can be taken apart to implement in a solar system for a house for example. As the efficiency is high it can be used for small houses or used at a more northern location than usual.

The subsystems that have been implemented to keep track of the health and safety of the pilot are all COTS components and can be taken apart to be implemented in every day use in different fields.

This is of course only possible if the mission is completed successful and the usable components survive the mission.

8.7 Reliability, Availability, Maintainability and Safety

The system in which the mission is performed should be reliable, available, maintainable and safe. In other words, the RAMS characteristics of the system should be sufficient to call the mission feasible. This subsection is divided in reliability, availability, maintainability and safety.

Reliability

There are basically five main characteristics of this system that lower the reliability drastically. Firstly, the wing design is a complete new concept. The way of inflating the wing is unique and besides that, an inflated wing with tension lines underneath are also not commonly used. Therefore validating the performance of the wing is very hard, which lowers the reliability.
Secondly, paragliders are usually non-rigid. The controllability is highly dependent on the fact that the wing is non-rigid. The wing that is designed in semi-rigid and therefore the controllability may be questioned.
Thirdly, the batteries are not yet used in real life. Their performance is based on lab tests and therefore their real life performance may drop dramatically.
The conductive lines are also rather critical. The assumption was made that a conductive material in one of the lines transfers the electricity from the PV cells to the fuselage to power the subsystems and the motor. The question is whether the conductive line maintains the expected performance throughout the mission. This topic is, like the wing design, innovative, but hard to validate.
Finally, the PV cells are essential for this mission. The reliability of the PV cells drop significantly since more than 7000 separate cells are used. These cells are stored in series and in parallel and if one cell fails, several other cells become useless as well. In addition, the PV cells are stored on an inflated structure, which adds complexity. In between the cells there are conductive lines that, like the cells, can fail during the mission.
Other systems that need further investigation regarding the reliability are the life raft and the battery drop system. The life raft is also not a COTS component and is therefore a design risk. The CO_2-capsules used for inflating the life raft are validated in other liferaft systems, but the shape and the exact configuration are subject to further research.
The battery drop system is a really nice system in case of emergency, since the most dangerous systems are dropped. The exact flight path of the dropped fuselage part is not known, which makes it a dangerous flying projectile.

Availability

The system mostly uses COTS components which are available at the moment. However, as mentioned in the MRR, the mission was not possible using conventional paraglider canopies. Therefore a new wing was designed, using technologies like inflated tubes in the wing and a semi-rigid structure, which made the system deviate from the definition of a paraglider. This wing design is unique and designed specifically for this mission.
Besides the wing, the batteries are also currently not available. The batteries are supposed to be available within 5 years, so the mission should be feasible in 5 years in that sense. However, as mentioned earlier, the energy density of the batteries is based on lab tests. The real life performance regarding energy density is assumed to be worse.

Maintainability

The mission is performed only one time and therefore maintenance is not a major issue. The maintenance is therefore limited to pre-operations inspections as mentioned in Section 1.8.3.

Safety

One of the main requirements of the mission was that it can be performed safely. The pilot's safety is improved by many safety measures. Firstly, the health of the pilot is monitored during the flight.

Secondly, the pilot is able to communicate with the ground station during the entire flight. A backup communication system is implemented in case the first one fails. In case of a critical system failure, the inflammable batteries and the propeller are dropped and a liferaft is inflated once the fuselage hits the water. The impact loads are taken by the fuselage frame and the G-force that the pilot experiences is within the range that is safe for a human being. In addition, there is a sufficient amount of food and drinks taken for the pilot. The pilot is, however, flying in a system that uses several design concepts that are new and innovative and therefore less reliable.

It can be concluded that a lot of tests are required in order to be able to rely on all the subsystems that are used for the paraglider. Especially the components that are unique for this mission and therefore designed specifically for the paraglider should be tested thoroughly. Examples are for instance a scale model of the wing to test in a wind tunnel or a life raft system inflation test.

8.8 Cost Analysis

A cost analysis has been constructed to get an idea of the costs of the project. Some costs, like the costs of the COTS components are known while others are less certain. For all costs an estimation has been made that resembles the reality as good as possible. The overview of the cost analysis is found in Table 8.19

The design has been approximated as ten engineers working full-time on the design, being paid € 120 per hour. An estimate of work hours has been made based on the work hours that the Team has put into the project up til now and estimating the work that still has to be completed after the end of the project. A division of 1.5:2.5:10 has been chosen to divide the workload between the different design phases.

The cost analysis of the components is easier as most components are COTS the actual price is known. The PV cells have been priced at € 150 a piece. They are currently priced between € 150-400 but the price of PV cells drops exponentially, so when the aircraft is designed the average price is expected to have dropped to the minimum price that they cost now. The manhours and manufacturing price for both the canopy and the airframe structures has been estimated and this cost has been implemented in the cost of the component.

The integration, testing and producing the aircraft has been estimated by taking the average pay of manual labourers in the US where most parts are fabricated. It is expected that the production takes five weeks and takes ten people, while the integration and testing is done in respectively three weeks and one week by three persons. The rent of the facilities is taken to be € 3'500 per month based on the average rent for an aircraft hangar.

The total mission has been estimated to 72 hours. This is from the moment that the GO is given for the mission until the landing of the paraglider. Therefore all man hours that are incorporated in the mission execution are a multiple of 72, depending on the number of people. All cost/unit have been based on the average pay of that profession[(i)][(ii)][(iii)]. It has been assumed that the Mission manager, is the funder of the project and therefore does not bill himself.

The last part of the cost analysis is based on the operations & logistics. The cost to find sponsors has been based on the average pay of a sales representative[(iv)] working for two weeks. This is deemed to be enough time to train the client in acquiring sponsorships. The cost for the pilot training has been based on the average cost of lessons that it takes for a laymen to become a qualified paraglider pilot. The certification cost is based on the costs for the certification of an ultra-light. The transport is based on

[(i)] URL `http://www1.salary.com/meteorologist-Salary.html`[Cited 21 January 2015]

[(ii)] URL `http://swz.salary.com/SalaryWizard/General-Maintenance-Worker-I-Salary-Details.aspx`[Cited 21 January 2015]

[(iii)] URL `http://www1.salary.com/Physician-Generalist-salary.html`[Cited 21 January 2015]

[(iv)] URL `http://swz.salary.com/SalaryWizard/Sales-Representative-III-Salary-Details.aspx`[Cited 21 January 2015]

the average price that it takes to rent a 26' truck for three days in the United States and that the average coverage is 100 milesṪhe catering service cost is based on the cost of serving three meals a day to 40 people[(v)]. Emergency Services, both ambulances and firetrucks, have to be stand-by at both the take-off and the landing. The cost of the emergency systems is based on the average price of an ambulance ride per hour [(vi)]. In case of failure of the mission and the coastal guard has to be called in the cost is about € 10'000 per hour, based on a search with one aircraft and two boats. A rescue time of 10 hours is assumed. Of course an insurance can be taken out so that this cost is lower. The total cost of the mission is estimated at € 3'481'551. The main contributors are the design cost and the cost of the PV cells. The cost of the PV cells may be lower at the point in time when the mission is performed as the cost of PV cells decline with respect to time.

[(v)] URL `http://www.setoutfitters.com/Film_Crew_Catering.html`[Cited 21 January 2015]
[(vi)] URL `http://www.usfa.fema.gov/pdf/efop/efo46087.pdf`[Cited 21 January 2015]

Table 8.19: Cost analysis of the project

Project Part		Units	Cost/Unit	Cost	Total Cost
					€ 3'481'732
Design					€ 1'680'000
	Preliminary Design	1'500	120	180'000	
	Conceptual Design	2'500	120	300'000	
	Detailed Design	10'000	120	1'200'000	
Components					€ 1'441'162
	Airframe Structure	1	38'500	38'500	
	Attitude System	1	40'966	41'292	
	Canopy	1	16'800	16'800	
	Communication System	1	2'048	1'948	
	Emergency System	1	6'396	6'496	
	Life Support	1	382	387	
	Lines	1	800	800	
	Miscellaneous	1	961	855	
	Power System	1	26'863	26'832	
	PV cells	7'470	150	1'307'250	
Integration/Testing					€ 119'300
	Integration facilities	1	7'000	7'000	
	Man hours contractors	2'000	40	80'000	
	Man hours integration	360	60	21'600	
	Man hours testing	120	60	7'200	
	Testing facilities	1	3'500	3'500	
Mission Execution					€ 79'920
	Health monitoring	216	100	21'600	
	Meteorology	216	50	10'800	
	Mission Manager	72	0	0	
	Mission Team	720	50	36'000	
	Tech support	576	20	11'520	
Operations & Logistics					€ 161'350
	Catering service	1	2'500	2'500	
	Certification	1	20'000	20'000	
	Coastal rescue services	10	10'000	100'000	
	Control centre facilities	1	5'000	5'000	
	Emergency services	48	150	7'200	
	Find sponsors	80	85	6'800	
	Miscellaneous	1	2'000	2'000	
	Pilot training	1	16'250	16'250	
	Transport	4	400	1'600	

Figure 8.8: Time planning of all activities relevant to the mission

9 Conclusion & Recommendations

This chapter presents the conclusions from the work done in this DSE and continues to give a number of recommendations to anyone interested in continuing the research.

9.1 Conclusions

The aim at the end of the DSE, for the Team, was to deliver a design that shows that it is feasible to cross the Atlantic with a manned solar powered paraglider in continuous flight. Chapter 2 investigates the stability and control behaviour that a potential wing or canopy has to have in order for the mission to work. Chapter 3 investigates the aerodynamic characteristic of the airfoil and wing need to achieve the mission goal as well as the drag produced by the fuselage. Chapter 4 elaborates on the canopy design, its structure and materials involved in the design. Chapter 5 shows the design methods used for the fuselage and presents a design for the fuselage. The subsystems for the design have been described in Chapter 6. All the tools and methods used in the design have been verified and validated in Chapter 7. And finally a feasibility check is performed in Chapter 8, this chapter also shows what a potential continuation of this project might look like.

Chapter 2 states that it is unavoidable to have some form of instability. This is due to the characteristics of the paraglider-fuselage system. Similar to regular paraglider designs the Team has chosen to have lateral and longitudinal stability, this means that the paraglider is allowed to have so form of spiral instability. In the design there is more than enough time for the pilot to counteract this instability. Subsequently the control forces needed to achieve a normal turn are well within the range of human capabilities.

Chapter 3 illustrates the design approach of the wing for the final design, going from values based on existing canopies to a new wing design. Regular paraglider fly at a low speed, to get optimum performance a thick airfoil has been selected to meet this requirement. As shown in Chapter 3 the current wing design for the wing meets all the aerodynamics requirements. It should be noted that the wing performance is sensitive to changes in profile drag. The wing has been a custom design in order to reach a higher GR than that of regular paragliders, which has succeeded and in the end is 13.1 with respect to around 10 for regular paragliders. In Chapter 4 a design solution is proposed that combines Tensairity® with a multibubble helium pressurised tube structure to yield a semi rigid and lightweight wing design capable of handling the loads present during the mission. Chapter 5 & Chapter 6 prove that it is possible to design a lightweight fuselage that can house all subsystem as well as be safe for the pilot in case of an emergency landing. The power budget has been the driven factor behind the optimisation of the design, in particular Equation (9.1). It shows the 3 variables that have been the key factor in the design synthesis. The tool used in all the calculations have been verified and the results from these tools have been validated as much as possible. The result of this process is presented in Chapter 7.

$$P_r = \frac{W}{GR} \cdot v \tag{9.1}$$

Finally Chapter 8 shows that after the velocity was set at 10 $m \cdot s^{-1}$ the resulting design is indeed feasible to cross the Atlantic using a solar powered paraglider!

9.2 Recommendations

Different hurdles were encountered throughout the DSE project. Some were solvable or approached with estimates or assumptions. The possible improvements or leftover research are listed in this section.

Mission Profile

Throughout the design process the mission duration was limited to a maximum of 26 h. For this

duration the chosen mission profile has been verified to be the optimal mission profile. However, due to iterating the design the mission duration was lengthened to 38 h. As described the cycle of the current mission profile ends at 32 h. It is recommended to investigate the possibility to investigate take-off in daytime, in which the PV system can be sized to no longer charge the battery, but to power the climb phase instead. This is only a viable mission profile for a mission duration of less than 40 h as the batteries are not charged for a second cruise phase in darkness and then the aircraft is rendered powerless.

Stability and control

For this design, only a qualitative analysis has been performed on the stability and control characteristics of the design. This prevents the design from having a needed anhedral wing span. Therefore it is recommended to perform a numerical analysis for the turn rates and magnitude of the stability modes.

Aircraft subsystems

The manufacturer of the propeller and motor did not have much data available and also refused to release detailed data. Because of this, the performance change of the propeller and motor when running at different rpm has not been estimated. If more data is received, exact efficiencies of the power system can be obtained. For the subsystems it is also recommended to look into the possibility to start emergency procedures remotely controlled. This way an emergency landing can still be performed.

Structures of the wing

A whole new wing design has been established by means of a numerical tool which builds on the stress constraint of the skin material and load bearing capability of the stiffening elements. These were considered the most critical design criteria for checking the feasibility of this mission. However, it is recommended to perform further research on torsion, deflection and wrinkling in order to improve the accuracy of the model. Also the bridle of the sispension lines should be further researched. The Tensairity® layout, and the cylindrical form of the pressurised tubes can also be further optimised. Research exists on other geometrical forms that have higher load capability, and a more optimal design for spanning the Tensairity® elements in combination with the bridle could be determined in order to accomplish an even lighter and stronger design. Since the wing is a unique design it is also highly recommended to perform tests on a prototype of the wing itself. Numerical values from similar wings are not accurate enough to validate the model. Also a pressurised prototype canopy may be built for experiments to validate the research.

Structures of the fuselage

Due to time and knowledge constraints it was not possible to come up with a detailed design for the fuselage yet. Based on the performed calculations and estimations the team made, a few recommendations for the next steps to be taken can be given. After obtaining an estimation for the impact load on water in case of an emergency landing, which is about $15G$ it is important to investigate possibilities of damping to ensure the pilot survives the impact unharmed. According to [57] an average human body can handle about $5G$ in spine (initial impact-) direction, a trained pilot can even handle up to $9G$ before passing out. This means, dependent on the pilot condition, approximately 6 to $10G$ has to be absorbed by the structure. This could be done using a spring-damper-system mounted to the pilot seat or by incorporating a sandwich structure as crumbling zone in the nose of the fuselage. For the horizontal impact after bounce back, the impact load is significantly lower and using the model explained in Section 5.2, it is found not to be a critical load case. In [57] it is mentioned, that the human body can take higher loads perpendicular to the spine, which also makes the horizontal landing less critical. It is recommended to conduct further research on load damping and human factors with high G-loadings to ensure a safe emergency landing. The determination of the peak load as well as the stresses on the structure where based on a number of simplifications and approximations as explained throughout the various sections. Only after a detailed finite element analysis, FEM, the point loads and local stresses can be simulated more precisely. To assure that the structure is indeed able to carry the loads in all possible situations during the mission and optimise thickness distribution and size required for the load carrying elements, it is recommended to perform an FEM of the structure. It is also recommended to use Finite Element Modelling to find peak loads and stresses for impact cases.

Fuselage window

The window is a critical point of the fuselage design. The windows has to be able to withstand the impact loads as well as remain waterproof during the submerged phase of the emergency landing. Making a FEM model will provide a more detailed load distribution across the fuselage. From the FEM model it can be seen if the reference window of PLEXIGLAS® can withstand the impact load. Further research is necessary in the window department to come to a more detail window design. Further more the window acts as door for the fuselage. Therefore it is important that during the emergency water landing the fuselage is waterproof. In order to make the connection between the fuselage and the window watertight, two ways can be considered. Using a sealant material or using a seal. The company PPG Aerospace [(i)] contains information about sealants and Esterline [(ii)] has examples of different aviation seals. Further research is required to come to a more detailed analysis which method would be favourable. Research should not be limited by these two method mentioned.

Canopy lines

The canopy lines have been sized for a $2G$ turn load case. According to Ozone glider inspection[(iii)], the conventional paraglider lines have to be able to hold a 6 to $8G$ load dependent on the type of line. More research has to be done to verify if the design still has to comply with a conventional paraglider certification. The canopy used for the PPG is a new design and hence the regulations in which category it complies is not yet determined.

Aerodynamics

The airfoil has been designed in the beginning for 12.5 $m \cdot s^{-1}$, but in the end a cruise speed of 10.0 $m \cdot s^{-1}$ has been used. Therefore it is recommended to investigate if this low speed would need a different airfoil. The climb performance of the airfoil has also not been investigated to a great extent, especially with the new cruise speed. So this would need more research. Also an extensive study could be done, that looks into the advantages of thicker airfoil that can store more helium, but also have more drag. An optimum for this could be found. One large assumption that has been made is using an AR of 9, because this has been stated in one reference paper. In this paper it is said that for regular pressurised wings the AR has never been above 9, however, since the wing has been custom designed, perhaps a larger AR can be used which would improve the glide ratio of the design greatly, as can be seen in Section 3.3. Lastly, the conversion from a 2D to a 3D wing has been done using lifting line theory, which is not completely valid for thick airfoils as has been used in this design. This could be investigated using CFD models of the wing.

Use of correct power budget tool

In Section 8.4, the consequences of using the corrected power budget tool are presented as Case 4. These consequences are significant and will therefore improve the design greatly. Implementing this is therefore highly recommended.

[(i)] URL `http://www.ppgaerospace.com/Products/Sealants/Windshield-and-Canopy.aspx`[cited 25-01-2015]
[(ii)] URL `http://www.esterline.com/Portals/8/PDF/Aircraft_Seals.pdf`
[(iii)] URL `http://www.flyozone.com/paragliders/en/infozone/glider-inspections/`[cited 26-01-2015]

Bibliography

[1] T. Buchenau, F. Fortman, M.P. Huijts, H. Hussain, L. Koomen, R.C. Kuipers, T.L. Mulders, L.M.C. Sijbers, D.L. da Silva Rosa, and A.J. Vrasdonk. Baseline Review Report - Solar Powered Paraglider to Cross the Atlantic. 2014.

[2] J. Mulder, W. van Staveren, J. van der Vaart, E. de Weerdt, C. de Visser, A. in 't Veld, and E. Mooij. Flight Dynamics Lecture Notes, March 2013.

[3] O. Prakash and N. Ananthkrishnan. Modeling and Simulation of 9-DOF Parafoil-Payload System Flight Dynamics. Technical report, Indian Institude of Technology, 2006.

[4] P. Crimi. Lateral Stability of Gliding Parachutes. Technical report, Textron Defense Systems, 1990.

[5] C. Schreuder Iacomini and C. Cerimele. Lateral-directional Aerodynamics from a Large Scale Parafoil Test Program. Technical report, NASA, 1999.

[6] U.S. Department of Transportation Federal Aviation Administration. *Powered Parachute Flying Handbook*, 2007.

[7] C. Schreuder Iacomini and C. Cerimele. Longitudinal Aerodynamics from a Large Scale Parafoil Test Program. Technical report, NASA, 1999.

[8] G. Brown. Parafoil Steady Turn Response To Control Input. Technical report, Vertigo Inc., 1993.

[9] Warren F. Phillips. *Mechanics of Flight*. John Wiley and Sons, 2009.

[10] J.D. Anderson. *Fundamentals of Aerodynamics*. McGraw-Hill, 2001.

[11] J.M Scott, J. D. Jacob, S.W. Smith, L.T. Asheghian, and J.N. Kudva. Development of a Novel Low Stored Volume High-Altitude Wing Design. In *50th AIAA/ASME/ASCE/AHS/ASC Structures, Structural Dynamics, and Materials Conference*, Palm Springs, California, May 2009.

[12] Manfred Kistler. Email Conversation. Private Communication, 2015.

[13] Sadraey M. *Aircraft Performance Analysis*. VDM Verlag Dr. Müller, 2009.

[14] T. Buchenau, F. Fortman, M.P. Huijts, H. Hussain, L. Koomen, R.C. Kuipers, T.L. Mulders, L.M.C. Sijbers, D.L. da Silva Rosa, and A.J. Vrasdonk. Midterm Review Report - Solar Powered Paraglider to Cross the Atlantic. 2014.

[15] R.H. Luchsinger, A. Pedretti, P. Steingruber, and M. Pedretti. Light Weight Structures with Tensairity. Technical report, Airlight Ltd and Prospective Concepts Ag, 2004.

[16] J. Breuer, W. Ockels, and R.H. Luchsinger. An Inflatable Wing Using the Principle of Tensairity. 48th AIAA Structures, Structural Dynamics and Materials Conference, 2007.

[17] *Material Selection and Joining Methods for the Purpose of a High-Altitude Inflatable Kite.*, 50th AIAA/ASME/ASCE/AHS/ASC Structures, Structural Dynamics, and Materials Conference, 2009.

[18] J.C.M. Breuer. The New Structural Concept Tensairity: Basic Principles. Technical report, TU Delft and EMPA, 2004.

[19] F.J.J.M.M. Geuskens, O.K. Bergsma, S. Koussios, and A. Beukers. Analysis of Conformable Pressure Vessels: Introducing the Multibubble. *AIAA Journal*, (8), 2011.

[20] F.J.J.M.M. Geuskens. *Conformable Pressure Vessels. Design & Analysis*. BOXPress, 's-Hertogenbosch, 2012.

[21] J.D. Anderson. *Introduction to Flight*. McGraw-Hill, 2008.

[22] J. G. Brown and R. Haggard. Inflatable Structure Paraglider, September 1993.

[23] R.H. Luchsinger. The New Structural Concept Tensairity: Basic Principles. Technical report, Propective Concepts AG, 2004.

[24] J.D. Jacob and S.W. Smith. Design Limitations of Deployable Wings for Small Low Altitude UAVs. Technical report, Oklahoma State University and University of Kentucky, 2009.

[25] J.P.H. Webber. Deflections of inflated cylindrical cantilever beams subjected to bending and torsion. *The Aeronautical Journal*, 86, 1982.

[26] S.L. Veldman. Wrinkling predictions of cylindrical and conical inflated cantilever beams under torsion and bending. *Thin-Walled Structures*, 44, 2006.

[27] J. F. Harvey. *Theory and Design of Modern Pressure Vessels*. Van Nostrand Reinhold, 1974.

[28] Y. C. Gal-Rom and D. E. Raveh. Simplified aerostructural static model for inflated wings. *AIAA Journal*, 49, 2011.

[29] A.D. Simpson. Design and Evaluation of Inflatable Wings for UAVs. Technical report, Uknowledge University of Kentucky, 2008.

[30] A. Yavrouian, G. Plett, S.P.S. Yen, J. Cutts, and D. Baek. Evaluation of Materials for Venus Aerobot Applications. 1999.

[31] G. A. Khoury. *Airship Technology*. Cambridge University Press, 1999.

[32] C. L. Staugaitis and Kobren L. Mechanical and Physical Properties of the Echo II Metal-Polymer Laminate. Technical Report NASA TN D-3409, NASA, August 1966.

[33] Downs R.J. Meldner H. Beach C. McDaniels, K. and C. Adams. High Strength-to-Weight Ratio Non-Woven Technical Fabrics for Aerospace Applications. Technical report, Cubic Tech Corp, 2009.

[34] ASTM F224-10. *Standard Specification for Design and Performance Requirements for Powered Parachute Aircraft*. West Conshohocken, PA, 2010.

[35] Serhan Yüksel. *Low Velocity Impact Analysis of a Composite Mini Unmanned Air Vehicle during Belly Landing*. PhD thesis, Middle East Technical University, May 2009.

[36] T. von Karman. The Impact on Seaplane Floats during Landing. *NACA*, 1929. Technical Note.

[37] Y. Hirano and K. Miura. Water Impact Accelerations of Axially Symmetric Bodies. *Spacecraft & Rockets*, 7, 1970.

[38] R.D. Lorenz. Huygens Probe Impact Dynamics. *ESA Journal*, 18, 1994.

[39] NASA Apollo Command Module News Reference. Apollo Lunar Surface Journal, 1972.

[40] inc Toray Carbon Fibers America. *Torayca T300 Data Sheet*, 2008.

[41] R. Wang, S. Zheng, and Y. George Zheng. *Polymer Matrix Composites and Technology*. Elsevier, July 2011.

[42] Evonik Industries. *PLEXIGLAS Product Description*, July 2008.

[43] R. Vos and B.T.C. Zandbergen. Systems Engineering Elements i Lecture Notes, 2010.

[44] J.M. Calavia1, M.and Perié1, J.F. Sanz, and J. Sallán. Solar Array Trades Between Very High-Efficiency Multi-Junction and Si Space Solar Cells. *Emcore Photovoltaics*, 2000.

[45] James R. Wertz, Jeffery J. Puschell, and David F. Everett. *Space Mission Engineering: The New SMAD*. Microcosm Press, 2008.

[46] M. Song, Y. Zhang, and E. J. Cairns. A Long-Life, High-Rate Lithium/Sulfur Cell: A Multifaceted Approach to Enhancing Cell Performance. *American Chemical Society*, 40, 2013.

[47] J.M. Calavia1, M.and Perié1, J.F. Sanz, and J. Sallán. Comparison of MPPT Strategies for Solar Modules. *ICREPQ*, 6, 2010.

[48] T. Yamakoshi, K. Matsumura, P. Rolfe, S. Hanaki, A. Ikarashi, Jihyoung Lee, and K.-I. Yamakoshi. Potential for Health Screening Using Long-Term Cardiovascular Parameters Measured by Finger Volume-Oscillometry: Pilot Comparative Evaluation in Regular and Sleep-Deprived Activities. *Biomedical and Health Informatics, IEEE Journal of*, 18(1):28–35, Jan 2014.

[49] S. Lockley, E. Evans, F. Scheer, G. Brainard, C. Czeisler, and D. Aeschbach. Short-Wavelength Sensitivity for the Direct Effects of Light on Alertness, Vigilance, and the Waking Electroencephalogram in Humans. *SLEEP*, 29(02), 2006.

[50] T. Murase, S. Haramizu, A. Shimotoyodome, A. Nagasawa, and I. Tokimitsu. Green Tea Extract Improves Endurance Capacity and Increases Muscle Lipid Oxidation in Mice. *Biological Science Laboratories, Kao Corporation, Ichikai-machi, Haga-gun, Tochigi, Japan*, 288(1), Oct 2005.

[51] B.F. Blackwell, T.L. DeVault, T.W. Seamans, S.L. Lima, P. Baumhardt, and E. Fernandez-Juricic. Exploiting Avian Vision with Aircraft Lighting to Reduce Bird Strikes. *Journal of Applied Ecology*, 1(1), Nov 2012.

[52] J. Chambers. Longitudinal Dynamic Modelling and Control of Powered Parachute Aircraft, 2007.

[53] F.M. Dekking, C. Kraaikamp, and L.E. Lopuhaa, H.P. and¨Meester. *A Modern Introduction to Probability and Statistics*. Springer-Verlag, January 2005.

[54] E. Moij, Q. Wijnands, and B. Schat. 9DOF Parafoil/Payload Simulator Development and Validation. Technical report, Dutch Space B.V., 2003.

[55] J. Lingard. The Aerodynamics of Gliding Parachutes. Technical report, G.Q. Defence Equipment Limited, 1986.

[56] M.J. Scott, D.J. Jacob, S.W. Smith, L.T. Ashegian, and J.N. Kudva. Development of a Novel Low Stored Volume High-Altitude Wing Design. Technical report, NextGen Aeronautics, Oklahoma State University and University of Kentucky, 2009.

[57] M.P.H. Dennis F. Shanahan, M.D. *Human Tolerance and Crash Survivability*. Injury Analysis, LLC, august 2005.

Appendices

A Stability Derivation

The stability derivation only a qualitative measure is done as only experiments and CFD could approximate the actual values for all stability derivation coefficients. Certain assumptions were made:

- The canopy exhibits a curvature or in technical terms a continuous polyanhedral
- The canopy has a taper ratio of less than 1 (i.e. the root is longer than the tip)
- The pendulum effect is greater than the positive moment the airfoil generates [52]
- The pendulum effect is greater than the pitching moment due to pitch rate [52]

If certain assumptions resulted in the instability of a certain mode this could be translated into the a different canopy design.

Longitudinal stability

From the longitudinal stability the phugoid was inspected. According to derivations made in Flight Dynamics lecture notes [2], the coefficients A to C for the characteristic determinant as presented in Equation (A.1) must be all positive or all negative to have stability.

$$A = 2\mu_c \left(C_{Z_\alpha} C_{m_q} - 2\mu_c C_{m_\alpha}\right), \tag{A.1a}$$
$$B = 2\mu_c \left(C_{X_u} C_{m_\alpha} - C_{m_u} C_{X_\alpha}\right) + C_{m_q} \left(C_{Z_u} C_{X_\alpha} - C_{X_u} C_{Z_\alpha}\right), \tag{A.1b}$$
$$C = C_{Z_0} \left(C_{m_u} C_{Z_\alpha} - C_{Z_u} C_{m_\alpha}\right), \tag{A.1c}$$

These stability derivatives are given and explained in Table A.1.

Table A.1: Longitudinal Stability Coefficients for a parafoil-payload system

Derivative	Sign	Explanation
C_{m_α}	< 0	Increase in pitching moment due to angle of attack increase
$C_{m_{\dot{\alpha}}}$	< 0	Increase in pitching moment due to angle of attack acceleration
C_{m_q}	< 0	Increase in pitching moment due to pitch rate increase
C_{m_u}	> 0	Increase in pitching moment due to horizontal speed increase
C_{X_α}	> 0	Increase in forward force due to angle of attack increase
C_{X_u}	< 0	Increase in forward force due to horizontal speed increase
C_{Z_0}	< 0	Inverse of C_L
C_{Z_α}	< 0	Increase in downward force due to angle of attack increase
C_{Z_u}	< 0	Increase in downward force due to horizontal speed increase
μ_c	> 0	Dimensionless weight

Inserting in Equation (A.1) gives:

$$A > 0, \tag{A.2a}$$
$$B > 0, \tag{A.2b}$$
$$C > 0, \tag{A.2c}$$

Assuming both C_{m_α} and C_{m_q} strong negative in comparison with other coefficients due to the pendulum effect, also verified by NASA X-38 parafoil-payload program [7].

Next the short period was investigated. Again, according to the equations of motions for constant speed and pitch rotation were derived in Flight Dynamics [2] and are presented in Equation (A.3).

$$A = -2\mu_c K_Y^2, \tag{A.3a}$$
$$B = C_{m_{\dot{\alpha}}} + C_{m_q} = C_{m_q}, \tag{A.3b}$$
$$C = C_{m_\alpha}, \tag{A.3c}$$

Restating, all A,B and C must have the same sign for stability. The parameter K_Y^2, the dimensionless moment of inertia around the Y-axis, is always positive due to the square. $C_{m_{\dot{\alpha}}}$ is approximately zero due to the absence of a tailplane and can also be ignored when changes in angle of attack occur slowly. The coefficients from Table A.1 are reused and easily can be seen that the condition for stability is met.

Lateral Stability

$$C_{l_\beta} C_{n_r} - C_{l_r} C_{n_\beta} > 0 \tag{A.4}$$

Table A.2: Spiral Stability Derivatives for a parafoil-payload system

Derivative	Sign	Explanation
C_{l_β}	< 0	Increase in roll moment due to sideslip
C_{l_r}	< 0	Increase in roll moment due to yaw rate
C_{n_β}	> 0	Increase in yaw moment due to sideslip
C_{n_r}	< 0	Increase in yaw moment due to yaw rate

Putting the signs into Equation (A.4) gives:

$$((< 0) \cdot (> 0) - (> 0) \cdot (> 0)) < 0 \tag{A.5}$$
$$((-) \cdot (+) - (+) \cdot (+)) < 0 \tag{A.6}$$

Remember that Equation (A.5) had to be positive for spiral stability, hence it could be concluded a typical parafoil-payload system exhibits spiral instability. Certain design option exist to counter this.

- A dihedral canopy; This makes the spiral stable, but designwise a dihedral canopy is harder to achieve.
- horizontal drag chute; An emergency tool to introduce drag to get out of a spiral. Not recommended as it is a one time use.
- Increasing line length; Consequence is increase in weight and drag.
- Yaw control; A vertical tail plane or winglets. Extra weight, drag and complexity.

B Ejection Cap Calculations

In this section the calculations for the required spring force for the ejectable fuselage part are done. Let's say the propeller must have rotated at least 90 degrees after 1 second so the parachute has enough time to deploy. The required spring force F_{spring} should induce a certain angular acceleration $\alpha_{rotation}$ to achieve this rotation $\theta_{rotation}$. The required acceleration was calculated in Equation (B.1).

$$\theta_{rotation} = \frac{1}{2} \cdot \alpha_{rotation} v \cdot t^2, \tag{B.1a}$$

$$\alpha_{rotation} = \frac{2\theta_{rotation}}{t^2}, \tag{B.1b}$$

$$= \frac{2 \cdot 0.5 \cdot 3.14}{1^2} = 3.14 \frac{rad}{s^2} \tag{B.1c}$$

With a mass moment of inertia I around its own axis, as derived using Catia's internal calculation, the moment M required can be found using Equation (B.2). As can be seen there is no thrust force present. The propeller blades' rotational energy should be removed before the manoeuvre can be done. A fast way of doing this is with a small explosive charge or mechanical decoupler which separates the blades from the shaft. Due to their rotational velocity they would fly away from the fuselage. Potentially, they could hit the canopy which would not be a problem as this procedure is only executed when the canopy would be ejected as well. The moment around hinge point a follows from the free body diagram in Figure B.1.

$$M = \alpha_{rotation} \cdot \left(I + m \cdot d^2\right) = \pi \cdot \left(5.916 + 69 \cdot 0.5^2\right) \approx 73 Nm \tag{B.2}$$

The worst-case scenario is for the case that the fuselage points straight down. For other cases the gravity helps rotating the section and in this case the spring has to do all the work.

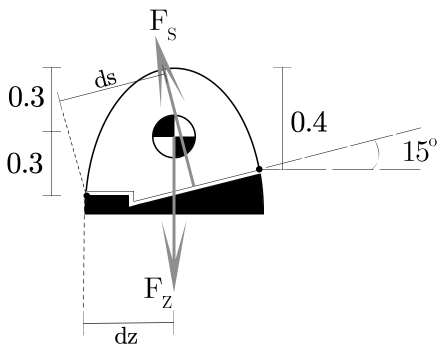

Figure B.1: Free body diagram for the worst ejection case scenario: fuselage pointing down

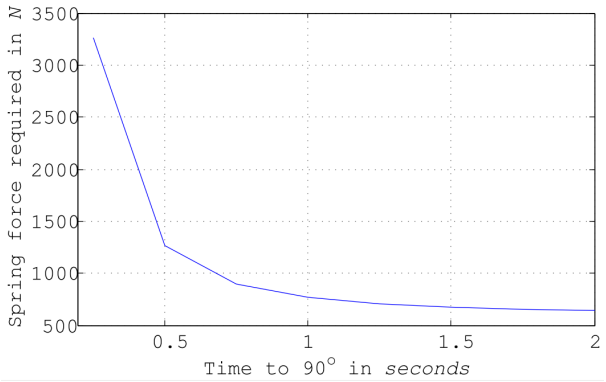

Figure B.2: Springforce required for a 90 degrees rotation of the ejection cap for different amounts of time

The section's mass was calculated to be 69 kg or in weight 677 N. With the only unknown being the spring force, it was calculated using Chapter B.

$$\sum M_a \approx d_s \cdot F_s - d_z \cdot F_z \approx, \tag{B.3}$$

$$0.41 \cdot F_s - 0.4 \cdot 677 \approx 73 Nm \tag{B.4}$$

The result was a plausible spring force F_s of approximately 838 N. For completeness, all calculations were done for a range of different time periods as shown in Figure B.2. Increasing F_s gives diminishing returns in terms of time. As there is no real reason to have a faster rotation the decision is to use a F_s of 838 N still stands. The design could easily incorporate a few springs that deliver this amount of force[(i)].

[(i)] `http://www.leespring.com/uk_compression_spec.asp?springType=C&forWhat=Search`[cited 17 January 2015]

C Contribution Chart

In this Appendix the contribution of all Team members on the report can be found.

Table C.1: Contribution chart of the final review

Final Review	Tim	Melchior	Theresa	Luuk	Haider	Rutger	Frits	Leon	Atilla	David
Preface								x		
Abstract								x		
1. Introduction										
1 Introduction	x									
1.1 Requirements								x		
1.2 Technical Risk Assessment								x		
1.3 Project Management								x	x	
1.4 Mission Profile			x					x		
1.5 Development Logic & Project Design								x		
1.6 N^2-Chart of the Design Iteration		x								
1.7 Market Analysis	x						x			
1.8 Operations & Logistics							x			
2. Stability & Control										
2.1 Stability	x							x		
2.2 Control	x							x		
3. Aerodynamics										
3.1 Preliminary Aerodynamic Characteristics		x	x							
3.2 Airfoil Selection					x					
3.3 Airfoil To Wing Conversion		x			x					
3.4 Wing Sizing	x	x								
3.5 Secondary Drag		x								
4. Canopy Structures & Materials										
4.1 Canopy Design Method									x	x
4.2 Canopy Structural Concept									x	x
4.3 Tensairity®									x	x
4.4 Canopy Structural Layout									x	x
4.5 Pressurised Multibubble Design									x	x
4.6 Structural Integrity Through Jet Flaps									x	x
4.7 Numerical Code for Structural Canopy Design									x	x
4.8 Canopy Materials					x				x	x
4.9 Effect of Assumptions									x	x

Table C.2: Contribution chart of the final review

Final Review	Tim	Melchior	Theresa	Luuk	Haider	Rutger	Frits	Leon	Atilla	David
5. Fuselage Structures & Materials										
5.1 Load Cases			x			x				
5.2 Fuselage Model			x			x				
5.3 Sensitivity			x			x				
5.4 Fuselage Frame			x			x				
5.5 Fuselage Materials			x			x				
5.6 Canopy Connectors			x			x				
5.7 Motor Frame			x			x				
6. Aircraft Subsystems										
6.1 Power system							x			
6.2 Power Management System							x			
6.3 Navigation				x						
6.4 Health & Safety				x						
6.5 Take-off & Landing				x						
6.6 Configuration				x						
6.7 Overview				x						
6.8 Helium		x								
7. Verification & Validation										
Verificaton	x	x	x	x	x	x	x	x	x	x
Validation	x	x	x	x	x	x	x	x	x	x
8. Feasibility										
8.1 Flightprofile		x	x		x					
8.2 Performance Analysis		x								
8.3 Sensitivity Analysis of the Full Design					x					
8.4 Feasibility Check		x								
8.5 Futre Project Planning							x			
8.6 Sustainable Development							x			
8.7 Realiability, Availability, Maintainability and Safety				x						
8.8 Cost Analysis							x			
9. Conclusion & Recommendations										
9.1 Conclusions	x									
9.2 Recommendations	x	x	x	x	x	x	x	x	x	x
Appendices										
Appendix A: Stability Derivation								x		
Appendix B: Ejection Cap calculations								x		
Appendix C: Contribution Chart						x				
Latex	x		x					x		
Layout	x		x							
Quality Control	x		x		x				x	
CATIA				x						
Sketch-up	x									